Development of a Framework for Identifying Critical Input Parameters for Effective Pediatric PBPK/PBTK Modelling

by

Yejin Esther Yun

A thesis

presented to the University of Waterloo

in fulfillment of the

thesis requirement for the degree of

Doctor of Philosophy

in

Pharmacy

Waterloo, Ontario, Canada, 2022

Examining Committee Membership

The following served on the Examining Committee for this thesis. The decision of the Examining Committee is by majority vote.

External Examiner	Jeffrey Fisher Senior Research Fellow, ScitoVation, Durham NC
Supervisor	Andrea Edginton Professor and Hallman Director
Internal Members	Praveen Nekkar Rao Associate Professor
	Rogelio Tornero-Velez Adjunct Assistant Professor
Internal-external Member	Rebecca Rooney Associate Professor

Author's Declaration

This thesis consists of material all of which I authored or co-authored: see Statement of Contributions included in the thesis. This is a true copy of the thesis, including any required final revisions, as accepted by my examiners.

I understand that my thesis may be made electronically available to the public.

Statement of Contributions

The contents of Chapter 2 were published as an original contribution manuscript by the PhD candidate (Yejin Yun). The original manuscript has been formatted according to thesis publication requirements. The PhD candidate conducted all the pertinent research and analyses and wrote the manuscript.

Yun, Yejin Esther, and Andrea N. Edginton. "Model qualification of the PK-Sim® pediatric module for pediatric exposure assessment of CYP450 metabolized compounds." Journal of Toxicology and Environmental Health, Part A 82.14 (2019): 789-814.

The contents of Chapter 3 were published as an original contribution manuscript by the Ph.D. candidate (Yejin Yun). The original manuscript has been formatted according to thesis publication requirements. The PhD candidate conducted the majority of pertinent research analyses and wrote the manuscript. Rogelio Tornero-Velez, S. Thomas Purucker, Daniel T. Chang conducted a portion of research analyses.

Yun, Yejin Esther, Rogelio Tornero-Velez, S. Thomas Purucker, Daniel T. Chang, and Andrea N. Edginton. "Evaluation of quantitative structure property relationship algorithms for predicting plasma protein binding in humans." Computational Toxicology 17 (2021): 100142.

The contents of Chapter 4 were published as an original contribution manuscript by the PhD candidate (Yejin Yun). The original manuscript has been formatted according to thesis publication requirements. The PhD candidate conducted all the pertinent research and analyses and wrote the manuscript.

Yun, Yejin Esther, and Andrea N. Edginton. "Evaluation of models for predicting pediatric fraction unbound in plasma for human health risk assessment." Journal of Toxicology and Environmental Health, Part A 84.2 (2021): 67-83.

The contents of Chapter 5 were published as an original contribution manuscript by the PhD candidate (Yejin Yun). The original manuscript has been formatted according to thesis publication requirements. The PhD candidate conducted all the pertinent research and analyses and wrote the manuscript.

Yun, Yejin Esther, and Andrea N. Edginton. "Prediction of fraction unbound in plasma in children in data-limited scenarios for human health risk assessment." Computational Toxicology 18 (2021): 100168.

The contents of Chapter 7 were published as an original contribution manuscript by the PhD candidate (Yejin Yun). The original manuscript has been formatted according to thesis publication requirements. The PhD candidate conducted all the pertinent research and analyses and wrote the manuscript.

Yun, Yejin Esther, Daniella Calderon-Nieva, Abdullah Hamadeh, and Andrea N. Edginton. "Development and Evaluation of an In Silico Dermal Absorption Model Relevant for Children." Pharmaceutics 14.1 (2022): 172.

Abstract

Within a physiologically based pharmacokinetic (PBPK) model framework, virtual children are built based on known trajectories of anatomy and physiology across age and a compounds transfer within the body is defined by physicochemical and biochemical properties. Pediatric PBPK models have been used to derive doses for pediatric clinical trials and to assess risk of exposure to environmental chemicals. The identification of critical system- and compound-specific input parameters for pediatric PBPK modeling is crucial to applying this approach where pharmacokinetic (PK) data are limited. The objective of this study is to suggest a framework for the development of effective pediatric PBPK models by (i) identifying the most critical input parameters affecting the model precision as a means of targeting experimentation and by (ii) developing a workflow that combines available in silico prediction methods to estimate PK parameters in children. It is hypothesized that the framework for pediatric PBPK modeling will decrease the uncertainty associated with human health risk assessment in children.

Pediatric PBPK models for 10 hepatically metabolized compounds were developed and their predictive performance was evaluated by comparing the predicted and observed PK values in children. Resonable prediction accuracy was demonstrated such that eighty-one percent of the comparisons between simulated and observed clearance values were within two-fold error. Through sensitivity analyses, the most important parameters for pediatric PBPK modeling were identified. It was found that protein binding and clearance parameters were important for pediatric PBPK models. In light of these findings, prediction methods of plasma protein binding and clearance in children were chosen as the main topics of this dissertation.

When experimentally determined plasma protein binding information is not available, quantitative structure–property relationship (QSPR) models can be used to predict fraction unbound in plasma (fup) in humans. Three available QSPR models were evaluated. The most important chemical descriptors for predicting fup were lipophilicity, positive polar surface area, and the number of basic functional groups. It was found that the prediction of fup was the most uncertain for highly bound compounds. The next step was to evaluate adult-to-children scaling algorithms (ontogeny models) for fup. The predictive performance of 4 ontogeny models for albumin and 5 ontogeny models for alpha1-acid glycoprotein (AAG) were evaluated. Plasma protein concentrations vs. age profiles

derived from non-linear equations (PK-Sim and Johnson et al.) were more in agreement with the observed levels than other models. Prediction accuracy of the ontogeny model depended on the appropriateness of the protein concentration vs. age profiles of ontogeny models particularly for highly bound compounds.

For environmentally relevant compounds which are data-poor (e.g. information on physicochemical, toxicokinetic, and toxicological properties is not available), the prediction accuracy for fup prediction in children (fup_{child}) can be different than pharmaceuticals where experimental data such as fup in adults (fup_{adult}) is often available. The prediction of fup_{child} for data-limited scenarios were evaluated with data-rich compounds such as pharmaceuticals as fup_{child} values are often available for those compounds. When QSPR-predicted fup in adult values were used as an input for predicting fup_{child}, over-predictions were observed for acids and neutrals with an average fold error (AFE) up to 8. The results indicated that an experimental determination of fup in adults was crucial.

Two methods were proposed for predicting clearance (CL) in children from compound structure. The workflow utilizes QSPR models, protein binding ontogeny models and virtual pediatric individuals. Hepatic intrinsic CL, renal CL and fup in adults were estimated from a compound structure based on QSPR methods. Appropriate scaling methods were used to estimate CL in children. The QSPR-predicted CL values showed an over-prediction with geometric mean fold error values ranging from 1.9 to 3.29. When a predominant clearance pathway (e.g. hepatic metabolism or renal excretion) was predicted based on physicochemical properties of compounds and this information was used for CL prediction in children, the prediction accuracy was improved. The proposed workflow is considered to provide a reasonable estimation of clearance in pediatric population for human health risk assessment for data-sparse compounds.

Prediction of dermal absorption in children is an important aspect in human health risk assessment. A pediatric dermal absorption model was developed by incorporating maturation functions into a MoBi implementation of the Dancik et al. 2013 skin permeation model.

Adult models were first developed by optimizing key chemical specific parameters using the observed dermal absorption data in adults (e.g. in vitro permeation testing experimentation). For predicting dermal absorption in children, chemical-specific parameters in the model remained the same as in the adult model and age-dependent components of dermal absorption (e.g., skin layer

thickness and hydration) were scaled as a function of age. This model can be used to predict dermal absorption in children by taking into account the physicochemical properties of the drug and the maturation of skin physiology and anatomy. In order to incorporate the information on the maturation of skin physiology and anatomy, extensive literature search was conducted. The predictive performance of the model was evaluated by comparing predicted and observed rate of dermal absorption for three compounds where IVPT data were available for neonates. The model described the trend of increased flux in neonates compared to adults. The predicted flux values were similar to the observed and predicted mean flux in neonates generally fell within the 90 percent prediction intervals. More IVPT data in children are required for model evaluation, however, the preliminary assessment with the limited set of data demonstrated favourable outcome.

The studies in this dissertation evaluated computational methods that can be used to estimate pediatric PK for data-sparse compounds (e.g. environmentally relevant compounds). The proposed workflows and developed models for estimating important PK parameters in children in this dissertation are considered to be useful in decreasing uncertainties associated with PK in children estimation from compound structure for environmentally relevant compounds. Furthermore, the proposed models are physiologically relevant and these models will help risk assessors to make informed decisions for human health risk assessment in children.

Acknowledgements

First of all, I'd like to thank God for everything. I'd like to thank my supervisor Dr. Andrea Edginton for her guidance, advice and kind help. I'd like to thank my committee members for providing their support and insight.

I'd like to give special thanks to my family for their support when undertaking my research and writing my papers. I'd like to thank my friends Maxene Smith and Renore Smith for always being there for me. Your prayer, support and care for me helped me reach this far.

I'd like to thank Dr. David Barrett from Nottingham University for providing a copy of his published paper. It was helpful for Chapter 7 of this thesis. I'd like to thank co-authors of Chapter 3 and Chapter 7. I'd like to give thanks to Rogelio (Mike) Tornero-Velez, S. Thomas Purucker and Daniel T. Chang from U.S. Environmental Protection Agency for providing me with calculations, feedback and suggestions. I'd like to thank Dasha Hajducek for helping me when I had questions regarding statistics. I'd like to thank Mickael, Alexandra and Andrew for their morale support.

Dedication

I dedicate my dissertation work to my family.

Table of Contents

List of Figures

List of Tables

List of Abbreviations

AAFE	absolute average fold error
AAG	Alpha-1 acid glycoprotein
ALB	albumin
AC50	A ratio of Cmax to half maximal effective concentration
ADI	acceptable daily intake
ADME	absorption, distribution, metabolism and elimination
AFE	average fold error
AU	arbitrary unit
AUC	area under the curve
AUCinf	the area under the plasma concentration vs. time profile from 0 to infinity
AUClast	the area under the plasma concentration vs. time profile from from dosing (time 0) to the time of the last measured concentration
B:P	blood-to-plasma ratio
BAP	benzo-a-pyrene
BMI	Body mass index
BPA	bisphenol A
CL	clearance
CLh	hepatic clearance
CLint	intrinsic clearance
CLp	plasma clearance
CLr	renal clearance

CLspec	specific clearance
Cmax	maximum concentration
CompTox	computational toxicology
CSAF	chemical specific adjustment factor
CV	coefficient of variation
CYP	cytochrome P450
D	diffusion coefficient
d	day
DDT	dichlorodiphenyltrichloroethane
DE	dermis
ECCS	Extended Clearance Classification System
ED	epidermis
EH	hepatic extraction ratio
EPA	Environmental Protection Agency
ERC	environmentally relevant compound
fe	fraction excreted unchanged in urine
$f_{hepatic\ uptake}$	fraction of hepatic uptake
fm	fraction metabolized of CYP enzyme(s)
fub	fraction unbound in blood
fumic	fraction unbound in human liver microsomes
fup	fraction unbound in plasma
fup_{adult}	fraction unbound in plasma in adults

fup_{child}	fraction unbound in plasma in children
GA	gestational age
GFR	glomerular filtration rate
GMFE	geometric mean fold error
GSD	geometric standard deviation
h	hour
hde	dermis thickness
HDL	high density lipoprotein
hed	epidermis thickness
HHRA	human health risk assessment
HKAF	human kinetic adjustment factor
HLM	human liver microsome
hsc	stratum corneum thickness
HTS	high throughput screening
ICRP	International Commission on Radiological Protection
IV	intravenous
IVIVE	in vitro-in vivo extrapolation
IVPT	in vitro skin permeation test
J	flux rate
K	partitioning coefficient
KA	absorption rate constant
Ki	Inhibition constant

Klip/w	partition coefficient of compound in SC lipids with respect to water
Ktrans	trans-lipid-bilayer permeability in SC
LDL	low-density lipoproteins
LOAEL	lowest-observed-adverse-effect level
LogP	partition coefficient of a compound between lipophilic phase (e.g. octanol) and water
LOOCV	leave-one-out cross validation
MAE	mean average error
MCMC	Markov-chain Monte-Carlo algorithm
MFE	mean fold error
mg	miligram
NOAEL	no-observed adverse-effect level
OF	ontogeny factor
PBPK	physiologically based pharmacokinetic
PCB	polychlorinated biphenyl
$PC_{prot/water}$	Partition coefficient of compound in corneocyte protein phase with respect to water
PDE	partial differential equation
PKA	negative base-10 logarithm of the acid dissociation constant
PMA	postmenstrual age
PNA	postnatal age
PO	oral administration
POD	point of departure
QH	hepatic blood flow

QSPR	quantitative structure–property relationship
r2	coefficient of determination
RCU	relative capacitance unit
RfC	reference concentration
RfD	reference dose
RFE	relative prediction error
RMSE	root mean squared error
SC	sensitivity coefficient
SC	stratum corneum
SD	standard deviation
SDF	structural data file
t1/2	half-life
TD	toxicodynamics
TDI	tolerable daily intake
TK	toxicokinetics
Tmax	time to reach Cmax
ToxCast	Toxicity Forecaster
UF	uncertainty factors
UGT	Uridine 5'-diphospho-glucuronosyltransferase
VLDL	very-low density lipoprotein
Vss	Volume of distribution at steady state
w	week

Chapter 1: Introduction and Background

1.1 Physiology Based Pharmacokinetic (PBPK) modeling in Human health risk assessment

Human Health Risk Assessment

Human health risk assessment is a process to estimate a health risk in human or (sub-)population, following an exposure to a compound, by accounting for the inherent characteristics of the compound and the specific target system [1]. In risk assessment, a potential hazard is identified and the associated risks are estimated [2]. In human health risk assessment, the mode of action and probability of adverse health effects are evaluated in humans who are exposed to environmental toxicants. As a result, risk managers can use the results of the risk assessment and design and implement risk management approaches.

For human health risk assessment, in order to estimate an acceptable chemical exposure limit or an allowable dose for humans, a dose-response relationship must be derived. This usually entails experimentation in animals where the dose-response relationship is evaluated and a point of departure (POD) for human extrapolation is determined such as a no-observed-adverse-effect level (NOAEL), or a lowest-observed-adverse-effect level (LOAEL) (Figure 1.1). In non-cancer risk assessment, the POD, as determined in animal experiments, is divided by an uncertainty factor (e.g. chemical specific adjustment factor (CSAF)) to derive an acceptable daily intake (ADI), reference dose (RfD), reference concentration (RfC), or tolerable daily intake (TDI) for humans [2-5]. For the protection of both healthy and susceptible human populations, the POD of interest is divided by a default uncertainty factor of 10 in order to address variations in interspecies (animal to human) and inter-individual (human to human) variations in toxicokinetics (TK) or toxicodynamics (TD) [5-7]. The 10-fold uncertainty factor for interspecies differences is subdivided into 4 (i.e. $10^{0.6}$) for toxicokinetics and 2.5 (i.e. $10^{0.4}$) for toxicodynamics. Whereas the 10-fold uncertainty factor for human variability is subdivided to 3.16 (i.e. $10^{0.5}$)-fold subfactors for each of toxicokinetics and toxicodynamics (Figure 1.2) [8-10].

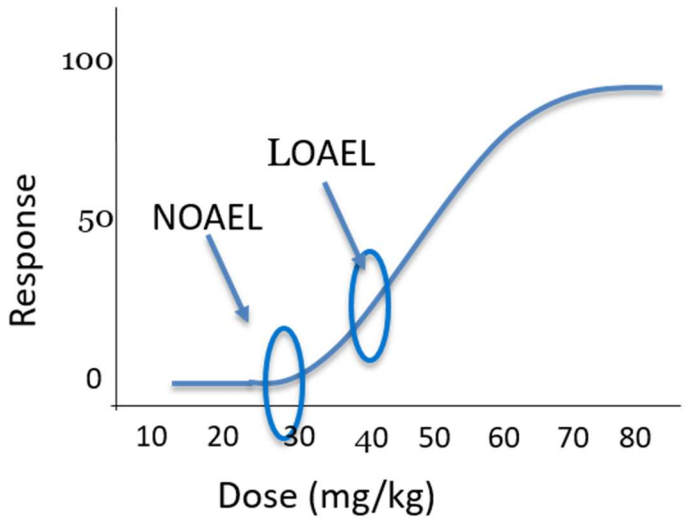

Figure 1.1 An example of dose-response curve and point of departures of LOAEL and NOAEL

Although the default value of 3.16 has been approved by regulatory agencies, this value may not address the extent of human variability. The International Programme on Chemical Safety [11] provided a method to replace default uncertainty factors with CSAFs so that the uncertainty factor of 3.16 can be replaced when sufficient toxicokinetic and/or pharmacokinetic data are available in various populations [10, 12]. The CSAF is obtained by the ratio between the upper percentile value of a pharmacokinetic parameter and the median values in a population [10, 13]. In terms of the CSAF for susceptible populations, CSAF can be obtained by the ratio between the upper percentile value of a pharmacokinetic parameter in a susceptible subpopulation and the median value in the healthy population [13, 14]. For example, Ginsberg et al. [15] showed that the range of the half-life ratios between neonate and adults for 26 test compounds was 2 to 4 indicating that the TK ratio of some compounds exceeded the uncertainty factor of 3.16. In this case, the CSAF values derived from adult and neonate PK data can be used for risk assessment to account for internal exposure [11].

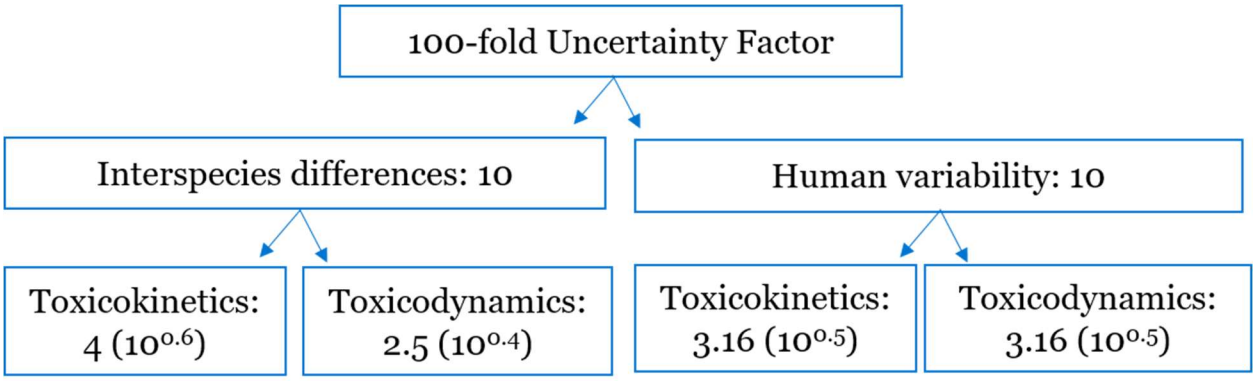

Figure 1.2 The derivation of CSAF via subdivision of uncertainty factors into TK and TD subfactors (Adapted from Meek et al. 2002 and Bhat et al. [6, 13])

Physiologically based pharmacokinetic/toxicokinetic (PBPK/PBTK) models

PBPK models are composed of integrative mathematical equations that quantitatively describe the processes of absorption, distribution, metabolism and elimination (ADME) of a compound in a biological system. The structure of a PBPK model represents an organism by defining compartments that correspond to different tissues such as heart, liver, kidney, bone, muscle, and spleen, etc (Figure 1.3). The organs are connected through the circulatory system and each compartment is defined by system-specific (e.g. volume, blood flow rate) or compound-specific (e.g. plasma-to-tissue partition coefficient) parameters. Chemical movement between organs or organ compartments (e.g. vascular space, interstitial space) is represented with a mass-balance ordinary differential equation that describes changes in chemical concentration over time. The chemicals are subject to processes including the distribution into a compartment and the clearance from the compartment through processes such as metabolism or elimination.

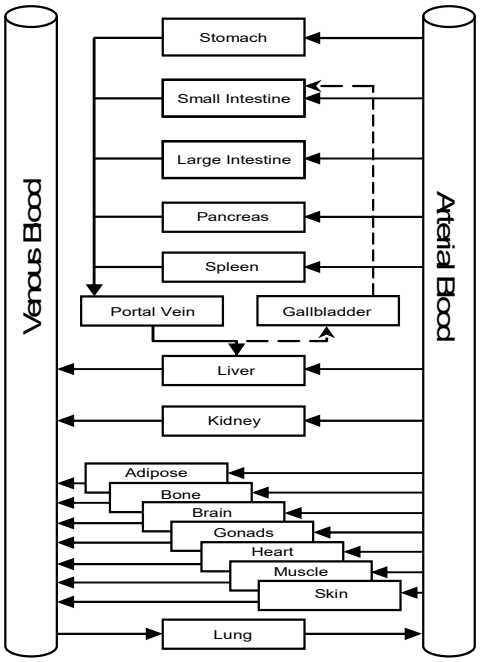

Figure 1.3 An example of model structure of a PBPK model

Application of PBPK models in human health risk assessment

PBPK models are used to predict tissue and plasma concentrations of a substance for dose-response analysis in animal toxicity or human toxicity studies [4]. Furthermore, PBPK models can facilitate many more applications in human risk assessment such as (i) interspecies extrapolation of equivalent doses, (ii) route-to-route extrapolation (iii) high-to-low dose extrapolation (iv) estimation of a tissue dosimetry from multi-route exposure and (v) screening and prioritization of chemicals [16-18].

One of the main applications of PBPK models in risk assessment is in interspecies extrapolation. PBPK models can inform the determination of the CSAF for interspecies differences in toxicokinetics such that toxicokinetic data that is determined in animal species can be used for predicting toxicokinetic profiles in humans by accounting for chemical specific data and species-specific anatomy and physiology [17, 19]. PBPK models can also be used to predict toxicokinetically equivalent doses in animals and humans. An animal PBPK model is first constructed to estimate the internal exposure given an external dose of a POD in the animal. The internal exposure in humans is estimated in human PBPK models using human equivalent doses that are estimated from animal doses. As stated previously, interspecies differences are taken into account by system-specific physiologic parameters, therefore, no

additional TK adjustment factors are necessary if a PBPK model is used for extrapolation of a dose metric value [6].

Pharmacokinetic and toxicokinetic differences in the pediatric population

As a result of the different rates of anatomic and physiological maturation or growth, ADME in children can be different from adults and harder to predict due to higher inter-individual variabilities [20, 21]. The metabolism, detoxification and excretion capacity in a system relies on the maturity of metabolizing enzymes and the function of a relevant organ [21]. For example, the activity of metabolic enzymes (e.g. cytochrome P450) and the renal elimination capacity is lower in neonates and infants [22] [23, 24]. The degree of protein binding to plasma proteins (e.g. human serum albumin) can differ in children as compared to adults. For example, plasma protein levels are lower in neonate leading to a higher unbound fraction in plasma than in adults. This can alter both the distribution and clearance processes [25]. In terms of the age-dependence of absorption, a higher skin surface area per body weight in children and the prematurity of skin in neonates can cause a higher vulnerability to environmental toxicants [20]. Further, with respect to oral absorption transit times [26, 27] and solubility [28] may differ from those in adults. When children are exposed to chemicals, immaturity can lead to higher blood concentration levels and a longer duration in the body as compared to adults.

By understanding the anatomy and physiology of children, the PBPK model can be used to integrate the interplay of numerous factors that are derived from growth and maturation. In drug development, PK data in children is often available whereas pediatric TK data is not available for human health risk assessment. Therefore, the use of pediatric PK data as derived in drug development allows for determination of process maturation that is responsible for compound disposition [25, 29, 30] and the use of those data to derive such age-related relationships benefits the development of virtual children that can be used in prediction of TK.

Applications of PBPK models in the pharmaceutical sector

In drug development, PBPK modeling can be used in multiple applications including (i) prediction of drug-drug interactions, (ii) initial dose selection in first-in-pediatric trials, (iii) initial dose selection in first-in-human trials, (iv) evaluation of formulation effects and (v) evaluation of the effects of disease (e.g. renal or hepatic impairment) [17, 31-36]

Furthermore, PBPK models in pharmaceutical studies will advance with technology and the improvement in predictive algorithms that describe various biological processes. For example, in order to improve the limitation in describing inter-individual variability for advanced

parameter identification in PBPK modeling, a new approach [37-39] was developed by applying the Markov-chain Monte-Carlo algorithm (MCMC) [40]. The MCMC algorithm allows for the estimation of posterior distributions of individual specific PBPK parameters (i.e. both physiologic and compound specific parameters). By using clinical PK data and the explicit definition of physiological parameters as defined in PBPK models, virtual organisms will continue to better represent real organisms thus improving model confidence.

A traditional method for predicting pediatric PK

From a regulatory perspective, it is a challenge to plan and conduct pediatric PK/PD studies using a safe and therapeutically effective dose in these populations [41]. The design of the initial PK studies in children has been derived from PK properties in adults and adolescents using allometry [41, 42]. Allometric scaling describes the age-dependent difference in PK using by accounting for body size and metabolic rate. However, the low hepatic metabolic capacity in pediatrics is not taken into account [43]. Furthermore, allometric scaling is derived from interspecies analysis from adult animals, therefore, it may not be sufficient to describe age-specific differences [16]. It has been shown that PBPK results yielded a better prediction of clearance in children than the results estimated from allometry [44].

Pediatric PBPK/TK model

From a regulatory perspective, a first-in-children dose selection for initial clinical studies are based on limited clinical data, therefore they can rely heavily on a pediatric PBPK model. As most pediatric PBPK models are developed using adult PK data [45-47] (Figure 1.3), the evaluation of adequate parameterization of variables that are related to growth and maturation is of most importance [5, 45, 48]

The assumptions of pediatric PBPK models are (i) the clearance pathway(s) is/are the same in both adults and children, and (ii) the disease pathophysiology and progression are similar in adults and children and (iii) the disease state does not affect the maturation process as compared to healthy children [49]. Pediatric PBPK/TK models can facilitate (i) dose selections in first in children clinical studies, (ii) PK-safety assessment, (iii) drug-drug interaction prediction and (iv) the effect of diseases [45, 50]. PBTK models for environmental toxicants have been widely used in human risk assessment for pediatrics (e.g. BPA [51], isopranolol and vinyl chloride [12])

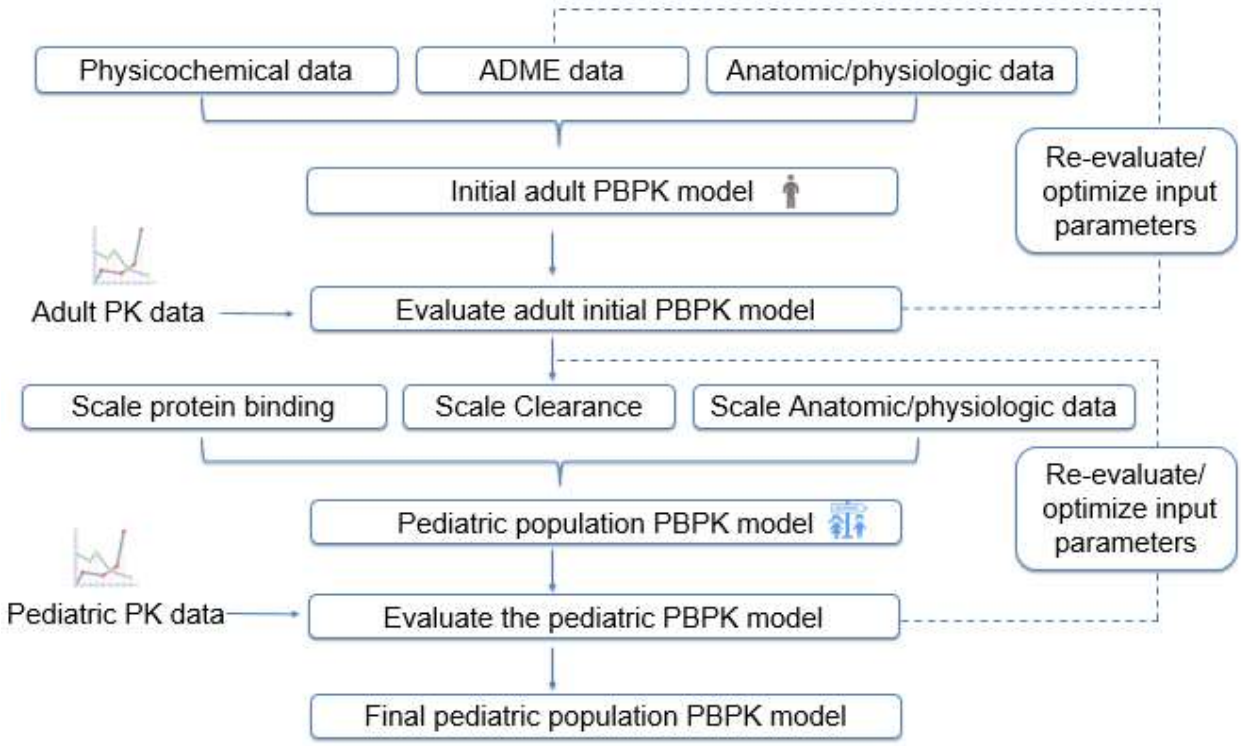

Figure 1.4 Model building workflow for a pediatric PBPK model (Adapted from Edginton and Maharaj [47])

PK-Sim®

PK-sim (Open Systems Pharmacology Suite) [52] is a whole body PBPK modelling software that has a graphical user interface. PK-Sim includes the database of anatomical and physiological parameters of humans and laboratory animals [53]. A whole body model in PK-Sim consists of 17 tissues that are composed of compartments including: plasma, red blood cells, interstitial as well as cellular space in a tissue. The PBPK model also takes into account different administration routes (e.g. subcutaneous or intravenous) and formulations (e.g. suspension or tablet) of a drug. Using the PK-Sim software for a pediatric model, the major maturation dependent processes such as metabolism (e.g. ontogeny of metabolizing enzymes) and excretion (renal clearance) are scaled to children [44, 45]. PK-Sim is an open-source

software (open-systems-pharmacology.com) that can facilitate many applications of PBPK modeling used in pharmaceutical studies and risk assessment.

PBPK modelling platform evaluation in predictive performance

As a PBPK model describes a complex biological system, it can have innate errors such as model structure errors and parameter uncertainties. Therefore, a model qualification should be performed for the intended use to increase the confidence in the model outcome. In terms of evaluating a PBPK model, (1) model structure, (2) mathematical representation of the biological processes (3) compound- and/or system- specific parameter estimation can be assessed for model qualification [16, 17]. The model adequacy of those components can be evaluated by comparing the model outputs (e.g. AUC) with the observed data. As a part of this study, model adequacy and predictive performance of PK-Sim for pediatric models will be investigated.

Sensitivity analysis

A PBPK model is mechanistic in nature with a set of equations that consists of numerous physiological and compound specific input parameters. In PBPK modeling, a sensitivity analysis can elucidate the relative contribution of single or multiple parameters (e.g. hepatic parameters or glomerular filtration rate) to a model output (predicted plasma concentration of a parent compound). Local sensitivity analysis measures how the model output changes by varying one parameter while keeping all other parameters constant. The sensitivity of the model output to the varied input parameter is calculated as the ratio of the relative change of that model output and the relative variation of the input parameter (Equation 1),

Eqn (1) $S_{ij} = \frac{\frac{\Delta AUC}{AUC}}{\frac{\Delta p}{p}}$

where S_{ij} is a sensitivity coefficient, p is a parameter. For example, a 20% change of a parameter results in a 20% change in a model output, then the resulting sensitivity coefficient is 1. Accordingly, the effect of an input parameter on a model output is regarded insignificant if the sensitivity coefficient is less than 0.1 [54]. In terms of global sensitivity analysis, all the input parameters are varied concurrently [55]. An example of a global sensitivity analysis on a PBPK model can be found in Malik et al. [56].

Sensitivity analysis of a PBPK model can be used to inform human health risk assessment. For example, McLanahan et al. [57] developed the PBPK model that predicted inhibition of

thyroidal radioactive iodine uptake by an environment contaminant perchlorate for different age groups at the POD (7 μg/kg-day). The researchers determined through sensitivity analysis that the near-term fetus (40 gestational weeks) is the most sensitive to perchlorate as compared to other age groups.

Limitations to the use of PBPK in drug development and in human health risk assessment

Challenges in both drug development and human risk assessment are the prediction of human PK/TK profiles from animal data and adults to children extrapolation. The availability of the required input parameters for a PBPK model can be a barrier as those input parameters are often not available, especially during the risk assessment process. Therefore, the identification of the critical input parameters will target limited resources and lessen the burden of experiments allowing efficient PBPK modeling in those applications.

1.2 Objectives

Pediatric PBPK modeling can be used to simulate various exposure scenarios to environmental toxicants in children. It can also suggest a safe and therapeutic dose for pediatric clinical studies in drug development. Due to ethical constraints, the experimental determination of TK parameters in children is not possible. Therefore, pediatric PBPK modeling plays an important role to utilize the most of the limited data and to help make informed decisions for risk assessors. The hypothesis of this study is that identifying input parameters, within the PBPK structure, that are important to PK outcomes enables us to decide where resources need to be directed in pursuit of having high confidence in pediatric PBPK model outcomes. The objective of this study is to suggest a framework for the development of effective pediatric PBPK models by (i) identifying the most critical input parameters affecting the model precision

as a means of targeting experimentation and by (ii) developing a workflow that combines available *in silico* prediction methods to estimate PK parameters in children. It is hypothesized that the resulting framework for pediatric PBPK modeling will decrease the uncertainty associated with human health risk assessment in children.

Chapter 2: Model qualification of the PK-Sim® pediatric module for pediatric exposure assessment of CYP450 metabolized compounds

2.1 Introduction

In human health risk assessment (HHRA), uncertainty factors (UF) are applied to a point of departure (POD) such as a no-observed-adverse-effect level (NOAEL), or a lowest-observed-adverse-effect level (LOAEL) to derive relevant toxicological indices such as tolerable daily intake (TDI) and average daily intake (ADI) [2, 11]. These factors serve a purpose of protecting healthy and potentially susceptible populations from exposure to contaminants such as children. The default uncertainty factor (UF) of 3.16 is used to address the toxicokinetic (TK) variability between adults and children [15, 17, 58]. However, this value might be too low or high depending upon the properties of a chemical and/or the characteristics of individuals who are exposed to the chemicals [59], hence, the default factor may not be adequate or may be overly protective of a subpopulation. To improve this limitation and account for chemical-specific data, the default UF may be replaced with a chemical-specific adjustment factor (CSAF) [10, 11]. A human kinetic adjustment factor (HKAF) is obtained by a ratio between the upper percentile (e.g. 95th) value of a pharmacokinetic parameter in a susceptible subpopulation and median value in the healthy population [13, 14]. As human TK data are scarce, physiologically based pharmacokinetic (PBPK) models might facilitate the estimation of a PK parameter in a population of interest such as infants or children and support determination of the HKAF. Examples of PBPK-based-HKAF include styrene [60], chloroform [61], toluene [62] and 1-4 dioxane [10].

PBPK models are composed of mathematical equations that quantitatively describe the processes of absorption, distribution, metabolism and excretion (ADME) of a compound in a biological system

[63]. The structure of a PBPK model represents an organism by defining compartments that correspond to different tissues such as heart, liver, kidneys, bone, muscle, and spleen. The organs are connected through the circulatory system and each compartment is defined by system-specific (e.g. volume, blood flow rate) or compound-specific (e.g. plasma-to-tissue partition coefficient) parameters. Chemical movement between organs or organ compartments (e.g. vascular space, interstitial space) is represented with a mass-balance ordinary differential equation that describes changes in chemical concentration over time. The chemicals are subject to processes including the distribution into a compartment and the clearance from the compartment through processes such as metabolism or elimination.

One of the advantages of using PBPK to define the dose-exposure relationship is its ability for extrapolation, for example between adults and children [64]. By understanding the anatomy and physiology of children, the PBPK model may be used to integrate the interplay of numerous factors that are derived from growth and maturation. The metabolism and excretion capacity of a system relies on the maturity of metabolizing enzymes and the function of a relevant organ [21]. For example, the activity of metabolic enzymes (e.g. cytochrome P450 (CYP)) and the renal elimination capacity is lower in neonates and infants [22, 23, 65]. The degree of protein binding to plasma proteins (e.g. human serum albumin) can be different in children compared to adults. For example, plasma protein levels are lower in neonates leading to a higher unbound fraction in plasma than adults. This may alter both distribution and clearance processes [25]. In terms of the age-dependence of absorption, a higher skin surface area per body weight in children and the prematurity of skin in neonates might result in higher vulnerability to environmental toxicants [20, 58]. Further, with respect to oral absorption, solubility may differ from those in adults due to developmental changes in gastrointestinal fluid composition [28, 66]. When children are exposed to chemicals, immaturity might lead to higher blood concentrations and a longer half-life in the body compared to adults.

When building PBPK models applicable to children, little, if any, information is usually available to evaluate the model outcomes. The process of model qualification aims to demonstrate that the model inputs (e.g. organ volumes, enzyme concentrations) are reasonable representations of reality that will ideally lead to a reasonable prediction accuracy of the model for an intended use, such as predicting pediatric systemic exposure. As pediatric PBPK models play a key role in decision making for

regulatory purposes in both the pharmaceutical sector (e.g. first-in-children dose recommendation [36, 67]) and human health risk assessment (e.g. PBPK-based-CSAF determination [10]), model qualification has become a topic of intense discussion [34, 68]. Model qualification is prominently featured in the European Medicines Agency guideline on the reporting of PBPK model and simulation with special attention paid to model qualification for pediatric PBPK models based upon a regulatory impact. In light of this, many academic and industry groups have made an effort to demonstrate the predictive performance for adult-to-children PK extrapolation [69-71].

PK-Sim is an open-source PBPK modeling tool within the Open Systems Pharmacology Suite (open-systems-pharmacology.org). While historically this software was a commercial product of Bayer Inc., as of 2017, it has been made freely available. There is significant push from within Bayer and throughout the community to qualify the platform [68, 72] and therefore increase certainty in the model structure and parameters contained therein.

Prediction of PK in children may be dependent upon a PBPK model's integrity to describe the effects of maturation and growth by combining relevant anatomic, biochemical and physiologic parameters at specific age stages with compound-specific parameters. The aim of this study was (i) to determine the appropriateness of the virtual individual creating algorithm in PK-Sim® in predicting PK parameters and their variability in children by comparing a model output, clearance, to observed data and (ii) to identify critical system-specific input parameters within a pediatric PBPK model structure for estimating exposure in children via a sensitivity analysis.

2.2 Methods

2.2.1 Compound selection and data collection

Compounds that are mainly metabolized by hepatic CYP enzymes were included in this study. Because the predictive capability of the platform was assessed by generating pediatric PK outputs, a full set of input data was required. The required data for building and evaluating a pediatric PBPK model included:

physicochemical data (e.g. lipophilicity (LogP), acid-base properties (pKa), water solubility)

fraction unbound in plasma in adults (fup)

plasma concentration vs. time profiles in adults

fraction excreted unchanged in urine (fe)

metabolism information (fraction metabolized, contributions of each metabolism process, enzymes involved)

The input parameters for each compound-specific pediatric PBPK model are listed in Table 2.1. All included compounds were pharmaceuticals. For these compounds, all required inputs listed above were available. Table 2.2 presents clinical studies that provided PK data for model development and evaluation. The collected compound-specific data and adult data was used for model development and the pediatric data was used for model evaluation. Pediatric data are categorized based upon age as follows: neonates or newborns are from 0 to <1 month, infants are 1 month to <2 years, children are from 2 years to <12 years and adolescents are 12 years to <18 years. PK profiles following intravenous (IV) administration were used with priority in order to accurately characterize distribution volume and clearance. When only pediatric PK profiles following an oral administration (PO) were available in the literature, both observed IV and PO profiles were used to characterize PK properties in adults. The simulation of PO profiles from the same formulation was employed in both adults and children. The numerical values of plasma concentration-time profiles in adults from the literature were obtained by using PlotDigitizer [73]. The mean and standard deviation of clearance values in pediatric clinical studies were obtained from the literature. When only a range was available, a standard deviation was estimated from the range based on an estimating equation (Supplementary Material Table S1.) in Hozo et al. [74].

Table 2.1 Compound-specific input parameters for PBPK model development

Compound	LogP (reported a / optimized) b	Molecular Weight (g/mol) a	pKa a	fup	Water solubility a	Specific clearance (min-1) b,c	ADME	Reference
Alfentanil	2.16 /1.69	416.5	7.5	0.1	34.60 mg/L	CYP3A4 0.47		[75, 76]
Diclofenac	1.90 /1.35	296.1	4.0 (acid)	0.003	2.37 mg/L	CYP2C9 460.0		[77-79]
Esomeprazole	0.6/ 1.34	345.4	9.68 (acid)/ 4.77 (base)	0.03	0.353 mg/mL	CYP2C19 5.6 CYP3A4 0.5	CYP2C19 inhibition Ki b, c 7.5µmol/L	[80]

Itraconazole	5.66/ 4.80	705.6	3.7	0.006	9.64 mg/L	CYP3A4 90.6	Ki b of itraconazole and hydroxy- itraconazole on CYP3A4 were 0.35 and 0.38 nmol/L, respectively	[81]
Lansoprazole	1.9 / 1.0	369.4	8.84 (acid), 4.15 (base)	0.03	0.97 mg/L	CYP2C19 5.1 CYP3A4 0.5		[82, 83]
Midazolam	3.33/ 3.03	325.8	6.15 (base)	0.02	49 mg/L	CYP3A4 3.9		[84, 85]
Ondansetron	2.4 / 1.59	293.4	7.34 (base)	0.27	0.36 mg/L	CYP3A4 0.02 CYP1A2 0.13	Fe d < 5%	[86, 87]
Sufentanil	3.95 / 2.56	386.6	8.01 (base)	0.12	76 mg/L	CYP3A4 4.57		[81, 88-90]

Theophylline	-0.02 / 1.23	180.1	8.81 (acid)	0.4	7360 mg/L	CYP1A2 0.03 CYP2E1 0.002	Fe 0.25	[91-93]
Tramadol	2.4 / 1.90	263.4	9.41	0.8	0.75 mg/mL	CYP2D6 0.31 CYP3A4 0.03 CYP2B6 0.02		[94, 95]

Lipophilicity (LogP), Molecular weight, pKa and solubility values taken from Drugbank [96].

LogP, specific clearance and Ki parameters were optimized based on plasma concentrations vs. time profiles in adults and used for pediatric model development.

Fraction metabolized values from Zhou et al. were applied [70]. Specific clearance is the internal clearance unit of PK-Sim (Specific clearance = intrinsic CL / (liver volume * fraction intracellular))

Ki: dissociation constant of the enzyme-substrate-inhibitor complex

Fe: Fraction excreted unchanged in urine.

Table 2.2 Clinical study data that were used for PBPK model development and evaluation

Compound	Age Group	Age Mean ± SD [range]	Weight (Kg)	Number of subjects	Administration protocol	Reference
Alfentanil	Adults	28.5 ± 4.8 yr	83.5 ± 11.2	10	IV infusion over 10 min, 15 mg	[97]
	Adults	45 ± 13 yr	59 ± 14	10	IV bolus, 50µg/kg	[98]
	Adults	31.3 ± 3.8 yr	NA	5	IV bolus, 20µg/kg	[99]
	Adults	38.2 [18-62] yr	61.3 ± 8.1	6	IV bolus, 50µg/kg	[76]
	Children	5.4 ± 1.1 yr	21 ± 3	8	IV bolus 20µg/kg	[99]

	Infants	0.73 ± 0.29 yr	6.12 ± 1.48	6	IV bolus 20µg/kg followed by 1µg/kg/min	[100]
	Children	4.05 ± 2.83 yr	15.81 ± 6.85	6	IV bolus 20µg/kg followed by 1µg/kg/min	[100]
	Infants	0.74 ± 0.51 yr	8.08 ± 2.58	7	IV infusion for 0.5 min, 50 µg/kg	[101]
	Children	6.7 ± 4.28 yr	23.58 ± 11.08	6	IV infusion for 0.5 min, 50 µg/kg	[101]
Diclofenac	Adults	[20-22] yr	NA	7	IV, 50mg	[102]
	Adults	≥ 18 yr	NA	22	IV infusion for 30min, 75 mg	[103]
	Children	5.4 ± 0.6 yr	19.6 ±1.1	5	IV infusion for 5 min	[104]
	Children	5.1 ± 1.0	19.8 ± 1.1	5	IV infusion for 15 min	[104]

Esomeprazole	Adults	NA	NA	32	IV infusion over 30 min, PO, 20 or 40mg	[105]
	Adults	[20-39] yr	NA	24	IV infusion over 3 ~30 min, 20 or 40 mg	[106]
	Adults	NA	NA	8	PO 40mg	[80]
	Newborn	1 mo	3 ± 0.6	6	IV, 0.5mg/kg	[107]
	Infants	[1-11] mo	6.1 ± 1.1	6	IV, 1 mg/kg	[107]
	Young Children	[1-5] yr	15.3 ± 5	7	IV, 10 mg	[107]
	Children	[6-11] yr	33.1 ± 9.8	8	IV, 10 mg	[107]
	Children	[6-11] yr	34.4 ± 15.6	8	IV, 20 mg	[107]
	Adolescents	[12-17] yr	57.6 ± 12.1	6	IV, 20 mg	[107]
	Adolescents	[12-17] yr	52.2 ± 4.9	6	IV, 40 mg	[107]
Itraconazole	Adults	43.2 ± 6.7 yr	NA	18	IV infusion over 1 hr, 50, 100, 200 mg	[108]

	Adults	NA	NA	6	IV infusion over 1 hour, 100 mg	[109]
	Infants	[0.7-2.0] yr	9.1	6	IV infusion over 1 hr, 2.5 mg/kg	[110]
	Children	[2.2-5.6] yr	18.2	9	IV infusion over 1 hr, 2.5 mg/kg	[110]
	Children	[8.0-11.0] yr	28.8	7	IV infusion over 1 hr, 2.5 mg/kg	[110]
	Adolescents	[12.3-16.9] yr	55.1	11	IV infusion over 1 hr, 2.5 mg/kg	[110]
Lansoprazole	Adults	[26-48] yr	NA	12	IV infusion over 10 min, 15 mg PO 15 or 30 mg.	[111]
	Adults	[19-53] yr	NA	36	PO 15 or 30 mg	[112]
	Adults	[29-54] yr	NA	12	PO 15 or 30 mg	[113]

	Neonates	[1-19] wk	3.0 ± 0.89	24	PO 0.5, 1.0 mg/kg	[114]
	Infants	[6-54] wk	6.4± 1.5	24	PO 1.0, 2.0 mg/kg	[114]
	Children	[0.21-13.54] yr	NA	18	PO 17 mg/m2	[115]
Midazolam	Adults	[22-27] yr	55-77	6	IV bolus 0.15 mg/kg	[116]
	Adults	[21-22] yr	66-78	6	IV 5mg	[117]
	Young Children	2.5 [1.75-4] yr	14.6 [11-17]	6	IV bolus 0.2mg/kg	[118]
	Infants	[0.5-2] yr	NA	5	IV bolus 0.15 mg/kg	[119]
	Children	[2-12] yr	NA	14	IV bolus 0.15 mg/kg	[119]
	Children	[12-16] yr	NA	2	IV bolus 0.15 mg/kg	[119]
	Children	5.52 ± 1.87 yr	17.3 ±4.43	8	IV bolus 0.15 mg/kg	[120]
Ondansetron	Adults	[20-69] yr	NA	6	IV infusion over 5 min, 8mg	[121]

	Adults	NA	NA	12	IV infusion over 20 min, 24mg	[122]
	Adults	[18-40] yr	NA	16	IV infusion over 15 min, 8mg	[123]
	Infants	[1-24] mo	7.1 a [3.3 - 12]	50	IV infusion over 0.5 min, 0.1 or 0.2 mg/kg	[124]
	Children	[3-7] yr	20.4 a [15.2-26.0]	10	IV infusion over 5min, 2mg	[125]
	Children	[7-11] yr	37.1a [20.3-51.2]	11	IV infusion over 5min, 4mg	[125]
Sufentanil	Adults	[22-64] yr	NA	10	IV bolus 5 µg/kg	[126]
	Adults	58 ± 13.9 yr	NA	10	IV bolus 150 µg	[127]

	Adults	[27-45] yr	NA	6	IV bolus injection 3 µg/kg	[128]
	Infants	5.2 ± 2.1 mo	5.3 ± 1.1	7	IV infusion for 1 min, 15 µg/kg	[129]
	Infants	15.5 ± 5.2 mo	8.9 ± 1.6	6	IV infusion for 1 min, 15 µg/kg	[129]
	Neonates	1 mo	3.2 ± 0.36	9	IV bolus, 10 - 15 µg/kg	[130]
	Infants	[1 – 23] mo	8.7± 3.1	7	IV bolus, 10 - 15 µg/kg	[130]
	Children	[2-11] yr	21 ± 6.71	7	IV bolus, 10 - 15 µg/kg	[130]
	Adolescence	[13-18] yr	58.4 ± 9.50	5	IV bolus, 10 - 15 µg/kg	[130]
	Children	[2 – 9] yr	19.1 ± 5.2	20	IV bolus, 1 – 3 µg/kg	[131]
Theophylline	Adults	[19-35] yr	NA	16	IV infusion over 30min, 4.5 mg/kg	[132]
	Adults	[24-33] yr	NA	12	IV infusion over 8 hours, 506 mg	[133]

	Infants	[3-23] mo	NA	15	IV infusion over 20min, 7mg/kg	[134]
	Infants- Children	[1.3 – 4.4] yr	12.5 ± 2.1	10	IV infusion over 5min, 3.2mg/kg	[135]
	Children	[7-12] yr	NA	8	IV infusion over 5min, 2-4 mg/kg	[136]
Tramadol	Adults	30.1 ± 7.3	71.9 ± 11.8	12	IV infusion over 30 min, 50 mg	[137]
	Adults	[23-40] yr	NA	12	IV infusion over 30 min, 50 mg	[138]
	Infants	[1.1-6.58] yr	13.3 ± 5.2	9	IV bolus, 2mg/kg	[139]

Yr: year, mo: month, wk: week, NA: Not available, IV: intravenous, PO: oral

a median

2.2.2 Model development

The established workflow for development of a pediatric PBPK model is described in Maharaj and Edginton [47] and Maharaj, Barrett [46]. Adult models were first developed based upon compound-specific physicochemical data and in vitro observations such as plasma protein binding and metabolism/excretion. Using observed PK results from clinical studies, key compound-specific parameters that were influential to the PK profile and deemed uncertain, such as lipophilicity (i.e. LogP) and specific clearance, were numerically optimized in PK-Sim (version 7.3). For a better characterization of clearance and distribution, a plasma concentration vs. time profile following a single IV dose was preferably used over PO. When only pediatric PK findings following an oral administration were available, adult IV data was first used for optimization of systemic parameters. Second, an adult PO model was created by adjusting parameters only related to the absorption process (e.g. intestinal permeability and dissolution time). The parameters of adult PO models were used for PK prediction in children following an oral administration. For the prediction of tissue: plasma partition coefficients, a major predictor of distribution, Rodgers and Rowland [140] and Rodgers et al. [141] method was used.

The goodness of fit of adult models were first assessed via visual inspection of superimposing observed and simulated plasma concentration time profiles. The two profiles were compared by examining similarity in maximum concentration (Cmax), time to reach Cmax (for PO), and slope of the curve in the elimination phase. Second, concordance correlation coefficients were calculated [142] to assess an agreement between observed and simulated plasma concentration vs. time profiles in adults.

The drug-specific properties, as defined in the adult model, were directly used in the pediatric models. In these models, the dose and route of administration employed for simulation were similar to the clinical study design as presented in Table 2.2. To simulate the dose-exposure relationship in children, virtual pediatric individuals (n=100) were created by setting the same ranges of age, body weight and height (if available) of the children in the available pediatric clinical studies. When ranges of age, weight and height of a desired population are provided, virtual individuals are created with varying physiological parameters such as organ volumes, blood flows and organ volume fractions of protein, water and lipids based upon the underlying database (e.g. International Commission on

Radiological Protection (ICRP) [143] study [144]. The algorithm for development of virtual populations, as implemented in PK-Sim, is described in principle in Willmann et al. [144]. The age dependence of physiological and anatomical parameters for pediatric individuals is presented in Edginton et al. [45]. For each created virtual individual, PK parameters such as volume of distribution, AUCinf, Cmax, time to reach Cmax (Tmax), Half-life (t1/2) and clearance were output.

In this study, 10 drug-specific PBPK models were developed and several assumptions are listed below.

The clearance pathway(s) was/were the same in both adults and children and the main driver of the metabolism of compounds were CYP enzyme mediated as listed in Table 2.1. In other words, the effect of other possible metabolizing enzymes (e.g. monoamine oxidases) were deemed negligible [145, 146] due to a broad substrate specificity.

The effects of a disease state did not markedly alter PK properties in children. In contrast to adult studies, pediatric investigations are often conducted in pediatric patients, therefore, a disease state might alter the PK properties in children. For example, during infectious disease, inflammation is associated with down-regulation of CYP enzymes [147]. Regardless, the influence of a disease on CYP enzyme mediated metabolism was not taken into account.

Genetic variations (polymorphism) were not taken into account. Due to point mutations or genetic alterations, enzyme functionality varies [148, 149]. In this study, it was assumed that genetic variation was not significant to alter PK properties in either adults or children.

2.2.3 Model qualification strategies

2.2.3.1 Evaluation of predictive performance and model precision

In order to assess the appropriateness of the virtual individual creating algorithm in PK-Sim for predicting PK parameters and their variability in children, 100 virtual individuals with similar ranges of age, weight and height were created and their predicted PK parameters compared to the observed data. The calculated PK parameters and characteristics of virtual individuals including age and body weight were exported from PK-Sim. One-hundred bootstrap replicates [150] using the 100 virtual individuals were created with the same sample size of the clinical study (n = 5 ~12). The calculation

of mean and standard deviation values of bootstrap samples of PK parameters from the virtual population were processed in R [151]. The mean and standard deviation of clearance values of all bootstrap replicates were then compared to those of the observed data and the ratio of predicted CL to observed CL calculated. An example of the comparison of CL between the bootstrap replicates and observed data are presented in Figure 2.1. The mean fold error (MFE) of predicted to observed CL values was calculated for each bootstrap replicate using equation 1:

Eqn. (1) $MFE = \frac{1}{n}\sum_{1}^{n}\frac{pred_i}{obs}$

where predi is a predicted CL value in i-th bootstrap replicate and obs is an observed mean CL value. The mean of bootstrap means is the same as the sample mean. MFE values within a 2-fold error range (i.e. $0.5 \leq MFE \leq 2$) were regarded to be a reasonable prediction.

In a second instance, the % bootstrap replicates with a ratio of mean CL values within 2-fold error of deviation (% within 2-fold) was calculated such that, among 100 comparisons, the number of events that the ratio of mean CL values of each replicate and the observed value was within the range of 0.5 to 2 was counted and expressed as % (For example, predicted mean values within the dotted lines in Figure 2.1).

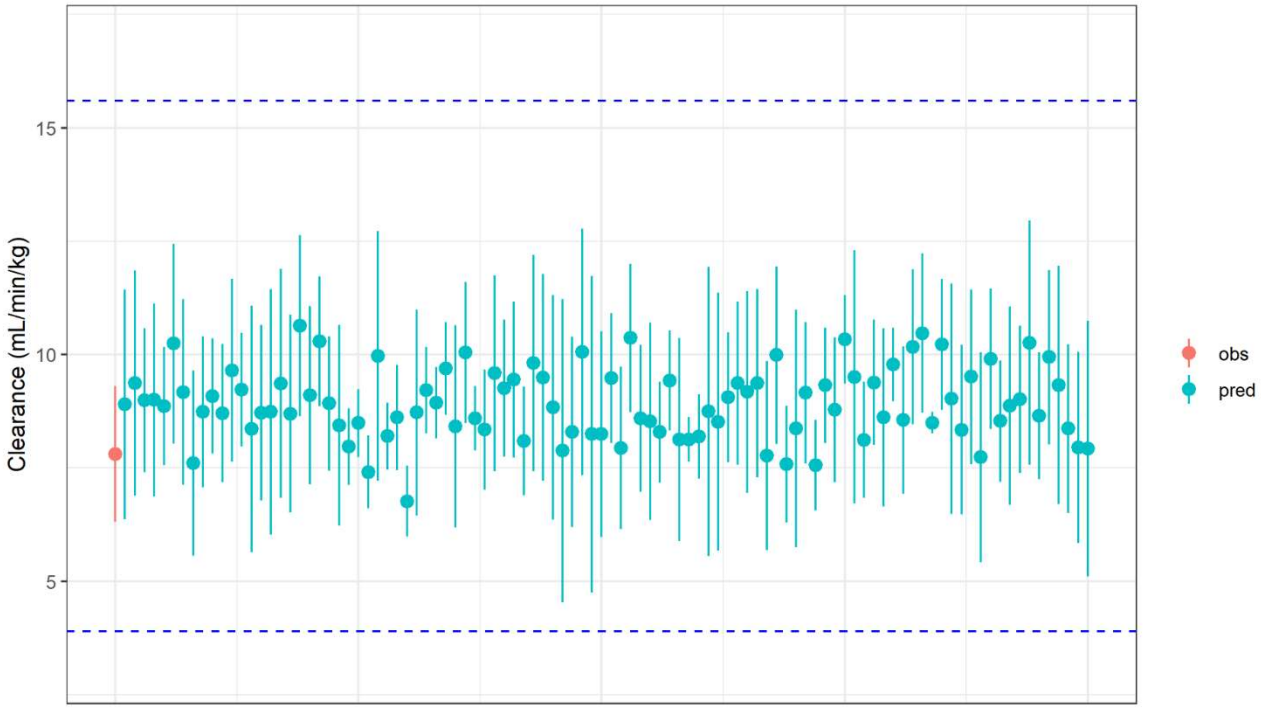

Figure 2.1 An example of a comparison between arithmetic means and SDs of CL values of the observed data and 100 bootstrap replicates. Dots indicate arithmetic means and solid vertical lines represents SDs. The blue dotted lines are the range of 2 fold error of deviation. Diclofenac data was presented. The observed data in children (CL: 7.8 ± 1.5 ml/min/kg) was obtained from Korpela and Olkkola (1990).

Third, as an additional measure to evaluate the predictive performance of pediatric PBPK models in CL prediction, a two sample Student's T-test was performed to compare the mean CL values of the bootstrap replicates to a mean observed CL value from clinical study data. This was assessed if the two populations (i.e. virtual vs. real pediatric individuals) exhibited an equal mean for CL given the same sample size. Among 100 comparisons, the number of events that a mean CL value of each replicate and an observed value were not statistically different at the significance level of α =

0.05 was counted and converted to %. This metric reflects the probability of predicting a reasonable PK parameter value for compounds that are metabolized by CYP enzymes in a certain pediatric age group using PK-Sim. When observed SDs of CL values were unavailable, this analysis was not applicable.

Fourth, in order to assess if the PBPK approach could capture CL variability, the observed (Eqn. 2) and predicted (Eqn. 3) coefficient of variation (CV) was calculated. The median and range of CVpred from the bootstrap was also obtained. When CVobs was within the range of CVpred,i, CL variability was deemed reasonably predicted. This comparison was only applicable in cases where observed mean and standard deviation (or the range of CL values) were available.

Eqn. (2) $CV_{obs} = \frac{standard\ deviation\ of\ observed\ CL\ values}{mean\ of observed\ CL\ values}$

Eqn. (3) $CV_{pred,i} = \frac{standard\ deviation\ of\ predicted\ CL\ values\ in\ \ i^{th}\ bootstrap\ replicate}{mean\ of\ predicted\ CL\ values\ in\ i^{th}\ bootstrap\ replicate}$

2.2.3.2 Critical Parameter Identification [Sensitivity analysis]

In order to identify the most critical parameters for accurately predicting the PK parameters in both pediatric and adult PBPK models, virtual newborn (1-month-old), infant (2-year-old) and adult (30-year-old) individuals were created. A simulation was performed separately for these individuals for each compound with the same administration protocol (1 mg, iv infusion of 5 min). When only PO models were available, the dosing was set at 1 mg and the same formulation setting was maintained as used in the model. The local sensitivity analysis was carried out using PK-Sim. To calculate the sensitivity of a model output of interest, an input parameter was altered ± 10 % [152, 153]. With the altered input parameter, simulation was conducted while all other parameters in the model remained unchanged. The sensitivity of the model output to the varied input parameter was calculated as the ratio of the relative change of that model output and relative variation of the input parameter (Eqn. 4).

Eqn. (4) Sensitivity coefficient (SC) $= \frac{\frac{\Delta PK\ parameter}{PK\ parameter}}{\frac{\Delta input\ parameter}{input\ parameter}}$

The input parameters were ranked based upon the resulting sensitivity coefficient values. Critical input parameters were identified by following criteria:

(i) parameters with SC values higher than 0.45 in newborn, infant and adult models were considered critical for PK parameter of interest for the compound.

(ii) parameters that were differentially sensitive with respect to age were identified by comparing the sensitivity coefficient values of infant or newborn to that of an adult (i.e. the sensitivity coefficient of a newborn or an infant is 30% higher than that of an adult).

The outcome of this analysis provided an understanding of the most critical and/or age-sensitive model parameters for the simulated compounds.

2.2.3.3 Evaluation of characteristics of virtual pediatric individuals

Ten thousand virtual pediatric individuals aged between 0 and 18 years (only criteria used) were created and based upon the ICRP [143] population. The mean and standard deviation of weight, height and age of children in the clinical studies were obtained as listed in Table 2.2 and compared to the virtual population. The observed data for liver volume in children were taken from Johnson et al. [154]. A visual inspection was performed to compare the observed liver volume in children and simulated values in virtual individuals.

2.3 Results

2.3.1 Predictive performance of pediatric PBPK models

Pediatric PBPK models were developed for 10 compounds that are primarily metabolized by CYP enzymes. These models were based upon an adult PBPK model for each compound (Supplemental Material Figure S1). The obtained input data from literature and optimized parameters from the adult model development process are summarized in Table 2.1. The goodness of fit was assessed based on graphical comparison between observed and simulated PK profiles. In addition, the simulated plasma

concentration vs. time profiles in adults were in a good agreement with the observed data with concordance correlation coefficients ranging from 0.75 to 0.98 (Supplementary Material Table S2).

The predictive performance of the models was determined by comparing the model output (i.e. CL) to the observed data from pediatric clinical investigations (Table 2.2). The calculated metrics (e.g. MFE, % within 2-fold error of deviation) for assessing the performance of pediatric PBPK models with respect to age groups are summarized in Table 2.3. Overall, 81% of 43 comparisons between simulated and observed CL were within 2-fold error of deviation and 56% of 40 comparisons of predicted vs. observed mean CL were not markedly different according to the Student's T-test at the significance level of α=0.05.

Table 2.3 Predictive performances of pediatric PBPK models

Compound	**Age Group**	**Mean Fold error (MFE)**	**% Within 2 fold error**	**% Equal means via T-test (α =0.05)**
Alfentanil	Infants	0.6	78	30
Alfentanil	Children	1	99	74
Diclofenac	Children	1.2	100	90
Esomeprazole	Neonates	1.7	87	67
Esomeprazole	Infants	1.1	100	100
Esomeprazole	Children	1.8	54.7	47.7
Esomeprazole	Adolescents	1.6	95.5	22

Itraconazole	Infants	0.4	10	4
Itraconazole	Children	0.5	61.5	69.5
Itraconazole	Adolescents	0.3	0	0
Lansoprazole	Neonates	2.4	9.5	5.5
Lansoprazole	Infants	0.6	68	47.7
Lansoprazole	Children	0.8	100	66
Midazolam	Infants	0.6	95	100
Midazolam	Children	0.8	99.5	85.5
Ondansetron	Infants	0.7	100	N/A
Ondansetron	Children	1.2	100	N/A
Sufentanil	Neonates	0.7	100	100
Sufentanil	Infants	0.7	72	43
Sufentanil	Children	0.8	100	32.7
Sufentanil	Adolescents	0.9	100	100
Theophylline	Infants	1	100	99
Theophylline	Children	0.7	100	58
Tramadol	Children	1.6	95	26

N/A: Not applicable as observed standard deviation values were not available.

To assess predictive accuracy as a function of age group, studies were sub-divided. In this investigation, observed CL data from 4 groups of adolescents, 23 groups of children, 12 groups of infants, 4 groups of neonates were compared to simulated CL values (Figure 2.2). The mean fold error of deviation by age group was 1.1, 1, 0.7 and 1.8 in adolescents, children, infants and neonates, respectively (Figure 2.3). Overall, pediatric PBPK models constructed in PK-Sim resulted in CL values within 2-fold error of deviation for adolescents, children and infants, with a few exceptions. In the case of alfentanil, diclofenac, midazolam, sufentanil, ondansetron, theophylline and tramadol, pediatric PBPK models reasonably predicted CL values with MFE within 2 fold error and % within 2-fold error higher than 70% (Table 2.3). Notably, % equal means were lower than % within 2-fold error in most cases. The MFE values are categorized by primary CYP enzyme and presented in Figure 2.4. For the compounds that are metabolized by CYP 1A2, 2D6, 2C8, 2C9 and 3A4, the clearance values were in concordance with the observed data with MFE values within the 2-fold range. The compounds that are metabolized by CYP2C19 and CYP3A4 showed high variability in terms of CL prediction accuracy.

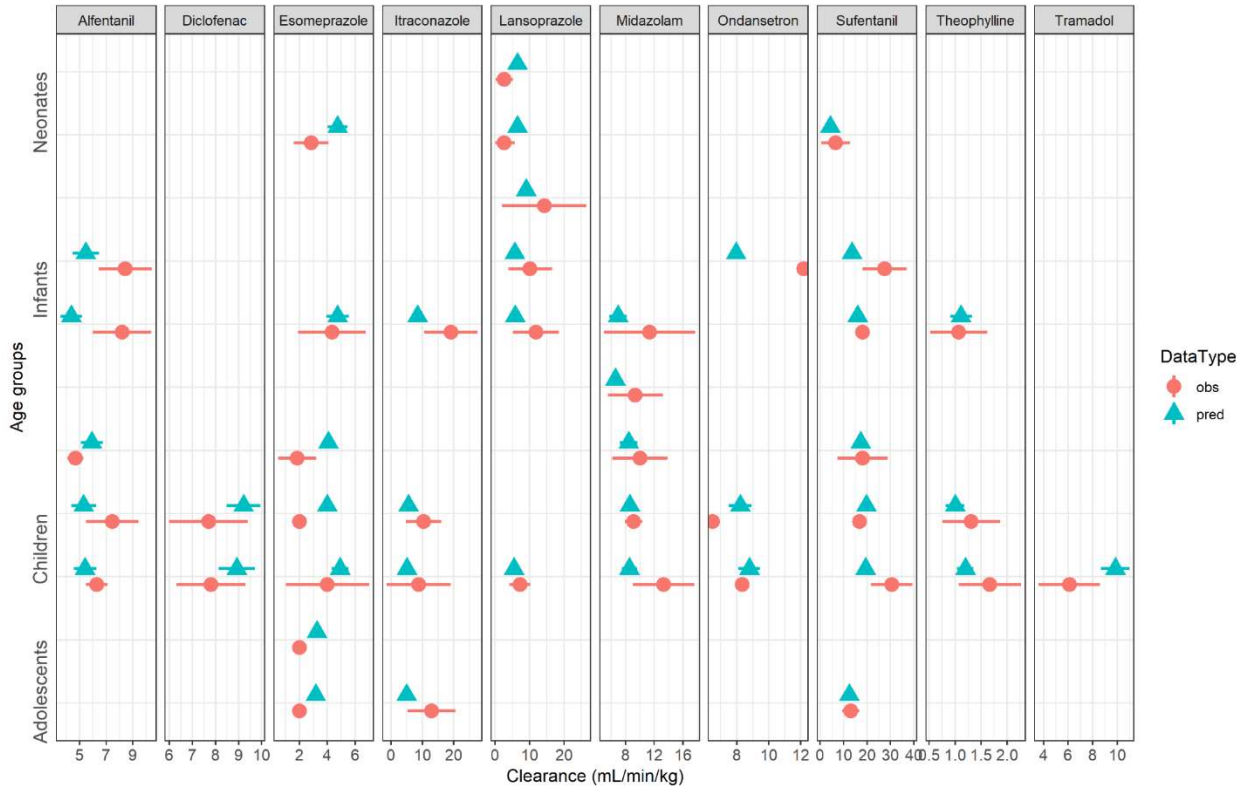

Figure 2.2 Comparison between predicted CL values from virtual pediatric individuals and observed data from clinical studies. The symbols represent means and the lines are standard deviations.

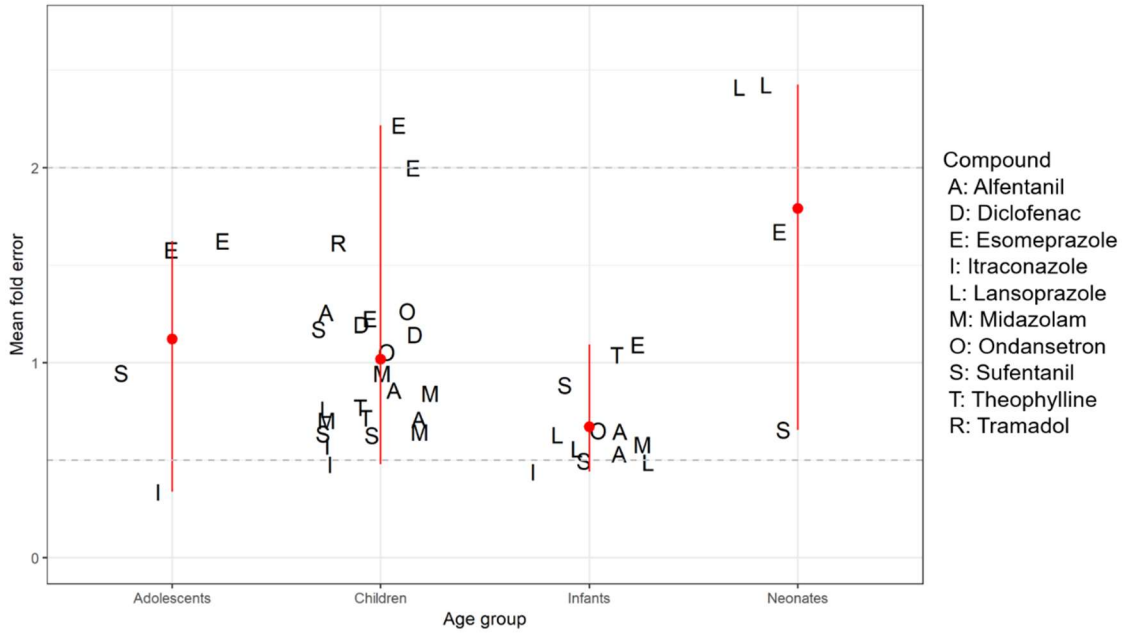

Figure 2.3 Mean fold error (MFE) for clearance in different age groups. Each black letter is a MFE value that indicates a comparison of CL between a pediatric study as defined in Table 2.2 and a virtual study created in PK-Sim. The red dot is the mean of the MFE values in each age group and the red line is the range. The grey horizontal line shows the range of a 2-fold error.

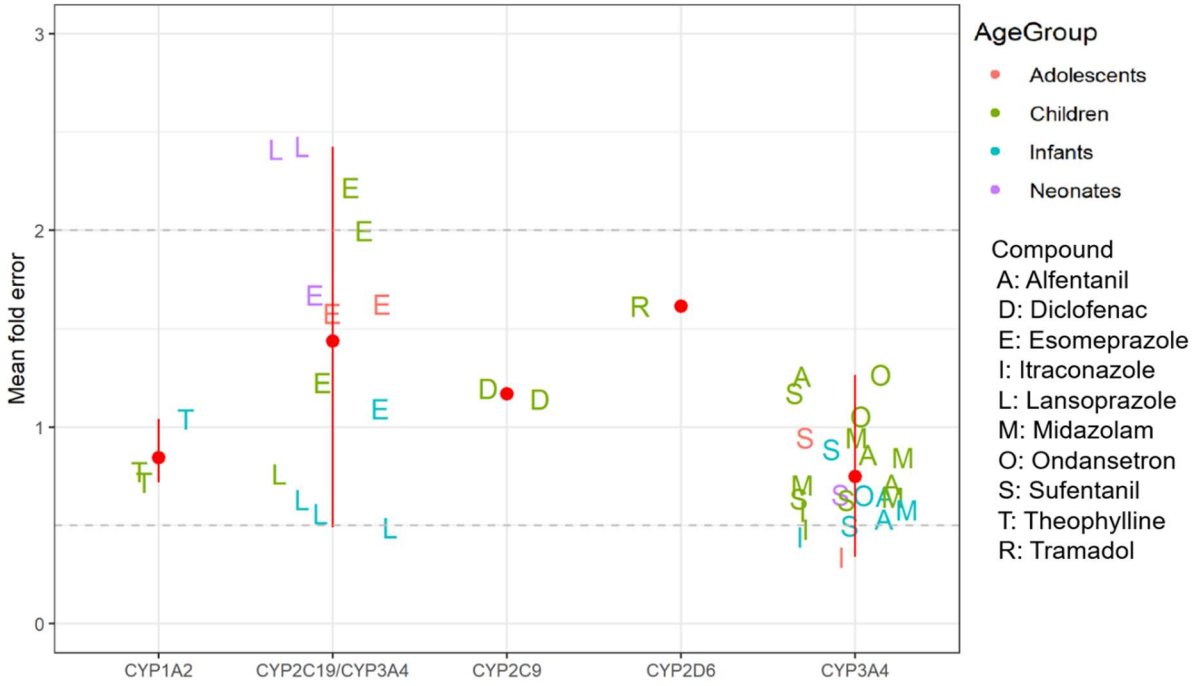

Figure 2.4 Mean fold error (MFE) for clearance stratified by the major metabolizing CYP enzyme. Each colored letter is a MFE value that indicates a comparison of CL between a pediatric study as defined in Table 2.2 and a virtual study created in PK-Sim. The MFE value was labeled with different color and letters such that pink letters are adolescents, green letters are children, blue letters are infants, and purple letters are neonates. The red symbols are the mean of the MFE values in each group and the red line is the range. The grey horizontal line shows the range of a 2-fold error.

A comparison between observed and predicted CL variabilities is presented in Figure 2.5. Observed standard deviations of CL values were not available for ondansetron. For 28 of 40 (70%) comparisons, CVobs was within the range of CVpred. For 11 out of 40 comparisons, CVobs was larger than CVpred and for 1 out of 40 comparisons, CL variability was over-estimated when compared to observed CL variability.

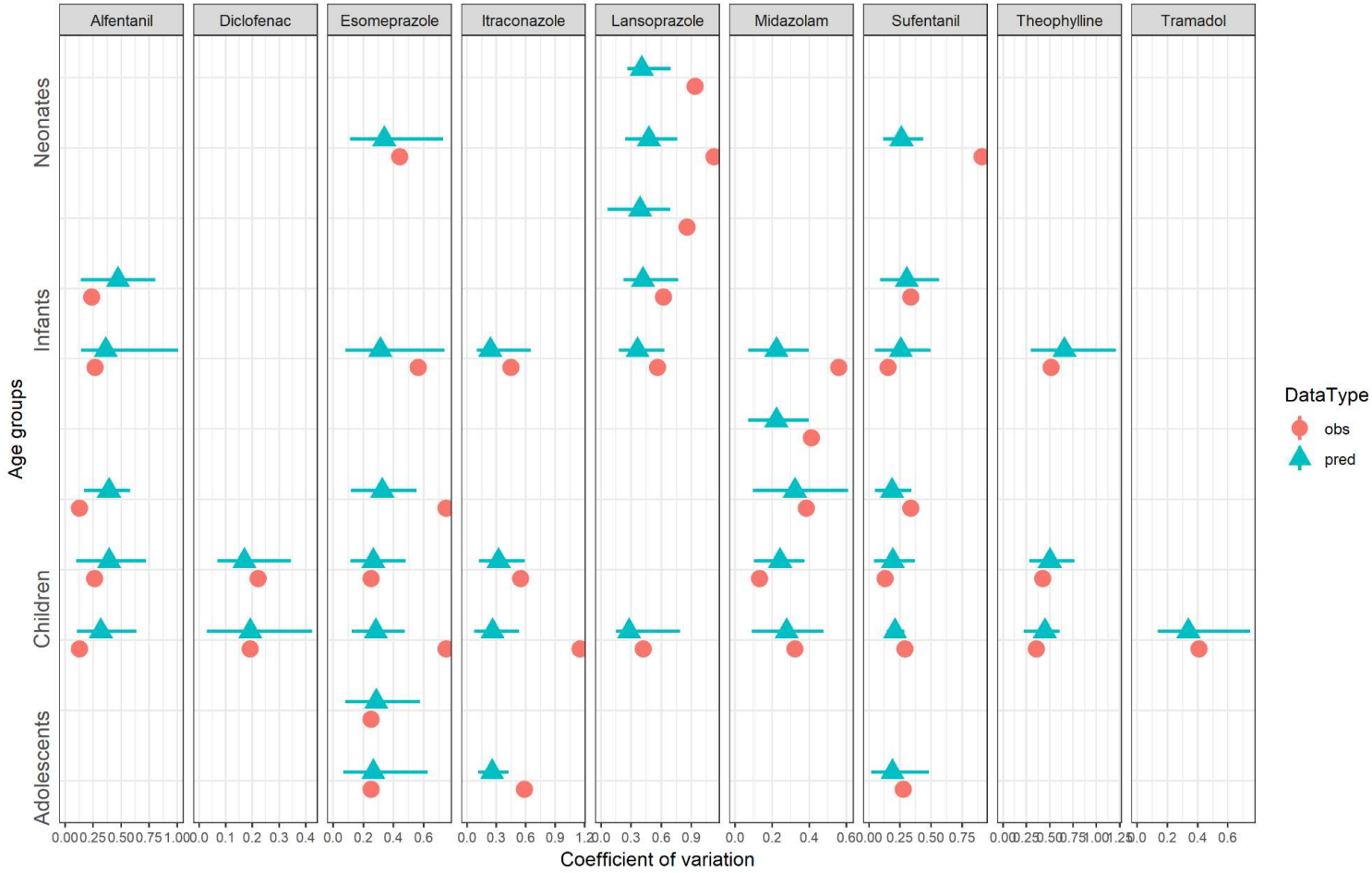
Alfentanil
Diclofenac
Esomeprazole
Itraconazole
Lansoprazole
Midazolam
Sufentanil
Theophylline
Tramadol
Neonates
Infants
Children
Adolescents
Age groups
Coefficient of variation
DataType
obs
pred

Figure 2.5 Age and drug-specific coefficients of variation for CL. The symbols represent observed (circles) and predicted (triangles) coefficients of variation. The lines are the range of CV values from the bootstrap samples of virtual individuals and the triangle is the median CV.

2.3.2 Sensitivity analysis

The sensitivity analysis was performed for all constant input parameters (i.e. not derived by equations such as tissue: plasma partition coefficients). The focus of this analysis was to evaluate the sensitivity of the area under the plasma concentration vs. time profile from 0 to infinity (AUCinf) to model parameters (Appendix 1). AUCinf is the critical exposure metric.

Parameters with high sensitivity coefficients in all age groups (absolute SC $\geq$ 0.45)

In terms of AUCinf prediction, the most important parameters were fraction unbound in plasma and liver volume. Further important inputs also related to CYP enzyme mediated metabolism-related parameters such as specific clearance, reference concentration, and relative expression in the liver in the midazolam model.

2.3.3 Age sensitive parameters

For alfentanil, sufentanil, lansoprazole, ondansetron and theophylline, CYP enzyme mediated metabolism-related parameters showed age-dependent importance in terms of AUC prediction. For alfentanil and sufentanil, CYP 3A4 metabolism-related parameters such as specific clearance, reference concentration, and relative expression in the liver were more influential in a newborn with higher absolute sensitivity coefficients when compared to those in an infant and adult.

For lansoprazole (metabolized by CYP2C19 and CYP3A4), CYP2C19 metabolism-related parameters such as specific clearance, reference concentration, and relative expression in the liver exhibited higher absolute sensitivity coefficients in a newborn compared to those in an infant and an adult.

For ondansetron and theophylline, lower absolute sensitivity coefficients for CYP1A2 related parameters and higher absolute sensitivity coefficients for kidney volume and glomerular filtration rate (GFR) fraction were observed in a newborn.

2.3.4 Evaluation of characteristics of virtual pediatric individuals

Figure 2.6 presents a comparison between weight, height and liver volume of the virtual population compared to children participating in each clinical study. The weight-for-age and height-for-age relationships were in a reliable agreement with the pediatric patient data whose clearance

values were employed in assessing predictive performance of PK-Sim (Table 2.2). The liver volume values of virtual individuals in relation to age were also in agreement with the observed data [154].

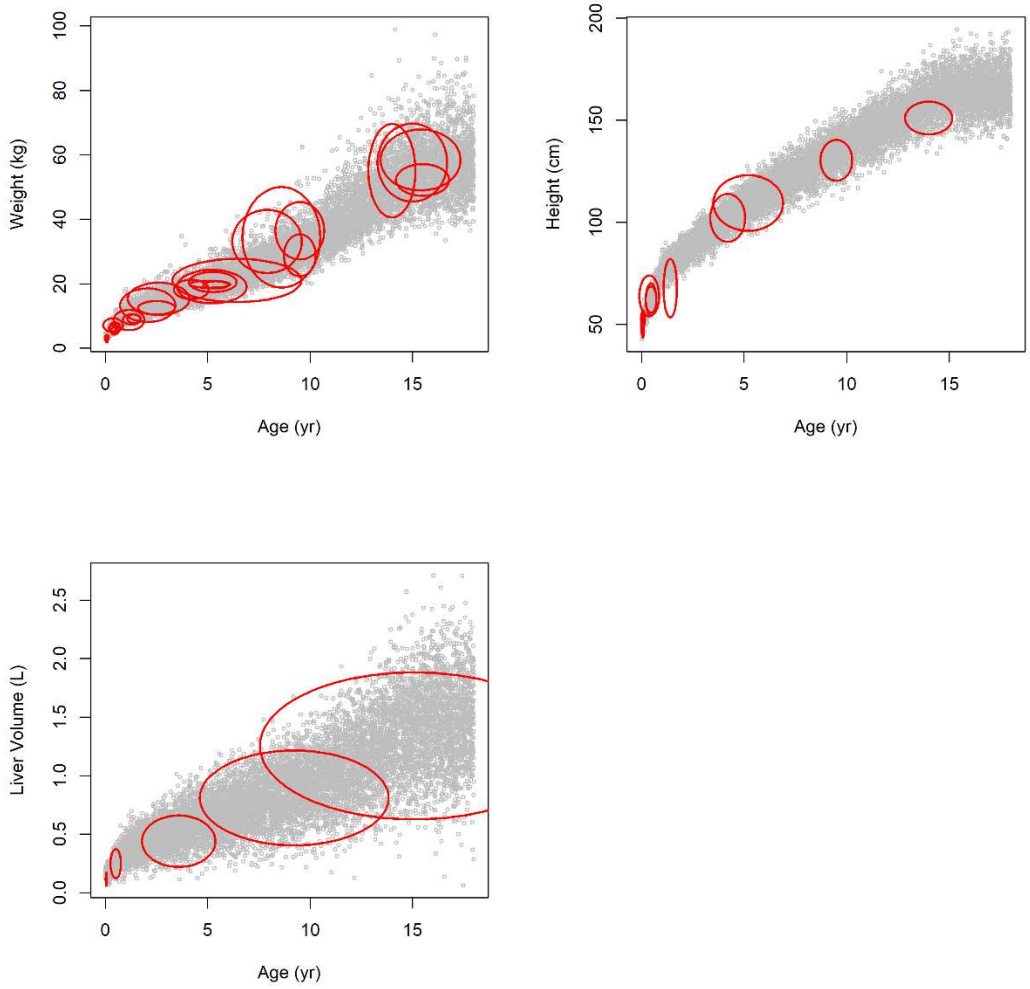

Figure 2.6 Visual comparisons of (a) weight, (b) height and (c) the liver volume in relation to age between the virtual pediatric individuals (n=10,000) and observed data. Grey dots are virtual individual data. The ellipses represent the observed means and standard deviations of the x and y variables. For example, in the case of (a), the center of an ellipse is the mean of weight and the mean of age of observed data. The halves of vertical and horizontal widths of an ellipse are standard deviations of weight and age of observed data, respectively.

In addition, input parameters that may contribute to inter-individual variability to CL in the virtual population were illustrated in Figure 2.7. Examples of input parameters of PK-Sim virtual pediatric population in an anthropometric level such as body mass index (BMI) (A), physiologic and anatomical level (B-C) such as liver volume and liver blood flow and biochemical level such as ontogeny of plasma proteins (D-E) and CYP enzyme (F) are presented. The sources of CL variability are summarized in Table 2.4.

Table 2.4 Sources of CL variabilities in a virtual pediatric population

	Parameter	**Is this critical parameter according to the sensitivity analysis?**	**Is this parameter varied in a virtual pediatric population?**
1st tier: anthropometric variabilities	Weight	N/A	✓
	Height	N/A	✓
	Body mass index (BMI)	N/A	✓
2nd tier: anatomic and physiologic parameters	Organ weight		✓
	Cardiac output		✓
	Organ volume	✓	✓
	Organ blood flow rate		✓
3rd tier: biochemical parameters	Intrinsic clearance per gram tissue weight	✓	✓
	Relative expression level of a metabolizing enzyme in liver	✓	
	Ontogeny of metabolizing enzymes (e.g. CYP, UGT)		✓

	Ontogeny of plasma proteins (e.g. albumin, alpha-acid glycoproteins)	✓	✓
	Reference concentration of metabolizing enzymes	✓	

N/A = not applicable as these define the 2nd tier parameters

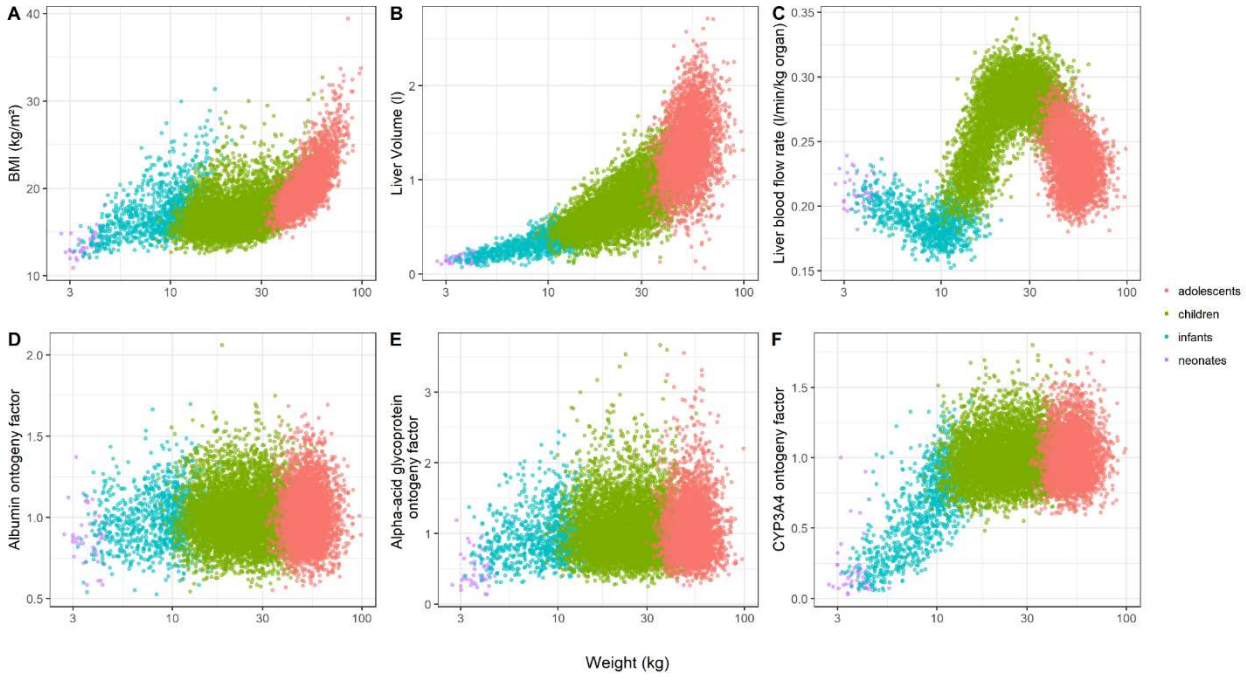

Figure 2.7 Visualization of example parameters that contribute to CL variabilities in virtual pediatric population created by PK-Sim (age 0 to 18, n=10,000) As an example of anthropometric characteristics, BMI was shown in (A). Examples anatomic and physiologic parameters such as liver volume and liver blood flow were presented in (B) and (C),

respectively. Biochemical parameters such as ontogeny factors of plasma proteins and a CYP enzyme were presented in (D) to (F).

2.4 Discussion

Chemical specific adjustment factors (CSAF) are determined to protect a susceptible population in human risk assessment [6, 155]. As compound-specific data are taken into account in the derivation of CSAF, these results are more evidence based than empirically derived default UF [9, 155-157]. Further, CSAF are context specific in that these factors can be determined as a function of exposure duration (e.g. acute, chronic), route (e.g. inhalation or oral) [158] and relevant dose metrics (e.g. Cmax, AUC or CL). Despite the superior characteristics of CSAF over UF, PBPK-derived-CSAF are not adopted in many cases by regulatory agencies mainly due to the lack of human data to support the model quality [6, 159]. Model qualification of PBPK models might improve reliability in model results by (1) clarifying model adequacy for an intended purpose, (2) identifying critical factors and (3) evaluating characteristics of virtual individuals.

Model qualification can be performed for types of compounds that undergo the same elimination pathway [67]. In this study, compounds that are primarily metabolized by CYP enzymes were selected. CYP enzymes are responsible for metabolizing exogenous compounds such as environmental toxicants as well as therapeutic compounds. As human TK data are limited, pharmaceutical data were utilized to determine the predictive performance and model adequacy of adult-to-children PK extrapolation using a PBPK modeling approach. This assessment is specific to the evaluation of the way virtual children are defined and, because an 'optimal' adult model was initially employed where chemical-specific inputs were used and assessed, this evaluation may not be used to assess the validity of experimental, in vitro chemical-specific inputs. In summary, this determination isolates one component of the PBPK modeling process in HHRA, that of virtual children development for the most important CYPs.

The accurate prediction of PK in pediatric individuals is dependent upon [17]:

Model structure: the series of equations that describe mass transfer of drug from one compartment to another in a physiologically relevant manner

Model parameterization: anatomical, physiological and biochemical parameter values relevant for the modelled organism (e.g. adult, children)

Because the model first assessed adults, it was assumed that item (i) above is a reasonable representation of reality and therefore there was focus on item (ii). Since all parameters (i.e. anatomical, physiological, biochemical) affect PK outcomes in an integrated manner, evaluation of virtual children depended upon comparison of predicted to observed PK outcomes in children. As concentration-time profiles in children are often not available, model adequacy was determined by comparing the most important exposure metric, CL, to the observed data. Clearance is one of the most important PK parameters with respect to both drug development for safety and optimal dosing and HHRA for estimating differential dosimetry of chemicals.

The sample size of pediatric clinical investigations is relatively small (n<30) (e.g. Table 2.2, Number of subjects). For a more fair comparison, a bootstrap sampling method [150] was adopted. Among the comparisons between predicted and observed mean CL values with clinical study data, 81% of 43 comparisons were within 2-fold error of deviation and 56% of 40 comparisons resulted in equal means. A 2-fold error was considered a reasonable prediction according to the WHO/IPCS guideline [6, 17]. With respect to CL variability, 70% of observed CL CVs were well described by the models with bias towards underprediction in the additional 30%. Underprediction of variability is somewhat expected in PBPK outcomes as protocol aberrations (e.g. vomiting after oral dosing), experimental (e.g. sample timing not at nominal times but recorded as such) and assay imprecision are not included [160]

An over prediction of lansoprazole CL/F in neonates was observed (metabolized by both CYP2C19 and CYP3A4) with a 2.4 -fold error (Figure 2.3-2.4). This may be due to the lack of a model component that explains potential disease effects on absorption. In the comparative study [114], CL/F was determined in neonates with gastroesophageal reflux disease (GERD). It is speculated that a significantly lower level of CL/F in neonates compared to older children may be due to disease effects such as varying stomach pH in newborn patients with GERD [114, 161]. Disease effects may affect bioavailability (F) and, therefore, exert influence on CL/F. In the case of another proton pump inhibitor agent, esomeprazole (metabolized by CYP2C19 and CYP3A4), following iv administration in neonates with GERD, PBPK-predicted CL was within 2-fold of

observed values (MFE = 1.7). Considering the CL predictions of compounds that are primarily metabolized by CYP3A4 were fairly reasonable (Figure 2.4), and CL prediction of those with CYP2C19 metabolism were also within 2-fold, the weight placed on lansoprazole to detect potential CYP2C19 ontogeny misspecification in neonates is limited; especially when masked by bioavailability.

For itraconazole, an underprediction of CL in adolescents (age 12.3 - 16.9 years) was observed with an MFE value of 0.33 (Figure 2.3 and 2.4). The observed weight-normalized CL in this cohort of 12.95 ml/min/kg was 2.5 higher than the reported adult CL value of 5.1 ml/min/kg [109] following iv administration, which is not unique to this adult study. It is expected that the weight-normalized CL is equivalent between adolescents and adults as maturation is complete [162, 163] and size is similar to adults. The PBPK-predicted CL value in adolescents was 4.38 ml/min/kg, which was similar to the reported adult value. In other pediatric clinical investigation [164], itraconazole CL in a group including children and adolescents (age 9.5 – 14.4 years) was approximately 2.2 ml/min/kg (3.8 ± 1.6 L/hr). Values indicate a high inter-individual variability or inter-study variability. Isoherranen, Kunze [165] suggested that this is probably due to complex PK behavior of this drug with inhibition effects of both parent and metabolite molecules on the metabolizing enzyme CYP3A4. The PK-Sim under-prediction of CL noted by Abdel-Rahman, Jacobs [110] was maintained in the assessment for transparency although it is clear that a virtual population of adolescents may not be able to recapitulate this study based upon the adult base model.

Identifying those input parameters, within the PBPK structure, that are important to PK outcomes enables us to decide where resources need to be directed in pursuit of having high confidence in PBPK model outcomes. Within this pediatric PBPK system, input parameters that were deemed, based upon sensitivity coefficient cut-offs, to markedly influence CL prediction for hepatic CYP enzyme-metabolized compounds, and therefore the exposure metric of AUC, were CYP enzyme reference concentration, CYP intrinsic clearance, CYP protein relative expression in the liver, CYP enzyme ontogeny, protein binding (fraction unbound in plasma), plasma protein ontogeny (e.g. ontogeny factor for albumin or alpha acid glycoprotein), liver volume and liver blood flow. Depending upon the molecule, factors that relate to the blood-to-plasma ratio related parameters such as red blood cell pH were also important.

With respect to CYP enzyme-mediated clearance, within the model structure assuming linear processes, hepatic intrinsic clearance (CLH) is calculated by the following equation.

Eqn. (5) $\mathrm{CLH} = \sum_1^n \mathrm{CL}_{spec,i} \cdot [\mathrm{CYP}]_{\mathrm{ref,i}} \cdot \text{relative expression}_{\mathrm{i}} \cdot \text{ontogeny factor}_{\mathrm{i}} \cdot f_{\text{intracellular}} \cdot \text{Liver volume} (\cdot \mathrm{fm_i})$

CLspec is specific clearance which is the internal clearance unit in PK-Sim (min-1) and n denotes the number of CYP enzymes if multiple enzymes were involved. [CYP]ref is a reference concentration of a CYP enzyme in liver (µmol CYP/L liver tissue) in an adult and relative expression is a parameter to account for the protein expression in an organ relative to the expression in the organ with the highest concentration of the enzyme (for example, the relative concentration of CYP3A4 in the liver is 100%). fintracellular is a fraction of intracellular space in liver. CYP enzyme ontogeny factors in PK-Sim are based upon age-specific enzyme activity [44, 166]. From equation 5, it is noted that the critical inputs to define CL are all multiplied in the equation which indicates that all are individually important.

As defined from the sensitivity analysis, unbound fraction in plasma was a key input parameter. This is the case especially for compounds with a low to moderate extraction ratio where, according to the venous equilibrium model (or well stirred model) [25, 167, 168], a hepatic extraction ratio (EH) can be expressed as.

Eqn (6) $E_H = \frac{fu_b CL_{Int}}{Q_H + fu_b\, CL_{Int}}$

QH: hepatic blood flow, CLInt: intrinsic clearance and fub: fraction unbound in blood where,

$Eqn\ (7)\ fu_b = \frac{fu_p C_p}{C_b} = \frac{fu_p}{B:P}$

fup: fraction unbound in plasma, Cp: concentration in plasma, Cb: concentration in blood, B:P: blood-to-plasma ratio.

For low EH compounds, hepatic clearance approximates fub · CLint. This was corroborated with the sensitivity analysis results such that for low extraction ratio compounds in liver (e.g.

lansoprazole [169]) fup resulted in a high absolute SC value whereas a compound with a high hepatic extraction ratio (e.g. sufentanil [170]), fup was not a critical parameter.

The sensitivity of CL-related parameters is predicted to be a function of age in some, but not all cases (Appendix 1). Parameters that exhibited age-dependent importance in CL predictions were CYP enzyme metabolism-related parameters. When there are multiple processes involved (e.g. a compound metabolized by multiple CYP enzymes), the sensitivity of each process was dependent on (i) importance of each process to the total clearance (e.g. fraction metabolized) and (ii) its maturation profile (e.g. ontogeny of a CYP enzyme). The importance of each process is proportional to its fraction metabolized value. For instance, in adults, lansoprazole is metabolized by both CYP2C19 (fm: 70%) and CYP3A4 (fm: 30%)[70] and absolute sensitivity coefficient values of CYP2C19 related parameters were higher than those of CYP3A4 related parameters.

Age-dependent sensitivity was noted when ontogeny was a rate-limiting process. For example, with theophylline, lower absolute sensitivity coefficients in CYP related parameters and higher absolute SC values in renal clearance related parameters were observed in a 1-month-old virtual individual as compared to the adult. This was the result of a low concentration of CYP1A2 as compared to adults, with a higher subsequent reliance on renal rather than hepatic clearance. CYP1A2 is one of slowest maturing enzymes [171]. The sensitivity analysis finding is in agreement with the reported observations of an inability to metabolize CYP1A2 substrates such as caffeine in young children [172, 173]).

From a HHRA perspective, it is necessary to capture inter-individual variability in PK/TK for a group of pediatric individuals. CSAFs are defined by using the upper (e.g. 95th) percentiles of PK parameters [13] and these might be derived through development of virtual individuals. When creating virtual pediatric populations, one needs to (i) account for growth and maturation of relevant parameters and (ii) incorporate reasonable inter-individual variability in anatomical and physiological inputs.

For a virtual pediatric population created using PK-Sim, inter-individual variability in clearance is introduced at three different levels (Table 2.4). The first tier is variability in anthropometric input of weight and height. In this study, virtual children were created by setting the same range of age, height and weight as in the clinical study design. In a HHRA scenario, the virtual

population is most likely to be created by setting only the age range of the population of interest such as age 1 month to 2 years for infants with or without restricting height, weight or BMI ranges. When only the age range was input to create virtual individuals, there was reasonable concordance between observed (Table 2.2) and simulated weights and heights confirming that these were reasonably assigned for virtual children. BMI is a function of weight and height. Data also showed that BMI of virtual individuals were in a reliable agreement with World Health Organization (e.g. 3rd to 97th percentiles of a 2-year-old-boy: 11.3 – 16.1 kg/m2, 3rd to 97th percentiles of a 18-year-old boy: 17.3 – 28.4 kg/m2) growth charts [174, 175]. Weight is important in that this parameter defines absolute dose in clinical settings and in HHRA, the TDI is expressed as a weight normalized value [2] (e.g. TDI for bisphenol A is 0.05 mg /kg body water [176]).

The second tier of deriving CL variability originates from anatomic and physiologic parameters such as organ volume and organ blood flow rate, which are predominantly dependent upon first tier variabilities but display additional variability assigned to ensure that not every virtual person with the same height and weight possess the equal organ weights and blood flows. The appropriate assignment of primarily height but also weight leads to parametrization of eliminating organ weight and their associated blood flow rates using scaling methods of Willmann et al. [144]. Liver volume, being a critical input identified in the sensitivity analysis, appears well defined in PK-Sim (Figure 2.6).

The third tier is the variabilities in biochemical inputs such as the ontogeny of metabolizing enzymes including CYP or uridine 5'-diphospho-glucuronosyltransferase (UGT) and the variability in organ enzyme concentrations and plasma protein levels including albumin and alpha-acid glycoprotein (AAG). Variability resulting from ontogeny and enzyme concentration are combined in PK-Sim where one function, with associated variability, is used to define both of these components since variability in enzyme concentration cannot be uniquely identified from varying rates of maturation [166]. Based upon Figure 2.1 and Figure 2.5, CL variability was reasonably predicted although, as illustrated in Figure 2.1, variability in the context of a small number of participants is heavily dependent upon which children are selected.

PK-Sim is an open-source software within the Open Systems Pharmacology Suite (open-systems-pharmacology.com) and is actively developed, moderated and versioned with use in the

pharmaceutical industry for regulatory filings. One of advantages of using PK-Sim is in its flexibility to incorporate the latest information. T'Jollyn et al. [177] derived an ontogeny profile for CYP2B6 from experimental data of Pearce et al. [178] and incorporated this user-defined CYP2B6 maturation profile into their pediatric PBPK model for tramadol. T'Jollyn et al. [177] compared the predictive accuracy with other commercially available PBPK platforms and found that PK-Sim resulted in the best predictive performance across ages; not solely a function of ontogeny but also anatomical and physiology inputs. As data are generated from various groups, once verified, may be implemented in an official PK-Sim version. Feedback from the community that revolves around an open forum in GitHub is already a place for open science and collaboration in this space.

2.5 Conclusion

The objective of this investigation was to assess the virtual population generation algorithm for children in PK-Sim. To isolate this, rich data were used from adults to define chemical-specific inputs and assessed, assuming accurate chemical-specific inputs, as to what is the accuracy of exposure predictions when utilizing PK-Sim to create virtual children. Of course, in HHRA, this scenario is not possible as PK data in adults and the plethora of in vitro observations to generate mechanistic understanding of drug ADME are usually not available. However, this is a necessary component to define which workflow steps in development of a pediatric PBPK model are most prone to error and therefore in greatest need of refinement. In conclusion, adequate estimation of systems-specific parameters based on age will increase the confidence in the use of PK-Sim to create virtual pediatric populations and to perform PK/TK predictions in children for human health risk assessment.

Chapter 3: Evaluation of Quantitative Structure Property Relationship Algorithms for Predicting Plasma Protein Binding in Humans

3.1 Introduction

Many endogenous and exogenous substances reversibly bind to plasma proteins such as albumin, alpha1-acid glycoprotein (AAG) and lipoproteins. The extent of binding, often expressed as a fraction unbound in plasma (fup), is a function of protein concentration and protein binding affinity as well as, to a lesser degree, a displacement by other molecules [179]. The extent of plasma protein binding is an important compound-specific property as it affects a compound's distribution, metabolism and elimination processes. Therefore, the characterization of protein binding is critical to the prediction of the pharmacokinetics (PK) of a compound and essential within a physiologically-based toxicokinetic (PBTK) modeling framework [180] to the estimation of human exposure to environmental toxicants.

Experimental determination of fraction unbound in plasma can be done by, for example, ultrafiltration or equilibrium dialysis methods [181-184]. When experimentally determined protein binding information is not available, in silico methods, such as predictive quantitative structure-property relationship (QSPR) modeling, can be used. QSPR models identify relationships between chemical structure and a chemical property, such as the degree of protein binding in plasma [185]. Chemical descriptors that capture structural properties and characteristics of compounds are used as predictors, while protein binding information is used as a response variable. The learned relationship between protein binding and chemical descriptors can provide an estimation of a fup for a new compound.

In one of the recently developed QSPR models, Ingle et al. [186] included both pharmaceutical and environmentally relevant compounds (ERC) in their training and test sets. For the pharmaceuticals, previously curated data from the literature [187-190] was included. In terms of ERCs, experimentally derived protein binding data of ToxCast compounds from Wetmore et al. [191, 192] were included and used as a test set. The data from ToxCast, implemented by the US Environmental Protection Agency (EPA), included in vitro assessment of fup for pesticides, food additives, consumer products, and industrial products [193]. Molecular Operating Environment (MOE, Chemical Computing group) was used to calculate the input chemical descriptors. To construct a predictive model, several machine

learning techniques such as k-nearest neighbours, support vector machines and random forest were employed. A consensus model resulted in the best predictive performance with mean absolute error (MAE) values of 0.15 and 0.11 for pharmaceuticals and ERCs, respectively.

Watanabe et al. [194] developed two kinds of predictive models using machine learning techniques. For the first model, a classification function was used to predict whether a new compound will have high or low protein binding separated by a fup value of 0.05 for binary classifiers (i.e. high or low) and by fup values of 0.05 and 0.2 for three-class (i.e. high, moderate and low) classifiers. For the second model, a regression function of machine learning methods was used to predict fup. For chemical descriptors, Mordred [195] and Padel [196] programs were used. The training set included 2192 compounds from the ChEMBL [197] and PharmaPendium [198] databases. The test set included 546 compounds from KEGG DRUG [199-201]. The classifier resulted in a true positive rate of 0.83 for the low fup class. Predictive performance was compared with the results of the S+PrUnbnd model from ADMET Predictor 8.1 (Simulation Plus, Inc.). The Watanabe et al. [194] model (MAE: 0.32) resulted in higher predictive accuracy as compared to the S+PrUnbnd model (MAE: 0.43) [194]. The online calculator provides both a fup estimate based on the regression algorithm and a compound's degree of binding classification based on the multi-state classifier.

The predictive performances of different QSPR models have been evaluated using a relatively small set of data, not fully encompassing the structural diversity of compounds. The QSPR models have not been evaluated with the same dataset. Therefore, the prediction accuracy that was determined in the QSPR studies is not comparatively informative. Furthermore, available QSPR models have been developed based on training sets containing pharmaceutical compounds. It is necessary, therefore, to compare the prediction accuracy of the QSPR models for both environmentally relevant (ERC) and pharmaceutical compounds.

In this study, (i) we will evaluate the predictive performance of QSPR models for predicting fup values in humans for ERCs and pharmaceuticals. The prediction accuracy of QSPR models, Ingle et al. [186] and Watanabe et al. [194], will be compared to that of a commercially available program ADMET Predictor. (ii) We will identify the most critical chemical characteristics that influence the predictive performance of each QSPR model. (iii) We will identify the chemical space that is different between QSPR training sets and ERCs.

3.2 Materials and Methods

3.2.1 Construction of the test dataset

Fup values in humans were obtained from the literature [186, 194, 202-205]. The workflow for the construction of the test set is illustrated in Figure 3.1. The training and test sets of Ingle et al. [186] and Watanabe et al. [194] were obtained from the respective supplemental materials. As each dataset included different chemical identifiers, the different chemical identifiers were then translated to the same type of identifier, PubChem ID (CID) using the PubChem Identifier Exchange Service (https://pubchem.ncbi.nlm.nih.gov/idexchange/idexchange.cgi) [206]. The test sets of Watanabe et al. [194] and Ingle et al. [186] were then combined with the literature data [202-205] that were not included in these datasets (Figure 3.1A). All the data sets were merged using R (version 3.6). To prevent overlap in compounds between the training and test sets, the compounds that were used for training sets for either Ingle et al. [186] or Watanabe et al. [194] were removed from the test set. Using the obtained PubChem IDs as input, 2-dimensional structure-data file (SDF) files were downloaded using the PubChem Download Service (https://pubchem.ncbi.nlm.nih.gov/pc_fetch/pc_fetch.cgi). In order to ensure the ID conversion process was properly done, the simplified molecular-input line-entry system (SMILES) identifiers in the original data set were visually compared to the PubChem canonical SMILES by using the SMILES checker (http://www.cheminfo.org/flavor/malaria/Utilities/SMILES_generator___checker/index.html). For consistency, PubChem canonical SMILES and SDF files were used as inputs for the QSPR models and for the calculation of fup values.

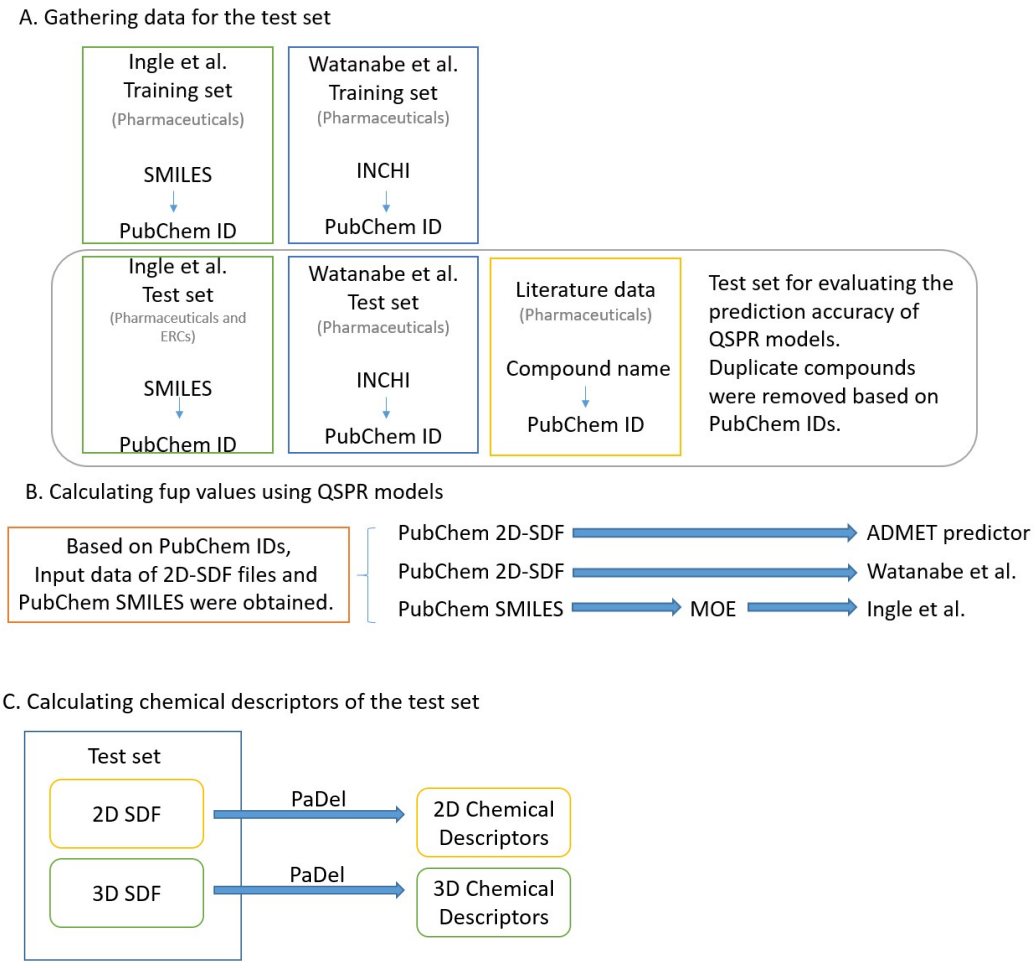

Figure 3.1 A workflow of the construction of the test dataset

3.2.2 Selection criteria for non-commercial QSPR models for predicting fup

Among the many available QSPR models, non-commercial models were selected for this study. The selection was based on the following criteria: (i) the training dataset used to build the QSPR model includes structurally diverse compounds (i.e. the training set included more than 1000 compounds), and (ii) either a freely available calculator or the source code for the model was available online. Selected non-commercial QSPR models were compared for prediction accuracy amongst themselves as well as against the commercial software, ADMET Predictor (Simulation Plus®).

3.2.3 Calculation of fup_{adult} based on QSPR methods

With the constructed test set, fup values were calculated (Figure 3.1B). For the ADMET Predictor, SDF files were imported into the program, and human fup values were calculated using the ADMET predict function (ADMET Predictor™ software provided by Simulations Plus, Inc., Lancaster, California, USA). For fup calculation using Watanabe et al. [194], SDF files that were obtained from PubChem were used as input in the online fup calculator (https://drumap.nibiohn.go.jp/fup/). For the fup calculation using Ingle et al. [186], using SMILES as an input, chemical descriptors that were required to predict a fup were calculated using MOE. The consensus model output was evaluated for the prediction accuracy. The calculated fup values based on each method were gathered and imported into R (version 3.6) for further analysis.

3.2.4 Predictive performance of QSPR models

In order to assess the predictive performance of the QSPR models, prediction error (Eqn. 1), relative prediction error (Eqn. 2), average absolute relative prediction error (Eqn 3), mean absolute error (Eqn 4), root mean squared error (Eqn 5) and correlation of determination (r2, Eqn 6) were calculated. Scatterplots of prediction errors and fup values were created using the "ggplot" package in the software R. Prediction error is the difference between the predicted and observed fup (Eqn 1). Relative prediction error (RPE) indicates the relative magnitude of a prediction error (Eqn 2). Mean absolute RPE indicates overall relative prediction deviation regardless of under- or over-prediction (Eqn 3). Mean absolute error indicates the average of prediction deviation from the observed value. An observed fup value of 0 was assumed to be 0.001. The evaluation metrics were calculated for compounds with observed fup values ranging from 0.01 to 1. Due to the uncertainty associated with experimental measurements of protein binding for highly bound compounds [207], compounds with fup less than 0.01 ($fup < 0.01$) were excluded for evaluating the prediction performance of QSPR models.

In order to evaluate the predictive performances of the QSPR models based on the types of compounds, the test set was subdivided by three categories, such as (i) highly binding (i.e. $0.01 \leq fupobs \leq 0.25$) or low-to-moderately binding compounds (i.e. $fupobs > 0.25$), (ii) pharmaceuticals and ERCs, and (iii) acid-base properties. For acid-base classification, the same criteria used in Ingle et al. [186] were applied to determine acid, base, neutral and zwitterion.

Eqn 1. Prediction error = fuppred – fupobs where fuppred and fupobs are predicted and observed fup values, respectively.

Eqn 2. Relative prediction error (RPE) = $\frac{fup_{pred} - fup_{obs}}{fup_{obs}} \cdot 100\ (\%)$

Eqn 3. Mean absolute RPE = $\frac{\sum_1^n |RPE_i|}{n}$

Eqn 4. Mean absolute error (MAE) = $\frac{1}{n}\sum_{i=1}^{n}\left|fup_{pred,i} - fup_{obs,i}\right| \cdot 100\ (\%)$

Eqn 5. Root mean squared error (RMSE) = $\sqrt{\frac{1}{n}\sum_{i=1}^{n}(fup_{pred,i} - fup_{obs,i})^2}$

Eqn 6. Coefficient of determination (r2) = $\left[\frac{(\sum_1^n fup_{pred,i} \cdot fup_{obs,i}) - n\overline{fup_{pred}} \cdot \overline{fu_{obs}}}{\sqrt{\left(\sum_1^n fu_{pred,i}^2 - n\overline{fup_{pred}}^2\right)\left(\sum_1^n fu_{obs,i}^2 - n\overline{fup_{obs}}^2\right)}}\right]^2$

3.2.5 Identification of important chemical descriptors on QSPR model prediction performance

Using PubChem 2D and 3D SDF files as inputs, chemical descriptors were obtained using the PaDel Descriptor program (version 2.21) [196] (Figure 3.1C). The total of 1045 2D chemical descriptors and 431 3D chemical descriptors were generated for the test set. Additional chemical information such as lipophilicity and polar surface area was obtained from the PubChem SDF files. The chemical descriptors with near zero variance (i.e. descriptor with one unique value or relative small number of unique values compared to the size of the sample) were removed using nearZeroVar function of Caret package in R [208]. The chemical descriptors were standardized for a statistical test (Eqn 7). The Pearson's correlation test was performed between the logarithm of RPE for each QSPR method and each chemical descriptor. The logarithm transformation of RPE was done because of the skewed distribution of RPE values. The correlation coefficients (r) and significance level (i.e. p-value < 0.05) were obtained for each chemical descriptor. The chemical descriptors with a p-value exceeding 0.05 were removed. The remaining descriptors were then ranked based on Pearson's correlation coefficients in order to identify the most correlated chemical descriptors with RPE values of each model.

Eqn 7. $Standardized\ (X_i) = \frac{X_i - \text{me}\quad (X)}{SD(X)}$

3.2.6 Comparison of chemical structures between training sets of QSPR models and environmentally relevant compounds

For training sets of Ingle et al. [186] and Watanabe et al. [194], 2- and 3- dimensional chemical descriptors were calculated using Padel. Chemical descriptors of compounds in those training sets were those of environmentally relevant compounds in the test set of this study. Each chemical descriptor in each training set and test set were subjected to Two-sample Student's T test (i.e. Welch's T test) to identify statistically different chemical descriptors. The significantly different chemical descriptors with p-value less than 0.05 between a training set and the test set of ERC compounds were then ranked based on p-values.

3.3 Results

3.3.1 Prediction performance of QSPR models for estimating fup

Data from a total of 1026 compounds was gathered. Among 208 compounds with observed fup values less than 0.01, only 0 %, 8.2 % and 1.4 % of fup values were calculated within the range of 0.001– 0.01 by ADMET Predictor, Watanabe et al. [194], and Ingle et al. [186], respectively (Figure S1). The test set for evaluating the predictive performance of QSPR models included a total of 818 compounds with fup values ranging from 0.01 to 1 of which 69% were pharmaceutical and 31% were environmentally relevant. The predicted fup values based on QSPR models were compared to the observed data. Overall, the three QSPR models resulted in over-prediction of fup for highly binding compounds and under-prediction for low or moderately binding compounds (Figure 3.2 A-B). All QSPR models resulted in higher relative prediction error for highly binding compounds (i.e. observed fup ranging from 0.01 to 0.25) (Figure 3.3 A-C). The highly deviating predictions by all QSPR models were observed for both types of compounds, namely pharmaceutical and environmentally relevant compounds (Figure 3.3D).

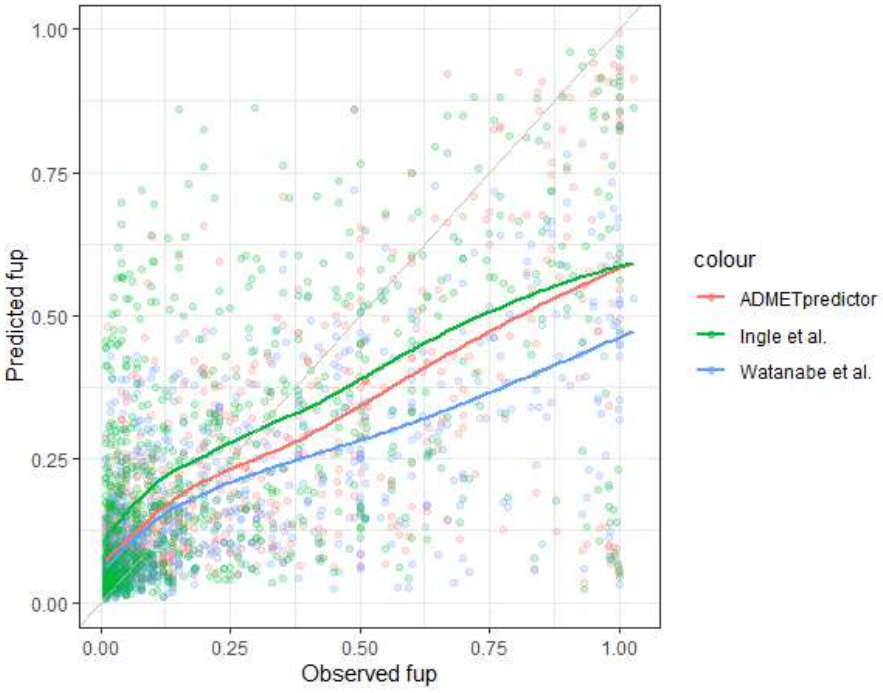
1.00
0.75
0.50
0.25
0.00
Predicted fup
0.00
0.25
0.50
0.75
1.00
Observed fup
colour
ADMETpredictor
Ingle et al.
Watanabe et al.

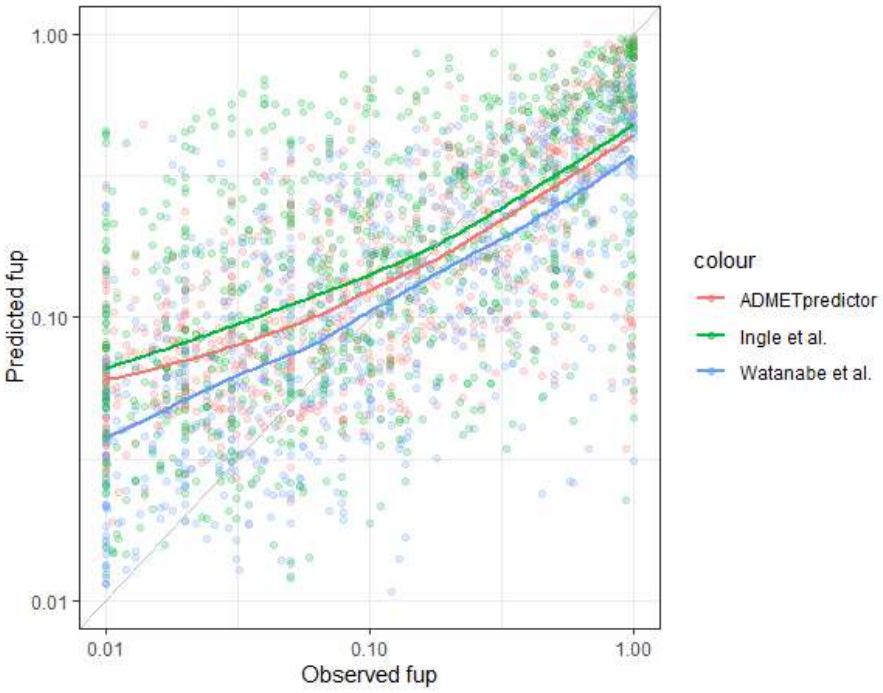
1.00
0.10
0.01
Predicted fup
0.01
0.10
1.00
Observed fup
colour
ADMETpredictor
Ingle et al.
Watanabe et al.

Figure 3.2 Predicted fup values versus the observed values in (A) linear and (B) logarithmic scale. Colored points are fup values. The lines represent the conditional means based on the locally estimated scatterplot smoothing (LOESS) method. The grey line is the line of unity.

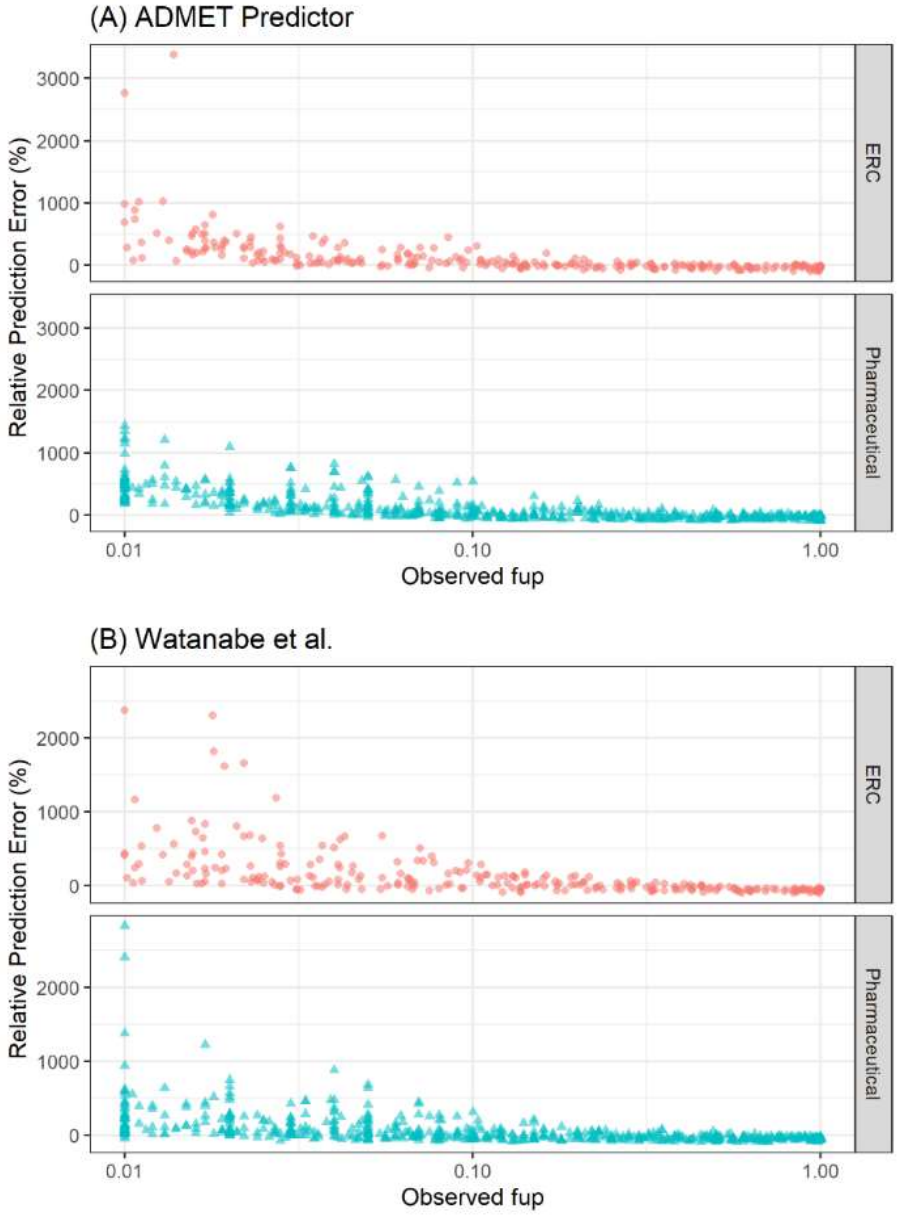

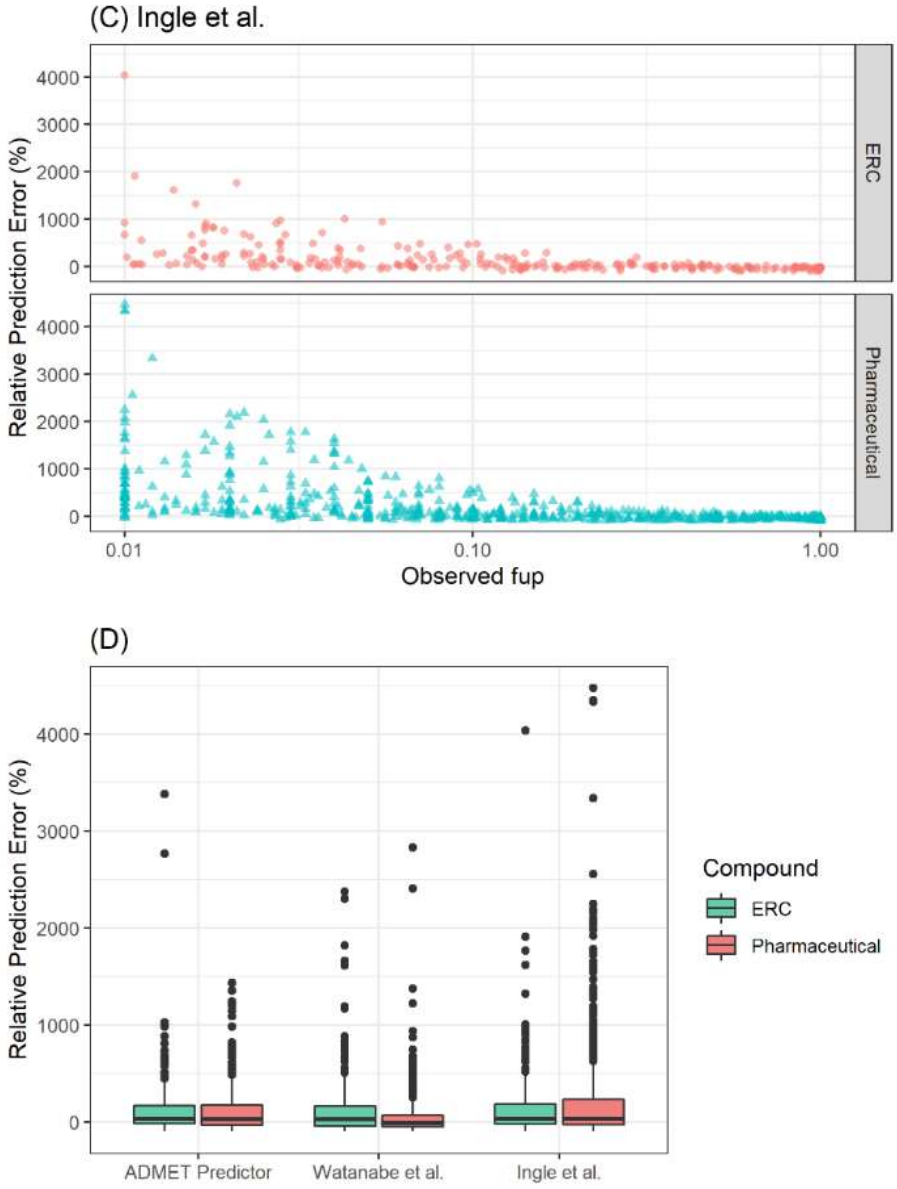

Figure 3.3 Relative prediction error of (A) ADMET predictor, (B) Watanabe et al. and (C) Ingle et al. (D) Relative prediction error of each QSPR model with respect to compound types, pharmaceutical and environmentally relevant compounds. The boxes represent the range of 25th and 75th percentiles. The line within a box indicates a median.

In terms of the overall predictive performance for both ERC and pharmaceuticals, ADMET Predictor and Watanabe et al. [194] resulted in the better predictive performance with lower mean absolute RPE, lower MAE and RMSE values than those of Ingle et al. [186] (Table 3.1). For highly binding compounds (i.e. $0.01 \leq fup \leq 0.25$), Watanabe et al. [194] performed better with a lower MAE of 6.7% and a lower mean absolute RPE of 171.7 % than other QSPR methods. For low or moderately binding compounds ($fup > 0.25$), both Ingle et al. [186] and ADMET Predictor performed better than Watanabe et al. [194] with superior MAE and mean absolute RPE values. For both pharmaceuticals and ERCs, ADMET Predictor and Watanabe et al. [194] performed better than Ingle et al. [186] with lower MAE and mean absolute RPE values. For all QSPR models, higher RPEs were observed for acids compared to those of other types of compounds. Based on RPE values, Watanabe et al. [194] performed better for bases, neutrals and zwitterions.

Table 3.1 Prediction performance of QSPR models for predicting fraction unbound in plasma

	ADMET Predictor	Watanabe et al.	Ingle et al.
All compounds (n=818)			
RMSE	0.21	0.22	0.24
R2	0.52	0.48	0.37
Mean absolute error	12.6	14.3	15.9
Mean absolute RPE	149.3	131.4	243.9
Median absolute error	6.5	7.2	9.5
Median absolute RPE	58.2	55.3	67.1
Highly binding compounds (0.01 ≤ fup ≤ 0.25, n=552)			
Mean absolute error	7	6.7	12

Mean absolute RPE	202.1	171.7	341.6
Median absolute error	4.9	4	6.4
Median absolute RPE	95.3	64	116.4
Lowly or moderately binding compounds (fup > 0.25, n=266)			
Mean absolute error	24.3	30	24
Mean absolute RPE	39.6	47.8	41.1
Median absolute error	17.5	26.5	18.6
Median absolute RPE	36.6	49.2	36.2
Pharmaceuticals (n=565)			
Mean absolute error	13	13.2	16.7
Mean absolute RPE	146.3	109	269.9
Median absolute error	6.6	6.1	10.1
Median absolute RPE	60	51.4	71.4
Environmentally relevant compounds (n=253)			
Mean absolute error	11.8	16.6	14.1
Mean absolute RPE	155.9	181.5	185.9
Median absolute error	6.5	10.2	8.2
Median absolute RPE	56.1	65	53.1
Acids (n=177)			
Mean absolute error	12.5	14.4	16.9
Mean absolute RPE	174.5	213.6	364.4

Median absolute error	6.2	7.8	11
Median absolute RPE	77.2	64	99.7
Bases (n=221)			
Mean absolute error	13.1	14.4	18.3
Mean absolute RPE	150.2	91.3	277.5
Median absolute error	8.1	7.7	11.5
Median absolute RPE	52.8	49.6	62.3
Neutrals (n=397)			
Mean absolute error	12	13.3	13.9
Mean absolute RPE	139.7	120	177.4
Median absolute error	5.7	6.2	7.2
Median absolute RPE	57.3	57.4	62.5
Zwitterions (n=23)			
Mean absolute error	20.1	29.5	21.6
Mean absolute RPE	111.6	82.7	142.4
Median absolute error	12.3	28.8	15.4
Median absolute RPE	49	62.8	38

3.3.2 Prediction accuracy as a function of chemical structure

Chemical descriptors that exhibited a significant correlation with RPE (p-values < 0.05) based on the Pearson correlation test were ranked. For ADMET Predictor, the number of basic functional groups,

the fraction of charged weighted partial positive surface area and lipophilicity were most correlated with the RPE (Figure 3.4 A-B). For Watanabe et al. [194] and Ingle et al. [186], the partial positive surface area, the number of basic functional groups and lipophilicity were the most important parameters (Figure 3.4 C-F). Taken together, for all three QSPR models, the positive polar surface area, the number of basic functional groups and lipophilicity were the most important chemical descriptors for predicting fup. Highly hydrophobic compounds with fewer basic functional groups were found to have high RPEs (>200%) or below the prediction limit (fup < 0.01). On the other hand, the QSPR models showed relatively low prediction error (RPE < 200%) for hydrophilic compounds with basic functional groups.

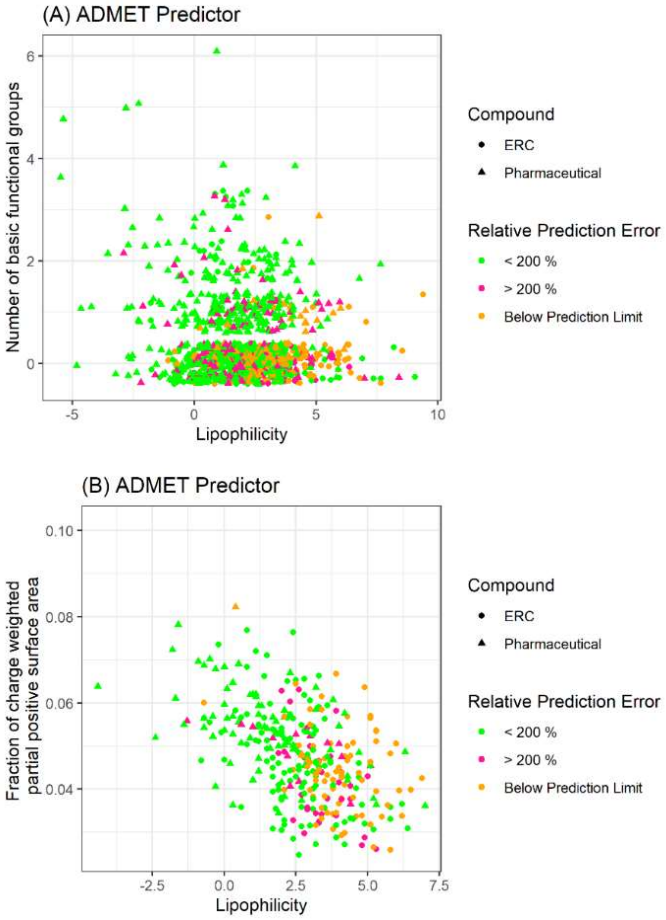

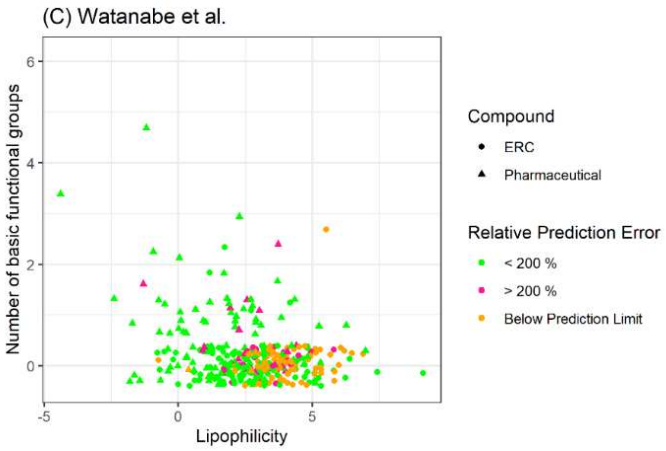
(C) Watanabe et al.
Number of basic functional groups
Lipophilicity
Compound
ERC
Pharmaceutical
Relative Prediction Error
< 200 %
> 200 %
Below Prediction Limit

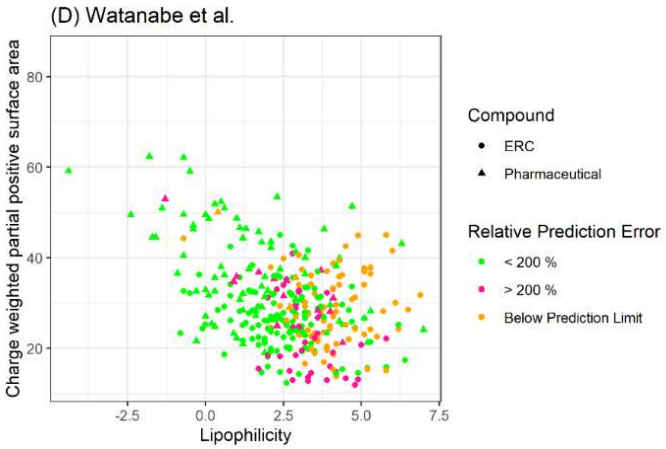
(D) Watanabe et al.
Charge weighted partial positive surface area
Lipophilicity
Compound
ERC
Pharmaceutical
Relative Prediction Error
< 200 %
> 200 %
Below Prediction Limit

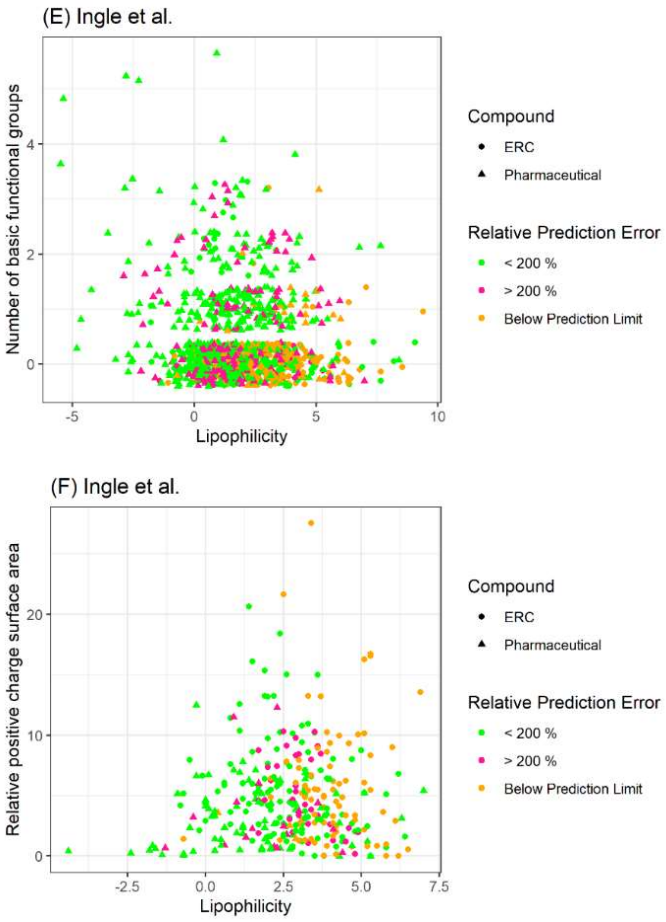

Figure 3.4 Relative prediction error of each QSAR models as a function of chemical descriptors. The triangular and circular points represent pharmaceuticals and environmentally relevant compounds data. The colors indicate a degree of relative prediction error of a QSPR method such that compounds with >200 % RPE and < 200 % RPEs are in red and green, respectively. Compounds that were below prediction limit of fup <0.01 are in orange.

3.3.3 Identification of significantly different chemical characteristics between ERCs and QSPR training set compounds

Environmentally relevant compounds were more lipophilic than the QSPR training set compounds (Figure 3.5A). Structurally, ERC contained a lower number of rings and a lower number of basic

functional groups and a higher number of halogens than those of compounds in the training sets (Figure 3.5 B-D). In terms of 3D chemical descriptors, partial positive surface areas of ERC compounds (i.e. the sum of surface area on an electropositive portion of a molecule, PPSA-2) were significantly lower than those in the QSPR training sets (Figure 3.5 E). The ERC compounds were smaller in size with significantly smaller geometrical radii (Figure 3.5 F) and geometrical diameters.

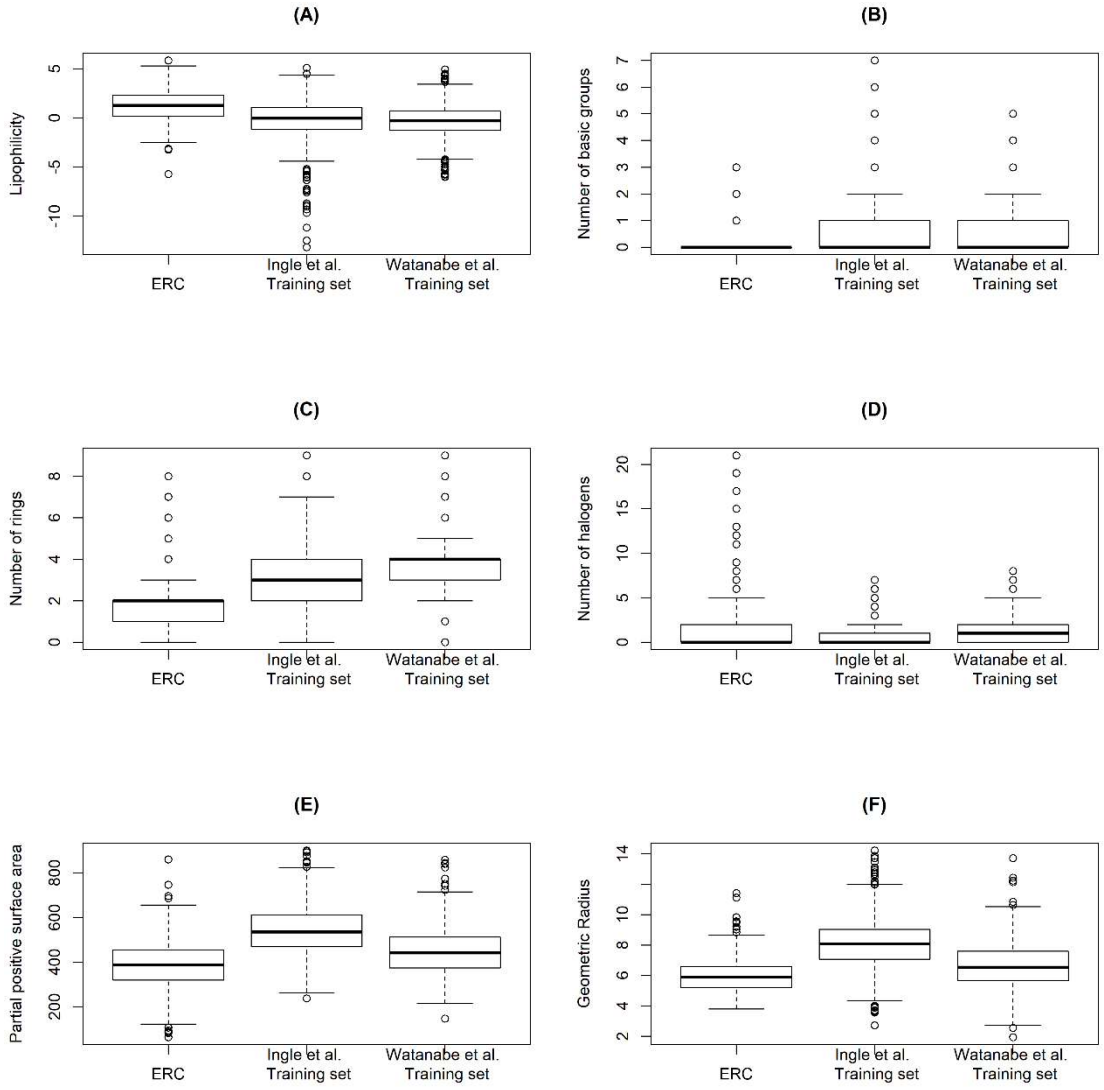

Figure 3.5 Significantly different chemical descriptors between compounds in the training sets of QSPR methods and environmentally relevant compounds.

3.4 Discussion

The degree of plasma protein binding is an important property of a compound influencing toxicokinetics (TK) and is a key parameter in PBTK modeling. Volume of distribution that affects the maximum concentration and the half-life, is directly proportional to fup. Further, the freely available portion of compounds elicit pharmacological/toxicological response [179]. Clearance reflects overall exposure (i.e. area under the curve (AUC)) and is almost proportional to fup for compounds with a low hepatic extraction ratio (EH). Its importance in in vitro-in vivo extrapolation (IVIVE) has been demonstrated with Trichloroethylene [209] where in vitro CLH is measured with a hepatocyte uptake assay using isolated hepatocytes in a medium in the absence of plasma proteins and fup is applied as in equation 8. The determined CLH information can be incorporated into a PBPK model.

Eqn. 8 $CL_H = \frac{Q \cdot R_{BP} \cdot fup \cdot CL_{int,in\ vitro} \cdot SF}{Q + R_{BP} \cdot fup \cdot CL_{int,in\ vitro} \cdot SF}$

Q: blood flow, RBP: blood-to-plasma ratio, CLint: in vitro intrinsic clearance, SF: scaling factor for 20 g liver/kg and 45 mg protein g/liver in humans [210].

An accurate determination of a fup is needed for use in PBTK models for human health risk assessment such that fup levels in potentially sensitive populations such as diseased, pediatric or elderly can be extrapolated by adjusting altered plasma protein concentrations [25, 211]. In a PBTK model, virtual individuals are built based on known trajectories of anatomy, biochemistry and physiology across age, and compounds are defined by physicochemical properties [45, 212]. Sensitivity analyses found that fup is one of the most critical input parameters for PBPK model outputs [70, 180] and when extrapolating across age or disease state, the reference value of fup defines the extrapolated fup. For example, Yun and Edginton [180] found that from 10 pediatric PBPK models that were extrapolated from adult models, the sensitivity coefficients of fup were high for compounds with low EH in

predicting AUC, compared to compounds with high EH. Therefore, in many cases, the precision of fup_{adult} must be ensured if there is to be confidence in the pediatric model outcomes.

In this study, we evaluated the performance of QSPR models for predicting protein binding as well as the chemical descriptors that were most associated with the resulting prediction errors. In terms of the overall predictive performance for all compounds, the RMSE and MAE values were the lowest for ADMET Predictor although Watanabe et al. [194] provided similar metrics. A clear distinguishing feature was that there was increased predictive performance for compounds having a fup >0.25 regardless of the model used.

In terms of extremely highly binding compounds (i.e. observed fup < 0.01), only a small fraction of fup values were predicted below fup of 0.01 indicating that the QSPR models may not be suitable for predicting fup values for extremely highly binding compounds. The reason for this is that during the data curation and the training set development, when a compound was stated to have protein binding higher than 99%, the fup value for the compound was assumed to be 0.01 [194]. This assumption is in line with U.S. Food Drug Administration guidelines that states when an experimentally determined value of fup is less than 0.01, the fup is then set to 0.01 due to uncertainties in the protein binding measurements [207]. However, this limitation makes the QSPR model inherently incapable of predicting a high degree of protein binding.

In terms of important chemical descriptors that were associated with the prediction errors of QSPR models, the commonly observed chemical characteristics of highly binding compounds were also correlated with a high prediction error. Lipophilicity was a critical chemical characteristic that was positively correlated with RPEs such that the compounds that had a high prediction error or below the limit of prediction (fup <0.01) tended to be highly lipophilic. This was expected because the lipophilicity of a compound is known to have a high correlation with plasma protein binding [213] and QSPR models, in general, resulted in poor prediction performance for highly binding compounds. In contrast, the number of basic functional groups and positive partial surface area were negatively correlated with RPEs.

The negative correlation between the chemical characteristics of positively charged states and the prediction error is in line with the albumin binding sites findings. There are three drug-like molecule binding sites in albumin, namely, warfarin (Site I), benzodiazepine (Site II), and digitoxin [179, 214-

218]. An affinity of a compound to each binding site depends on the functional groups of that compound. The binding site II of the major carrier protein albumin has positively charged groups on the surface of its' binding site [219]. The cationic center of binding sites and the positively charged portion of compounds are likely to have an electropositive repulsion. This is in accordance with an earlier finding that the presence of positive charges in a compound precludes binding to binding site II [219].

For the most part, QSPR models are built based on pharmaceutical compounds as a training set primarily due to the availability of experimental fup for these compounds as compared to ERCs. Therefore, it is necessary to evaluate the predictive performance of QSPR models for non-pharmaceutical compounds. For all evaluated QSPR models, the prediction accuracy was lower for ERCs than for pharmaceuticals. This suggested that the structural difference between the two types of compounds may have contributed to the discrepancy in the prediction accuracy of QSPR models. The ERCs were more lipophilic and smaller in size, furthermore, there were a lower number of basic functional groups and rings in ERCs compared to the training set compounds (Figure 3.5). These tendencies of ERCs lead to high binding affinity towards plasma proteins. This suggest that QSPR models are less equipped to predict ERCs that have the chemical characteristics listed above.

Some of the ERCs were highly halogenated compared to the QSPR training set compounds (Figure 3.5D). The highly halogenated compounds included organochlorines, pyrethroids, perfluoroalkyl and polyfluoroalkyl substances. The presence of halogens increases binding affinity to proteins through halogen bonding (e.g. halothane [220]). The majority (18 of 28 compounds) of highly halogenated compounds (i.e. the number of halogens > 5) were highly protein binding with the observed fup values less than 0.01. The absence of highly halogenated compounds in the QSPR training sets implies that the relationship between high halogenation and protein binding may not be well captured. This suggests that QSPR models may not be suitable to make predictions for the highly halogenated ERCs.

As regression models, QSPR models are suitable for predicting the target property within or near the chemical space of a training set [221]. For the predictions outside the intended chemical space, Tan et al. [221] suggested re-parameterizing or creating a new model. In the previous findings of Yin et al. [222] and Ingle et al. [186], the chemical spaces of pharmaceutical and ToxCast compounds [192, 223] overlap and the application domain [224] of the Ingle et al. [186] model covered the chemical properties

of ERCs with a few exceptions. This leveraged the use of pharmaceutical data to predict fup values for ERCs. However, our study identified several chemical descriptors that were significantly different between ERC and pharmaceuticals (Figure 3.5). It is thought that expanding a training set to include ERC data may improve the prediction performance of a QSPR model. In addition, different sets of chemical descriptors and different machine learning techniques may result in different prediction performance [225]. With this in mind, multiple alternative QSPR models can be developed and consensus prediction can be applied [225, 226]. When predictions from multiple QSPR models converge, the confidence of an output increases and moving forward, this multiple model prediction approach should be considered.

A critical concern in the use of PBTK modeling for human health risk assessment is the availability of input parameters [212]. When an experimentally determined fup is not available, the use of QSPR models for predicting fup seems the most viable option and has been accepted as a de facto standard [221, 227]. This study suggests that the use of QSPR models for fup prediction in human and for further extrapolations using PBTK modeling or IVIVE may not be an optimal choice especially for highly binding ERCs. To improve prediction of fup, better mechanistic understanding is needed between the protein binding properties and chemical structure. Also, the uncertainty associated with experimental determination for highly binding compounds should be improved [228] as this uncertainty is carried forward into the QSPR models. Prediction of fup values using the QSPR approach is an alternative to experiments; however, if certainty is required, experimental determination is required.

3.5 Declaration of Interest

The authors have no conflict of interest, financial or otherwise.

Chapter 4: Evaluation of models for predicting pediatric fraction unbound in plasma for human health risk assessment

4.1 Introduction

Pediatric physiologically based pharmacokinetic (PBPK) models mathematically describe a compound's absorption, distribution, metabolism and excretion processes by taking into account age-dependent changes in a child's anatomy, biochemistry and physiology along with physicochemical properties of a compound [17, 44, 45, 47]. These models inform human health risk assessment by providing a justifiable estimation of chemical-specific adjustment factors (CSAF) [11, 61, 229] that rely on reasonable estimation of PK inter-individual variability. This is achieved through the creation of virtual pediatric populations that allow for PK parameter distributions to be delineated. The human kinetic adjustment factor (HKAF) uses the PK parameter distribution differences between adults and children such that the HKAF ratio is the 95th percentile PK parameter in a pediatric group to the median in an adult population [6, 12, 13]. Similar adult and pediatric distributions bring confidence that the adult variability is a good surrogate for children and divergent distributions reflect that children (or some children) may not be covered if only adults are considered during human health risk assessment.

To instill confidence in PBPK model outputs, an accurate determination of the fraction unbound in plasma (fup) is essential and has been identified as one of the most important inputs driving pediatric PBPK model outputs [180]. Among the sixty plasma proteins in humans, albumin, alpha acid glycoprotein (AAG), and lipoproteins meaningfully bind to exogenous compounds [179, 230]. While the acid-base properties of a compound generally determine which plasma protein it preferentially binds this assumption is not always valid. Neutral and acidic compounds tend to bind to albumin, and basic compounds tend to bind to AAG and lipoproteins [179]. The physiological roles of these plasma proteins are manifold, in that they serve as both a transporter and a storage depot for endogenous and exogenous substances [231]. Albumin maintains the osmotic pressure in the bloodstream and transports endogenous molecules such as bilirubin and fatty acids [232]. AAG is an acute-phase reactant; when presented with injury and inflammation, plasma AAG levels increase [233]. A decreased AAG level is associated with severe liver diseases (e.g. cirrhosis [233, 234]). AAG serves

as a carrier of exogenous substances. Lipoproteins transport lipid molecules or lipid-soluble compounds [235].

The degree of protein binding can differ between children and adults due to the effects of growth and maturation [24]. Neonates and young infants have a lower degree of protein binding compared to that of adults due to a lower plasma protein concentration level than adults [24, 236]. In the case of albumin, adult concentrations are reached in 10 - 12 months. Preterm neonates have a lower level of albumin than term neonates [237]. In terms of AAG, the adult level is reached in 12 months [238] and concerning low-density lipoproteins (LDL), there is a sharp increase in the level of LDL particles during the first week of life and is maintained in the neonatal phase, 1 month after birth [239].

A lower degree of protein binding, i.e. a high unbound fraction, may impose a greater health risk to children especially for infants and neonates compared to adults. For example, the study of Sethi et al. [205], highlighted the potential health risk for neonates when exposed to a pyrethroid insecticide due to low protein binding. Pharmaceutical agents may also be associated with adverse effects in neonates due to low protein binding. For example, fentanyl can result in respiratory depression even at a low dose in neonates [240-242].

The age-dependent changes in protein binding to albumin [25, 166, 211, 243] and AAG [25, 166, 211, 243, 244] can be predicted by several methods. These ontogeny models estimate the fraction unbound in plasma in children (fup_{child}) as a function of the concentration of a plasma protein at a specific age and a fup value in adults (fup_{adult}). In these models, the binding affinity of a compound to albumin is assumed to be the same in both adults and children. When an experimentally determined fup_{adult} value is not available, an in silico method, quantitative structure -property relationship (QSPR) model, can be used [185, 186, 194]. QSPR models predict fup in human based on the learned relationships between chemical structure and the degree of protein binding in plasma. As fup_{adult} for environmentally relevant compounds is often not available, the overall uncertainty of using both QSPR approach for predicting fup_{adult} from compound structure and an ontogeny model for predicting a fup_{child} need to be assessed.

The objectives of this study are (i) to evaluate the protein concentration vs. age profile derived from various ontogeny models by comparison to observed concentrations, (ii) to assess the predictive performances of the ontogeny models by comparing predicted fupchild values to observed values, and

(iii) to evaluate the overall uncertainty in fup_{child} prediction resulting from a combination of QSPR models and ontogeny models.

4.2 Methods

4.2.1 Data collection

Plasma protein concentration data for children (age 0 – 12 years) was obtained from literature to evaluate the appropriateness of the ontogeny models in predicting age-dependent changes in albumin (Johnson et al. [243], McNamara and Alcorn [25], McNamara and Meiman [211], PK-Sim [166]) and AAG (Johnson et al.[243], Maharaj et al. [244], McNamara and Alcorn [25], McNamara and Meiman [211]) plasma concentrations. The observed values were obtained from MEDLINE database by searching keywords, for example, 'plasma protein concentrations', 'protein binding', and 'infant or newborn'. Arithmetic mean and standard deviation (SD) of plasma (or serum) protein concentrations vs. age were gathered. When a range was reported, the mean and SD were calculated based on equations in Hozo et al. [74]. The pediatric data was categorized based on age such that neonates were 0 to ≤1 month, infants were 1 month to ≤2 years, children were 2 years to ≤12 years and adolescents were 12 years to ≤18 years. Any age that was expressed in years or months was converted to postnatal age (PNA) in days. Graphically presented data was digitized using Plot-digitizer [73]. Data from individuals with reported disease was not included, for example, albumin levels in critically ill patients in the intensive care unit were not included (e.g. [245]).

To evaluate the predictive performance of ontogeny models for the prediction of unbound fraction in plasma, the fraction unbound in plasma data in both children and adults were obtained from literature. The arithmetic mean and SD of fup values vs. age was obtained. Relevant information such as disease status (i.e. healthy or patients) and binding partner (i.e. albumin or AAG) were also collected.

4.2.2 Models for predicting fup_{child}

Fup_{child} values were calculated by using the following equations (Eqn 1) [25]. According to McNamara and Alcorn [25] method, the ratio of protein concentrations in children relative to adult is determined by using linear equations (Eqn. 2-3):

Eqn 1. $fup_{child} = \frac{1}{1+\frac{[P]_{child}}{[P]_{adult}} \cdot \frac{(1-fup_{adult})}{fup_{adult}}}$

Eqn 2. $\frac{[ALB]_{child}}{[ALB]_{adult}}(\%) = 0.005627 \cdot Days \cdot 76.7$

Eqn 3. $\frac{[AAG]_{child}}{[AAG]_{adult}}(\%) = 0.01137 \cdot Days \cdot 53.4$

[P], [ALB], [AAG] are the concentrations of protein, albumin and alpha1-acid glycoprotein, respectively.

According to Johnson et al. [243], albumin and AAG concentrations in children are calculated by following equations:

Eqn 4. [ALB] (g/L) = $1.1287 \cdot \ln(\text{Days}) + 33.746$

Eqn 5. [AAG] (g/L) = $\frac{0.887 \cdot Days^{0.38}}{8.89^{0.38}+Days^{0.38}}$

Maharaj et al. [244] provided the AAG ontogeny models for both healthy children and pediatric patients who were diagnosed or suspected of having an infection. Age-dependent changes in AAG concentrations can be estimated by using the following equation:

Eqn 6. [AAG] (mg/dL) = $\frac{AA\_max \cdot Age^{P}}{TM^{P}_{50}+Days^{0.38}} = \frac{93.17 \cdot Days^{0.498}}{7.76^{0.498}+Days^{0.498}}$

AAGmax: maximum plasma AAG concentration (mg/dL), TM50: age at 50% AAGmax, P: Hill coefficient

In terms of PK-Sim [166], the ratio of albumin concentrations in children relative to adult is determined by using a following equation:

Eqn 7. $\frac{[ALB]_{child}}{[ALB]_{adult}} = \frac{PMA^{k}}{(A_{0.5}{}^{k}+PMA^{k})}$

PMA: postmenstrual age, A0.5: PMA at 50% level compared to adults (21.533), k: Hill coefficient (3.240).

In terms of the AAG ontogeny model incorporated in PK-Sim [166], the ratio of AAG concentrations in children relative to adults was determined by using the Markov Chain Monte Carlo (MCMC)

approach and the age-dependent changes in the ontogeny factors were described in detail in Mayer et al. [246] and listed in the PK-Sim Ontogeny Database version 7.3 [166].

According to McNamara and Meiman [211], the ratios of albumin concentrations in children relative to adults for neonates, infants and children are 0.777 ± 0.025, 0.899 ± 0.028 and 0.853 ± 0.037, respectively. For AAG, the ratios of concentrations in children relative to adults for neonates, infants and children are 0.456 ± 0.053, 0.814 ± 0.067 and 1.12 ± 0.084, respectively.

The calculation of fup_{child} was carried out under the following assumptions. (i) An equilibrium affinity constant of a compound to plasma proteins was the same in children and adults. (ii) The equilibrium dissociation constant was less than the plasma concentrations of a compound, therefore, the degree of protein binding was independent of compound concentrations in plasma.

4.2.3 Evaluation of the appropriateness of protein concentration vs. age profile for each model

Using the ontogeny factors (i.e. the ratio of protein concentrations in children relative to adults) calculated from each model, plasma protein concentration vs. age profiles were calculated. For PK-Sim, PMA (in weeks) was converted to PNA (in days) using the following relationship: PMA= postnatal age + gestational age. For full-term neonates, the gestational age of 40 weeks was assumed.

The estimated albumin concentration vs. age profiles were obtained by multiplying the ontogeny factors by the reference albumin concentration in adults of 4.5 g/dL [25]. These concentrations were then compared to the observed albumin concentration data in children. To note, PK-Sim [166], McNamara and Alcorn [25] and McNamara and Meiman [211] do not use the adult reference albumin concentration because these models directly estimate ontogeny factors. The reference protein concentration in adults was applied only for comparison purposes.

In terms of AAG adult reference concentrations, the values of each model were different. The AAG adult reference concentrations were 0.60 g/L, 0.83g/L, 0.93 g/L, 0.70 g/L and 0.77 g/L for McNamara and Alcorn [25], Johnson et al. [243], Maharaj et al. [244], McNamara and Meiman [211] and PK-Sim [166], respectively. The AAG adult reference concentrations were obtained from the text or digitized from the graphs using the Plot-digitizer [73].

4.2.4 Evaluating the divergence of ontogeny models as a function of age

By examining the consensus or the discrepancy in ontogeny factors produced by each model as a function of age, the uncertainty surrounding the choice of an ontogeny model was examined. The maximal difference in ontogeny factors between models was attained by subtracting the minimum possible ontogeny factor from the maximum possible ontogeny factors over the pediatric period. The minimum, maximum and differential ontogeny factors vs. age profiles were plotted for visual comparison.

To evaluate the conditions in which ontogeny model choice affects the outcome of fup_{child}, the combinatorial effects of the differences in the ontogeny factors of the models and a compound's degree of protein binding on fup_{child} predictions, the ratio of fup_{child} to fupadult (fup_{child} / fup_{adult}) values, were simulated. The fup_{child}, maxOF and fup_{child}, minOF estimates were calculated by using the maximum and minimum possible ontogeny factor (OF) at a specific age, respectively (Eqn 8-9). Fup_{adult} values of 0.01, 0.1, 0.5 and 0.9 were used in the calculations.

Eqn 8. $$fup_{chil\ ,\mathrm{maxOF}} = \frac{1}{1+\left(\frac{[P]_{child,max}}{[P]_{adult}}\right).\frac{(1-fup_{adult})}{fu\ _{adult}}}$$

Eqn 9. $$fup_{chi\ \ ,\mathrm{minOF}} = \frac{1}{1+\left(\frac{[P]_{child,min}}{[P]_{adult}}\right).\frac{(1-fup_{adult})}{fu\ _{adult}}}$$

4.2.5 Evaluation of the overall uncertainty of using QSPR predicted fup values for predicting fup_{child}

Fup values for all compounds were calculated based on a QSPR approach using ADMET Predictor (Simulations Plus, ver. 9.5). Two-dimensional structural data files (2D-SDF) for each compound were obtained using PubChem [206]. Human fup values were calculated using the ADMET predict function. It was assumed that a QSAR-predicted fup value in humans was equivalent to the fup value in adults. As ADMET Predictor does not provide information on whether a compound primarily binds to albumin or AAG, the binding partner information of a compound was obtained from literature. Fup_{child} was calculated with each ontogeny model using the QSPR-predicted-fup_{adult} as an input. For albumin binding compounds, albumin ontogeny models were applied in order to calculate QSPR-predicted fup_{child}. For AAG binding compounds, AAG ontogeny models were applied. QSPR-

predicted fup_{child} were then compared to observed fup_{child}. QSPR-predicted fup_{child} were then compared to observed fup_{child}. The overall uncertainty of the combined use of the QSPR method to predict a degree of protein binding in humans and the ontogeny models that predict the fup_{child} was evaluated.

4.2.6 Evaluation of the predictive performance of QSPR and ontogeny models

To assess the predictive performance of models, the average fold error (AFE) (Eqn 10), absolute average fold error (AAFE) (Eqn 11), relative prediction error (Eqn 12), mean absolute relative prediction error (Eqn 13), mean absolute error (Eqn 14), root mean squared error (RMSE) (Eqn 15) and coefficient of determination (r2) (Eqn 16) were calculated.

AFE >1 and AFE<1 indicate over-and under-predictions, respectively. AAFE indicates an overall magnitude of errors. The higher AAFE values indicate the lower overall prediction accuracy. RPE indicates relative magnitude of prediction error with respect to the observed value. MAE will indicate an average of prediction errors. For example, if MAE is 0.3, then predicted fup values deviate on average by 0.3. RMSE and coefficient of determination are the metrics that are commonly used for measuring the difference between predicted and observed values.

Eqn 10. Average fold error (AFE) = $10^{\frac{1}{n}\sum \log\left(\frac{fu\ \ pred}{fu\ \ obs}\right)}$ where fuppred and fupobs are predicted and observed fup values, respectively.

Eqn 11. Absolute average fold error (AAFE) = $10^{\frac{1}{n}\sum\left|\log\left(\frac{fu\ \ pred}{fup_{obs}}\right)\right|}$

Eqn 12. Relative prediction error (RPE) = $\frac{fup_{pred} - fup_{obs}}{fu\ \ obs} \cdot 100\ (\%)$

Eqn 13. Mean absolute RPE = $\frac{\sum_1^n |RP\ \ _i|}{n} \cdot 100\ (\%)$

Eqn 14. Mean absolute error (MAE) = $\frac{1}{n}\sum_{i=1}^{n}\left|fup_{pred,i} - fup_{obs,i}\right| \cdot 100\ (\%)$

Eqn 15. Root mean squared error (RMSE) = $\sqrt{\frac{1}{n}\sum_{i=1}^{n}(fup_{pred,i} - fup_{obs,i})^2}$

Eqn 16. Coefficient of determination (r2) = $\left[\frac{(\sum_1^n fup_{pred,i} \cdot fu_{obs,i}) - n\overline{fup_{pred}} \cdot \overline{fup_{obs}}}{\sqrt{\left(\sum_1^n fu_{pr,i}^2 - n\overline{fup_{pred}}^2\right)\left(\sum_1^n fu_{obs,i}^2 - n\overline{fup_{obs}}^2\right)}}\right]^2$

4.3 Results

4.3.1 Evaluation of the appropriateness of protein concentration vs. age profile for each model

The estimated albumin ontogeny factors at birth were similar across models and ranged from 74 % ~ 88 % (Table 4.1, Figure 4.1). In the case of McNamara and Alcorn [25] and Johnson et al. [243], the albumin concentration level at 2 years reached 81 % and 92 % of the adult level, respectively. The adult plasma albumin concentrations were reached at 11.3, 17.2 and 1.4 years according to McNamara and Alcorn [25], Johnson et al.[243] and PK-Sim [166], respectively (Table 4.2).

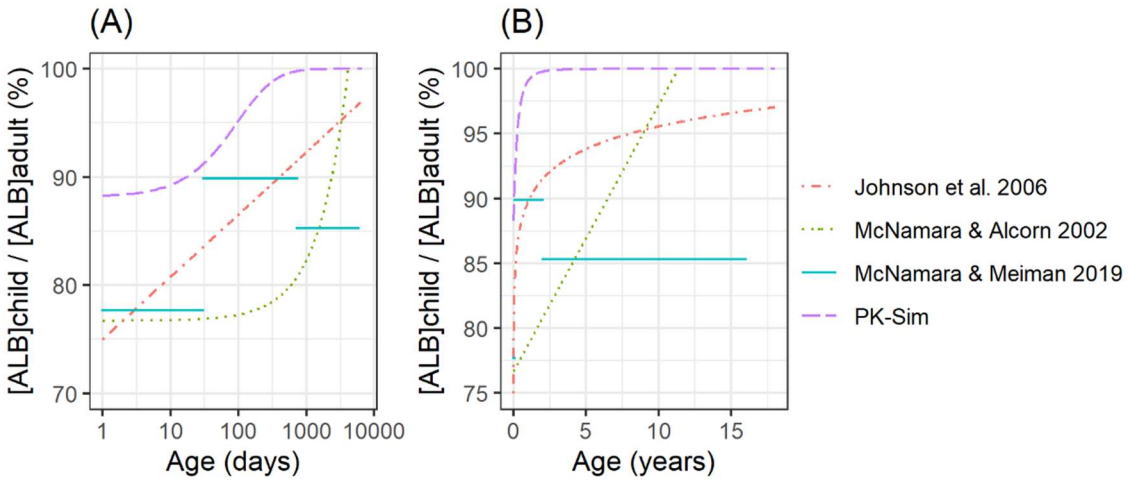

Figure 4.1 Calculated ratios of albumin concentration in children relative to an adult level as a function of age of each models were presented in (A) logarithm and (B) linear scales.

Table 4.1 Albumin concentration ratios of ontogeny models

	At birth (Full term neonate; Gestational age of 40 weeks was assumed)	Age at which the adult level is reached
McNamara and Alcorn (2002)	77%	11.3 years
Johnson et al. (2006)	74%	17.2 years
McNamara and Meiman (2019)	77.7%	N/A[a]
PK-Sim	88%	17 months
a N/A: not applicable		

Table 4.2 AAG concentration ratios of ontogeny models

	At birth (Full term neonate; Gestational age of 40 weeks was assumed)	Age at which the adult level is reached
McNamara and Alcorn (2002)	53.4%	9.3 years
Johnson et al. (2006)	28.9%	Reaches 88% by 17.7 years
Maharaj et al. (2018)	26.4%	Reaches 92% by 3 years
McNamara and Meiman (2019)	45.6%	2 years
PK-Sim	28.8%	11.4 years Reaches 99% by 3 years

A comparison between the albumin concentration vs. age profiles derived from the models (Figure 4.2) revealed that the models with non-linear equations, PK-Sim [166] and Johnson et al. [243], were more in agreement with the observed albumin concentrations (Table S1) than those derived from McNamara and Alcorn [25] and McNamara and Meiman [211].

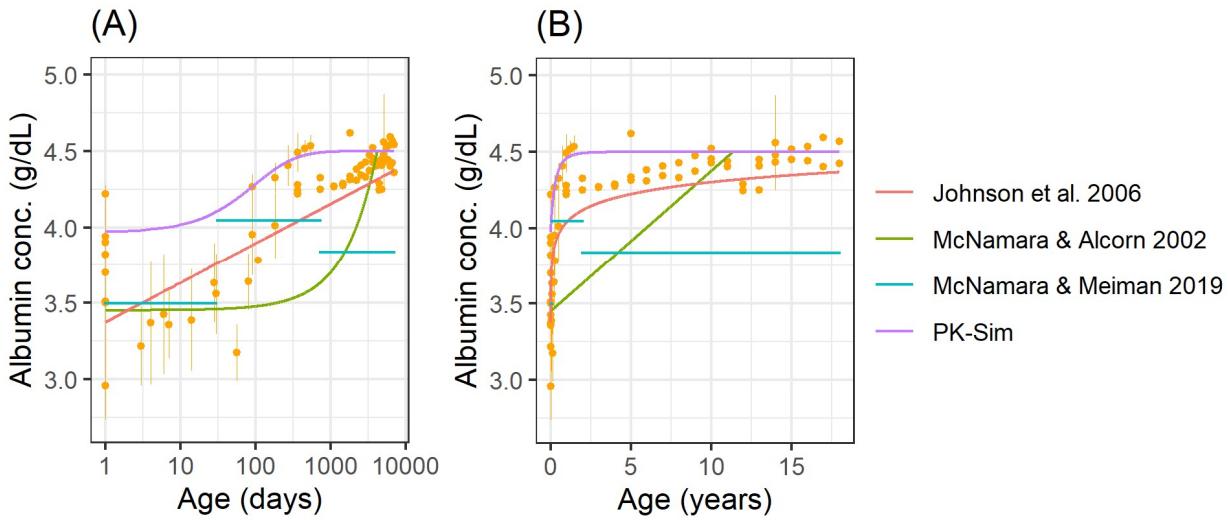

Figure 4.2 Estimated albumin concentrations vs. age profiles (coloured lines) were compared to the observed albumin concentrations in children in (A) logarithm and (B) linear scales. Points are observed mean or median values and vertical lines represent standard deviations. The adult reference concentration of 4.5 g/dL was assumed for all models.

The estimated AAG ontogeny factors at birth ranged from 28 ~ 53% (Figure 4.3). The Johnson et al. [243], Maharaj et al. [244] and PK-Sim [166] models showed similar profiles with low starting ontogeny factors in neonates and a rapid increase up to an adult level in the neonatal or infant periods. For both the Maharaj et al. [244] and the PK-Sim [166] models, the ratio reaches 90% by 2-year of age. Whereas for Johnson et al. [243], the ratio was 80% for a 2-year old and slowly increased to 88% in adolescents.

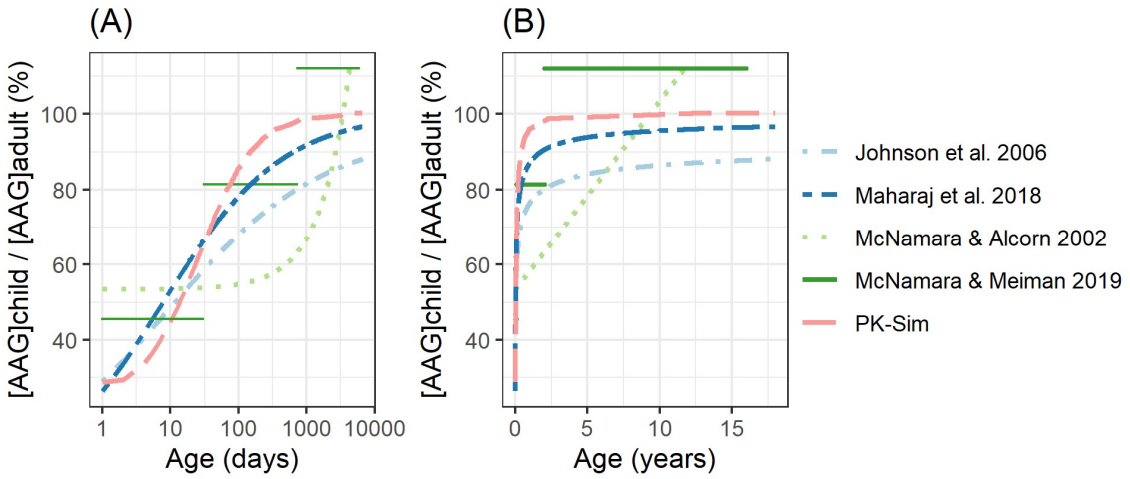

Figure 4.3 Calculated ratios of AAG concentration in children relative to an adult level as a function of age of each models were presented in logarithm and linear scales.

The comparison between the AAG concentration vs. age profiles derived from the models (Figure 4.4) showed that the models with non-linear equations, PK-Sim [166], Johnson et al. [243] and Maharaj et al. [244], were more in line with the observed AAG concentrations (Table S2) than those of McNamara and Alcorn [25] and McNamara and Meiman [211].

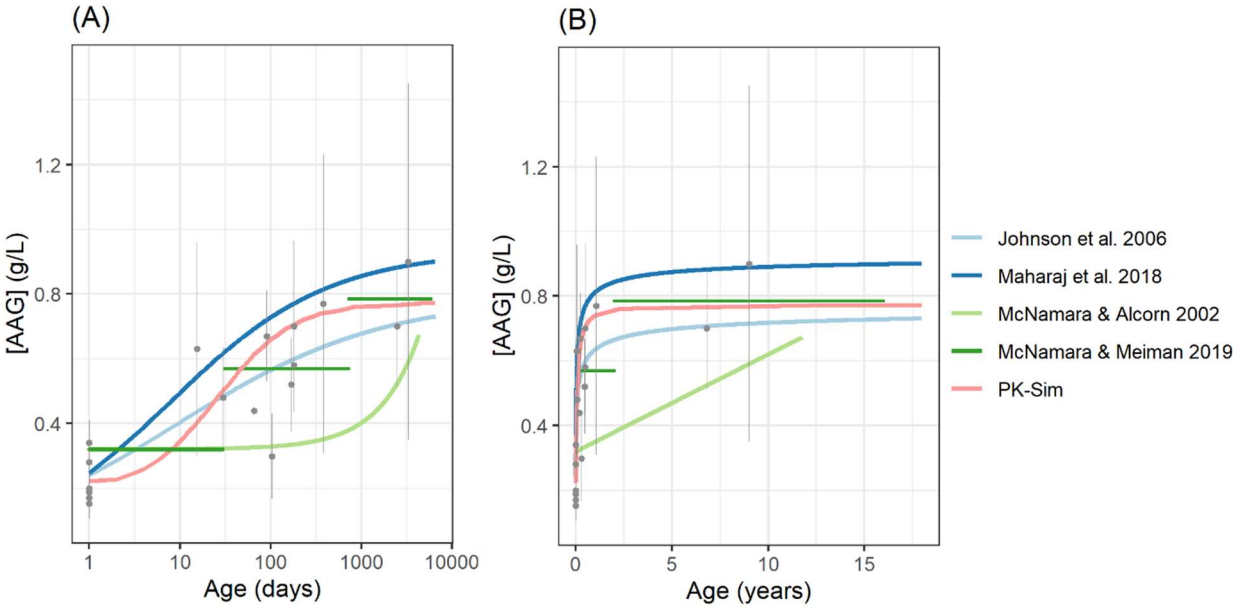

Figure 4.4 Estimated AAG concentrations vs. age profiles (coloured lines) were compared to the observe AAG concentrations in children in (A) logarithm and (B) linear scales. Points are observed mean or median values and vertical lines represent standard deviations. The adult reference concentrations were assumed for all models.

4.3.2 Evaluating the divergence of ontogeny models as a function of age

The differences in ontogeny factors at specific ages were calculated (Figure 4.5). These calculations were used to identify which age groups fup_{child} estimates would be most affected by choice of ontogeny model. For albumin, the difference in the ratio ranged from 3 to ~20 %, depending on the compared models. These differences were highest in infants and young children (age 3 months - 3 years).

In terms of the AAG ontogeny models, the difference in the ontogeny factors ranged from 8 to 48 % (Figure 4.6). Ontogeny factor differences were more prominent in neonates, infants and young children (i.e. age 0 to 6 years). The prediction of fup_{child} is a function of the ontogeny factor and also the degree of binding of a compound to plasma proteins which is reflected by the fup_{adult}. In this section, we evaluated how the choice of ontogeny model influences the fup_{child} estimates for high and

low binding compounds. Fup_{child} values were simulated based on the maximum and minimum ontogeny factor vs. age profiles plus the fup_{adult} values (Figure 4.7 - 4.8).

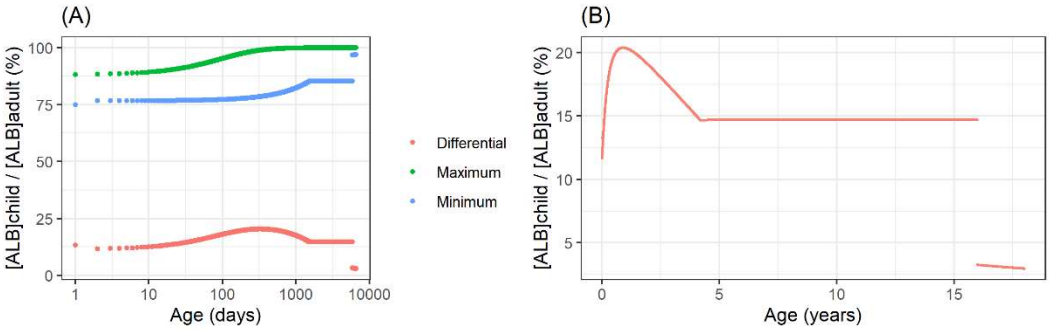

Figure 4.5 Differential ontogeny factors as a function of age between ontogeny models in (A) logarithmic and (B) linear scales. Green and blue dots represent the maximum and minimum ratio differences at a specific age, respectively. The red dots are the differences between the maximum and the minimum ratio differences. The schematic (B) presents the differences between the maximum and the minimum ratios vs. age (in years) profile.

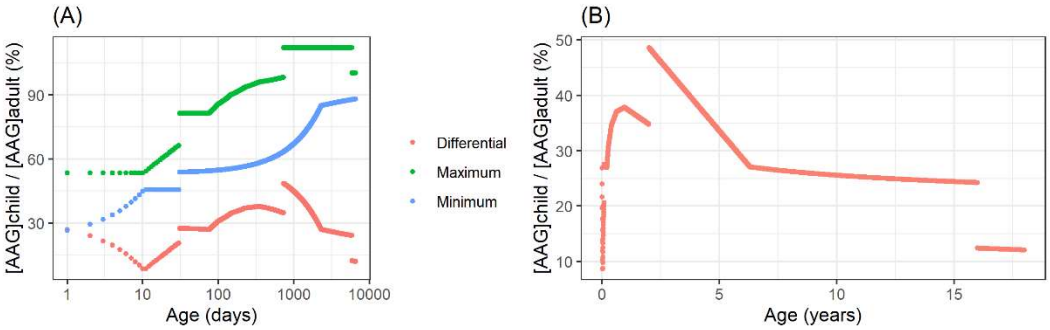

Figure 4.6 Differential ontogeny factors as a function of age between ontogeny models in logarithmic scales. Green and blue dots represent the maximum and minimum ratio differences at a specific age, respectively. The red dots are the differences between the maximum and the minimum ratio differences. The schematic (B) presents the differences between the maximum and the minimum ratios vs. age (in years) profile.

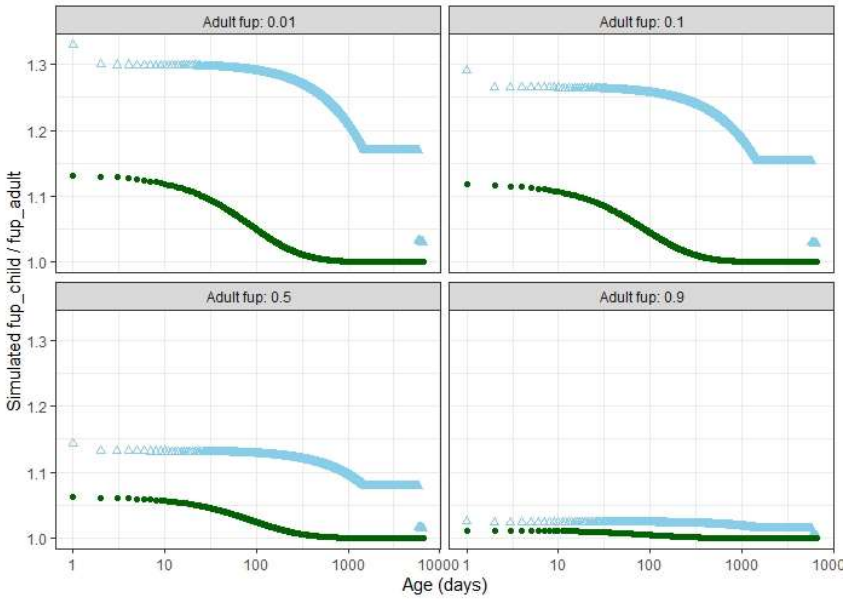

Figure 4.7 Simulated fup_{child} values based on the maximum or the minimum possible albumin concentration ratios (i.e. $[ALB]_{child}/[ALB]_{adult}$) of models. The simulated fup_{child} normalized by fup_{adult} values of 0.01, 0.1, 0.5 and 0.9. The blue triangles are the simulated fup_{child} values with the possible minimum albumin ontogeny factors as a function of age. The green circles are the simulated fup_{child} values with the possible maximum albumin ontogeny factors as a function of age.

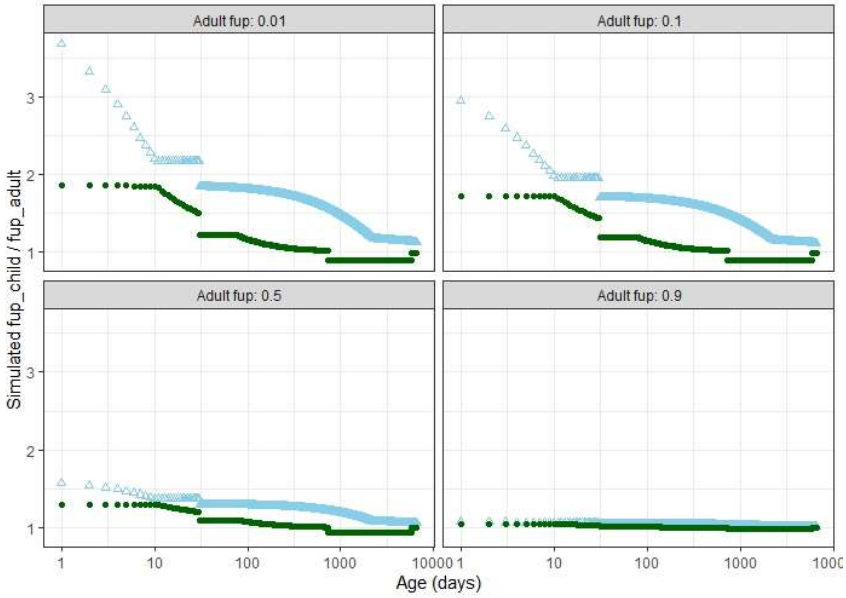

Figure 4.8 Simulated fup_{child} values based on the maximum or the minimum possible AAG concentration ratios (i.e. $[AAG]_{child}/[AAG]_{adult}$) of models. The simulated fup_{child} normalized by fup_{adult} values of 0.01, 0.1, 0.5 and 0.9. The blue triangles are the simulated fup_{child} values with the possible minimum AAG ontogeny factors as a function of age. The green circles are the simulated fup_{child} values with the possible maximum AAG ontogeny factors as a function of age.

In the case of high binding compounds where fup_{adult} values were 0.01 and 0.1, the deviation between the fup ratios (i.e. fup_{child}/fup_{adult}) calculated using the maximum and the minimum ontogeny factors were larger as compared to low-to-moderate binding compounds with fup_{adult} values of 0.5 and 0.9. The deviations in the fup ratios decreased as age increased. For AAG, the deviation in the fup ratio resulting from the wide differences in the ontogeny factors between models was larger than that of albumin. When a compound is highly bound with fup_{adult} of 0.01, the simulated fup ratios in all ages ranged from 1 to 3.7 for AAG models whereas the fup ratios for albumin models ranged from 1.1 to 1.3.

4.3.3 Predictive performance of ontogeny models

In order to evaluate predictive performances of ontogeny models, a total of 61 compounds data was gathered. The summary of chemical properties was listed in Supplementary materials (Table S3, Figure S1). In this data set, there were 24 acids, 24 bases and 13 neutrals. The mean and standard deviation values of lipophilicity (LogP) and molecular weight were 2.2 ± 1.6 and 385.6 ± 223.3 da, respectively.

The fup_{child} predictions for compounds bound to albumin based on four ontogeny models were comparable with similar AFE values across age groups (Table 4.3). For the majority of compounds, the fup_{child} values were under-predicted (Figure 4.9A) with AFE values ranging from 0.79 ~ 0.81. The fup values were under-predicted in neonates, and a higher variability in the prediction errors in neonates was also observed as compared to other age groups (Figure 4.9B).

Table 4.3 Predictive performance of albumin ontogeny models in predicting fup_{child}

	data	McNamara & Alcorn 2002	Johnson et al. 2006	McNamara & Meiman 2019	PK-Sim	Average
RMSE	All	0.07	0.07	0.07	0.08	0.07
R2	All	97.9	97.9	97.9	97.8	95.8
MAE (%)	All	4.5	4.6	4.5	5.5	4.8
mean absolute RPE (%)	All	23.1	23.2	23.8	26.8	24.2
AFE	All	0.81	0.79	0.81	0.73	0.79
AAFE	All	1.32	1.34	1.34	1.42	1.36
AFE	Highly binding compounds	0.79	0.76	0.79	0.69	-
AAFE	Highly binding compounds	1.39	1.41	1.41	1.5	-
AFE	Low to moderately binding compounds	0.87	0.86	0.88	0.82	-
AAFE	Low to moderately	1.16	1.17	1.16	1.22	-

	binding compounds					
AFE	Healthy subjects	0.87	0.85	0.86	0.78	-
AAFE	Healthy subjects	1.25	1.24	1.25	1.33	-
AFE	Patients	0.7	0.66	0.7	0.62	-
AAFE	Patients	1.53	1.58	1.57	1.66	-
R2 (%)	QSPR-predicted fup_{adult} as input	58.6	59.3	59	58.6	58.9
MAE (%)	QSPR-predicted fup_{adult} as input	12.4	12.2	12.3	12.3	12.3
AFE	QSPR-predicted fup_{adult} as input	1.35	1.3	1.34	1.2	1.3
AAFE	QSPR-predicted fup_{adult} as input	2.24	2.22	2.23	2.2	2.22

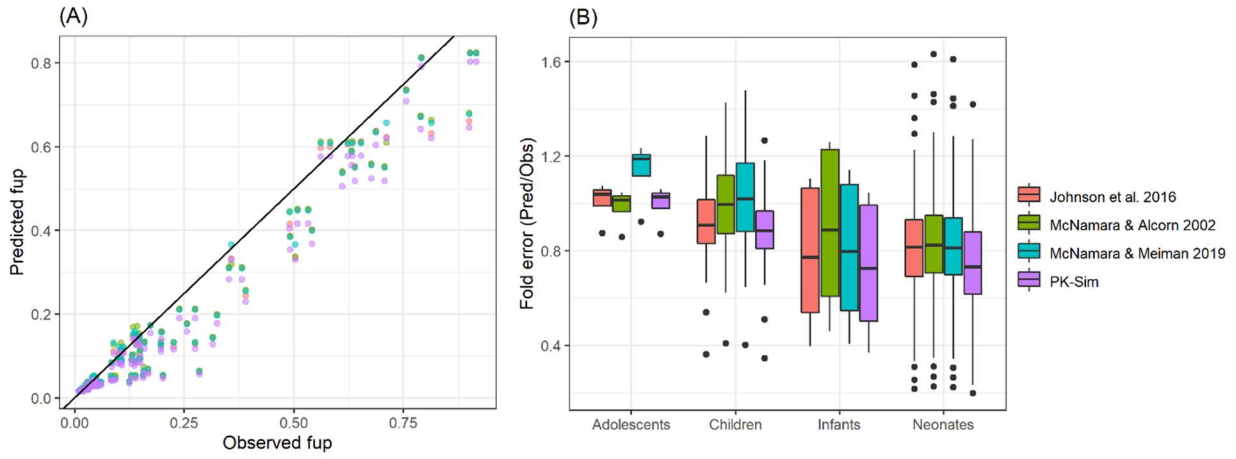

Figure 4.9 (A) Comparison of predicted and the observed fup_{child} values for albumin binding compounds. Dots are fup_{child} values calculated using different ontogeny models and the line is the line of unity. (B) Comparison of fold error values with respect to age groups.

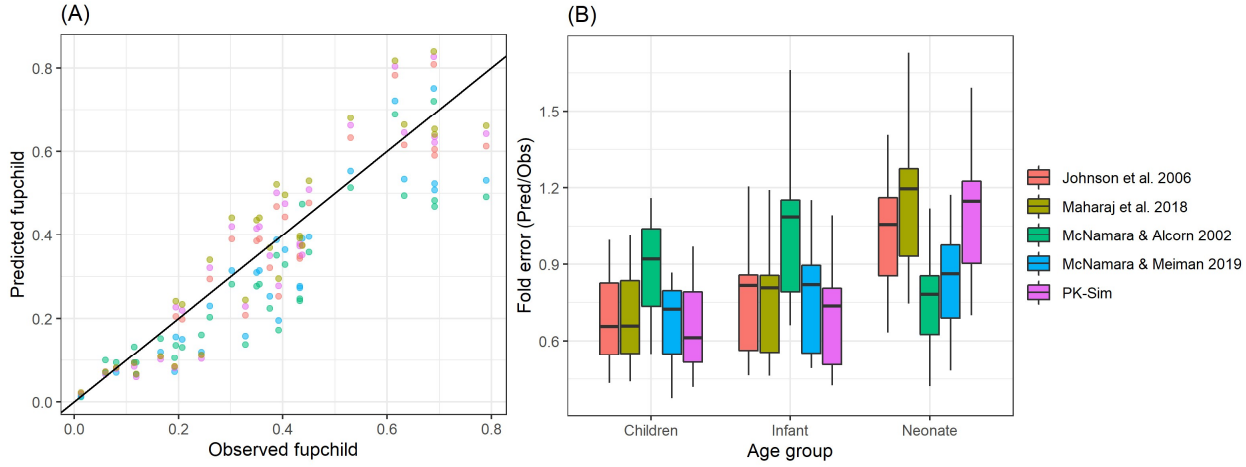

Figure 4.10 (A) Comparison of predicted and the observed fup_{child} values for AAG binding compounds. Dots are fup_{child} values calculated using different ontogeny models and the line is the line of unity. (B) Comparison of fold error values with respect to age groups.

For compounds bound to AAG, the fup_{child} values were under-predicted with AFE values ranging from 0.77 ~ 0.97 (Table 4.4, Figure 4.10). Overall, PK-Sim [166], Johnson et al. [243] and Maharaj et al. [244] resulted in similar predictive performances with similar RMSE, R^2, AFE and AAFE values (n=29). Highly bound compounds (i.e. $0.01 < fup_{adult} \leq 0.2$) had lower AFE and higher AAFE as compared to low-to-moderate binding compounds (i.e. $0.2 < fup_{adult}$).

Table 4.4 Predictive performance of AAG ontogeny models in predicting fup_{child}

	Data type	McNamara & Alcorn 2002	Johnson et al. 2006	McNamara & Meiman 2019	PK-Sim	Maharaj et al. 2018	Average
RMSE	All	0.12	0.09	0.11	0.09	0.09	0.1
R2 (%)	All	78.1	84.8	83.1	84.6	84.8	83.1
MAE (%)	All	9.7	7.1	8.4	7.6	7.7	8.1
mean absolute RPE (%)	All	26.9	20.5	23.7	22.5	23	23.3
AFE	All	0.78	0.89	0.77	0.92	0.97	0.87
AAFE	All	1.38	1.26	1.34	1.29	1.28	1.31
AFE	Highly binding compounds	0.74	0.82	0.7	0.84	0.9	-
AAFE	Highly binding compounds	1.48	1.33	1.46	1.36	1.34	-
AFE	Low to moderately binding	0.85	1.02	0.9	1.06	1.09	-

	compounds						
AAFE	Low to moderately binding compounds	1.23	1.16	1.18	1.18	1.19	-
AFE	Healthy subjects	0.75	0.96	0.8	1.01	1.06	-
AAFE	Healthy subjects	1.41	1.22	1.31	1.23	1.24	-
AFE	Patients	0.87	0.71	0.69	0.67	0.72	-
AAFE	Patients	1.28	1.41	1.46	1.49	1.42	-
R2	QSPR-predicted fup_{adult} as input	47.9	63.4	59.4	65.5	65.5	60.3
MAE (%)	QSPR-predicted fup_{adult} as input	12.6	10.9	10.5	11.4	12.2	11.5
AFE	QSPR-predicted fup_{adult} as input	0.98	1.11	0.97	1.15	1.2	1.08

AAFE	QSPR-predicted fup_{adult} as input	1.56	1.37	1.41	1.37	1.39	1.42

4.3.4 Evaluation of the overall uncertainty of using QSPR predicted fup values for predicting fup_{child}

When QSPR-predicted fup_{adult} values were compared to the observed fup_{adult} values, the MAEs were 10.4 % and 13.4 % for albumin and AAG binding compounds, respectively (Table 4.5). Although both under- and over-predictions were observed (Figure 4.11), over-predictions were prominent with the AFE values of 1.44 and 1.25 for albumin and AAG bound compounds, respectively. The AAFE values were 2.04 and 1.93 for albumin and AAG binding compounds, respectively.

Table 4.5 Predictive performance of QSPR model in predicting fup_{adult}

	Evaluation metric	**value**
Albumin binding compounds (n=51)	RMSE	0.15
	R2	0.58
	MAE(%)	10.4
	mean absolute RPE (%)	126.5
	AFE	1.44
	AAFE	2.04
AAG binding compounds (n=24)	RMSE	0.17
	R2	0.34
	MAE(%)	13.4

	mean absolute RPE (%)	88.2
	AFE	1.25
	AAFE	1.93

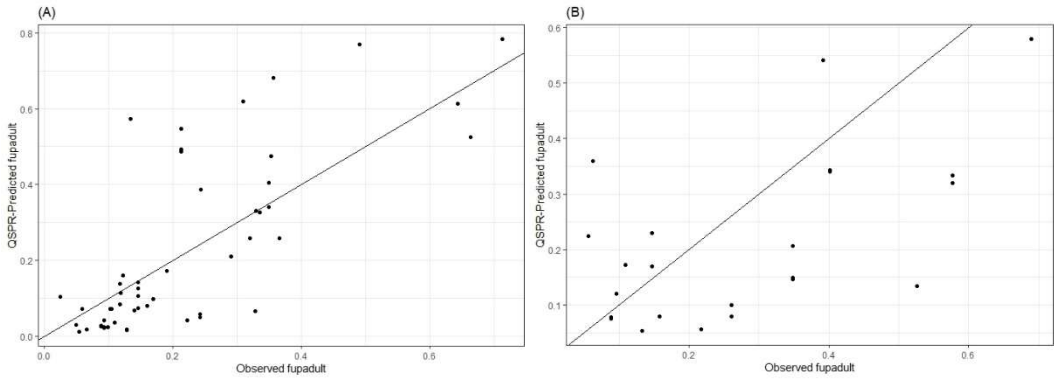

Figure 4.11 Comparison of QSPR-predicted and the observed fup_{adult} values for (A) albumin and (B) AAG binding compounds. Dots are fup_{adult} values and the line is the line of unity.

Assuming a human fup is equivalent to that of a fup_{adult}, the fup_{child} values were calculated using the ontogeny models with QSPR-predicted-fup_{adult} values as inputs. In order to evaluate the overall uncertainty of using QSPR-predicted fup_{adult} values as inputs, the average values of evaluation metrics (i.e. R2, MAE, AFE and AAFE) of models was compared when observed fup_{adult} vs. when QSPR-predicted fup_{adult} were used to calculate fup_{child} (Table 4.3). For compounds bound to albumin, on average, the coefficient of determination between predicted vs. observed fup_{child} values was decreased by 37% when QSPR-predicted fup_{adult} was used. MAE increased by 7.5%. AFE on average increased by 0.51 indicating that QSPR-predicted fup_{child} values were over-predicted (AFE: 1.2 ~ 1.35) compared to the fup_{child} that was derived from the observed fup_{adult} (AFE: 0.79 ~ 0.81).

For compounds bound to AAG, on average, the MAE value increased by 3.4 %, the AAFE increased by 0.11 and coefficient of determination decreased by 23 % (Table 4.4). AFE was increased by 0.2

indicating that QSPR-predicted fup_{child} values (AFE: 0.77 ~ 0.97) were on average over-predicted by 20% when compared to the observed fup_{adult} values that were used as inputs (AFE: 0.98~1.2).

4.4 Discussion

Ontogeny models describing plasma protein concentrations as a function of age are a critical component in pediatric PBPK modeling as they provide an estimate of fup_{child}. According to the established workflow in Maharaj and Edginton [47], pediatric PBPK models are extrapolated from the PBPK model in adults. The fup_{adult} is subjected to the ontogeny equations to estimate fup_{child}. The results of a sensitivity analysis within pediatric PBPK models revealed that fup was one of the most important input parameters, with importance to systemic distribution and clearance for low to moderately extracted compounds [70, 180]. This indicates that the confidence in the pediatric PBPK model outputs are dependent on the accuracy of fup_{child}. In light of this, we evaluated the appropriateness of the concentrations of albumin and AAG vs. age profiles and predictive performance of ontogeny models. In addition, we examined an overall uncertainty of the combined use of QSPR approach and ontogeny model in predicting fup_{child}.

These ontogeny models for albumin or AAG binding compounds are largely different in their mathematical structures. Johnson et al. [243] and PK-Sim [166] both adopted non-linear equations assuming that the predicted protein concentrations increase steeply during the neonatal and infant periods. In contrast, McNamara and Alcorn [25] employed a linear equation to describe age-dependent changes in protein concentrations and McNamara and Meiman [211] used a fixed concentration ratio for each age group. The observed protein concentration data shown in Figure 4.2 and 4.4, Table S1 and S2 was used in at least one model development process except for that of Weaving et al. [247], which presented albumin concentration data at 1 year and above. These plasma protein concentration data was used as a means to assess the appropriateness of a curve shape (i.e. continuous vs. discontinuous, linear vs. non-linear) and physiological relevance of the predicted protein concentration vs. age profiles.

Albumin plasma concentrations at birth (i.e. full-term neonate), depending on the model, are between 74% to 88% of those in adults, which is similar to observed values (i.e. measured in cord plasma or serum of neonates) of 80 ~ 81% [25, 248]. In terms of infants and children, both the albumin concentration vs. age profiles of PK-Sim [166] and Johnson et al. [243] were in line with the observed

concentration data. However, the projection of albumin concentration vs. age for PK-Sim [166] was slightly higher than in the other models, especially in neonates. In the case of both the McNamara and Alcorn [25] and the McNamara and Meiman [211] models, the predicted albumin concentrations in the neonate and infant period (i.e. age 0 -2) were in agreement with the observed data. However, predicted albumin concentrations in children were lower than observed.

AAG plasma concentrations at birth are relatively immature with, depending on the model, between 28 to 53% of those in adults. This is in line with observed ratios of AAG plasma concentrations in neonates at birth relative to adults of 33 to 46 % [25, 242, 249]. In terms of the McNamara and Alcorn [25] and the McNamara and Neiman [211] models, the predicted AAG concentration ratios in neonates were higher than those of the other models (Figure 4.3). This over-estimation in the concentration ratios resulted in an under-prediction in neonate fup values (Figure 4.10). On the other hand, throughout the pediatric period, the predicted AAG concentrations derived from PK-Sim [166], Johnson et al. [243] and Maharaj et al. [244] were in line with the observed data. This indicates that those models are physiologically relevant and can reasonably describe the age-dependent maturation of the AAG levels. This agreement in turn contributed to a better overall prediction performance with AAFE values ranging from 1.26 to 1.29 compared to AAFE values of 1.34 and 1.38 in the other models.

Depending on the ontogeny model used, the predicted fup in neonates can differ from fup_{adult} values up to 1.3 fold for albumin (Figure 4.7) and 3.7-fold for AAG (Figure 4.8). The discrepancy between the AAG ontogeny models was more prominent than the albumin models with the difference of the ontogeny factors ranging from 20 to 48 % in the neonate and infant periods (Figure 4.6). The large deviation between AAG concentrations vs. age profiles of each model is attributed to the lower AAG levels of the McNamara and Alcorn [25] model compared to the non-linear models such as the Johnson et al. [243], Maharaj et al. [244] and PK-Sim [166]. Furthermore, the discrepancy between models is greatest when fup_{adult} is low with little difference when fup_{adult} is high. As such, it is expected that the choice of ontogeny model is most important to the confidence in pediatric PBPK model outputs when the compound is bound to AAG, the child is a neonate and the compound is highly bound. The choice of model is much less important, regardless of age, if the compound is albumin bound and/or has low binding to either AAG or albumin.

Based on the test set of compound data obtained from the literature, it was found that the ontogeny models under-predicted fup_{child} with the average AFE values of 0.79 and 0.87 for albumin and AAG ontogeny models, respectively. According to Figure 4.9B, albumin ontogeny models under-predicted fup_{child} for neonate and infants compared to children and adolescent groups. Possible reasons for this under-estimation of fupchild are manifold. First, fetal albumin has a lower binding affinity for weakly acidic compounds, therefore the presence of fetal albumin in neonates may lower the degree of protein binding [24, 250]. Fetal albumin is replaced by albumin at 3-4 weeks of age. Second, the binding capacity of plasma proteins is reduced in neonates. It was suggested that endogenous molecules such as non-esterified fatty acids may lower the binding capacity of albumin [179, 251-253]. Furthermore, high concentrations of other blood constituents such as bilirubin and free fatty acids may displace a compound from albumin [24, 252, 254]. These qualitative differences in protein binding may violate the assumptions of ontogeny models and subsequently lead to less accurate fup_{child} prediction. More research is needed to elucidate how the levels of impeding endogenous substances affect protein binding in neonates.

In addition, we evaluated the predictive performance of the models using fup_{child} data of patients requiring a drug administration for treatment purposes in clinical studies. The identification of disease status of the patients and how it may alter the plasma protein concentration levels was beyond the scope of our investigation. However, we could not rule out that the underlying physiological condition of the subjects may have influenced the protein concentrations, thereby affecting fup_{child} values. In the case of McNamara and Alcorn [25], for the period of infants, children and adolescents, both predicted albumin and AAG concentration levels were lower than the rest of the models. The prediction error was low for patients (Table 4.3-4.4) compared to other models with the AAFE values of 1.53 and 1.28 for both the albumin and AAG models, respectively. This implied that the altered protein concentration levels due to a possible disease effect in patients better matched with the protein concentration vs. age profiles of McNamara and Alcorn [25].

Currently available protein ontogeny models predict fup_{child} based on age-dependent maturation of albumin or AAG concentrations in children, however, some compounds bind preferentially to other proteins. For example, lipophilic bases and neutrals such as probucol bind extensively to lipoproteins [235, 255]. Many environmental contaminants such as polychlorinated biphenyl (PCB),

Dichlorodiphenyltrichloroethane (DDT), benzo-a-pyrene (BAP) bind to both albumin and lipoproteins [256-258].

Lipoproteins are heterogeneous, vary in size and in lipophilic contents [259]. The concentration of lipoproteins is smaller than that of albumin [low density lipoprotein (LDL, 0.23-0.35 g/dL), high density lipoprotein (HDL, 0.1-0.2 g/dL) and very-low density lipoprotein (VLDL, <0.05 g/dL), albumin (3.5 – 5.5 g/dL)] [179, 233, 259, 260]. Incorporation of lipoprotein binding may help improve fupchild prediction for those compounds that preferentially bind to lipoproteins, however, observed fup_{child} for compounds preferentially bind to lipoproteins are not available.

The ontogeny models are thought to be crucial for human health risk assessment applications. The accuracy of these models is of the utmost importance because they contribute to the evaluation of pharmacokinetic variability in the health risk assessment for children. The use of an under-estimated fup_{child} in PBPK modeling would result in an under-estimation of clearance for low-to-moderately extracted compounds and volume of distribution. This would then lead to an over-estimation of the area under the curve of the plasma concentration vs. time profile (AUC). These inaccurate PK predictions would then lead to an inadequate determination of a toxicology index such as tolerable daily intake (TDI) in the human health risk assessment for children.

Due to the scarcity of the observed fup_{child} data, the results of prediction performance on this data set should be interpreted with caution as another test set of compounds may result in a different prediction performance depending on the chemical properties of the compounds being used. Furthermore, evaluating the appropriateness of the protein concentrations vs. age profile is more important than comparing the models' predictive performances alone. Compared to the albumin data, the availability of AAG concentration data and observed fup_{child} for AAG binding compounds were limited. It is thought that more observed AAG concentrations and fup_{child} data in heathy individuals will help in evaluating the appropriateness of the AAG concentration vs. age profile and the prediction accuracy of the AAG ontogeny models.

The findings of this study provide sufficient evidence that albumin ontogeny models are physiologically relevant and are likely to result in consensus estimation with a reasonable prediction accuracy when fup_{adult} is available. Even though AAG models presented a larger model discrepancy in predicting protein concentration ratios (i.e. $[AAG]_{child}/[AAG]_{adult}$), the non-linear models of PK-Sim

[166], Johnson et al. [243] and Maharaj et al. [244] were expected to produce consensus fup_{child} estimation. Overall, the use of QSPR-predicted fup_{adult} as an input decreased prediction accuracy, indicating that an experimental determination of fup in adults is, at minimum, required for PK prediction in children. The prediction of fup_{child} for highly binding compounds can be more sensitive to the appropriateness of the projected protein concentration vs. age profiles, especially in the neonate and young infant periods. Therefore, for these compounds and scenarios, experimental determination of fup_{child} for inclusion into a pediatric PBPK model is necessary to have confidence in PBPK model outputs.

Chapter 5: Prediction of Fraction Unbound in Plasma in Children in Data-limited Scenarios for Human Health Risk Assessment

5.1 Introduction

Exposure of children to environmental chemicals is an active area of research in human health risk assessment. The characterization of toxicokinetic (TK) behavior in humans, such as absorption, distribution, metabolism and excretion (ADME) of environmentally relevant compounds, is ethically restricted in vulnerable populations. When children are exposed to environmental toxicants, their immaturity in anatomy and physiology can lead to higher blood concentration levels and a longer duration of the toxicant in the body compared to adults [20, 261]. Regulatory agencies face challenges in identifying associated human health risks [262] and there are only a fraction of compounds with well-characterized chemical safety profiles [262, 263]. In most cases, human exposure data to environmental chemicals is not available [264]. Furthermore, limited data availability (i.e. data-poor compounds) can hinder prompt response for appropriate and timely regulatory decisions.

In order to overcome the challenge, regulatory agencies such as US Environmental Protection Agency (EPA) and European Commission's Joint Research Centre have adopted and utilized computational toxicology to make the most of the best available science to protect the environment and human health. The computational toxicology initiative proposed by these agencies is described in review articles [262, 265, 266]. Briefly, the Joint Research Centre encourages developing, evaluating and implementing computational methods for regulatory assessment. Actions involve (i) developing publically available computational programs to evaluate chemical toxicity based on chemical properties and (ii) constructing regulatory guidance on the use of those programs [265]. In light of EPA's mandate to apply the best available science to human health risk assessment, computational toxicology (CompTox) research program and Toxicity Forecaster (ToxCast) project were developed. The agency's missions through these initiatives involve interdisciplinary integration of sciences to evaluate chemical safety in efficient and economical manner [262].

One important quantitative computational toxicology tool is the use of physiologically based pharmacokinetic (PBPK) modeling. In children, PBPK models can facilitate the prediction of PK parameters under specific exposure conditions [45, 51, 58]. In human health risk assessment, PBPK

modeling has been used to indicate chemical-specific human toxicokinetic adjustment factors (HKAF) [10]. Pediatric PBPK models provide an estimation of the pharmacokinetic inter-individual variability in children as well as predicting the HKAF. The HKAF is a ratio of the 95th percentile PK parameter in a pediatric group and 50th percentile PK parameter in an adult population [6, 13].

From a previous study of pediatric PBPK model qualification for cytochrome P450 (CYP) metabolized compounds [180], the fraction unbound in plasma value (fup) in children was one of the most critical input parameters for the estimation of exposure. This indicates that an accurate determination of fup in children (fup_{child}) is critical for predicting the PK in children. When an experimentally determined fup in adult (fup_{adult}) of a compound is available, the precision of the fup_{child} estimate will depend on the predictive performance of the ontogeny model (adult to child scaling model). This ontogeny model is a function of the plasma albumin or alpha-acid glycoproteins (AAG) concentrations at a specific age and fup_{adult} [25, 211, 243, 244]. Ontogeny models were developed based on the correlation between the increase in plasma albumin and AAG levels with age and fup values [25, 267]. In fup_{child} prediction, the protein maturation in protein binding levels is taken into account by applying the ratio of protein concentrations at a specific age and the ratio of protein concentrations vs. age profiles determine the prediction accuracy of the protein binding ontogeny models.

When the experimentally determined value of the fraction unbound in plasma in adults is not available, the input parameter can be estimated using a computational method which is known as predictive quantitative structure-property relationship (QSPR) modeling. Recent QSPR models [186, 194] employ machine learning techniques to predict the fup from chemical structures and properties. For this, various software (e.g. PaDel [196], Molecular Operating Environment (MOE, Chemical Computing Group)) is available to determine chemical descriptors and physicochemical properties. For data-poor chemicals, the use of predicted chemical properties from a compound structure such as lipophilicity, ionization state at physiological pH as well as fup can aid in the prediction of children PK. It was found from the previous investigation [268] that currently available QSPR models for predicting fup resulted in comparable prediction performances with mean absolute error values ranging from 12.6 ~15.9 %. The commercially available ADMET Predictor resulted in a slightly better prediction performance and, therefore, was chosen for evaluation in this study.

In this study, we will focus on the evaluation of the prediction of plasma protein binding in children for data-limited applications with data-rich compounds. The objectives of this study are (i) to evaluate the uncertainty of the ontogeny models in different data availability scenarios and (ii) to evaluate how these different data availabilities can impact the over-all prediction accuracy of protein binding estimates in children. In addition, the prediction error due to ontogeny model misspecification will also be assessed. This data availability scenario-based evaluation will provide an understanding of what chemical-specific information is necessary to reduce uncertainty in pediatric PK prediction.

5.2 Methods

5.2.1 Data collection

The observed fup_{child} and fup_{adult} values were obtained from MEDLINE database by searching relevant keywords, e.g. 'fraction unbound in plasma in infants' and 'protein binding in children'. Pediatric data was classified into four age groups such that neonates were 0 to ≤1 month, infants were 1 month to ≤2 years, children were 2 years to ≤12 years and adolescents were 12 years to ≤18 years. Age in years or months was converted to postnatal age (PNA) in days. The data presented in graphs was obtained by digitizing data points using the Plot-digitizer (ver 2.6.8). Relative differences between observed fup_{child} and fup_{adult} values were calculated by using the following equation (Eqn 1).

Eqn 1. $Relative\ difference\ = \frac{fup_{child} - fup_{adult}}{fup_{adult}} \cdot 100\ (\%)$

Human fup values were calculated using the ADMET predict function (ADMET Predictor™, Simulations Plus, Inc., Lancaster, California, USA). The estimated fup value in human value was assumed to be equivalent to fup_{adult}. The input of 2-dimensional structural data files were obtained from PubChem [206]. Along with human fup values, chemical descriptors such as lipophilicity, the fraction of anion, and the fraction of cation were calculated by using the ADMET Predictor.

Acid-base properties were then obtained by using the same criteria described in Ingle et al. [186] and were applied to determine acid, base, neutral and zwitterion. Briefly, the ionization state at a physiological pH of 7.4 was calculated by using the ADMET Predictor. When fractions of anion or cation of a compound exceeded 10 %, they were classified as an acid or a base, respectively. When a fraction of anion and cation of a compound was less than 10%, it was classified as a neutral

compound and when both a fraction of anion and a fraction of cation exceeded 10%, it was classified as a zwitterion.

5.2.2 Calculation of fup_{child} values

Fup_{child} values were calculated as a function of fup_{adult} and the protein concentration ratios between adults and children by using the following equations (Eqn 2) [25]. [P] is the concentrations of protein.

Eqn 2. $$fup_{child} = \frac{1}{1+\frac{[P]_{child}}{[P]_{adult}} \cdot \frac{(1-fup_{adult})}{fu_{adult}}}$$

The protein concentration ratio between children and adults ($\frac{[P]_{child}}{[P]_{adult}}$) can be determined with respect to the plasma protein to which a compound primarily binds. The protein concentration ratios vs. age profiles that were derived from albumin and AAG ontogeny models were plotted for comparison. With the albumin models, the albumin level in neonates was 75 ~88% of the adult level (Figure 5.1). The ratio of albumin incrementally increased throughout the pediatric period (i.e. age from birth to 18 years). The AAG ontogeny models projected the AAG level in neonates to be 25% of the adult level. There was a steep increase in the AAG level in the first year of life and it then reaches the plateau in older children and the adolescent periods (age from 10 to 18 years).

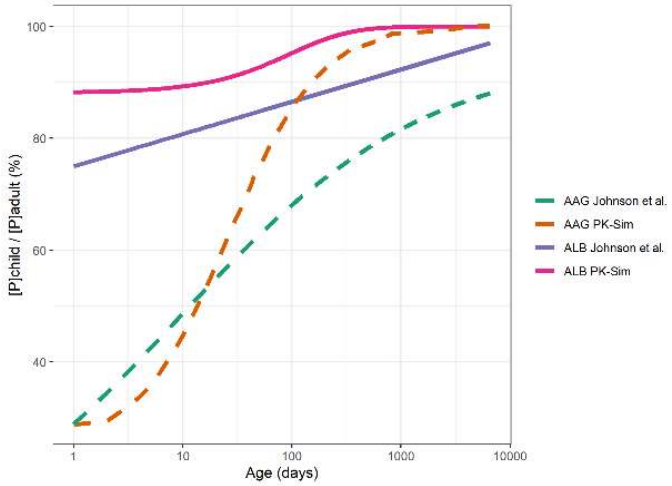

Figure 5.1 The protein concentration ratios between children and adults vs. age profiles derived from ontogeny models in logarithmic scale. ALB and AAG refer to albumin and alpha-acid glycoprotein ontogeny models, respectively.

Bases preferentially bind to AAG, and acids and neutrals bind to albumin [179, 233, 269]. When the protein binding partner information is not available, an AAG ontogeny model was used for bases and an albumin ontogeny model was used for acids and neutrals. In terms of the input fup_{adult}, either an observed fup_{adult} value from literature or a QSPR-predicted fup in human value was used. Fup_{child} values were calculated using Johnson et al. [243] and PK-Sim ontogeny models [166] according to the following scenarios listed below (Method 1-6, Table 5.1). These ontogeny models were selected because, in our previous investigation [270], these models [166, 243] showed more physiologically relevant plasma protein concentrations vs. age profiles compared to other models [25, 211].

Table 5.1 Fup_{child} predictions in data availability specific scenarios

Available data	**Ontogeny models**	**Inputs for ontogeny models**
Specific binding protein information	ALB ontogeny models for ALB binding compounds AAG ontogeny models for AAG binding compounds	Observed fup_{adult} QSPR-predicted fup_{adult}
Acid-base properties	ALB ontogeny models for acids and neutrals AAG ontogeny models for bases	Observed fup_{adult} QSPR-predicted fup_{adult}

Method 1. $\frac{[P]_{child}}{[P]_{adult}}$ was estimated based on albumin concentrations using albumin ontogeny models for all compounds. For fup_{child} calculation, observed fup_{adult} was used.

Method 2. $\frac{[P]_{child}}{[P]_{adult}}$ was estimated based on AAG concentrations using AAG ontogeny models for all compounds. For fup_{child} calculation, observed fup_{adult} was used.

Method 3. For $\frac{[P]_{child}}{[P]_{adult}}$ estimation, the albumin ontogeny models were used for acids and neutrals and AAG ontogeny models were used for bases. For fup_{child} calculation, observed fup_{adult} was used.

Method 4. For $\frac{[P]_{chil}}{[P]_{adult}}$ estimation, the albumin ontogeny models were used for acids and neutrals and AAG ontogeny models were used for bases. For fup_{child} calculation, QSPR-predicted fup_{adult} was used.

Method 5. For $\frac{[P]_{child}}{[P]_{adult}}$ estimation, the albumin ontogeny models were used for albumin binding compounds and AAG ontogeny models were used for AAG binding compounds. For fup_{child} calculation, observed fup_{adult} was used.

Method 6. For $\frac{[P]_{child}}{[P]_{adult}}$ estimation, the albumin ontogeny models were used for albumin binding compounds and AAG ontogeny models were used for AAG binding compounds. For fup_{child} calculation, QSPR-predicted fup_{adult} was used.

Method 1 and 2 will show the prediction error associated with the misspecification of ontogeny models with respect to a lack of binding partner information. Method 5 shows the prediction error of ontogeny models when ontogeny models are applied based on known binding partner information and the experimentally determined fup_{adult} is used as an input. The comparison between Method 3 and 5 will indicate the prediction error associated with calculating fup_{child} based on the assumption that acids and neutrals bind to albumin and bases bind to AAG, when experimentally determined fup_{adult} is used as an input. The comparison between Method 5 and 6 will show the prediction error associated with calculating fup_{child} when QSPR-predicted fup_{adult} values are used for ontogeny model input.

5.2.3 Evaluation of predictive performance of the model

The predicted fup_{adult} and fup_{child} values according to the 6 scenarios listed above were then compared to the observed values. The equations for evaluation metrics for assessing the predictive performance of the model are listed below.

Eqn 3. Prediction error = $fup_{pred} - fup_{obs}$ where fup_{pred} and fup_{obs} are predicted and observed fup values, respectively.

Eqn 4. Relative prediction error (RPE) = $\frac{fu_{pred} - fup_{obs}}{fup_{obs}} \cdot 100\ (\%)$

Eqn 5. Mean absolute RPE = $\frac{\sum_1^n |RPE_i|}{n}$

Eqn 6. Mean absolute error (MAE) = $\frac{1}{n}\sum_{i=1}^{n}\left|fup_{pred,i} - fup_{obs,i}\right| \cdot 100\ (\%)$

5.3 Results

5.3.1 Comparison of the observed fup_{child} and fup_{adult} values based on chemical properties

From literature, 139 fup_{child} values were obtained from a total of 61 compounds [25, 211, 236, 242, 248, 258, 271-285]. When individual fup_{child} values were reported (e.g. [272]), mean fup_{child} values were used for the analysis in this study. The relationship between fup_{adult} and fup_{child} is mostly linear for acids and neutrals. For all compounds, fup_{child} values were higher than fup_{adult}. This trend was expected because the protein concentration in children is lower than in adults (Figure 5.1) and, therefore, children tended to have a higher fup value than the adults. Acids and neutrals tended to be highly binding to plasma proteins compared to bases such that both fup_{adult} and fup_{child} were less than 0.1 for 32.8% of acids, 51.1% of neutrals and 5.9% of bases (Figure 5.2A). Albumin binding compounds revealed a higher degree of protein binding compared to the AAG binding compounds (Figure 5.2B).

For moderately lipophilic compounds (0<logP<3), the relative differences of fup between adults and children were higher than those of acids and neutrals with higher median values in all age groups (Figure 5.3). For highly lipophilic compounds (LogP > 3), relative differences of bases and neutrals were higher than the acids. Hydrophilic compounds (LogP <0) tended to have higher relative differences in all age groups.

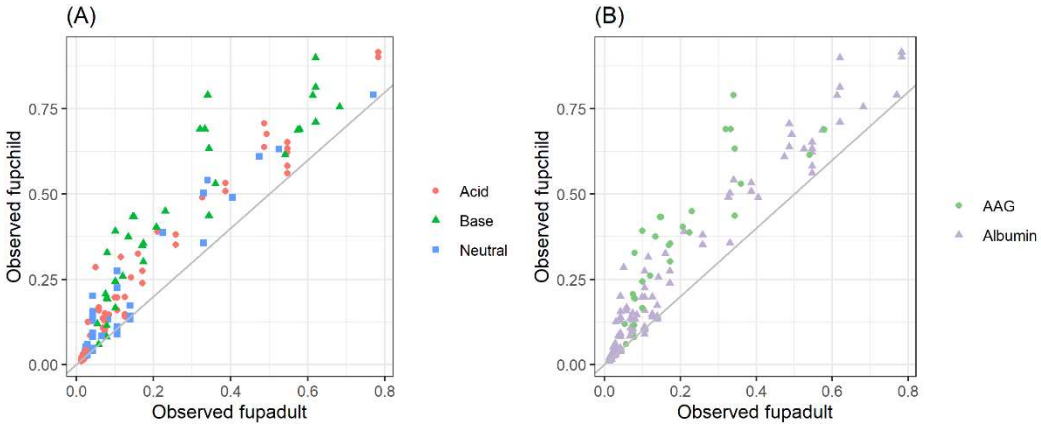

Figure 5.2 The relationship between observed fup_{child} and fup_{adult} on log-linear scale. Fup values were labeled based on (A) acid base properties and (B) specific binding protein. The line is the line of unity.

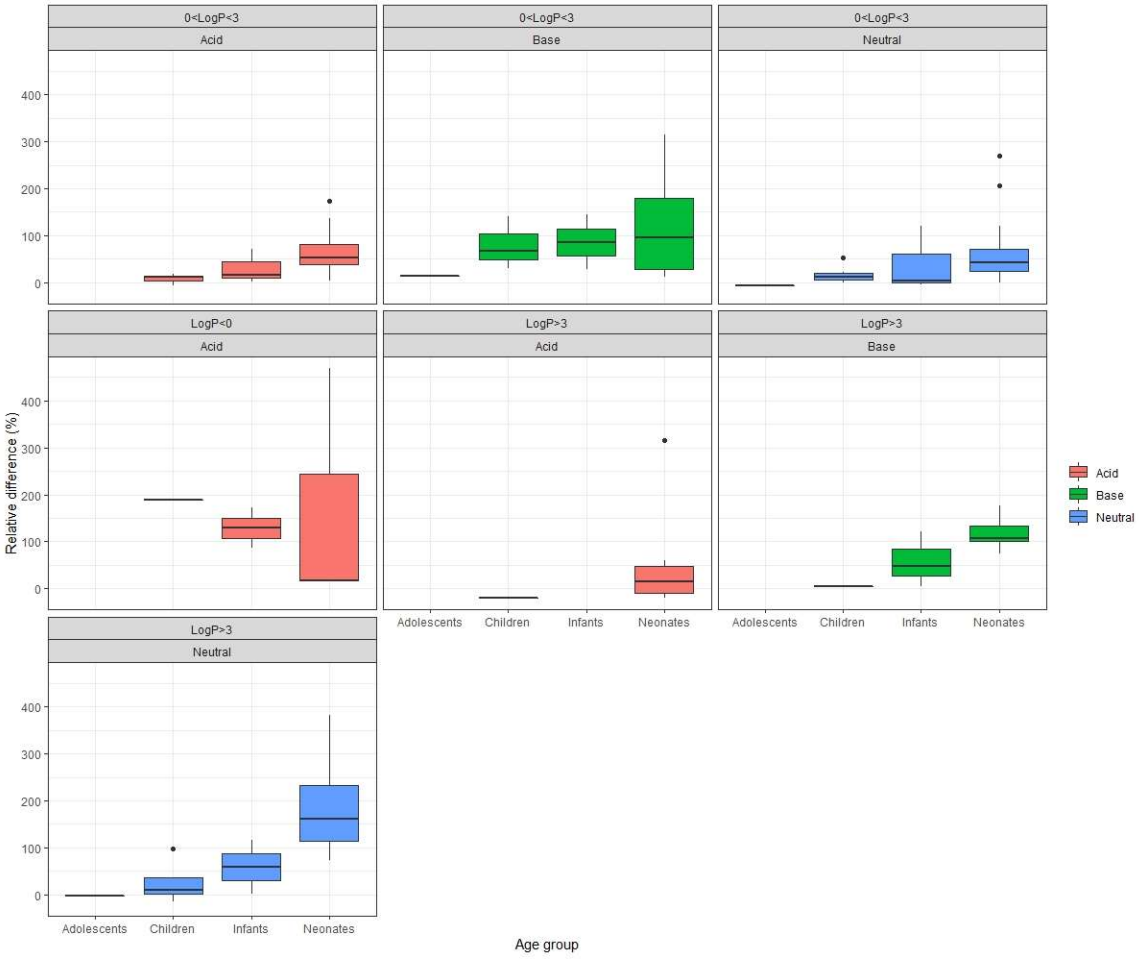

Figure 5.3 Comparison of relative differences between fup_{child} and fup_{adult} values as a function of chemical properties such as lipophilicity and acid-base properties.

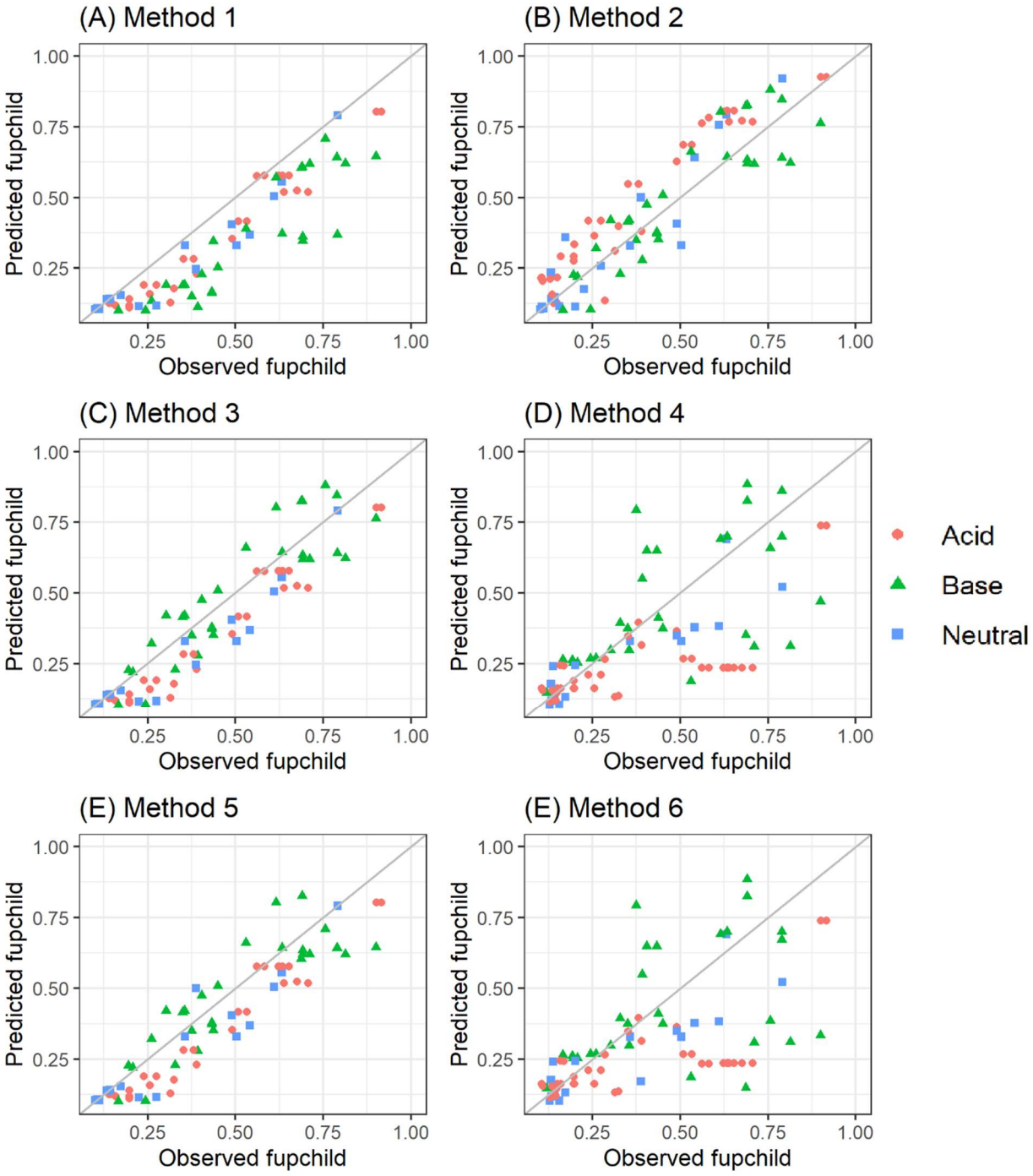

Figure 5.4 Comparison between observed fup_{child} values and QSPR-based fup_{child} calculated using PK-Sim according to different data-availability scenarios.

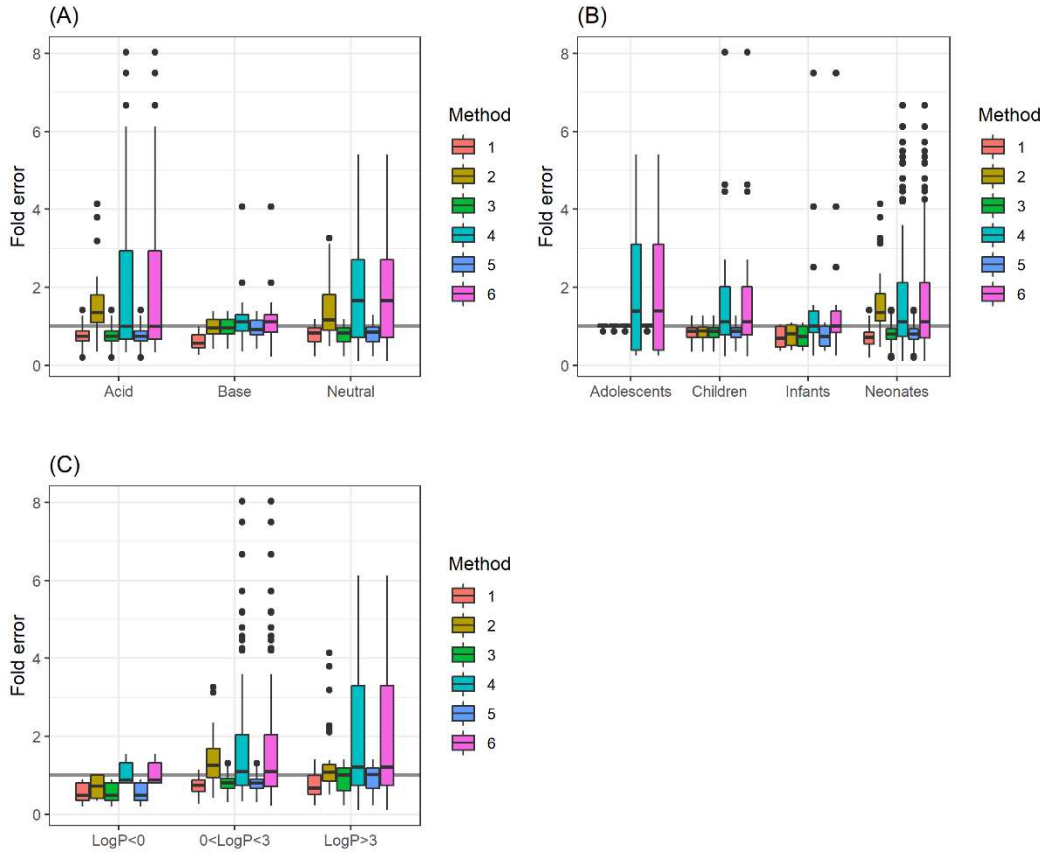

Figure 5.5 Comparison of predictive performance of protein binding ontogeny models as a function of (A) acid-base properties, (B) age group, and (C) lipophilicity.

5.3.2 Evaluation of the predictive performance of the model

When the albumin ontogeny equation was applied to calculate fup_{child} for all compounds (Method 1), fup_{child} values were under-predicted compared to observed fup_{child} with an AFE value of 0.68 for Johnson et al. [243] and an AFE value of 0.74 for PK-Sim [166] (Table 5.2 and 5.3, Figure 5.4A, Figure S1A). Fup_{child} values were slightly under-predicted for bases (Figure 5.5A).

When the AAG model was used to predict fup_{child} values for all compounds using fup_{adult} values as an input (Method 2, Figure 5.4B), a lesser degree of bias was observed with most fup values centered around the line of unity compared to the cases seen using the albumin models where the majority of

data points fell below the line of unity (Method 1, Figure 5.4A). Fup_{child} values were over-predicted especially for acids and neutrals with a fold error up to 4 (Figure 5.5A). In terms of Method 1 and 2, the degree of bias was greater in neonates than any other age group such that fup_{child} estimates were under-predicted with Method 1 and over-predicted with Method 2 (Figure 5.5B).

When the binding partner was assumed based on acid-base properties and the corresponding equations were applied to calculate fup_{child} using observed fup_{adult} as an input (Method 5.3, Figure 5.4C), the prediction accuracy was similar to the cases where fup_{child} values were calculated based on known binding partner information (Method 5.5, Figure 5.4E).

When QSPR-predicted fup_{adult} values were used as an input (Method 4 and 6), substantial over-prediction was observed for acids and neutrals up to an 8-fold of deviation from the observed values (Figure 5.4D, 5.4F, 5.5A). However, the degree of the over-prediction for bases was not as severe compared to the other groups of compounds. Lipophilic compounds tended to have a higher over-prediction in QSPR-predicted fup_{child} values than hydrophilic compounds (Figure 5.5C).

Table 5.2 Predictive accuracy according to different calculation methods for PK-Sim.

data	n	Evaluation metrics	Method 1	Method 2	Method 3	Method 4	Method 5	Method 6
Total	139	RMSE	0.11	0.09	0.08	0.17	0.08	0.17
	139	R2 (%)	90	90.6	92.1	57	92.1	52.9
	139	MAE (%)	7.7	7	5.9	11.7	5.9	12.1
	139	mean absolute RPE (%)	30.1	47.6	25.8	106.8	25.8	107.2
	139	AFE	0.68	1.18	0.76	1.2	0.76	1.19
	139	AAFE	1.5	1.46	1.39	1.98	1.39	1.99
	110	AFE	0.73	1.26	0.73	1.22	0.73	1.2

Albumin binding compounds	110	AAFE	1.42	1.52	1.42	2.16	1.42	2.2
AAG binding compounds	29	AFE	0.54	0.92	0.9	1.11	0.92	1.15
	29	AAFE	1.85	1.29	1.3	1.42	1.29	1.37
Acids	58	AFE	0.71	1.36	0.71	1.27	0.71	1.27
	58	AAFE	1.46	1.56	1.46	2.12	1.46	2.12
Bases	34	AFE	0.58	0.92	0.92	1.05	0.89	0.99
	34	AAFE	1.73	1.27	1.27	1.41	1.27	1.48
Neutral	47	AFE	0.73	1.19	0.73	1.23	0.74	1.25
	47	AAFE	1.41	1.51	1.41	2.33	1.41	2.28
Modately lipophlic compounds	101	AFE	0.7	1.24	0.77	1.22	0.76	1.2
	101	AAFE	1.44	1.45	1.35	1.86	1.35	1.9
highly-lipophlic compounds	32	AFE	0.68	1.14	0.82	1.15	0.84	1.19
	32	AAFE	1.6	1.49	1.44	2.6	1.43	2.52
Hydrophilic	6	AFE	0.48	0.63	0.48	1.02	0.48	1.02
	6	AAFE	2.1	1.6	2.1	1.29	2.1	1.29

compounds								

Table 5.3 Predictive accuracy according to different calculation methods for Johnson et al.

data	**n**	**Evaluation metrics**	**Method 1**	**Method 2**	**Method 3**	**Method 4**	**Method 5**	**Method 6**
Total	139	RMSE	0.10	0.08	0.07	0.16	0.07	0.17
	139	R2 (%)	90.8	91.5	93.5	58.4	93.7	55.2
	139	MAE (%)	6.7	6.1	5.2	11.6	5.1	11.9
	139	mean absolute RPE (%)	26.4	37.3	22.7	115.8	22.6	116.1
	139	AFE	0.74	1.1	0.81	1.27	0.81	1.26
	139	AAFE	1.41	1.39	1.33	2	1.33	2.01
Albumin binding compounds	110	AFE	0.79	1.17	0.79	1.32	0.79	1.3
	110	AAFE	1.34	1.42	1.34	2.19	1.34	2.22
AAG binding compounds	29	AFE	0.59	0.89	0.87	1.09	0.89	1.11
	29	AAFE	1.71	1.26	1.27	1.41	1.26	1.37
Acids	58	AFE	0.78	1.25	0.78	1.39	0.78	1.39
	58	AAFE	1.36	1.45	1.36	2.13	1.36	2.13

Bases	34	AFE	0.63	0.9	0.9	1.02	0.88	0.98
	34	AAFE	1.61	1.25	1.25	1.41	1.25	1.47
Neutral	47	AFE	0.78	1.1	0.78	1.31	0.79	1.34
	47	AAFE	1.35	1.42	1.35	2.38	1.34	2.34
Modately lipophlic compounds	101	AFE	0.76	1.16	0.82	1.3	0.81	1.28
	101	AAFE	1.35	1.36	1.28	1.88	1.28	1.91
highly-lipophlic compounds	32	AFE	0.73	1.07	0.85	1.2	0.87	1.23
	32	AAFE	1.54	1.43	1.39	2.64	1.38	2.58
Hydrophilic compounds	6	AFE	0.5	0.61	0.5	1.07	0.5	1.07
	6	AAFE	2	1.66	2	1.26	2	1.26

5.4 Discussion

Due to the difficulties in obtaining toxicology-relevant data in pediatric populations, in silico approaches such as QSPR or PBPK models can be a valuable aid in addressing the knowledge gaps by applying the best available science. These models are most needed for evaluating the health risk in children by predicting the dose-response relationships under various exposure scenarios. This is achieved by integrating age-specific physiological and anatomical parameters and chemical properties into the model (e.g. pediatric PBPK model of bisphenol A [51]) [12, 20]. When using computational toxicology methods for human health risk assessment purposes, it is important to characterize the

level of uncertainty and strength of these models based on the input data-availability. In this study, fup_{child} prediction in data-availability-specific scenarios was carried out for data-rich compounds. This was performed in order to identify the data-availability-specific uncertainty associated with the combined use of QSPR (i.e. predicting a degree of plasma protein binding from chemical structure) and ontogeny models (i.e. adult-to-children scaling).

Traditional plasma protein binding measurement methods include equilibrium dialysis, ultrafiltration and ultracentrifugation [179, 182]. These methods measure the overall degree of binding of compounds to plasma proteins and do not provide information about which plasma protein a compound preferentially binds to. In order to determine which protein a compound primarily binds (e.g. albumin binding or AAG binding), analyses such as affinity chromatography [183] and circular dichroism spectroscopy [286] are used and provide information on ligand-protein interactions and the compound binding to specific binding sites of albumin and AAG. These in vitro experimental analysis can be time-consuming and resource-intensive.

When experimental determination is not readily available, calculating the ionization state using chemical structural information can help to predict the primary binding partner as well as help to choose the right ontogeny model. Due to the microenvironment of binding sites of albumin and AAG, electrostatic interactions play a key role in compound binding. The binding site I and II of albumin are hydrophobic clefts and the hydrophobic force drives the binding of compounds to these sites [269, 287]. However, in terms of binding site II, there are positively charged residues at the entrance of the binding site which allow attractive electrostatic interactions with anionic compounds while contributing to repulsive interactions with cationic compounds [219]. In terms of AAG, there is one high-affinity binding site that is clinically relevant and six low-affinity binding sites [179, 233]. The binding sites of AAG have both polar (lobe I) and negatively charged residues (lobe II and III) [288]. In addition, the negatively charged carbohydrate and sialic acid portions of AAG contribute to attracting cationic compounds [233, 289]. Therefore, both electrostatic and hydrophobic interactions play a role in the binding of compounds to AAG. The similar prediction accuracies of calculation Method 3 and 5 indicate that choosing an ontogeny model based on acid-base property that is predicted from chemical structure is a reasonable alternative to experimental determination.

According to the previous investigation [270], the non-linear equations of Johnson et al. [243] and PK-Sim [166] were physiologically more relevant compared to the linear models of McNamara and Alcorn [25]. These non-linear equations are incorporated in the available PBPK modeling platforms such as PK-Sim. The results of this study indicated that these ontogeny models would provide a reasonable prediction of fup_{child} values as long as the fup_{adult} values were accurate (i.e. experimentally determined rather than computationally predicted).

Accurate determination of fup_{adult} is highly important to fup_{child} prediction. The use of QSPR-predicted fup_{adult} resulted in a larger deviation in fup_{child} estimates from the observed values compared to the cases where the ontogeny model was misspecified. In other words, the prediction accuracy of fup_{adult} is much more influential in fup_{child} estimates than the ontogeny model misspecification (e.g. using AAG equation for an albumin binding compound).

When QSPR-predicted fup_{adult} was used for acids and neutrals, the prediction errors were relatively higher compared to bases (Figure 5.5A, Method 4 and 6). The reason for this might be that in our test set, fup_{adult} values of acids and neutrals tend to be lower than that of bases. This was in line with the tendency presented by multiple researchers [187, 213, 290] that stated that compounds that are anionic and neutral at pH 7.4 showed higher protein binding compared to bases.

For bases, fup_{child} prediction via the combined use of the QSPR method and ontogeny model results were associated with the smallest error compared to the other classes of compounds. However, considering the over-prediction in fup_{adult} estimate with AFE of 1.32, the experimental determination fup_{adult} is still required to be confident in the PK prediction in children.

The European Medical Agency (EMA) advises determining free concentrations in neonates for highly binding compounds [291, 292]. Also, the US Food and Drug Administration (FDA) suggests characterizing the protein binding for highly binding compounds in neonates and to evaluate the potential impact on PK in neonates by applying modeling and simulation approaches such as PBPK modeling [293]. These guidelines are applicable to medicinal products. However, it is thought that the same should be applied for human health risk assessment purposes to appropriately protect this vulnerable population.

QSPR prediction of fup_{adult} is not optimal to use for PK prediction in children when precision is required [268, 270]. The results of this study demonstrated that an additional experimental step of assessing the primary plasma protein binding partner may not be necessary and prediction of acidic or basic ionization status at pH 7.4 was sufficient to select the most appropriate ontogeny model that could predict fup_{child} from fup_{adult}.

5.5 Declaration of Interest

The authors have no conflict of interest, financial or otherwise.

5.6 Author Contribution

Yejin Esther Yun: Conceptualization, Methodology, Data Curation, Formal analysis, Software, Investigation, Visualization, Writing - Original Draft

Andrea N. Edginton: Conceptualization, Investigation, Writing - Review & Editing, Supervision, Funding acquisition, Project administration

Chapter 6: Development of a Framework for Predicting Clearance in Children Using QSPR Models and Virtual Children in PBPK modeling

6.1 Introduction

In human health risk assessment, clearance (CL) is one of the crucial pharmacokinetic parameters as it a significant predictor of a compound's exposure in a system. As such, the prediction of clearance is important to characterize dose-response relationships.

Some methods for predicting human CL are interspecies scaling and in-vitro in-vivo extrapolation. In terms of interspecies scaling, human CL values can be estimated using in vivo experimental determination in preclinical species and human CL values can be extrapolated based on allometry. This interspecies extrapolation requires experimental determination in animals, which can be resource-intensive and time-consuming. Several equations are available to extrapolate human CL from animal CL values [294-296]. This approach assumes that clearance is a function of size or body weight. Allometric scaling of clearance can be useful in the situations where (i) compound disposition follows linear kinetics and (ii) the degree of plasma protein binding is similar in different species [297], and (iii) drug elimination is primarily via either the renal route or through metabolism [298].

Characterizing clearance of an environmentally relevant chemical in children is important for human health risk assessment [20, 299]. Children are a vulnerable population who often have a higher exposure compared to adults because of lower CL in the immature stages of life. The use of adult exposure estimates for children may result in under-estimating the risk associated with exposure to environmentally relevant chemicals [299]. Therefore, the reasonable estimation of CL in children is crucial for a successful human health risk assessment for children.

Clearance in children is predicted based on information of CL from adults as well as knowledge of CL mechanisms (e.g. major clearance pathway such as renal or hepatic). The information of a major clearance pathway is important because each clearance pathway matures at a different rate [171, 300].

This adult information on intrinsic clearances of each pathway can come from various sources. First, in vitro intrinsic hepatic clearance can be measured using hepatocytes or liver microsomes that are

obtained from human donors. This approach assumes that the rate of compound disappearance from the incubation medium is correlated with in vivo metabolic clearance. The in vivo hepatic intrinsic clearance can be then calculated from the in vitro hepatic clearance by applying appropriate scaling factors [301]. With the well-stirred model [167, 168], hepatic clearance can be calculated by inputting the in vivo hepatic intrinsic clearance and other physiological parameters in humans such as fraction unbound in plasma and hepatic blood flow. Second, when plasma and/or renal CL from an adult PK study is available, one can partition CL into different mechanisms. Subsequently, Well-stirred model can be used to calculate intrinsic clearance.

Once intrinsic CL for each pathway in adults is known, each intrinsic CL in children can be scaled by using ontogeny factors for metabolizing enzymes (e.g. PK-Sim® Ontogeny Database [166]) or by using the equation to estimate renal glomerular filtration maturation (e.g. Rhodin et al. [302]). For compounds that undergo cytochrome P450 (CYP) metabolism, the CYP specific ontogeny factors are determined based on age-dependent enzyme activity or relevant biomarker levels such as mRNA or protein concentrations levels [166, 243, 303, 304]. When multiple CYP enzymes are involved for hepatic metabolism, the intrinsic clearance in adults is multiplied by each CYP enzyme ontogeny factor. The sum of CYP specific intrinsic clearance is then converted to plasma clearance in children by using physiological parameters in children (e.g. hepatic blood flow, body weight). Alternatively, an allometric method can be used in order to scale plasma clearance in adults to plasma clearance in children by accounting for body weight differences [305].

The allometric method has been widely utilized in pediatric PK community and its precision has been demonstrated in numerous investigations[42, 306-309]. Unlike the physiologically relevant methods described above, the allometric method does not partition out clearance pathways (e.g. hepatic or renal).

Pediatric PBPK modeling can also provide the estimation of CL in children [44, 47, 58, 180]. According to the established workflow of pediatric PBPK modeling by Maharaj and Edginton [47], plasma concentration vs. time profiles in adults are used to predict intrinsic clearance. Based on CYP specific ontogeny models [166], age-dependent enzyme activity is taken into account along with the physiological and anatomical parameters. Yun and Edginton 2019 [180] demonstrated that CL prediction in children using pediatric PBPK platform PK-Sim (Open Systems Pharmacology) produce a reasonable prediction accuracy of the mean and variability of CL in children. However, for

environmentally relevant compounds, in vitro or PK data in adults is often unavailable and *in silico* methods are required.

The in silico prediction of pediatric CL requires numerous steps. Beyond the knowledge of how body weight and physiological changes change with age, to predict CL requires knowledge of a compound's primary clearance mechanism (e.g. hepatic metabolism or renal excretion).Varma et al. (2015) [310] developed an Extended Clearance Classification System (ECCS) that predicts the predominant clearance mechanism (e.g. renal or hepatic) based on a compound's physicochemical properties such as lipophilicity, permeability, ionization state and polarity. This classification method predicted the predominant clearance mechanism for 92% of the evaluated compounds (n=307).

Quantitative structural-property relationship (QSPR) models are built based on the relationship of a compounds' structural information and physiological properties. Many QSPR methods are available to predict a compound's clearance in a system. Several QSPR models predict CYP enzyme-mediated metabolism by identifying a potential metabolic site (e.g. [311-313]). Another type of QSPR model provides the prediction of the rate of hepatic intrinsic clearance (e.g. in vitro CLint in hepatocyte or human liver microsomes) (e.g. [314-317]) based on chemical descriptors. The model performance had a coefficient of determination (R^2) range from 0.30 to 0.79. Watanabe et al. [318] developed an *in silico* method for predicting renal clearance using chemical descriptors and a combination of a regression model and a classification algorithm. For renal clearance values higher than 1.02 ml/min/kg, 78.6% of compounds fell within two-fold error of deviation.

In addition, several research groups (e.g. Ingle et al.[186] and Watanabe et al. [194]) developed QSPR methods using machine learning algorithms to predict fraction unbound in plasma in human. The predictive performances of these algorithms for predicting human fups for environmentally relevant compound was evaluated in our previous investigation [268].

The *in silico* prediction of pediatric CL is a function of multiple pieces of information and algorithms, which have not been assessed in an entire workflow. The objectives of this study are (i) to establish a workflow of prediction of PK in children using in silico based clearance and fup estimates calculated from a chemical structure and (ii) to evaluate its predictive performance.

6.2 Methods

6.2.1 Data collection

For this study, clearance values in adults and children that were determined following an intravenous administration were gathered from the literature. CL values following IV administration were included in order to ensure CL values were not confounded by absorption. Age (postnatal age) was collected from the same source. When available, standard deviation values of CL were also obtained to estimate coefficient of variation (%).

For each molecule where both adult and pediatric CL were available, a database of the chemical descriptors was generated. Chemical specific data such as primary protein binding partner (i.e. albumin or alpha acid glycoprotein) and observed fup in adults was collected from the literature. The observed clearance and fup values were obtained from MEDLINE database by searching relevant keywords, e.g. 'clearance in pediatrics'.

6.2.2 Physiological data obtained from virtual individuals

To obtain relevant physiological parameters that are necessary for CL prediction in children and adults, a virtual population (n=1200, age range from 0 to 30, uniform age distribution) was created using PK-Sim ver. 9 (Open Systems Pharmacology). In PK-Sim®, when an age range is given, virtual individuals are created with varying system-specific parameters such as height, weight, organ volumes, organ-specific blood flows, maturation factors (e.g. plasma protein levels or enzyme concentration levels) and fractions of protein, water and lipids based on the underlying database (e.g. ICRP study [48]). Details of system specific parameters of virtual individuals can be found in Willmann et al 2007 [144].

The population was split into groups as listed in Table 6.1. For infants, virtual individuals were grouped with 3-month intervals. This was because anatomical, biochemical and physiological maturation takes place during infancy and therefore CL prediction can be sensitive to age-dependent parameters.

For the observed CL values in children, the mean of age was obtained from the same source. When the mean of age in the subjects who CL values were determined was within the age range of a group of virtual individuals, the predicted CL values were compared to the observed CL value. For example, if an observed CL value was determined in subjects with the mean postnatal age of 7 months, the predicted

CL values of the group pop 03 was compared to the observed CL value. The observed CL_{child} values were assumed to represent CL values in each groups of virtual children.

Table 6.1 Groups of virtual individuals

Group	Postnatal age	Number of virtual individuals	Age group
pop 01	0 – 3 months	100	Neonates/infants
pop 02	3 – 6 months	100	Infants
pop 03	6 – 9 months	100	
pop 04	9 – 12 months	100	
pop 05	12 – 15 months	100	
pop 06	15 – 18 months	100	
pop 07	18 - 21 months	100	
pop 08	21 – 24 months	100	
pop 09	2 – 6 years	100	Children
pop 10	6 – 12 years	100	
pop 11	12 – 18 years	100	Adolescents
pop 12	18 – 30 years	100	Adults

6.2.3 QSPR based CLchild calculation

For each compound, the two-dimensional structure-data file (SDF) was downloaded from PubChem [319]. Three methods to generate pediatric CL values were compared.

Method 1

In Method 1, hepatic CLint and CLr in adults were predicted based on QSPR approaches, respectively. The hepatic CLint and CLr in adults were then scaled to hepatic CLint and CLr in children using appropriate scaling methods. The calculation steps are as following.

1. Adult CL calculation

1.1. Hepatic CL prediction in adults

1.1.1. Metabolizing enzyme classification

The Substrate Classification Model in the ADMET Predictor (ADMET Predictor™ software provided by Simulations Plus, Inc., Lancaster, California, USA v9.5) was used. This model predicted the potential metabolizing enzymes (9 CYP isoforms and 9 UGT isoforms) for a compound. When confidence of the prediction was high (e.g. ≥ 75%), it was assumed that the compound was a substrate of the predicted enzyme and the enzyme (e.g. CYP3A4) was the primary enzyme that is responsible for hepatic metabolism. If a compound is predicted to be a substrate with a confidence higher than 75% for two enzymes, a fraction metabolized value of 50% was applied. This step was important because the matching CYP enzyme specific intrinsic clearance and ontogeny factor were applied to calculate CLchild. Once potential metabolizing enzyme(s) for a compound were identified, the next step was to predict a rate of the metabolic reaction (e.g. kinetic parameter).

1.1.2. Hepatic intrinsic clearance calculation

The ADMET Predictor provided an estimate of specific intrinsic clearance for five CYP enzymes (CYP1A2, CYP2D6, CYP3A4, CYP2C9, CYP2C19, μL/min/mg HLM protein for CYP enzyme mediated oxidation). When metabolizing enzyme specific intrinsic clearance was not available (e.g. CYP2E1), intrinsic clearance in human liver microsome (μL/min/mg HLM protein, unbound form) was used instead. The QSPR predicted intrinsic clearance was used to estimate in vivo intrinsic clearance (CLint, in vivo). The extrapolation of QSPR-predicted CLint to in vivo intrinsic hepatic clearance (CLint) in adults was done based on the following equation. QSPR-predicted hepatic intrinsic clearance was assumed to represent a mean value in the adult population.

$$CLint, in\ vivo\ (mL/min) = \frac{QSPR\ CLint, u}{fu_{mic}} * microsomal\ protein * liver\ weight * 70\ kg * 0.001$$

fu_{mic}: QSPR predicted fraction unbound in human liver microsomes (fu_{mic}), Microsomal protein: 52.5 mg protein/ g liver [320], Liver weight: 1800 g liver or 25.7 g liver/kg body weight [321]. An average adult human body weight was assumed to be 70 kg.

1.2. Renal clearance prediction in adults

For renal clearance prediction, each SDF file obtained from PubChem [319] was input to Renal-ex Predictor [318] (https://adme.nibiohn.go.jp/renal_ex). QSPR-predicted renal clearance in human was assumed to be equivalent to renal clearance values in adults. QSPR-predicted renal clearance values were assumed to represent a mean value in adult population.

2. Scale Pathway-specific Adult CL to Children

Scaling Adult CL to children requires two steps. First, protein binding must be scaled by taking into account the maturation of plasma protein concentrations. Second, respective clearance process (hepatic or renal) must be scaled by considering maturation.

2.1 Scaling fraction unbound in plasma

Human fup values were calculated using the ADMET predictor. The estimated human fup value was assumed to be equivalent to adult fup. Acid-base properties were predicted based on the method described in Ingle et al. [186]. Based on the ionization properties, acid-base properties were determined. It was assumed that acids and neutrals bind to albumin and bases bind to AAG. A more detailed description of this approach can be found in Yun and Edginton [322]. Fup in children was estimated by applying the ontogeny factors of virtual individuals created from PK-Sim as shown below.

$$For\ acids\ and\ neutrals: fup_{child,i} = fup_{adult} \cdot albumin\ ontogeny\ factor_i$$

$$For\ bases: fup_{child,i} = fup_{adult} \cdot AAG\ ontogeny\ factor_i$$

$Fup_{child,i}$ denotes an estimated fup value in i^{th} virtual individual. Albumin ontogeny $factor_i$ and AAG ontogeny $factor_i$: Albumin or AAG ontogeny factor for i^{th} virtual individual.

2.2 Scaling hepatic clearance

QSPR-predicted hepatic intrinsic clearance values were used to scale clearance for virtual children in each group (Pop01 ~ Pop11). First, ontogeny factors of each pediatric individual were used. By using substrate classification information described in the previous step (section 1.1.1), hepatic intrinsic clearance in adult was multiplied by the corresponding ontogeny factor for the predicted enzyme to estimate intrinsic clearance in children ($CL_{int,child}$). For this calculation, the following equation was used. As mentioned, fraction metabolized of a CYP enzyme was assumed to be 1 when a compound was predicted to be a substrate of a single metabolizing enzyme. Fraction metabolized of a CYP enzyme of 0.5 was applied when a compound was predicted to be a substrate of two metabolizing enzymes.

$CL_{int,child} = CL_{int,adult} \cdot ontogeny\ factor_{enz}$ or

$CL_{int,child} = CL_{int,adult} \cdot 0.5 \cdot ontogeny\ factor_{enz1} + CL_{int,adult} \cdot 0.5 \cdot ontogeny\ factor_{enz2}$

ontogeny $factor_{enz(1\ or\ 2)}$: ontogeny factor of a metabolizing enzyme (e.g. CYP3A4 or CYP1A2), $CL_{int,adult}$: intrinsic clearance in adults

Hepatic clearance in children ($CL_{h,child}$) values were calculated by using the well-stirred model [167, 168]. For the calculation of fub_{child}, $fup_{child,i}$ was divided by blood to plasma ratio (B:P). For B:P calculation, the following equation was used [323].

$$CL_{h,chil} = \frac{Q_H fub_{child} \cdot CL_{int,child}}{Q_H + fub_{child} \cdot CL_{int,child}}$$

$$\text{Log (B:P)} = -0.004282 + 0.067028\ \text{LogP} + 0.214590\ \text{Log (fup)}$$

Q_H: hepatic blood flow, fub: fraction unbound in blood, B:P: blood to plasma ratio

2.3 Scaling renal clearance

Renal clearance in children values ($CL_{r,child}$) were predicted using the following equation. For renal clearance, the QSPR-predicted CLr was assumed to be CLr in adults ($CL_{r,\ adult}$). GFR in child was calculated by using the GFR estimation equation from Rhodin et al. [302].

$$CL_{r,child} = \frac{GFR_{child} \cdot fup_{child}}{GFR_{child} \cdot fup_{adult}} \cdot CL_{r,adult}$$

3. Estimation of Total Plasma CL in Children

QSPR-predicted hepatic and renal clearance (CL_h and CL_r) values in each pediatric individual were added to calculate plasma clearance in children.

$$CL_{p,child} = CL_{h,child} + CL_{r,child}$$

Method 2

In Method 2, a predominant route of elimination (e.g. hepatic metabolism or renal excretion) was predicted based on physicochemical properties of compounds. For compounds hepatically metabolized, QSPR methods for hepatic CL prediction was used to estimate hepatic CL in adults. Subsequently, hepatic CL in adults was scaled to hepatic CL in children by taking into account maturation of metabolizing enzymes and plasma protein levels. For renally cleared compounds, renal clearance in adults were predicted based on a QSPR method. The renal clearance value in adults were then scaled to renal clearance in children by taking into account the maturation of glomerular filtration rate and plasma protein levels. A QSPR-predicted CL value of the predominant route of elimination (e.g. $CL_{h,child}$ or $CL_{r,child}$) was assumed to approximate plasma clearance in virtual individuals.

1. Identification of predominant route of elimination – ECCS

Clearance classification system was used to predict a predominant route of elimination (e.g. metabolism or renal excretion). This classification method was based on Varma et al. [310]. Using ADMET predictor, clearance mechanisms were predicted based on compound structure.

Class 1A and 2: Metabolism

Class 3A and 4: Renal CL

Class 1B: Hepatic uptake

Class 3B: Renal CL or Hepatic uptake

2. Clearance prediction for ECCS Class 1A and 2 compounds

2.1 Metabolizing enzyme classification

The same steps were taken as described in the Section 1.1.1 in Method 1

2.2 Prediction of hepatic intrinsic clearance in adults

The same steps were taken as described in the Section 1.1.2 in Method 1

2.3 Scaling fraction unbound in plasma

The same steps were taken as described in the Section 2.1 in Method 1

2.4 Scaling hepatic clearance

The same steps were taken as described in the Section 2.2 in Method 1

2.5 Estimation of Plasma CL in Children

Hepatic clearance in children ($CL_{h,child}$) values were calculated by using the well-strirred model. For hepatically metabolized compounds (ECCS Class 1A and 2), the QSPR-calculated $CL_{h,child}$ values were assumed to be equivalent to $CL_{p,child}$. This approach was employed based on the results of a preliminary analysis of Method 1. The errors due to the use of hepatic CLint prediction for renally excreted compounds (e.g. misspecification) were high.

$$CL_{h,child} = \frac{Q_H fub_{child} \cdot CL_{int,child}}{Q_H + fub_{child} \cdot CL_{int,child}}$$

$$CL_{p,child} \approx CL_{h,child}$$

3. Clearance prediction for ECCS Class 3A, 3B and 4 compounds

3.1 Renal clearance prediction in adults

For renal clearance prediction, each SDF file obtained from PubChem [319] was input to Renal-ex Predictor [318] (https://adme.nibiohn.go.jp/renal_ex). QSPR-predicted renal clearance in human was assumed to be equivalent to renal clearance values in adults. QSPR-predicted renal clearance values were assumed to represent a mean value in adult population.

3.2 Scaling renal clearance

Renal clearance in children values ($CL_{r,child}$) were predicted using the following equation. GFR in children was calculated by using the GFR estimation equation from Rhodin et al. [302]. Fraction unbound in plasma values in children were scaled from adults values as described in the section 2.3.

$$CL_{r,child} = \frac{GFR_{child} \cdot fup_{child}}{GFR_{child} \cdot fup_{adult}} \cdot CL_{r,adult}$$

3.3 Estimation of Total Plasma CL in Children

For mainly renally cleared compounds (i.e. Class 3A and 4), the QSPR calculated $CL_{r,child}$ values were assumed equivalent to $CL_{p,child}$. This approach was employed based on the results of a preliminary analysis of Method 1. The errors due to the use of hepatic CLint prediction for renally excreted compounds (e.g. misspecification) were high.

$$CL_{p,child} \approx CL_{r,chil}$$

Method 3

Observed CL_{adult} was scaled to CL_{child} using allometry. The weight of a virtual individual was used for calculation. As observed systemic clearance in adults is not readily available for environmentally relevant compounds, this calculation method was used in this study only for comparative purposes to compare predictive performance of Method 3 to that of Methods 1 and 2.

$$CL_{child,i} = CL_{adult} \cdot \left(\frac{weight_i}{70\ kg}\right)^{0.75}$$

6.2.4 Model evaluation

6.2.4.1 Predictive performance for $CL_{p,child}$ to compare Methods 1-3

In order to evaluate the prediction accuracy, the predicted $CL_{p,child}$ values were compared to the observed values that were obtained from literature. The equations for evaluation metrics for assessing the predictive performance of the model are listed below. GMFE and AAFE indicates the degree of deviation between observed and predicted values. Geometric coefficient of variation These metrics were used to compare predictive performances of Methods 1-3.

$$Geometric\ mean\ fold\ error = 10^{\frac{1}{n}\sum_1^n \log(\frac{CL_{p,child,pred,i}}{CL_{p,chil\ \ ,obs}})}$$

$$Absolute\ average\ fold\ error = \ 10^{\left[\frac{1}{n}\sum_1^n \left|\log(\frac{CL_{p,child,pred,i}}{CL_{p,child,obs}})\right|\right]}$$

$$Geometric\ coefficient\ of\ variation = \sqrt{exp^{GSD^2} - 1} \cdot 100\%$$

$CL_{p,child,pred,i}$: predicted plasma clearance in i^{th} child, $CL_{p,child,obs,i}$: observed plasma clearance in i^{th} child, GSD: geometric standard deviation of fold error ($CL_{p,child,pred}/CL_{p,child,obs}$).

6.2.4.2 Evaluation of the predictive performance of the ECCS classification system

To evaluate the predictive performance of the ECCS classification system, the predicted and the observed clearance mechanism was compared. For the observed data, if a compound has ≥ 60% hepatic (e.g. CYP fraction metabolized) or renal (e.g. fraction excreted unchanged in urine) contributions to systemic clearance, the primary route of elimination was labeled as hepatic or renal, respectively. For the ECCS classification results, the Class 1A, 2A and 2B compounds Class 1A, 2A and 2B were labeled as hepatic, and Class 3A, 3B and 4 compounds were labeled as renal.

6.2.4.3 Evaluation of predictive performance for QSPR-predicted fup in adults and its impact on $CL_{p,child}$ prediction

To evaluate the predictive performance for QSPR-predicted fup in adults, the observed fup values in adults and QSPR predicted fup values were compared. As mentioned previously, QSPR-predicted fup in human was assumed to be equivalent to fup in adults. For evaluating the predictive performance, absolute error and absolute relative prediction error (RPE) values were calculated. These evaluation metrics were previously used in Yun and Edginton [270]. In order to evaluate if prediction errors for fup and $CL_{p,child}$ were correlated, the evaluation metrics for fup (i.e. absolute error and absolute RPE) were then compared to AAFE values for $CL_{p,child}$ prediction.

$$Absolute\ error = \left|fup_{pred} - fup_{obs}\right| \cdot 100(\%)$$

$$Absolute\ relative\ predicion\ error = \left|\frac{fup_{pred} - fup_{obs}}{fup_{obs}}\right| \cdot 100(\%)$$

6.3 Results

6.3.1 Data

A total of 71 observed CL_{child} and 25 observed CL_{adult} values were obtained from literature [44, 100, 102, 104, 122, 124, 125, 128-131, 133-139, 171, 300, 304, 324-337]. Each virtual individual in each group were assigned with age, weight, ontogeny factors (which are necessary for CL predictions). For each individual and each drug, $CL_{p,child}$ values were calculated based on Method 1-3.

6.3.2 Contributions of Inter-individuality in CL_{child} Prediction

For $CL_{p,child}$ prediction, several system-specific parameters were involved and those were obtained from virtual individuals (Table 6.1). Key system-specific parameters used for adult-to-children scaling of CL were weight, CYP ontogeny factors, GFR ratios, and hepatic blood flow. As $CL_{p,child}$ was estimated for virtual individuals in each group, the distribution and mean of those parameters that contribute to inter-individual variability of $CL_{p,child}$ were visualized in Figure S1.

6.3.3 ECCS classification results

Among 71 predicted CLchild values, the majority were Class 2, 3A or 4. This indicates that 61% and 35% of CLchild was predicted by assuming the compounds' main route of elimination is hepatic metabolism and renal excretion, respectively. The predicted and the observed primary route of elimination matched 100% indicating that the ECCS classification reasonably predicted the predominant route of elimination.

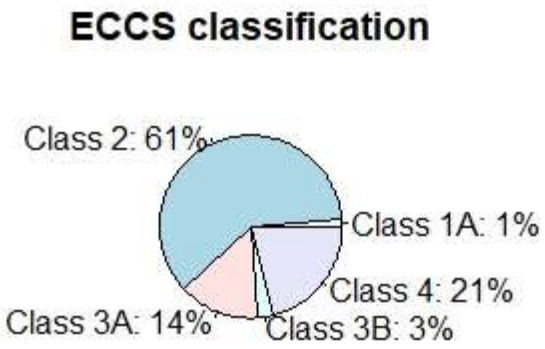

Figure 6.1 The distribution of ECCS classes.

6.3.4 Evaluation of the predictive performance

The predicted CLchild values were compared to the observed values. The QSPR-based methods (Methods 1 and 2) showed over-prediction with GMFE values of 3.29 and 1.90 (Table 6.2). The GMFE and AAFE values of Class 3 and 4 of Method 1 were higher than those values of Class 3 and 4 of Method 2. This indicates that the over-prediction was more prominent when QSPR based hepatic CLint was used for CLp prediction for renally excreted compounds.

For renally cleared compounds (i.e. Class 3A and 4), when the QSPR calculated $CL_{r,child}$ values were assumed to approximate $CL_{p,child}$ (Method 2), the predictive performance was improved with GMFE of 1.06 and AAFE of 2.01 compared to those of Method 1. This indicated that ECCS classification informed prediction of $CL_{p,child}$ resulted in a better prediction accuracy (Figure 6.2).

Table 6.2 Predictive performance according to different calculation methods

ECCS Class	Evaluation metric	Method 1	Method 2	Method 3
Class 1 and 2	GMFE	2.50	2.42	1.34

Class 1 and 2	AAFE	2.11	2.19	1.59
Class 3 and 4	GMFE	4.59	1.06	1.16
Class 3 and 4	AAFE	3.48	2.01	1.63
All	GMFE	3.29	1.90	1.27
All	AAFE	2.55	2.13	1.61
All	Geometric CV	30.1%	33.9%	9.34%

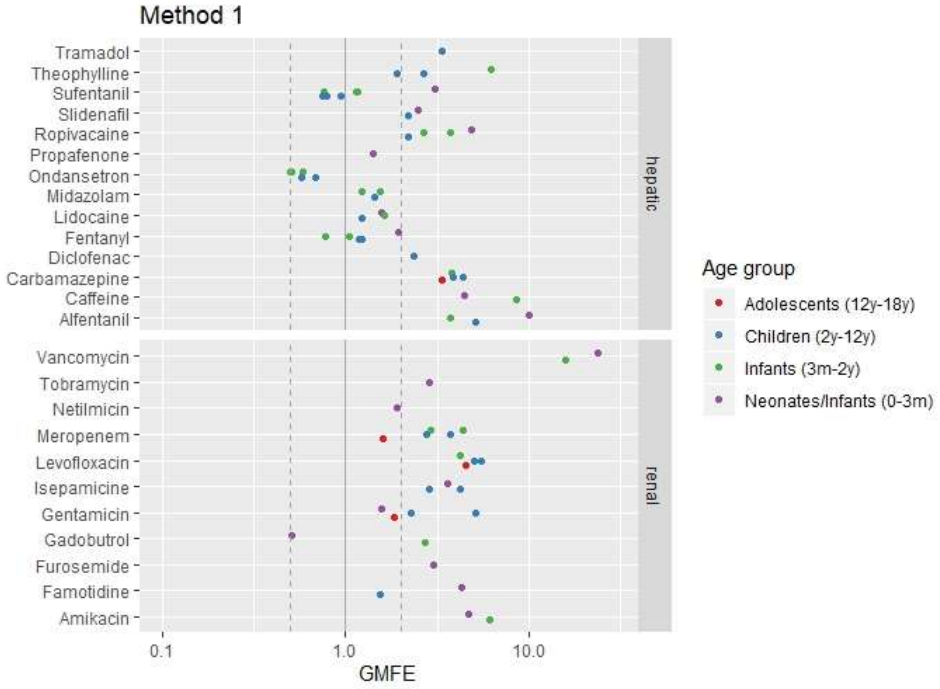

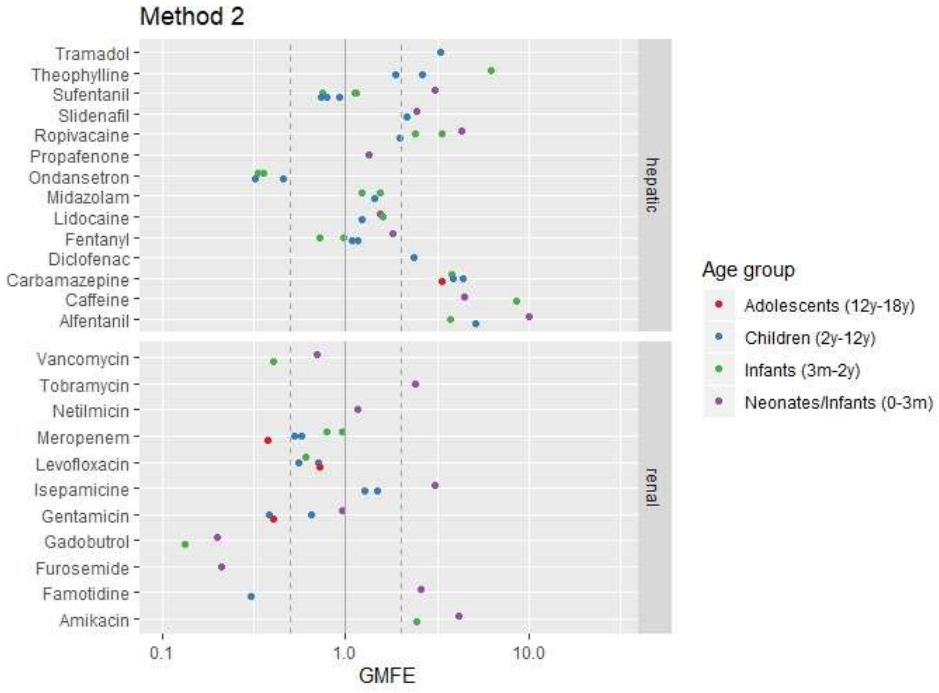
Method 2
Tramadol
Theophylline
Sufentanil
Slidenafil
Ropivacaine
Propafenone
Ondansetron
Midazolam
Lidocaine
Fentanyl
Diclofenac
Carbamazepine
Caffeine
Alfentanil
hepatic
Vancomycin
Tobramycin
Netilmicin
Meropenem
Levofloxacin
Isepamicine
Gentamicin
Gadobutrol
Furosemide
Famotidine
Amikacin
renal
0.1
1.0
10.0
GMFE
Age group
Adolescents (12y-18y)
Children (2y-12y)
Infants (3m-2y)
Neonates/Infants (0-3m)

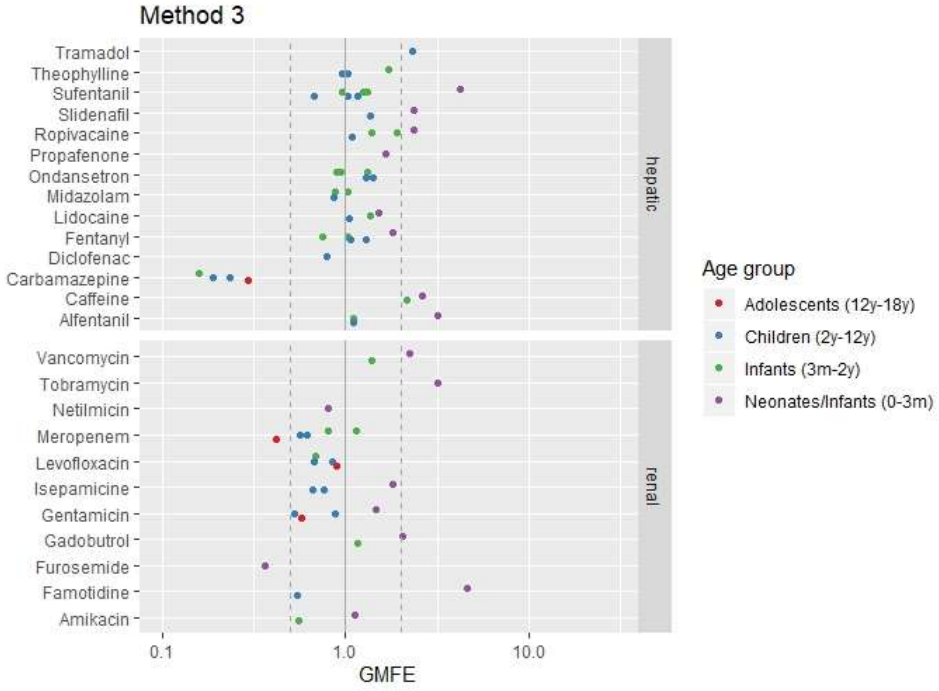
Method 3
Tramadol
Theophylline
Sufentanil
Slidenafil
Ropivacaine
Propafenone
Ondansetron
Midazolam
Lidocaine
Fentanyl
Diclofenac
Carbamazepine
Caffeine
Alfentanil
hepatic
Vancomycin
Tobramycin
Netilmicin
Meropenem
Levofloxacin
Isepamicine
Gentamicin
Gadobutrol
Furosemide
Famotidine
Amikacin
renal
0.1
1.0
10.0
GMFE
Age group
Adolescents (12y-18y)
Children (2y-12y)
Infants (3m-2y)
Neonates/Infants (0-3m)

Figure 6.2 The geometric mean fold difference according to the calculation methods 1- 3. The colors represent age group.

6.3.5 Evaluation of inter-individual variability of the predicted $CL_{p,child}$ values in each pediatric group

In each pediatric group, the each virtual individual (n=100) had a unique predicted-$CL_{p,child}$ value due to the virtual individuals' unique anatomical, biochemical and physiological parameters. The variation of $CL_{p,child}$ values within each group (n=100) was quantified by calculating geometric coefficient of variation. For each group, geometric coefficient of variation of $CL_{p,child}$ values predicted using each method (i.e. Method 1, Method 2, Method 3) and compared. The QSPR-based methods showed similar variability in predicted $CL_{p,child}$ with geometric coefficient of variation of 30.1% and 33.9% for Method 1 and Method 2, respectively. Method 3 resulted in smaller variability (CV: 9.34%) than QSPR-based methods (Table 6.2).

Not all the pediatric studies reported coefficient of variation or standard deviation values. When available variability information were gathered, observed coefficient of variation on average was 33.8%. This indicates that estimated variability in CL based on Method 1 and Method 2 may be more relevant compared to estimated variability in CL based on Method 3. However, due to the limited sample size in pediatric clinical studies, this observed coefficient variation may not reflect a true degree of inter-individual variability in a pediatric population. This comparison was therefore needs to be interpreted with caution.

6.3.6 Evaluation of predictive performance for QSPR-predicted fup in adults and its impact on $CL_{p,child}$ prediction

The comparison between the observed fup in adults and QSPR-predicted fup in adults was shown in Figure 6.3. Median and mean absolute error values were 11.6% and 18.2%, respectively. Median and mean of absolute RPE values were 37.0 % and 105.9% respectively. The next step was to evaluate if the prediction errors for fup in adults prediction was correlated with the prediction error for $CL_{p,child}$. For this, absolute error and absolute RPE values for fup adults and AAFE values for $CL_{p,child}$ was compared. The pearson correlation test showed that correlation between these prediction error values was not statistically significant with p-value > 0.05 except one case. When Absolute error for fup vs. AAFE for Method 2 $CL_{p,child,}$ the correlation was statistically significant with p-value less than 0.05 and r value of 0.25. This indicated that the precision of QSPR-predicted fup in adults affects the prediction accuracy of $CL_{p,child}$ when Method 2 (ECCS classficiation informed CLpchild prediction) was used (Figure 6.4). Overall, there was a weak correlation between prediction errors for fup and clearance based on QSPR approach. This suggested that prediction accuracy of QSPR predicted fup value was not the only contributing factor for prediction accuracy of $CL_{p,child}$. This suggested that the precision of QSPR methods for predicting both clearance and protein binding are important for a reasonable prediction of $CL_{p,child}$.

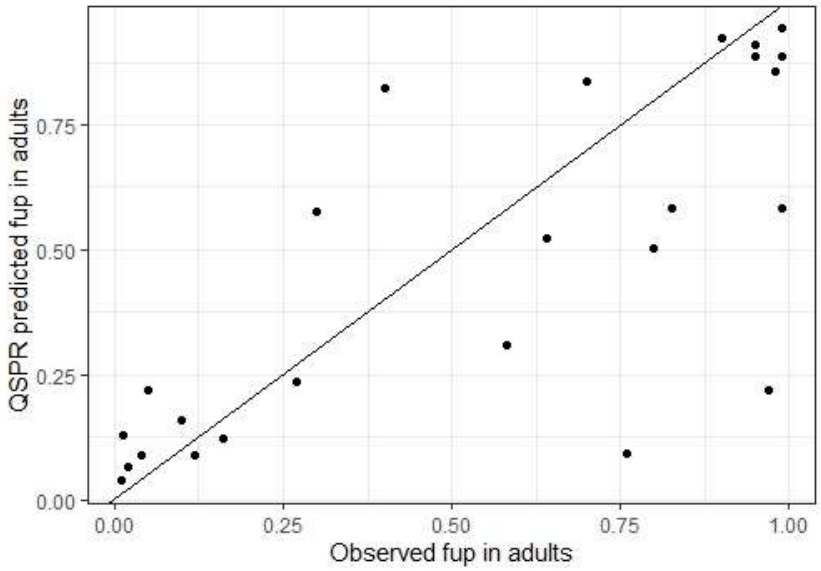

Figure 6.3 Comparison between observed fup in adults and QSPR-predicted fup values in adults.

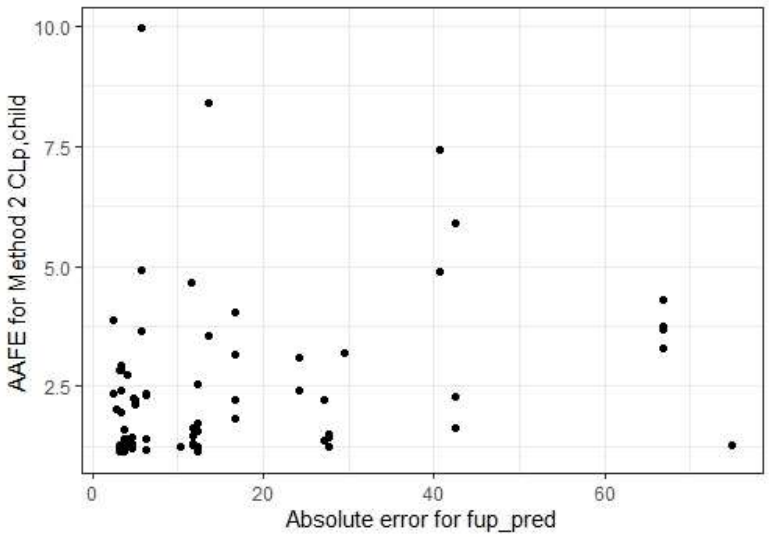

Figure 6.4 Comparison between absolute error values for QSPR predicted fup in adults and AAFE values for $CL_{p,child}$ calculated by Method 2.

6.4 Discussion

In human health risk assessment (HHRA), uncertainty factors (UF) are applied to a point of departure (POD) such as a no-observed-adverse-effect level (NOAEL) to estimate toxicological indices (e.g. tolerable daily intake (TDI) and average daily intake (ADI) (International Programme on Chemical Safety 2003; 2001)). The default uncertainty factor of 3.16 is applied to address the toxicokinetic (TK) variability between pediatrics and adults (World Health Organization 2010, Ginsberg et al. 2002, 2004b). This UF of 3.16 can be replaced with a human kinetic adjustment factor (HKAF) - a ratio between the upper percentile (e.g. 95th) value of a toxicokinetic parameter in a susceptible subpopulation such as children and median value in a reference population (e.g. healthy adults) (Meek et al. 2002, Price et al. 1999).

Physiologically based pharmacokinetic (PBPK) models can be used to estimate a HKAF by predicting the 95th percentile and median PK values in both children and adult populations [6]. Pediatric PBPK modeling requires many system-specific inputs and in vitro data for a reliable model output. Prediction of HKAF using a PBPK model can be challenging for environmentally relevant compounds because experimental determination of system-specific input parameters (e.g. fraction unbound in plasma) are not readily available [212]. Furthermore, many chemicals are screened for potential toxicity often with a high throughput screening (HTS) approach [223, 299, 338-340].

For example, as an extension of the Toxicology in the 21st Century (Tox21) federal collaboration, US EPA recently developed a high-throughput risk assessment framework utilizing both in silico- and in vitro- derived PK data [338]. This framework provides an estimation of likelihood of human in vivo chemical biological interactions. A ratio of Cmax to half maximal effective concentration (AC50) was used to evaluate this likelihood. This ratio is similar to Cmax/Ki used in evaluation of drug-drug interaction. Due to computational complexity and requirement of many system-specific input parameter, pediatric PBPK model may not be easily integrated into toxicity testing with HTS approach.

This study presents a framework for CL prediction in children for environmentally relevant compounds, that can be integrated to the high-throughput risk assessment. This framework utilized (i) virtual pediatric populations that were generated from open-source PBPK modeling software, PK-Sim, and

(ii) various QSPR-based methods for predicting clearance mechanisms, hepatic intrinsic clearance, renal clearance and fraction unbound in plasma in human from chemical structures.

In Method 1, hepatic CLint and CLr in adults were estimated from a compound structure based on QSPR methods. By using appropriate scaling methods, the hepatic CLint and CLr in adults were then scaled to hepatic CLint and CLr in children. In Method 2, a predominant route of clearance pathway (e.g. hepatic metabolism or renal excretion) was predicted based on physicochemical properties of compounds. The same steps were taken as in the Method 1 for calculating hepatic CL and renal CL in children. For estimating plasma CL in children, a QSPR-predicted CL value of the predominant route of elimination was assumed to approximate plasma clearance in virtual individuals. For Method 3, observed CLadult was scaled to CLchild using allometry based on weight of a virtual individual. This method was used only for comparative purposes to compare predictive performance of Method 3 to that of Methods 1 and 2.

The predictive performances of those methods were evaluated by comparing the predicted CL values in children to the observed values. The QSPR-predicted CL values based on Methods 1 and 2 showed an over-prediction with geometric mean fold error values of 3.29 and 1.90, respectively. The deviation from the observe value was lower for Method 2 compared to Method 1 indicating that ECCS classification informed prediction of $CL_{p,child}$ resulted in a better predictive performance.

The system-specific parameters that are necessary for predicting children CL includes fup, hepatic blood flow, liver weight, body weight, CYP ontogeny factor. These parameters contribute inter-individual variability of CL values in children, that can be crucial for HKAF determination. In our previous investigation [180], the virtual pediatric individuals were created by setting the same ranges of age and body weight of the children in the available clinical investigations. This was to evaluate the predictive performance of pediatric PBPK model. In this study, groups of virtual children were created based on a broader range of age (Table 6.1) to evaluate the predictive performance in the relevant pediatric populations. This method was adopted in order to apply this framework for HTS-based human health risk assessment for children. The observed CL_{child} values were assumed to represent CL values in each groups of virtual children. As the ranges of age and weight of the virtual children were not matched to those ranges of clinical studies, slight deviations (e.g, GMFE 1.9~3.29) were expected.

Allometric scaling with exponent of 0.75 on clearance assumes that clearance increases less than proportionally to weight increase [42]. The inter-individual variability of CL_{child} prediction based on allometry (Method 3) was largely attributed to weight (inter-individuality of weight in each group of virtual children). Method 3 is likely to under-estimate the variability of CL in a pediatric population as it is assumed that the individuals with same weight have the same systemic clearance values. On the other hand, using virtual children (Method 1 and 2) takes into account inter-individuality in anatomical, biochemical and physiological parameters (as shown in the Figure 6.2) in estimating CL_{child}.

In terms of hepatic CLint, a use case for QSPR-predicted can be found in Sipes et al. [338]. For input to High-Throughput Toxicokinetic (HTTK) package [341] developed by EPA researchers, CLint was calculated by aggregating CLint predictions of the five metabolizing enzymes CYP1A2, CYP2C9, CYP2C19, CYP2D6, and CYP3A4 [338]. In this study, a different approach was undertaken by utilizing structure-based prediction of a metabolizing enzyme. We used the predicted information that a compound is a substrate for a specific enzyme and if the predicted CYP CLint is available, specific CYP enzyme CLint was preferably used. This was because a virtual individual's specific CYP ontogeny factors are used for CL_{child} prediction. It was considered that, for applying CYP ontogeny factors, CYP enzyme specific CLint is most physiologically relevant. When a specific CYP enzyme CLint value was not available, in vivo CLint was estimated by using QSPR predicted CLint in human liver microsome.

This study presents a framework for predicting CL in children using QSPR-based PK predictions and virtual children. This combined approach will be useful especially for data-poor compounds. The comparison between predicted and observed CL values in children indicated a reasonable prediction accuracy with geometric mean fold error of 1.6 – 2.1. This framework can inform human health risk assessment for children by providing an *in silico* estimation of CLchild and its inter-individual variability within children population.

Chapter 7: Development and Evaluation of an In Silico Dermal Absorption Model Relevant for Children

7.1 Introduction

Mathematical in silico models of skin permeation simulate the dermal permeation and systemic exposure of a chemical through human skin. Given the limited availability of human and animal skin samples for permeability experiments and the differences between human and animal skin, in silico models can be used in lieu of experimental studies to estimate dermal exposure to chemicals and drugs and to predict systemic exposure under various dosing conditions and exposure scenarios [342]. This is especially valuable in pediatric patients where skin samples for in vitro studies are even more limited.

The mechanistic dermal absorption model by Dancik et al. [343] integrates a series of pharmacokinetic models, as previously described [344-350], that represent the penetration pathways of a chemical through skin. The components of the model were derived using data gathered from in vitro studies of chemical permeation in animal models and adult human skin samples [342]. The model also incorporates structural and physiological properties of adult human skin, which have been extensively described in detail [345, 351-356]. The model can generate longitudinal estimates of the flux (e.g., μm/cm2/h) and accumulation (e.g., μm/cm2) of small molecule compounds in the various skin layers under both in vitro and in vivo conditions. In the in vivo context, the model can additionally generate estimates of the bioavailability of dermally absorbed chemicals.

Pediatric exposure to environmental chemicals is an important component of human health risk assessment. Although rare, cases of chemical poisoning through skin exposure have been reported in pediatric patients under 17 years of age [357]. This is especially concerning given the presence, in children's bath products, of chemicals such as 1,4-dioxane and formaldehyde, which have been classified as carcinogens by the US Environmental Protection Agency (EPA) [358]. Moreover, the French Agency for Food, Environmental and Occupational Health and Safety has reported the identification of 60 hazardous chemicals in infant disposable diapers [359]. An increase in skin exposure to harmful chemicals may be a serious health risk in children, given the higher skin surface area to body weight ratio and the prematurity of skin in neonates [20]. Accounting for the anatomical

and physiological changes in skin associated with age using the Dancik et al. model [343] may therefore help to guide the risk assessment of chemicals and pharmaceutical products in children.

Skin development and maturation begins in utero, and a full-term infant's skin is histologically similar to adult skin, as it has a well-defined stratum corneum in addition to the other epidermal layers [360, 361]. However, in vivo studies using confocal laser scanning microscopy in the last 20 years have shown that differences in skin anatomy and physiology do exist as a function of age following birth, which was not previously well-captured in light microscopy and chemically fixed skin samples in infants. Physiological and structural skin features that differ between infants and adults, which were identified from the analysis of non-invasive in vivo measurements, have been previously reviewed [362]. These variations in pediatric skin anatomy and physiology with respect to adults can induce differences in the dermal absorption of a given chemical between the two populations. As a result, in silico predictions generated by dermal models tailored to adult skin may fail to correctly predict exposure in the pediatric population. The objectives of this study were therefore: (i) to provide a comprehensive review of the anatomical and physiological changes associated with the skin of children and (ii) to construct and evaluate a pediatric dermal absorption model that accounts for skin maturation with age.

7.2 Materials and Methods

7.2.1 Dermal Absorption Modeling Preliminaries

The Dancik et al. [343] skin permeation model has previously been programmed into MoBi (Open Systems Pharmacology v.8.21) and is currently available on GitHub (https://github.com/Open-Systems-Pharmacology/Skin-permeation-model, last accessed on 01 November 2021). The predictive accuracy of this model for the case of volatile vehicles was evaluated in Hamadeh et al. [363] with respect to in vitro skin permeation data reported in Hewitt et al. [364]. The model assumes that skin sections are composed of three stacked compartments that correspond to the stratum corneum (SC), the epidermis (ED) and the dermis (DE) (Figure 7.1), which have the respective thicknesses h_{sc}, h_{ed}, and h_{de}. The permeating compound is applied via a vehicle to the surface of the SC. The applied permeant is assumed to subsequently diffuse into the skin according to Fick's law of diffusion [346] as detailed in Dancik et al. [343]. The permeant in each compartment can partition into sub-

compartments that represent different phases within the skin sublayers, such as the lipid, protein or aqueous phases. The aggregate, layer-specific, diffusivity and partitioning processes in each skin layer are quantified by the diffusion coefficients (D_{sc}, D_{ed}, D_{de}) and the partitioning coefficients ($K_{sc/w}$, $K_{ed/w}$, $K_{de/w}$), respectively. These aggregate coefficients can be decomposed into diffusion and partition coefficients specific to each phase, as detailed in Dancik et al. [343]. These more fundamental coefficients can, furthermore, be decomposed into quantitative structure property relationships (QSPRs) that are functions of the physical/chemical properties of the permeant. The permeant concentration at depth x, as measured from the top of the SC, at time t, can be expressed as $c(x,t)$. The complete partial differential equation model (PDE) describing permeant diffusion and clearance from the skin can be found in [343, 365].

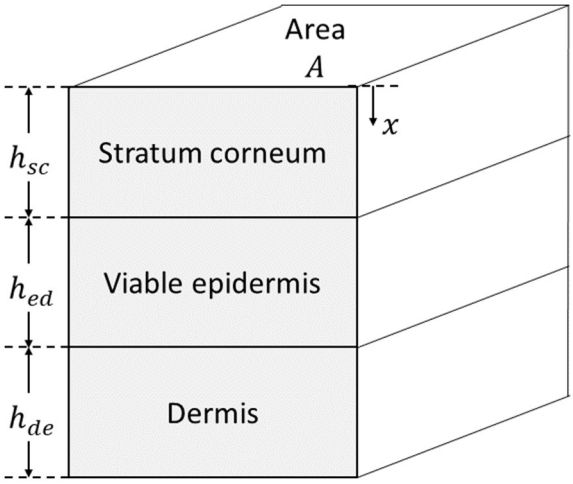

Figure 7.1 Structure of skin in the dermal absorption model.

7.2.2 Physiological and Anatomical Changes in Skin as a Function of Age

A comprehensive literature review was conducted of the anatomical and physiological properties of skin that impact dermal absorption according to the Dancik et al. [343] model. Skin-specific parameters of this model include the stratum corneum thickness, the thickness of the viable epidermis, dermis thickness, stratum corneum hydration, lipid, and protein fraction of the stratum corneum, skin surface pH, corneocyte size and volume fraction of the stratum corneum, follicle size and density, albumin concentration in skin, and skin blood flow. Each parameter was searched on MEDLINE and EMBASE or PUBMED to identify articles that reported quantifiable data in healthy

full-term infants and children up to 18 years of age (Tables S1-S6). The search strategy for each parameter is displayed in the Supplementary Materials (Tables S7–S14). The results were limited to the English language and human studies. Child and adult estimates were obtained for the stratum corneum thickness, epidermis thickness, dermis thickness, and skin hydration.

7.2.3 Development of an Age-Dependent Dermal Absorption Model

7.2.3.1 Development of Model Structure

We generalized the dermal absorption model in [343, 365] to include the effect of subject postnatal age (Age). This model can be expressed using the following shorthand representation:

PDE	$\frac{\partial c}{\partial t} = f\left(t, c, \frac{\partial c}{\partial x}, \frac{\partial^2 c}{\partial x^2}, P, P_A(Age)\right)$	(1)
Initial conditions	$c(0) = c_0(P, P_A(Age))$	(2)
Boundary conditions	$h\left(c, \frac{\partial c}{\partial x}, P, P_A(Age)\right) = 0$	(3)
Model outputs	$y(t) = g(t, P, P_A(Age))$	(4)

The model represented by (1)–(4) is assumed to have the same structure as the model in [343, 365]; however, we allowed for some of the parameters in the original model to vary with postnatal age. Model parameters that do not change with postnatal age were grouped into the parameter set P, while postnatal age-dependent parameters were grouped into the set $P_A(Age)$. The skin layer thicknesses (h_{sc}, h_{ed}, h_{de}), permeant diffusivities (D_{sc}, D_{ed}, D_{de}) and partitioning coefficients ($K_{sc/w}$, $K_{ed/w}$, $K_{de/w}$) can be expressed as lump parameters that are functions of the parameters in the sets P and $P_A(Age)$.

For the purposes of this study, the model outputs $y(t)$ were limited to estimates of two in vitro skin permeation test (IVPT) observations: (1) the permeant flux from the dermis into receptor fluid ($y_J(t)$), and (2) the permeant accumulation in receptor fluid ($y_Q(t)$). Assuming receptor fluid

conditions that replicate permeant solubility and diffusivity in the dermis, these estimates can be derived from Fick's law as models (5) and (6):

$$y_J(t) = D_{de} \frac{\partial c(x,t)}{\partial x}_{|x=h_{sc}+h_{ed}+h_{de}} \quad (5)$$

$$y_Q(t) = \int_{\tau=0}^{\tau=t} D_{de} \frac{\partial c(x,\tau)}{\partial x}_{|x=h_{sc}+h_{ed}+h_{de}} d\tau \quad (6)$$

7.2.3.2 Maturation Models for Age-Dependent Model Parameters

Candidate models of postnatal age-dependence for each parameter within the set P_A were developed as functions of postnatal age (in days) from birth to adulthood. Each such parameter was assumed to be expressible as a scaling with respect to a reference adult value P_{adult} that depends on postnatal age (Age). The i^{th} postnatal age-dependent parameter, $P_{A_i}(Age)$, was assumed, a priori, to have one of three candidate functional forms with respect to Age:

Sigmoid equation	$\frac{P_{A_i}(Age)}{P_{adult}} = \frac{a \cdot Age}{b + Age} + c$	(5)
Hill equation	$\frac{P_{A_i}(Age)}{P_{adult}} = \frac{a \cdot Age^n}{b^n + Age^n} + c$	(6)
Polynomial equation	$\frac{P_{A_i}(Age)}{P_{adult}} = a \cdot Age^n + b \cdot Age^m + c$	(7)

The nlstools R package (R version: 3.6.1, nlstools version: 1.0-2) [151, 366] was used to fit each of the models (5)–(7) for each postnatal age-dependent parameter to the literature-sourced data collected through the literature review. To evaluate the test error rate of the models, leave-one-out cross validation (LOOCV) [367] was carried out. For each parameter, the functional form with the lowest LOOCV test error was selected as the final model.

For each $\frac{P_{A_i}(Age)}{P_{adult}}$ ratio used in model optimization, the values of $P_{A_i}(Age)$ and P_{adult} were sourced, where possible, from the same study from the literature. Mean levels in adults of the SC, ED and DE thicknesses (h_{sc}, h_{ed}, h_{de}) were collected, and the geometric mean of those mean values was

calculated as a reference level in adults. When the adult level was not reported in the same study as the child level, a reference level in adults was used for P_{adult}. This reference level was estimated as the mean of all adult values collected in the literature.

7.2.4 Age-Dependent Dermal Absorption Model Optimization and Evaluation

The MoBi dermal absorption model was updated with the optimized maturation functions $P_A(Age)$ to form an integrated, postnatal age-dependent, dermal absorption model. The ability of the integrated model to capture changes in dermal absorption across postnatal age was evaluated using literature-sourced data on the skin permeation by three compounds: buprenorphine, diamorphine, and phenobarbital. These three compounds were selected based on the availability of experimental in vitro skin penetration data in adults and infants within the same study [368-370]. To assess the predictive performance of the model, the difference between observed and predicted flux values (fold error) was calculated by using Equation (10).

$$fold\ error = \frac{Predicted\ flux\ (y_J)}{Observed\ flux} \tag{10}$$

7.2.4.1 Dermal Absorption Model Sensitivity Analysis and Parameter Uncertainty

A local sensitivity analysis was conducted on the adult (Age = 30 years) models (1)–(4) for each of the three compounds to identify the uncertain model parameters that strongly impact estimates of the outputs y_J and y_Q. For each of buprenorphine, diamorphine, and phenobarbital, these sensitivities were evaluated after updating the model with the compound's corresponding parameters in Table 7.1 and Table 7.2. The uncertain model parameters to which the outputs y_J and y_Q are sensitive were classified into two sets: those that vary with postnatal age (denoted P_A^*) and those that are independent of postnatal age (denoted P^*).

A probability distribution for parameters P_A^* for adults was obtained from the literature. Parameters P_A^* for different ages were assumed to be distributed according to a corresponding probability distribution that is conditional on postnatal age, $p(P_A^*|Age)$. A sample from this conditional distribution is obtained, first, by sampling the adult distribution for parameters P_A^*, and then scaling the sample according to the optimized maturation model.

Table 7.1 Compound-specific model input parameters.

Property	Buprenorphine	Diamorphine	Phenobarbital
Molecular formula	C29H41NO4	C21H23NO5	C12H12N2O3
Molecular weight (g/mol)	467.6	369.4	232.2
Lipophilicity (Log P)	4	1.5	1.47
Boiling point (°C)	578.7	272	
Melting point (°C)	217	173	174
Water Solubility (mg/L)	16.8	600	1110
Solubility in ethanol (mg/mL)	N/A	N/A	100
pKa	8.65 (basic)	7.83 (basic)	7.3 (acidic)
Vapor pressure (mmHg)	N/A	N/A	1.4 × 10−11

N/A: not available.

Table 7.2 Experimental conditions and observed permeant flux values in adults.

Compound (Reference)	Dose (µg/cm2)	Experiment Duration (h)	Solvent	Observed Steady-State Flux (µg/cm2/h)	Final Receptor Fluid Accumulation (µg/cm2)
Buprenorphine (Barret et al., 1994)	2656	72	0.1 M acetate buffer, pH 4	0.08 ± 0.02 (mean ± SD)	5.54
Diamorphine (Barret et al., 1993)	53,100	72	0.1 M acetate buffer, pH 4	0.07	2.59

Phenobarbital (Bonina et al., 1993)	78	12	Ethanol	0.1 ± 0.02	0.91

7.2.4.2 Model Optimization and Evaluation

For each compound, the model evaluation consisted of the following steps:

The models (1)–(4) were updated with the compound-specific parameters from Table 7.1 and age-dependent parameters corresponding to adult skin (in which parameter $Age = 30$ years) gathered from the PubChem database [206].

The uncertain age-independent parameters P^*, to which the model outputs (5) and (6) are sensitive, were estimated by fitting outputs y_J and y_Q from the adult model generated in step 0 to the observed adult flux and receptor fluid accumulation in Table 7.2. Model fitting was performed via the Monte Carlo parameter identification algorithm in MoBi (Open Systems Pharmacology v.9.1), initiated from 10 randomly selected initial values.

Infant skin permeation by the compound was simulated assuming the experimental conditions and skin ages in Table 7.3 using the optimized parameter values P^*obtained in step 0. A total of 100 simulations of the model were run for each infant skin Age on which the compound was experimentally tested. Each such simulation was run after updating the model with a new sample from the distribution of age-dependent parameters $p(P_A^*|Age)$. For each experiment, the mean and 95% confidence intervals of the simulated permeant flux y_J were evaluated and compared with the corresponding observed flux in Table 7.3.

Table 7.3 Experimental conditions and observed permeant flux values in infants.

Compound (Reference)	Gestational Age (Postnatal Age)	Dose (µg/cm2)	Experiment Duration (h)	Solvent	Observed Steady-State Flux (µg/cm2/h)

Buprenorphine (Barret et al., 1994)	38w (1d) 40w (7h) 37w (1d) 37w (1d)	2656	72	0.1 M acetate buffer pH 4	0.01 0.36 0.08 0.11
Diamorphine (Barret et al., 1993)	38w (26d) 40w (7d) 36w (3d)	53,100	72	0.1 M acetate buffer pH 4	0.23 0.08 0.18
Phenobarbital (Bonina et al., 1993)	38w (2d) 40w (5d) 37w (5d) 35w (2d)	78	12	Ethanol	0.11 0.14 0.11 0.24

Neonates who were born before a gestational age (GA) of 37 weeks were considered to be preterm, whereas infants who were born after 37 weeks (i.e., GA ≥ 37 weeks) were classified as full-term [371]. The observed data for full-term and late preterm neonates with a gestational age from 35 to 40 weeks were included in this study. The review of skin anatomy and physiology did not focus on pre-term neonates, and this evaluation was for preliminary assessment only.

7.2.5 Identification of Critical Input Parameter

To assess which parameters were both important to the outcome of flux and had an importance that differed between adults and children, a post hoc sensitivity analysis was performed. The age of adults was set to 30 years and the age of children was set to the same age in the corresponding studies. Parameters that were differentially sensitive with respect to age were identified by calculating the absolute difference in sensitivity coefficients between children and adults. If the difference was equal to or greater than 15% (Equation (11)), the parameter was considered to be age-sensitive.

$$|sensitivity\ coefficient\ in\ children - sensitivity\ coefficient\ in\ adults| \geq 15\% \qquad (11)$$

7.3 Results

7.3.1 Physiological and Anatomical Changes in Skin as a Function of Age

7.3.1.1 Differences in Stratum Corneum Thickness

The geometrical properties of the stratum corneum (SC) are critical parameters used to determine the steady state permeation, lag time, and the flux of a substance transiting intercellularly through the SC [372]. Thus, studies investigating SC thickness in children were reviewed and quantifiable data were collected to determine whether SC thickness changed as a function of age.

A total of 43 relevant articles were identified in PUBMED, and 17 were identified as containing child-specific epidermis thickness data compared to adult epidermis thickness data (Supplementary Tables S1 and S7). It is important to note that the epidermis consists of the SC and the viable epidermis. The viable epidermis is distinct from the SC, as it contains nucleated keratinocytes, melanocytes, Langerhans cells, and Merkel cells [373]. Some investigations of epidermis thickness in children include SC thickness and identify it as the supra-papillary epidermis or epidermis thickness [374-376]. Of the 17 articles, only eight specifically measured SC thickness in children compared to adults. The body areas in which SC thickness was most often measured in children were the forearms, upper arm, and abdomen [361, 374-378], although data from other body areas such as the buttocks and thighs have also been collected [374-376, 378]. Measurements of histological skin samples ex vivo and confocal microscopy in vivo were the most common methods used to measure skin thickness.

Earlier studies measuring SC thickness using histological methods did not identify a significant distinct difference in the thickness of the SC between infants and adults [361, 377, 379, 380]. This was unlike in vivo SC measurements using confocal microscopy and confocal Raman spectroscopy, which revealed that infant SC is thinner than adult SC [36,37,43]. Stamatas et al. [374] found that the SC thickness of lower thigh skin from 20 infants from 3 months to 2 years old was on average 30% thinner than adults (7.3 ± 1.1 μm versus 10.5 ± 2.1 μm). Similarly, Liu et al. [375] also recorded that 52 infants and children of the same age range had a 34% thinner SC in the lower thigh compared to adults. In the same study, SC thickness measurements at the upper inner arm also revealed a thinner

SC in children compared to adults, although the magnitude of the difference was smaller, at only 18% thinner (5.3 ± 1.4 μm vs 7.9 ± 1.8 μm) [375].

Another investigation by Walters et al. [381] aimed to more closely identify the relationship between SC thickness and age by grouping infants and children 3 months old to 5 years old into different age bins. The SC thickness of the upper inner arm and dorsal forearm increased from 8 μm at 3 months of age to 14 μm at 4 years of age, at which point it became similar to adult (25–40 years old, average: 32 years) SC thickness, which ranged from 13 to 14 μm in this study. The SC thickness of dorsal forearm and inner arms were also similar in thickness in this study. Only one study was retrieved that measured SC thickness in neonates and infants less than 3 months of age [376]. This study pooled SC measurements of neonates aged 4–7 days old and compared this thickness to measurements taken at 1, 3 and 6 months after birth in the same infants. Measurements were taken from the buttock, thigh, and forearm skin. Unlike the previous studies, Miyauchi et al. [376] found that the SC was thicker at 4–7 days of age compared to 3 months of age at all three measured sites.

The ratio of child SC thickness to adult SC thickness was plotted as a function of postnatal age (Figure 7.2A). Overall, SC thickness approaches adult values at around 4 years of age.

7.3.1.2 Differences in the Thickness of the Viable Epidermis between Children and Adults

After diffusion through the SC, a chemical next permeates through the viable epidermis. Like SC thickness, the thickness of the viable dermis is important for calculating diffusion and permeability rates. A total of nine publications investigating epidermal thickness in children were identified (Supplementary Tables S2 and S8).

Measurements of abdominal viable epidermis thickness were first recorded by Evans and Rutter (1986). They measured the viable epidermal thickness of post-mortem infant skin samples ex vivo and identified that it increased linearly with postnatal age up to 16 weeks of life [361]. Moreover, they also recorded that the distinct undulating nature of the epidermis develops after birth and becomes more distinct with age. Similar findings were recorded by de Viragh et al. [382] a few years later in scalp skin isolated from biopsy specimens [382]. However, a distinction between maximum epidermis thickness and minimal epidermis thickness was identified. The maximum epidermis was defined as the distance from the start of the viable epidermis to the most prominent projection of the

collagen fibers, which identifies the border between the epidermal and dermis skin layers. The maximum epidermis thickness increased with age, unlike the minimal epidermis thickness, which did not vary. This was similar to the study by Evans et al. (1986) [361], which identified an increase in the undulating nature of the epidermis.

Similarly, more recent studies measuring epidermal thickness in vivo also concluded that infants have a thinner epidermis than adults. Stamatas et al. [374] and Liu et al. [375], both found that pooled epidermis thickness values of thigh skin in infants aged 3–24 months were 20% and 8% lower, respectively, than adult values. Liu et al. [375] also measured a 22% thinner inner arm epidermis in children compared to adults. The changes in epidermis thickness in neonates was also more closely identified by Miyauchi et al. [376], where epidermal thickness was measured in four day old infants until they were 6 months of age. Given the undulating nature of the epidermis, two thickness values were measured, which corresponded with the top of the dermal papillae and the bottom of the rete ridges (i.e., bottom of dermal papillae). The epidermis thickness increased with age until one month of age, where it reached a thickness of 25 and 58 μm in minimal and maximal epidermis thickness, respectively [376]. At this time point, the maximal epidermis thickness was similar to adult maximal epidermis thickness (60 μm) [376]. A final study measuring epidermal thickness in children aged six months to three years of age also concluded that epidermal thickness is thinner in children compared to adults, but did not show the data for this [383].

The viable epidermis in children was thinner than the adult epidermis. Since the data collected from Evans et al. [361], de Viragh et al. [382], Miyauchi et al. [376], and Mogensen et al. [383] included thickness values stratified by age group, the ratio of child epidermis thickness to adult epidermis thickness was plotted as a function of postnatal age (Figure 7.2B). In terms of de Viragh et al. [382], as the minimum and maximum values were reported, the averages of the minimum and the maximum values were used. These data outline that the epidermis thickness in the first week of life is thinner than in adults, and remains relatively similar until 10 days postnatal age, at which point the epidermal thickness increases rapidly until four months of age, where it reaches adult values.

7.3.1.3 Differences in the Dermal Thickness between Children and Adults

The dermis layer of the skin is the thickest layer, and although it contributes to a significant amount of variability for in vitro experiments [384], this layer is important when predicting systemic drug

delivery through the transdermal route [385]. As such, differences in dermis thickness (h_{de}) between children and adults were investigated. A total of four relevant articles were identified as having quantifiable data of dermis thickness values in children (Supplementary Tables S3 and S9). It is important to note that of the four articles, one was grey literature and the data were not extracted [386].

As with the epidermal layer, the dermis layer also has an undulating structure because of the dermal papillae. Additionally, it is made up of two layers: the papillary and reticular dermis. As such, thickness values were measured in a different way in each publication. Dermis thickness values from children aged one week to three years old were attained [382, 387], in addition to children aged 18 years [388]. Scalp dermis thickness data sourced from De Viragh et al. [382] identified an increase in maximal dermis thickness as a function of age from 1125 μm at 2 weeks old to 1500 μm at 21 years of age. The minimal dermis thickness in this study also increased from 850 μm at 2 weeks old to 2200 μm at 21 years of age. Marcos et al. [388] also found a similar trend in skin samples obtained from 5-month-old infants up to 95 years of age. They found a thickness of 1603.88 μm at birth and 3236.18 μm in adults at 50 years of age. Finally, Hughes et al. [387] more closely identified the relationship between age and dermis thickness in infants that were 1 week old up to 3 years old. However, the bounds of the dermis that were measured to gather thickness values were not clear in this study. They found dermal thickness in the forearm to be highest at 1 week of age (1200 μm), which decreased to 1100 μm at 4 weeks of age and then was similar from 6 to 36 months of age at a thickness of 1050 μm.

The ratio of child dermis thickness to adult dermis thickness measured by de Viragh et al. [382], Marcos et al. [388], and Hughes et al. [387] was plotted as a function of postnatal age (Figure 7.2C). In terms of de Viragh et al. [382], as the minimum and maximum values were reported, the average of the minimum and the maximum values were used. The dermis thickness in children does not change and remains at around 40% of adult thickness until around 2 years of age (730 days postnatal), where the dermis thickness increases rapidly into adulthood and continues to increase until 27 years of age.

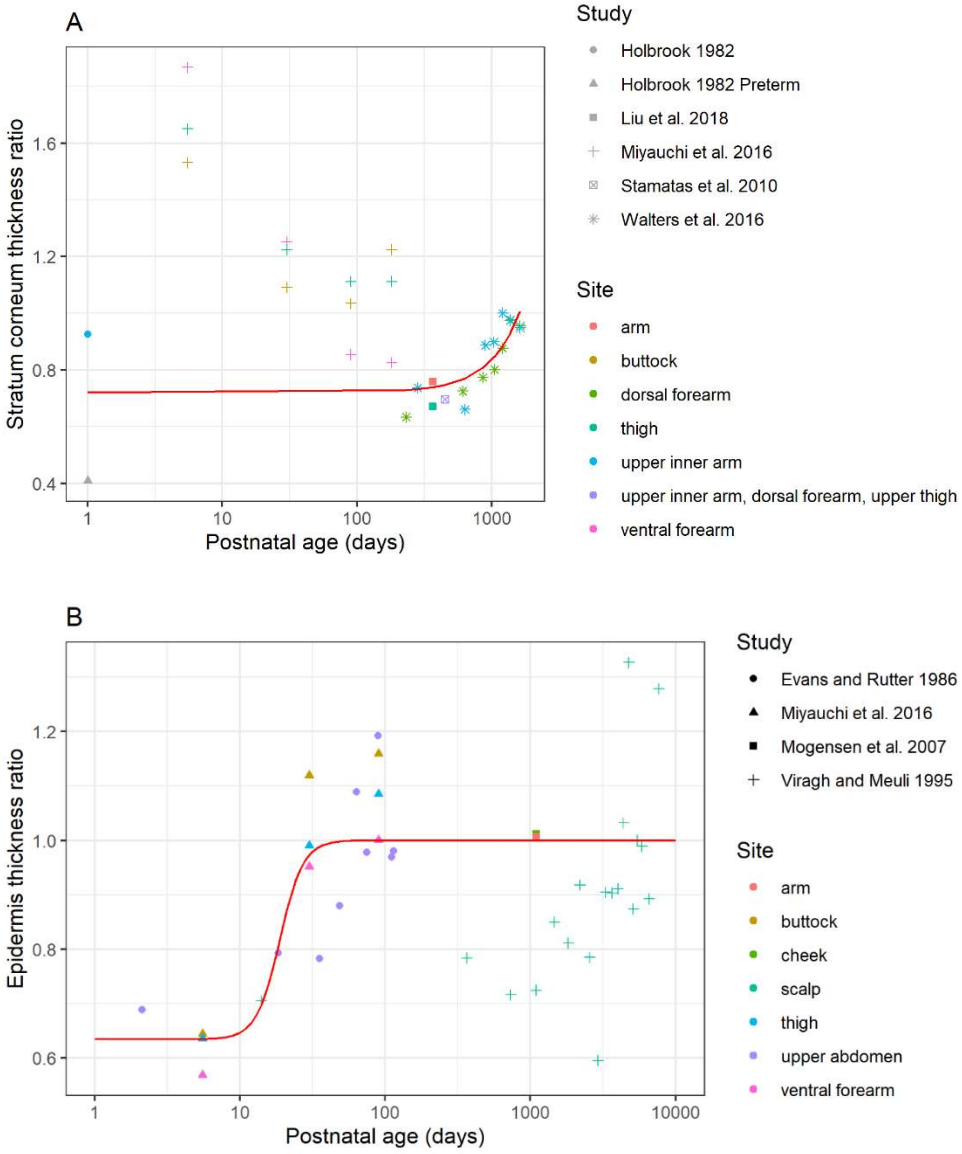
A
Stratum corneum thickness ratio
0.4
0.8
1.2
1.6
1
10
100
1000
Postnatal age (days)
Study
Holbrook 1982
Holbrook 1982 Preterm
Liu et al. 2018
Miyauchi et al. 2016
Stamatas et al. 2010
Walters et al. 2016
Site
arm
buttock
dorsal forearm
thigh
upper inner arm
upper inner arm, dorsal forearm, upper thigh
ventral forearm
B
Epidermis thickness ratio
0.6
0.8
1.0
1.2
1
10
100
1000
10000
Postnatal age (days)
Study
Evans and Rutter 1986
Miyauchi et al. 2016
Mogensen et al. 2007
Viragh and Meuli 1995
Site
arm
buttock
cheek
scalp
thigh
upper abdomen
ventral forearm

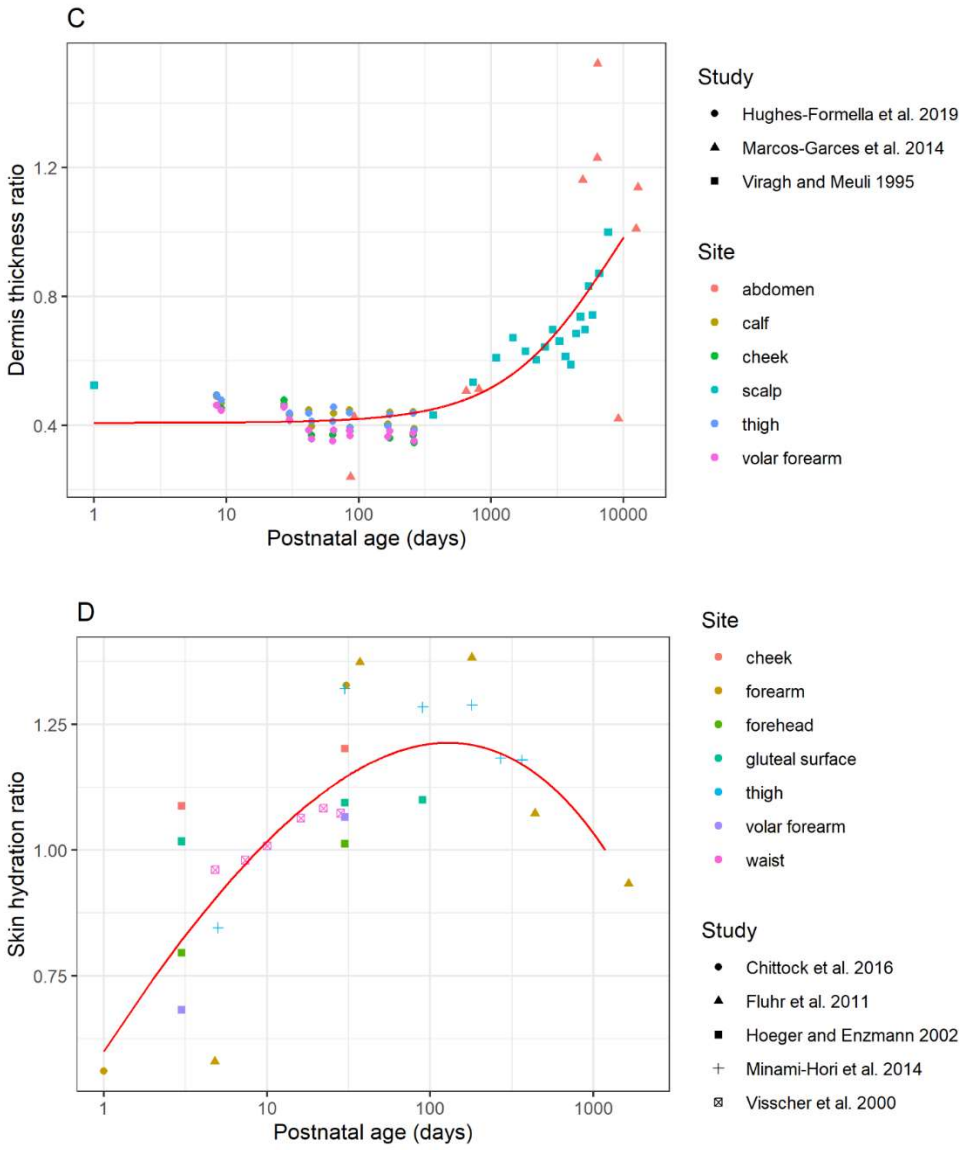

Figure 7.2 Maturation ratios vs. age profiles of (A) stratum corneum thickness (SC maturation model 2), (B) epidermis thickness, (C) dermis thickness, and (D) skin hydration. The model structures and coefficients are listed in Table 7.4. For the stratum corneum thickness model, Miyauchi 2016 data and Holbrook 1982 preterm data were not included in the development of SC maturation model 2.

7.3.1.4 Difference in Skin Hydration of Child and Adult Epidermal Barrier

The level of hydration of the skin and stratum corneum plays a role in permeability and chemical penetration. An increase in water content results in an increase in skin permeability, since the stratum corneum can act as a reservoir to promote percutaneous absorption [349, 389]. Therefore, differences in surface skin hydration as a function of age in children were investigated. Skin hydration in the stratum corneum can be measured indirectly using a corneometer. The corneometer measures skin capacitance, which is related to the dielectric properties of the skin and is proportional to the water content in the skin [390]. A total of 16 publications measured surface skin hydration indirectly via skin capacitance (Supplementary Tables S4 and S10).

Several investigations have identified that newborns in the first 2 weeks of life have lower skin hydration than adults [391-399]. Chittock et al. [391] found that infants <72 h old had skin capacitance of 17.66 ± 4.55 relative capacitance units (RCU), which was lower than adults at 31.47 ± 6.9 RCU. Similar trends were identified by Bartels et al. [393]. Additionally, a study by Yosipovitch et al. [399] also suggests that skin hydration begins significantly increasing in the first 24 hours of life [399]. As the neonate grows, skin hydration increases rapidly. The study by Bartels et al. [393] found that the highest increase in skin capacitance was by 7 arbitrary units (AU) in the abdomen from 2–7 days of age. Moreover, Visscher et al. [398] found that skin hydration continues to increase until 2 weeks of life then plateaus. However, several other investigations have found that the rapid increase in skin hydration in infants continues until approximately one month of age [393, 395-397].

At the 1 month mark, the skin capacitance in the infant is higher than adults [396]. Visscher et al. [398] and Fluhr et al. [392] also identified similar trends. The study by Fluhr et al. (2012) [392] suggests that the hydration remains high above adult values until 6 months of age (41.5 AU) and decreases to adult values (30 AU) in the first 1–2 years of life. At 6 months to 1 year of age, several investigators have found that skin hydration in children is not significantly different than in adults [392, 400, 401].

The change in skin hydration as a function of postnatal age is shown in Figure 7.2D. Skin capacitance values from Chittock et al. [391], Fluhr et al. [392], Hoeger and Enzmann [395], Minami-Hori et al. [396], and Visscher et al. [398] were used to calculate a ratio of children's skin hydration to adult skin

hydration. These ratios are plotted as a function of postnatal age. As previously described, skin hydration increases until 1 month of age, then decreases to adult values.

7.3.1.5 Differences in the Corneocyte Volume Fraction

The corneocyte phase of the SC is involved in model calculations that determine partition coefficients and saturation concentration of a substance in the SC [343]. The literature search identified four relevant articles related to differences in corneocyte size, shape, volume in the stratum corneum in children compared to adults (Supplementary Tables S5 and S11). Changes in cell density, cluster formation, cell shape, thickness, and adhesion in corneocytes of the stratum corneum exist in infants and children until 5 years of age, with the most drastic changes occurring during the first two years of life [343, 344]. Corneocytes in the stratum corneum of infants from 6 to 24 months old were smaller than adult corneocytes, which was attributed to a higher proliferation rate of corneocytes in infants [346]. During infancy and into adulthood, corneocytes became larger and flatter and assumed a greater surface area, which was correlated with a decrease in proliferation rate [2,3,5]. Since the relationship between these data and the effect on the volume of corneocytes in the SC are unknown, the corneocyte phase volume fraction in children was kept the same as in adults in the model.

7.3.1.6 Differences in the Lipid/Protein Ratio

Since the lipid contents in the SC, viable epidermis, and dermis affect the permeability of a substance through the corresponding layers, quantitative data regarding differences in lipid mass or volume between children and adults were investigated. Of the nine relevant articles identified looking at lipid composition in children, only two conference abstract articles from the same research group specifically measured whole lipid contents in infant skin compared to adults [402, 403] (Supplementary Table S12). Stamatas et al. [402, 403] measured the lipid content in the SC of the volar forearm of infants aged 3–24 months and their respective mothers. Similar amounts of urea, lipids (cholesterol and ceramides), and keratin (protein) were found in infants and adults. As a result, the same parameter values were used in adults and child simulations for the following parameters in the model: the protein phase volume fraction of the stratum corneum, the mass of proteins in relationship to the dry weight of the SC, and the mass of lipids in relation to the dry weight of the SC.

7.3.1.7 Differences in Albumin Concentration

The albumin content in the skin affects chemical or drug protein binding in the skin and therefore unbound and bound concentrations within the dermis [343]. There are limited data regarding albumin content in full term infant skin, and a search only revealed one article that quantified albumin content in newborn skin [404] (Supplementary Table S14). From this article, it was evident that albumin concentration in premature infants is greater than adults and full-term newborns. However, the albumin content in adults and newborn skin were similar, both within 2.5–5 ng/µg of protein. As such, the parameter value of the fraction of aqueous phase accessible to albumin was kept the same between children and adults.

7.3.1.8 Differences in Skin Blood Flow in Children

Skin blood flow is an important limiting parameter that helps to predict systemic drug clearance from the skin in vivo. In the Dancik et al. model [343], capillary clearance can be used to predict systemic clearance using the capillary surface area and estimated blood flow limited clearance. The modeling of dermal capillary clearance was reviewed by Kretsos and Kasting (2004) [405], who described several parameters such as geometry, vessel size, and surface area that affect capillary clearance. They also proposed a new microscopic model for the dermal capillary clearance process based on the physiologic capillary structure [406]. In infants, the microvascular structure is disorganized after birth and matures over the first 4–5 weeks post birth, when the papillary loops are seen as in adult skin [407]. More recently, Miyauchi et al. [376] also observed capillary loop formation in infants at 1 to 3 months of age. The relationship between vessel geometry and blood flow is complex, and several models are available with an aim to capture capillary transport [405]. An early study by Poschl et al. [408] identified that the skin blood flow in full-term and preterm neonates changes in the first week of life. In full-term neonates, the blood flow oscillations reached the lower range of the adult value within the 4 to 5 days of life [408]. The relationship between skin blood blow changes and microvessel structural changes in infant skin are not known and need to be further studied for future model development. Skin blood flow is not included in the Dancik et al. model [343]; however, the maturation of skin blood flow data will be useful in the in vivo prediction of dermal absorption.

7.3.1.9 Differences in Surface Skin pH and Follicle Density/Size of Children and Adults

The skin pH is a crucial element of skin barrier function as it affects enzymatic activity in the skin and lipid processing [409]. Although surface skin pH is not an input parameter in the Dancik et al. model [343], the pH of newborn skin is near neutral, unlike in adults [410]. The differences between adult and child skin pH have been extensively and recently reviewed [409, 410]. In short, skin surface pH in infants immediately after birth is higher and less acidic around 6.5 [398] than the pH in adult skin [409], which ranges from 4–6 [411]. The pH then decreases within 7–14 days and can normalize by 6 months [412]. Moreover, it appears similar to adults [400, 412] in later infancy. While skin pH is not currently in the model, this review provides information that may be used in future.

Similarly, the transfollicular shunt route is another parameter not currently included in the Dancik model [343]. Given the importance of the transfollicular shunt route of drug permeation through the skin, differences in follicle size or density between children and adults were also investigated for future model development. The literature search on EMBASE and MEDLINE identified two articles with quantifiable data regarding follicle density, length, or diameter (Supplementary Tables S6 and S13). Marchini et al. [413] identified that the number of visible hair structures per mm2 in infants 1–2 days of age was approximately 10 times greater than in adults. Additionally, a grey literature source suggested that there may also be a relationship between hair follicle dimensions and age [414].

7.3.2 Development of an Age-Dependent Dermal Absorption Model

7.3.2.1 Maturation Models for Age-Dependent Model Parameters

Based on the pediatric dermal data collated from literature, a predictive maturation model was developed for the stratum corneum thickness, epidermis thickness, dermis thickness, and stratum corneum hydration. Among the three tested models for each parameter, the model that resulted in the lowest test error value was selected as a final model. The final model equations and coefficients are listed in Table 7.4. For the SC thickness, a preliminary maturation (SC Maturation Model 1 in Table 7.4) was constructed based on a dataset that includes measurements reported by Miyauchi et al., 2016 [376]. However, these data report SC thickness values in neonates that exceed values reported in adults (Appendix Figure A1), in contradiction to previous literature findings. An alternate model, SC Maturation Model 2 in Table 7.4, was therefore developed based on a dataset that excludes

measurements from Miyauchi et al., 2016 [376]. The alternative model (SC Maturation Model 2) was chosen as the final model.

Table 7.4 Maturation ratio estimating equations.

Parameter	Equation	Coefficients
Stratum corneum thickness (P_{A_1})	SC Maturation Model 1 $\frac{P_{A_1}(Age)}{P_{adult}} = a \cdot Age^b + c \cdot Age^d + e$ for $Age \leq 1510$ days $\frac{P_{A_1}(Age)}{P_{adult}} = 1$ for age > 1510 days	$a = 2.401 \times 10{-}7$ $b = 2.000$ $c = {-}99.43$ $d = 2.071 \times 10{-}3$ $e = 101.4$
	SC Maturation Model 2 $\frac{P_{A_1}(Age)}{P_{adult}} = a \cdot Age^b + c$ for $Age \leq 1604$ days $\frac{P_{A_1}(Age)}{P_{adult}} = 1$ for $Age >$ 1604 days	$a = 2.662 \times 10{-}7$ $b = 1.878$ $c = 0.724$
Epidermis thickness (P_{A_2})	$\frac{P_{A_2}(Age)}{P_{adult}} = \frac{(1-c) \cdot Age^n}{b^n + Age^n} + c$	$b = 18.702$ $c = 0.634$ $n = 5.363$
Dermis thickness (P_{A_3})	$\frac{P_{A_3}(Age)}{P_{adult}} = \frac{(1.5-c) \cdot Age}{b + Age} + c$ for $Age \leq 9883$ days $\frac{P_{A_3}(Age)}{P_{adult}} = 1$ for $Age >$ 9883 days	$b = 8.974 \times 103$ $c = 0.407$
Stratum corneum hydration (P_{A_4})	$\frac{P_{A_4}(Age)}{P_{adult}} = a \cdot Age^n + b \cdot Age^m + c$ for $Age \leq 1182$ days $\frac{P_{A_4}(Age)}{P_{adult}} = 1$ for $Age >$ 1182 days	$a = {-}0.344$ $b = {-}17.585$ $c = 18.530$

$n = 0.245$

$m = -0.0171$

7.3.3 Age-Dependent Dermal Absorption Model Optimization and Evaluation

7.3.3.1 Dermal Absorption Model Sensitivity Analysis and Parameter Uncertainty

Local sensitivity analysis was conducted on the dermal absorption models (1)–(4) for adults for each of buprenorphine, diamorphine, and phenobarbital. This analysis assessed the impact on model outputs y_J and y_Q of local changes in the diffusion coefficients (D_{sc}, D_{ed}, D_{de}), partition coefficients ($K_{sc/w}$, $K_{ed/w}$, $K_{de/w}$) and skin layer thicknesses (h_{sc}, h_{ed}, h_{de}). The results of the sensitivity analysis are shown in Figure 7.3. For all three compounds, sensitivity was highest with respect to the stratum corneum parameters (D_{sc}, $K_{sc/w}$, h_{sc}).

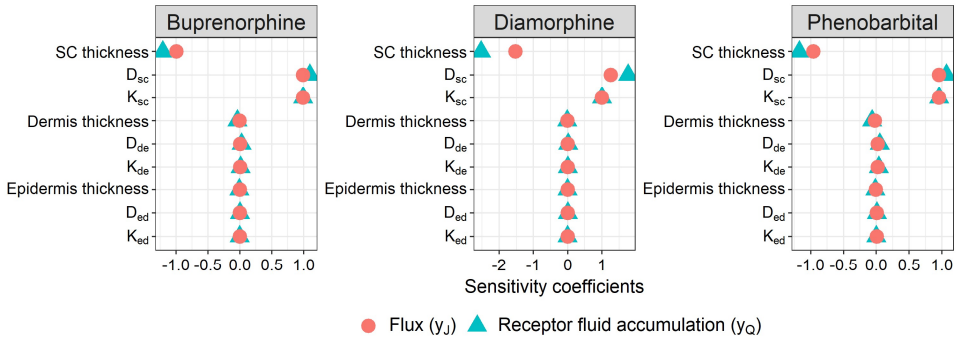

Figure 7.3 Local sensitivity analysis of the outputs y_J and y_Q of the dermal absorption models (1)–(4).

The SC diffusivity and partitioning coefficients, D_{sc} and $K_{sc/w}$, are functions of three uncertain quantitative structure property relationships (QSPR): 1) the permeant trans-lipid bilayer permeability, denoted as $\log_{10} k_{trans}$ [415]; 2) the permeant's SC lipid phase/water partition coefficient, $K_{lip/w}$ [416]; and 3) the permeant's SC protein phase/water partition coefficient, $PC_{pro/w}$ [417]. Nominal values and uncertainties in these QSPRs are summarized in Table 7.5. These three parameters were taken to be the set P^* of uncertain, age-independent model parameters.

Table 7.5 Nominal values and uncertainties in stratum corneum parameters.

Parameter (units)	Nominal value (Uncertainty range)	Source
$\log_{10} k_{trans}$ (cm/s)	Nominal value = $-0.570 - 0.840MW^{\frac{1}{3}}$ Uncertainty range = Nominal value ± 1.26	Wang et al., 2006 [415]
$\log_{10} PC_{pro/w}$	Nominal value = $0.27 \log_{10} K_{o/w} + \log_{10} 5.4$ Uncertainty range = Nominal value ± 0.32	Anderson and Raykar 1989 [416]
$\log_{10} K_{lip/w}$	Nominal value = $0.81 \log_{10} K_{o/w} + \log_{10} 0.43$ Uncertainty range = Nominal value ± 0.434	Nitsche et al., 2006 [417]

The SC thickness, h_{sc}, constitutes the set P_A^* of age-dependent, uncertain parameters of the model.

This quantity varies with the degree of SC hydration [343]. In the case of in vitro diffusion experiments, the SC is assumed to be fully hydrated, with a nominal thickness of 43 μm (Nitsche et al., 2006 [417]). The uncertainty in this model parameter for the case of adult skin, under in vitro (hydrated) conditions, was derived from literature-sourced measurements of the thickness of the partially hydrated SC at various anatomical sites, which are summarized in Table 7.6. First, the coefficient of variation in these measurements was estimated, under the assumption that they are log-normally distributed, to be 0.43. The fully hydrated SC thickness was similarly assumed to be log-normally distributed with a mean of 43 μm and a coefficient of variation equal to that of the partially hydrated SC measurements. From these estimates, the distribution in the fully hydrated h_{sc} for adults was approximated by Lognormal ($\mu = 3.68,\ \sigma^2 = 0.17$), which is taken to be the distribution $p(P_A^*|\text{Age})$ for Age values representing adults.

Table 7.6 Stratum corneum thickness measurements collected from the literature.

Mean (SD) SC Thickness (μm)	Skin Anatomical Site	Reference
13.2 (2.3)	Abdomen	Khiao In et al., 2019 [418]
21 (2.3)	Forearm	Choe et al., 2018 [419]

19 (1.3)	Forearm	
10.4 (3.2)	Forearm	Sauermann et al., 2002 [420]
11.2 (1.9)	Forearm	
13.3	Buttock	Therkildsen et al., 1998 [421]
18.3 (4.9)	Dorsal forearm	
11 (2.2)	Shoulder	Sandby-Møller et al., 2003 [422]
14.9 (3.4)	Buttock	
9.3	Back of hand	
8.7	Centre of calf	
10.9	Outer forearm	
6.2	Inner forearm	
6.4	Inner upper arm	Robertson and Rees 2010 [423]
8.4	Upper back	
6.5	Chest	
6.3	Abdomen	
5.8	Corner of eye	
6.3	Temple	

7.3.3.2 Model Optimization and Evaluation

The model optimization and evaluation steps 0–0 in Methods were implemented for each of buprenorphine, diamorphine, and phenobarbital. Figure 7.4 shows the step 0 fits of the adult dermal absorption model (where parameter $\text{Age} = 30$ years) to the three compounds' flux and receptor fluid

measurements in Table 7.2. Figure 7.5 shows the predictive performance of the fitted model for each compound with respect to permeant flux across neonate and preterm infant skin, as generated by step 0. The pediatric dermal models described the general observed trends of higher dermal absorption (i.e., higher flux) in younger infants. For diamorphine and phenobarbital (Figure 7.5 B,C), the dermal model provided reasonable predictions with most simulation outputs within the 95% confidence intervals. The fold error values of flux in neonates for diamorphine ranged from 0.55 to 1.4 (Table 7.7). For phenobarbital, the fold error values of flux rate in neonates ranged from 0.96 to 1.26. In terms of prediction for preterm neonates, the predicted flux was in good agreement with the observed data with fold error values of 1.2 and 0.93 for diamorphine and phenobarbital, respectively. For buprenorphine (Figure 7.5A), the model could not describe the inter-individual variability observed in full-term neonates (gestational ages of 38 and 40 weeks). The model predicted reasonably for an early term neonate (gestational age of 37 week) with 1–1.37 -fold error.

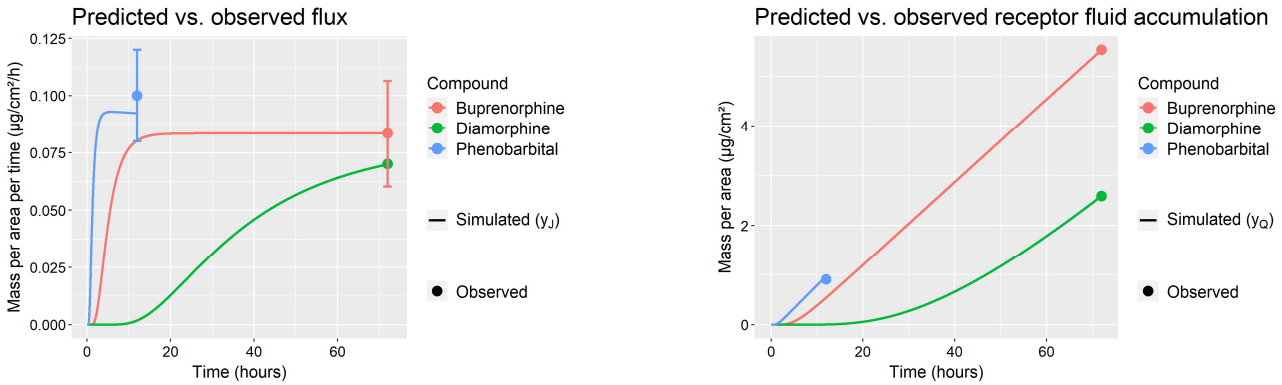

Figure 7.4 Observations and fitted dermal model simulations of flux (A) and receptor fluid accumulation (B). Error bars represent the mean observations ± one standard deviation.

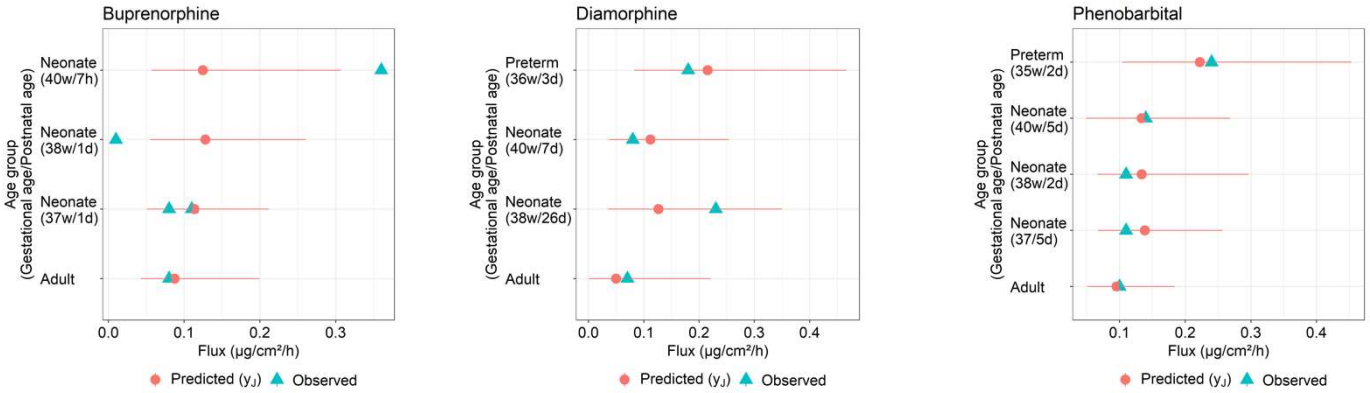

(A) (B) (C)

Figure 7.5 Observed and predicted (mean, 95% CI) flux for adults and newborns for (A) buprenorphine, (B) diamorphine, and (C) phenobarbital.

Table 7.7 Observed and predicted flux values in adults and infants.

Compound (Reference)	Gestational Age (Postnatal Age)	Observed Steady-State Flux (µg/cm2/h)	Predicted Terminal Flux (µm/cm2/h)		Predicted Geometric Mean/Observed Flux Ratio (Fold Error)
			Geometric Mean	95% CI	
Buprenorphine (Barret et al., 1994)	38w (1d)	0.01	0.13	0.06–0.26	12.8
	40w (7h)	0.36	0.12	0.06–0.31	0.35
	37w (1d)	0.08	0.11	0.05–0.21	1.37
	37w (1d)	0.11	0.11	0.05–0.21	1.0
Diamorphine (Barret et al., 1993)	38w (26d)	0.23	0.13	0.04–0.35	0.55
	40w (7d)	0.08	0.11	0.04–0.25	1.4
	36w (3d)	0.18	0.22	0.08–0.47	1.2

	38w (2d)	0.11	0.13	0.07–0.3	1.22
Phenobarbital	40w (5d)	0.14	0.13	0.05–0.27	0.96
(Bonina et al., 1993)	37w (5d)	0.11	0.14	0.07–0.26	1.26
	35w (2d)	0.24	0.22	0.1–0.45	0.93

h: hours, d: days, w: weeks.

7.3.4 Sensitivity Analysis

Post hoc sensitivity analysis was carried out to identify age-dependent parameters for which the outcomes were sensitive. The flux prediction showed age-dependent sensitivity to the SC thickness and a permeability-related parameter (i.e., $\log_{10} k_{trans}$), such that the absolute sensitivity coefficients of these parameters were higher in neonates than those seen in adults.

7.4 Discussion

In this study, the previously published dermal absorption model of Dancik et al. [343] was adapted to incorporate the maturation of skin anatomy and physiology in children. Through a literature review of physiological and anatomical skin parameters, it was found that that all skin layer thicknesses and the skin hydration state of the stratum corneum were age-dependent. Based on literature data, maturation equations were developed and incorporated into the model.

Adult-to-children PK extrapolation was performed using pediatric physiologically based pharmacokinetic modeling (e.g., [45, 180]). In this workflow, adult models were first constructed by optimizing key chemical specific parameters using the observed PK data in adults. Then, the age-dependent components of the model such as hepatic clearance and protein binding are scaled for children. In light of the established workflow of pediatric physiologically based pharmacokinetic (PBPK) modeling, the same steps were followed in this study. The adult model was optimized using the observed data in adults (e.g., flux and cumulative amount) obtained from IVPT experimentation. While chemical-specific parameters in the model remained unchanged, age-dependent components of dermal absorption (e.g., skin layer thickness and SC hydration) were parameterized as a function of age in children.

The model adequately described the relative difference in dermal absorption between adults and infants that were observed in in vitro experiments. In general, infants tended to have a higher absorption rate with higher flux rates (J) compared to that of the adults for buprenorphine, diamorphine, and phenobarbital. In other words, the model successfully predicted the relative differences in dermal absorption between adults and children by taking into account the maturation of skin layer thicknesses and skin hydration.

The predicted flux values agreed with the observed values in neonates for diamorphine and phenobarbital. In the case of buprenorphine, a high inter-individual variability was observed in experimental results between the 40 week-7 h child and the 38 week-1 day child. The 30-fold difference in flux values between these two skin samples could not be captured by the model and this discrepancy is thought to be due to an experimental error. The improbable values could have been due to the handling of the skin samples before the experiment, such as the freezing, thawing and treating the samples with water for rehydration [368], causing the neonatal skin to become damaged.

Pre-term infants with a lower gestational age exhibited higher absorption rates compared to full-term neonates [368-370, 424]. These trends were captured by the developed dermal absorption model accounting only for SC thickness being the difference between pre-term and term neonates. This speaks to the importance of SC thickness in driving flux rate in the model. The model could reasonably describe the flux rate in preterm neonates (i.e., GA: 35–36 weeks), with fold error values ranging from 0.93 to 1.2.

Clearly, these results provide only a small amount of evidence that the anatomy and physiology changes in the model are correct. This study as a whole is limited by the amount of in vitro skin penetration data available for this age group. However, the limited data that were found could generally be recapitulated by the model, although further experimentation would strengthen the basis to say that the model is predictive of age-related changes in dermal absorption.

The prediction of dermal absorption in children is critical for pediatric clinical applications. Transdermal drug delivery in neonates is advantageous because it can replace an invasive procedure of an intravenous line or an oral administration [425]. The smaller dose requirements and high permeability in neonates makes transdermal drug delivery more plausible [426]. This form of delivery

has already been used in children—for example, fentanyl, tulobuterol and lindocaine:prilocaine (EMLA) [425].

Topical bioavailability can be determined by the physicochemical properties of a drug and the vehicle, such as: temperature, skin anatomy and physiology, skin hydration and metabolism in dermis and epidermis [427]. The stratum corneum plays an important role in dermal absorption as a skin barrier [361, 425, 428]. The lipid composition and integrity of the SC are important components in the regulation of skin permeability [346, 429]. Therefore, the maturation of the SC determines the extent and the rate of dermal absorption in children [425]. The post hoc sensitivity analysis indicated that the flux rate prediction was the most sensitive to the SC thickness, indicating that the pediatric model appropriately reflected these literature findings. This was also corroborated in the flux prediction for preterm infants.

Compound-specific parameters of $\log_{10} k_{trans}$, $K_{lip/w}$ and $PC_{pro/w}$ were optimized based on the available dermal absorption data in adults (e.g., flux, cumulated amounts), and these parameters were kept the same in both adult and children models. According to the post hoc sensitivity analysis, the parameters that were the most important in predicting the relative difference of dermal absorption between adults and children was the SC thickness and $\log_{10} k_{trans}$. The satisfactory prediction accuracy of the model output indicated that the most important age-related parameters were appropriately parameterized in the model.

According to Code of Federal Regulations Title 21 Part 320 (§320.23) [430], it was stated that "For drug products that are not intended to be absorbed into the bloodstream, bioavailability may be assessed by measurements intended to reflect the rate and extent to which the active ingredient or moiety becomes available at the site of action". In vitro permeation testing is an important tool for evaluating the permeation amount and the rate of active compounds with the use of excised human skin [431]. It is required to characterize the rate and extent of drug delivery via transdermal or topical routes to demonstrate bioequivalence [432]. The relative difference in dermal absorption between adults and children can be predicted by taking into account the physicochemical properties of the drug and the maturation of skin physiology and anatomy. With the available in vitro permeation test data in adults, this dermal model in children can provide an estimation of a rate of absorption (flux y_J) following topical exposure.

Supplementary Materials: The following are available online at https://www.mdpi.com/article/10.3390/pharmaceutics14010172/s1, Table S1. Stratum corneum (SC) thickness in infants and children, Table S2. Thickness of the viable epidermis in infants and children, Table S3. Thickness of the dermis in infants and children, Table S4. Stratum corneum (SC) hydration in infants and children, Table S5. Corneocyte volume fraction, Table S6. Follicle size and Volume, Table S7. Stratum corneum thickness literature review and search strategy, Table S8. Epidermis thickness literature review and search strategy, Table S9. Dermis thickness literature review and search strategy, Table S10. Stratum corneum hydration literature review and search strategy, Table S11. Corneocyte volume fraction literature review and search strategy, Table S12. Lipid and protein ratio literature review and search strategy, Table S13. Follicle size, density, volume literature review and search strategy, Table S14. Albumin concentration literature review and search strategy.

7.5 Author Contributions

Conceptualization, Y.E.Y. and A.N.E.; Methodology, Y.E.Y., D.C.-N., A.H. and A.N.E.; Software, Y.E.Y. and A.H.; Validation, Y.E.Y. and A.H.; Formal Analysis, Y.E.Y., D.C.-N. and A.H.; Investigation, Y.E.Y., D.C.-N., A.H. and A.N.E.; Resources, Y.E.Y., A.H. and A.N.E.; Data Curation, Y.E.Y. and D.C.-N.; Writing—Original Draft Preparation, Y.E.Y., D.C.-N., A.H. and A.N.E.; Writing—Review and Editing, Y.E.Y., D.C.-N., A.H. and A.N.E.; Visualization, Y.E.Y. and A.H.; Supervision, A.N.E.; Project Administration, A.N.E.; Funding Acquisition, Y.E.Y. and A.N.E. All authors have read and agreed to the published version of the manuscript.

Appendix A. Alternative Maturation Model

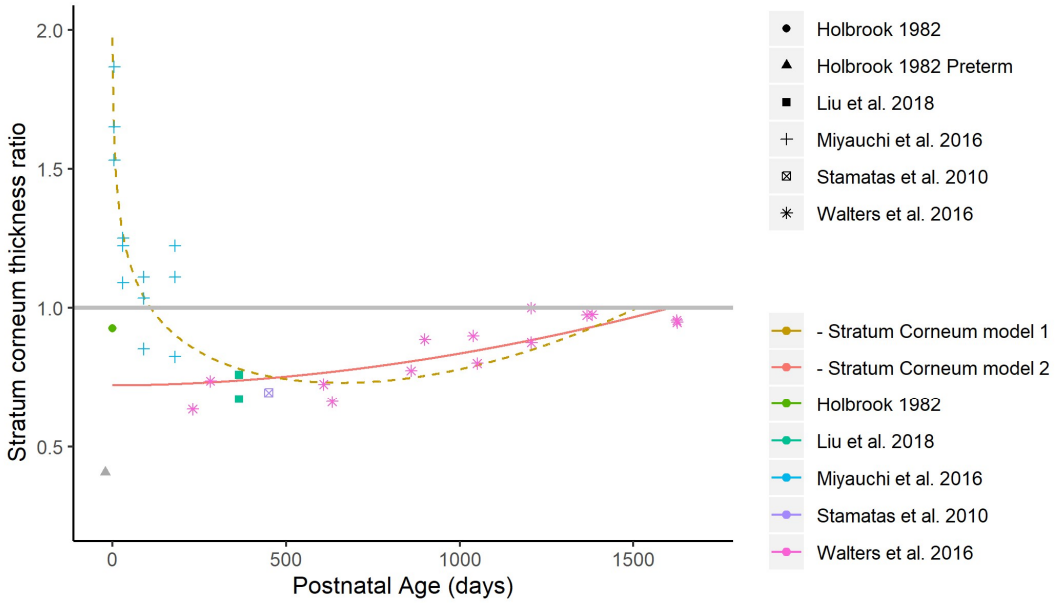

Figure A1. Alternative maturation model for stratum corneum thickness.

Chapter 8: Discussion, Future directions and Conclusions

8.1 Discussion

The main objective of this dissertation was to develop a framework for effective pediatric PBPK modeling to inform human health risk assessment for children. Pediatric toxicokinetics refers to absorption, distribution, metabolism and excretion of environmental toxicants in children. The objective of toxicological and pharmacological assessments can differ [433]. In pharmacology, following a therapeutic drug administerationd to children, pharmacokinetics and pharmacodynamics are characterized to evaluate the drug's dose-exposure and exposure-therapeutic effect, respectively. In toxicology, following an environmental exposure to a toxicant, toxicokinetics can be characterized to evaluate the dose-exposure profile with extrapolation to health risk. With the lack of pediatric toxicokinetic studies due to ethical reasons, relatively rich pediatric pharmacokinetic data has been utilized for health risk characterization of environmental chemicals in children [434].

In Chapter 2, pediatric PBPK models for 10 hepatically metabolized compounds were developed and qualified. Through sensitivity analyses of these models, the most important parameters for pediatric PBPK modeling were identified. It was found that protein binding and clearance parameters were important for pediatric PBPK model outcome. In light of these findings, prediction methods of plasma protein binding and clearance in children were chosen as the topics of next chapters of this thesis. Chapters 3, 4 and 5 pertain to prediction methods for protein binding in children, and Chapter 6 pertain to development of a framework to predict clearance in children for data-sparse compounds.

In Chapter 3, quantitative structure–property relationship (QSPR) models predicting fraction unbound in plasma in humans were evaluated. For human health risk assessment in children, fup_{child} or fup_{adult} for environmentally relevant compounds may not be readily available. This study was undertaken in order to investigate the available models that predict fup values in humans from chemical structures of compounds. Predictive performances of Watanabe et al. [194] and Ingle et al. [186] were compared to that of a commercial software ADMET predictor. The test set was comprised of 818 pharmaceutical and environmentally relevant compounds with fup values ranging from 0.01 to 1. For predicting human fup from chemical structures, the positive polar surface area, the number of basic functional groups and lipophilicity were the most important chemical descriptors. This study found

that that the fup prediction can be uncertain for highly binding compounds (i.e. $0.01 \leq fup \leq 0.25$). This result suggested that, when high prediction accuracy is required, an experimental determination of fup is needed.

In Chapter 4, an evaluation of predictive performance of adult-to-children scaling algorithms (ontogeny models) for fup was undertaken. The ontogeny models describe the plasma protein concentrations (i.e. albumin or AAG) as a function of age. These ontogeny models are important because those models provide an estimate of fup_{child} for pediatric PBPK modeling. Although many ontogeny models were available (4 ontogeny models for albumin and 5 ontogeny models for AAG), the predictive performance of the model had not been evaluated with the same test dataset. In this study, in order to evaluate of the appropriateness of protein concentration vs. age profile for each model, the predicted plasma protein concentrations were compared to the observed values obtained from the literature. Plasma protein concentrations vs. age profiles derived from non-linear equations (e.g. PK-Sim and Johnson et al. [243]) were more in agreement with the observed levels than other models (e.g. McNamara et al.[211], Alcorn and McNamara [25]). The findings were in line with the results from the Chapter 3 such that highly binding compounds were more sensitive to the appropriateness of the protein concentration vs. age profiles of ontogeny models. For prediction accuracy, the choice of ontogeny model was more important for AAG, highly bound compounds and infants.

In Chapter 5, the prediction methods evaluated in Chapters 3 and 4 were combined. This study was conducted in order to evaluate the overall uncertainty when both QSPR models for predicting human fup and protein binding ontogeny models are used to predict fup_{child} from a chemical structure. These models are most needed especially for evaluating the health risk in children for environmentally relevant compounds because fup values in children are not readily available due to ethical reasons. The protein binding information – whether a compound primarily binds to either albumin or AAG is also not readily available for environmentally relevant compounds. In this study, the impact of data availability for predicting protein binding in children using the ontogeny models was investigated. The use of QSPR-predicted fup_{adult} for fup_{child} prediction resulted in over-predictions for acids and neutrals indicating that an experimental determination of fup_{adult} is required when high precision is needed. In addition, it was found that chemical ionization information derived from a compound's

structural data can help to select the most appropriate ontogeny model for predicting protein binding in children.

From Chapter 2, it was discovered that parameters related clearance and fup are crucial for pediatric PBPK modeling. Following the extensive investigation on the topic of prediction of protein binding in children, the next topic was about a prediction of clearance in children. In chapter 6, all of the findings from Chapter 2 to 5 were amalgamated in order to develop a framework for predicting clearance in children for human health risk assessment. This workflow utilizes QSPR models, protein binding ontogeny models and virtual pediatric individuals. In order to predict pediatric CL values from a compound structure, many steps are required. Compound-specific input parameters include rate of clearance (e.g. hepatic intrinsic clearance, renal clearance), route of predominant clearance pathway, acid-base properties, plasma protein binding, metabolizing enzymes. For these compound-specific input parameters various QSPR methods were used. System-specific input parameters include ontogeny factors of metabolizing enzyme and protein binding, anatomical, biochemical and physiological parameters of a child at a specific age. These system-specific input parameters were obtained from virtual pediatric population created from PK-Sim.

Two QSPR approach based methods for predicting CL in children were proposed. The two methods (Method 1 and Method 2) share the same steps but the last step of estimating plasma CL in children was different. Briefly, hepatic CLint and CLr in adults were predicted from a compound structure using QSPR methods. By using appropriate scaling methods, the hepatic CLint and CLr in adults were scaled to hepatic CLint and CLr in children. For Method 1, plasma CL in children was calculated by adding predicted hepatic CL and CLr in children. For Method 2, a predominant route of clearance pathway (e.g. hepatic metabolism or renal excretion) was predicted based on physicochemical properties of compounds. For estimating plasma CL in children, a QSPR-predicted CL value of the predominant route of elimination was assumed to approximate plasma clearance in virtual individuals.

When the predicted predominant route of clearance pathway information was used (e.g. Method 2), the predictive accuracy was better than the case where the predominant route of clearance pathway information was not used (Method 1). This indicates that determination of the predominant route of

clearance pathway from compound structure can improve a prediction accuracy for estimating plasma CL in child for data-sparse compounds.

Another important aspect of this study was to estimate an inter-individual variability in pediatric CL values. The weight based allometry of Method 3 resulted in a smaller inter-individual variability (CV 9.34 %) compared to that in Method 1 (30.1%) and Method 2 (33.9%). This was because the method 3 only accounts for the variability of weight of virtual individuals. Method 1 and Method 2 were considered more physiologically relevant as those methods take into account variabilities in biochemical and physiological parameters (e.g. GFR, ontogeny factors CYP enzymes and plasma protein binding). The proposed workflow is thought to provide a reasonable estimation of clearance in pediatric population for human health risk assessment for data-sparse compounds.

In the next chapter, a predictive model for dermal absorption in children which is another important aspect of pediatric pharmacokinetics was developed. For important model parameters that are age-dependent (e.g. skin layer thicknesses and the skin hydration state of the stratum corneum), maturation equations were generated based on observed data in literature. A pediatric dermal absorption model was developed by updating a MoBi implementation of the Dancik et al. 2013 [343] skin permeation model. This model provides prediction of the relative difference in dermal absorption between adults and children by taking into account the physicochemical properties of the drug and the maturation of skin physiology and anatomy. Key chemical specific parameters in adult models were optimized by using the observed dermal absorption data in adults (e.g. in vitro permeation testing experimentation). For predicting dermal absorption in children, chemical-specific parameters in the model remained the same as in the adult model and age-dependent components of dermal absorption (e.g., skin layer thickness and hydration) were scaled as a function of age.

Due to sparsity in the observed dermal absorption data in children, the predictive performance of this model was evaluated using a limited set of compounds. The prediction accuracy of this model was reasonable for most comparisons between the predicted and observed flux values except one case where an experimental error was suspected (e.g. damaging of a neonatal skin sample when freezing and thawing). Dermal absorption prediction in children is an important aspect in human health risk assessment. This model is considered useful in predicting dermal absorption for environmentally relevant compounds and product chemicals (e.g. sunscreen [435]).

In drug development, observed PK data in children are often available and helpful for determining an appropriate dosing regimen. However, for human health risk assessment, PK data in pediatrics are not readily available. When the critical PK parameters are not available, various computational methods can be used. The studies in this dissertation evaluated computational methods that can be used to estimate pediatric PK for data-sparse compounds (e.g. environmentally relevant compounds).

In this dissertation, two types of models were investigated. First, predictive performances of QSPR models that predict PK values in human from compound structures were evaluated in Chapters 3 and 6. Second, predictive performances of adult to children scaling methods were evaluated in Chapters 2 and 4. In Chapter 5, theoverall uncertainty when QSPR methods for fup prediction in human and ontogeny model are combined to predict fup in children was assessed. In Chapter 6, overall uncertainty when QSPR methods and ontogeny models for both fup and CL were combined to predict CL in children were evaluated. These studies evaluated model appropriateness (e.g. observed vs. predicted protein concentrations in children for ontogeny models) and predictive performances of the workflows. The evaluations shed light on whether these computational methods provide reasonable estimation in children PK. The evaluations also identified areas of uncertainty.

In human health risk assessment, scaling of PK is often conducted by using simplified approaches such as applying HKAF or allometry scaling. In order to account relative difference in PK between adult and children population, HKAF of 3.16 can be applied to toxicological index [6]. On the other hand, scaling based on allometry assumes that relative difference in PK between adults and children is a function of weight or size. These simplified methods do not fully consider maturation and inter-individual variabilities in anatomical, biochemical and physiological aspects of children. Physiologically based estimation methods are considered more relevant as the models take into account for those aspects. The evaluations in Chapters 2 and 5 demonstrated that adult-to-children scaling of protein binding and clearance showed reasonable predictions (physiologically relevant methods). However, the predictive performance of the QSPR methods to estimate protein binding and clearance from structural data requires improvement.

CL prediction in children is more complicated than the prediction of plasma protein binding in children. For predicting fup in children, adult fup values are predicted using QSPR methods and plasma protein ontogeny models were used to scale adult value (human value predicted from QSPR

method was assumed to equivalent to adult values) to fup in children value. On the other hand, CL prediction in children required many compound-specific and system-specific parameters and also predicted fup_{child}. The prediction accuracy of fup_{child} depended on the prediction accuracy of two models – QSPR model and ontogeny model. The prediction accuracy of CLchild depended on prediction performances of numerous models including the fup_{child} prediction models. The predictive performance of QSPR methods can be improved by (i) using more advanced technique such as deep learning for model development and (ii) expanding the chemical space of training set.

One of advantages of QSPR models is that those models can be incorporated into High Through-put Screening (HTS) projects. HTS of environmental toxicants is fast and easy compared to traditional toxicological studies that can be expensive and time-consuming. Sipes et al. [338] presents estimated daily exposure of 56 compounds that can possibly elicit human in vivo interaction. Unlike higher dose amounts that are usually administered to elicit therapeutic effect of drugs (e.g. 1~100 mg/kg/day), the magnitude of doses eliciting a 'possible' human in vivo interaction can be small for environmental chemicals (e.g. 10^{-6} ~ 0.1 mg/kg/day) [338]. Considering the low exposure levels of environmental chemicals compared to pharmaceuticals, the high precision of QSPR models that would be required for pharmaceutical applications may not be necessary. This is because these models are used in the context of HTS. These models can be useful for risk assessors to prioritize compounds and identify potential health risks.

8.2 Future directions and Limitations

One of challenges for evaluating the available QSPR models or ontogeny models for predicting pediatric PK was the sparsity of observed PK data in children. More observed data in children is needed to evaluate the predictive performance of the available models and to improve a framework of predicting PK in children. For example, more observed CL and dermal absorption data in both adults and children is needed to evaluate the presented models.

In addition, clearance prediction in children is focused on well-studied metabolizing enzymes such as CYPs or UGTs. However, there are compounds that are mainly metabolized by less known enzymes such as hydrolases (e.g. carboxyesterase) and flavin-containing monooxygenase (FMO). A possible

ontogeny effect of these enzyme needs to be studied and incorporated into *in silico* systems to better estimate clearance in children.

One of limitations of this study is that pharmacogenomic effects (e.g. CYP2C19 poor metabolizer, CYP2C19 rapid metabolizer) on clearance and racial effects on PK were not taken into account. Incorporation of those system-specific factors in PK prediction in children can help risk assessors to identify a vulnerable subgroup in children.

8.3 Conclusions

The proposed workflows and developed models for predicting important PK parameters in children in this dissertation are considered to be useful in decreasing uncertainties associated with PK in children estimation from compound structure for environmentally relevant compounds. Furthermore, the proposed models are physiologically relevant and these models will help risk assessors to make informed decisions for human health risk assessment in children.

Letters of Copyright Permission

Chapter 2

May 4, 2022

Dear Author,

Thank you for your correspondence requesting permission to reproduce the above content from our Journal in your thesis to be posted on your University's repository.

We will be pleased to grant permission to reproduce your '**Accepted/Original Manuscript'** (please check the embargo: Open access cost finder - Author Services (taylorandfrancis.com) on the sole condition that you acknowledge the original source of publication.

This is an '**Accepted/Original Manuscript'** of an article published by Taylor & Francis Group in Journal of Toxicology and Environmental Health, Part A on 12 Aug 2019, available online: https://wwww.tandfonline.com/10.1080/15287394.2019.1652215."

This permission does not cover any third party copyrighted work which may appear in the material requested. Please ensure you have checked all original source details for the rights holder.

Further permission will be required if your thesis is published. (Please see information for sharing your work https://authorservices.taylorandfrancis.com/sharing-your-work/)

Thank you for your interest in our Journal.

With best wishes,

Annabel
Annabel Flude| Permissions Administrator
Journals, Taylor & Francis Group
Permissions e-mail: permissionrequest@tandf.co.uk
Web: www.tandfonline.com

4 Park Square, Milton Park, Abingdon, OX14 4RN
+44 (0)20 8052 0659

Chapter 3

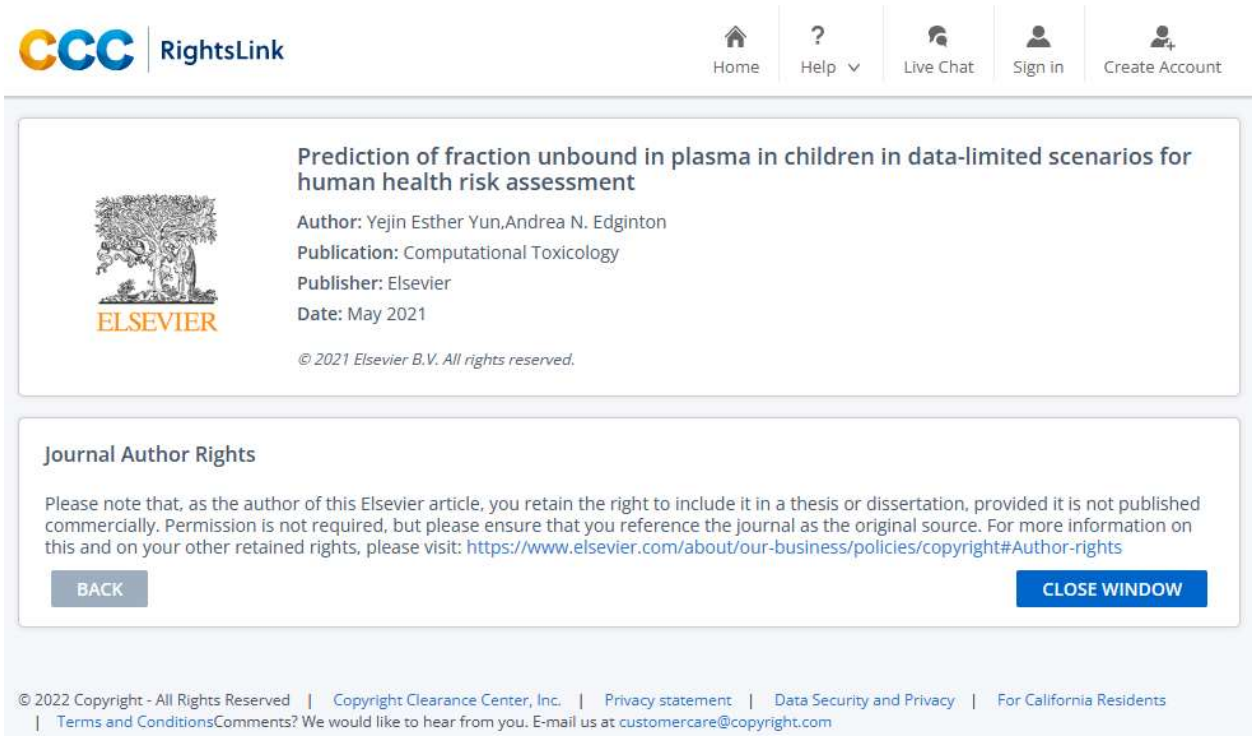
RightsLink
Home
Help
Live Chat
Sign in
Create Account
Prediction of fraction unbound in plasma in children in data-limited scenarios for human health risk assessment
Author: Yejin Esther Yun,Andrea N. Edginton
Publication: Computational Toxicology
Publisher: Elsevier
Date: May 2021
© 2021 Elsevier B.V. All rights reserved.
Journal Author Rights
Please note that, as the author of this Elsevier article, you retain the right to include it in a thesis or dissertation, provided it is not published commercially. Permission is not required, but please ensure that you reference the journal as the original source. For more information on this and on your other retained rights, please visit: https://www.elsevier.com/about/our-business/policies/copyright#Author-rights
BACK
CLOSE WINDOW
© 2022 Copyright - All Rights Reserved | Copyright Clearance Center, Inc. | Privacy statement | Data Security and Privacy | For California Residents | Terms and ConditionsComments? We would like to hear from you. E-mail us at customercare@copyright.com

Chapter 4

May 4, 2022

Dear Author,

Thank you for your correspondence requesting permission to reproduce the above content from our Journal in your thesis to be posted on your University's repository.

We will be pleased to grant permission to reproduce your '**Accepted/Original Manuscript'** (please check the embargo: Open access cost finder - Author Services (taylorandfrancis.com) on the sole condition that you acknowledge the original source of publication.

This is an '**Accepted/Original Manuscript'** of an article published by Taylor & Francis Group in Journal of Toxicology and Environmental Health, Part A on 26 Oct 2020, available online: https://wwww.tandfonline.com/10.1080/15287394.2020.1835761"

This permission does not cover any third party copyrighted work which may appear in the material requested. Please ensure you have checked all original source details for the rights holder.

Further permission will be required if your thesis is published. (Please see information for sharing your work https://authorservices.taylorandfrancis.com/sharing-your-work/)

Thank you for your interest in our Journal.

With best wishes,

Annabel
Annabel Flude| Permissions Administrator
Journals, Taylor & Francis Group
Permissions e-mail: permissionrequest@tandf.co.uk
Web: www.tandfonline.com

4 Park Square, Milton Park, Abingdon, OX14 4RN
☎·+44 (0)20 8052 0659

Chapter 5


RightsLink
Home
Help
Live Chat
Sign in
Create Account
Evaluation of quantitative structure property relationship algorithms for predicting plasma protein binding in humans
Author: Yejin Esther Yun,Rogelio Tornero-Velez,S. Thomas Purucker,Daniel T. Chang,Andrea N. Edginton
Publication: Computational Toxicology
Publisher: Elsevier
Date: February 2021
© 2020 The Authors. Published by Elsevier B.V.
ELSEVIER
Journal Author Rights
Please note that, as the author of this Elsevier article, you retain the right to include it in a thesis or dissertation, provided it is not published commercially. Permission is not required, but please ensure that you reference the journal as the original source. For more information on this and on your other retained rights, please visit: https://www.elsevier.com/about/our-business/policies/copyright#Author-rights
BACK
CLOSE WINDOW
© 2022 Copyright - All Rights Reserved | Copyright Clearance Center, Inc. | Privacy statement | Data Security and Privacy | For California Residents | Terms and ConditionsComments? We would like to hear from you. E-mail us at customercare@copyright.com

Chapter 7

Citation: Yun, Y.E.; Calderon-Nieva, D.; Hamadeh, A.; Edginton, A.N. Development and Evaluation of an In Silico Dermal Absorption Model Relevant for Children. *Pharmaceutics* **2022**, *14*, 172. https://doi.org/10.3390/pharmaceutics14010172

Academic Editor: Cheong-Weon Cho

Received: 16 November 2021
Accepted: 29 December 2021
Published: 12 January 2022

References

1. World Health Organization, *WHO human health risk assessment toolkit: chemical hazards*. 2010: World Health Organization.
2. International Programme on Chemical Safety, *Descriptions of selected key generic terms used in chemical hazard/risk assessment. International Programme on Chemical Safety Joint Project with OECD on Harmonisation of Hazard/Risk Assessment Terminology*. 2003.
3. Barnes, D.G., et al., *Reference dose (RfD): description and use in health risk assessments.* Regulatory toxicology and pharmacology, 1988. **8**(4): p. 471-486.
4. Thompson, C.M., et al., *Approaches for applications of physiologically based pharmacokinetic models in risk assessment.* J Toxicol Environ Health B Crit Rev, 2008. **11**(7): p. 519-47.
5. WHO, *Principles for evaluating health risks in children associated with exposure to chemicals*. 2006: World Health Organization.
6. Bhat, V.S., et al., *Evolution of chemical-specific adjustment factors (CSAF) based on recent international experience; increasing utility and facilitating regulatory acceptance.* Critical reviews in toxicology, 2017. **47**(9): p. 733-753.
7. United States Environmental Protection Agency, *A framework for assessing health risks of environmental exposures to children.* US Environmental Protection Agency, Washington, DC, EPA/600/R-05/093F, 2006.
8. World Health Organization, *Assessing human health risks of chemicals: derivation of guidance values for health-based exposure limits.* 1994.
9. Renwick, A.G., *Data-derived safety factors for the evaluation of food additives and environmental contaminants.* Food Addit Contam, 1993. **10**(3): p. 275-305.
10. Valcke, M. and K. Krishnan, *Characterization of the human kinetic adjustment factor for the health risk assessment of environmental contaminants.* J Appl Toxicol, 2014. **34**(3): p. 227-40.
11. International Programme on Chemical Safety, *Guidance document for the use of data in development of chemical-specific adjustment factors (CSAFs) for-interspecies differences and human variability in dose/concentration–response assessment*. 2001, World Health Organization Geneva, Switzerland.
12. Clewell, H.J., et al., *Evaluation of the potential impact of age-and gender-specific pharmacokinetic differences on tissue dosimetry.* Toxicological Sciences, 2004. **79**(2): p. 381-393.
13. Meek, M.E., et al., *Guidelines for application of chemical-specific adjustment factors in dose/concentration-response assessment.* Toxicology, 2002. **181-182**: p. 115-20.
14. Price, P.S., R.E. Keenan, and B. Schwab, *Defining the interindividual (intraspecies) uncertainty factor.* Human and Ecological Risk Assessment, 1999. **5**(5): p. 1023-1033.

15. Ginsberg, G., et al., *Evaluation of child/adult pharmacokinetic differences from a database derived from the therapeutic drug literature.* Toxicol Sci, 2002. **66**(2): p. 185-200.

16. EPA, U.S., *Approaches for the Application of Physiologically Based Pharmacokinetic (PBPK) Models and Supporting Data in Risk Assessment.* U.S. Environmental Protection Agency, Washington, D.C., EPA/600/R-05/043F, 2006., 2006.
17. World Health Organization, *Characterization and Application of Physiologically Based Pharmacokinetic Models in Risk Assessment*. 2010, World Health Organization, International Programme on Chemical Safety
18. Zhao, P., et al., *Applications of physiologically based pharmacokinetic (PBPK) modeling and simulation during regulatory review.* Clinical Pharmacology & Therapeutics, 2011. **89**(2): p. 259-267.
19. Health Canada, *Human health risk assessment for priority substances.* Canadian Environmental Protection Act Report, 1994.
20. Ginsberg, G., D. Hattis, and B. Sonawane, *Incorporating pharmacokinetic differences between children and adults in assessing children's risks to environmental toxicants.* Toxicology and applied pharmacology, 2004a. **198**(2): p. 164-183.
21. Scheuplein, R., G. Charnley, and M. Dourson, *Differential sensitivity of children and adults to chemical toxicity. I. Biological basis.* Regul Toxicol Pharmacol, 2002. **35**(3): p. 429-47.
22. Hines, R.N. and D.G. McCarver, *The ontogeny of human drug-metabolizing enzymes: phase I oxidative enzymes.* Journal of Pharmacology and Experimental Therapeutics, 2002. **300**(2): p. 355-360.
23. Arant Jr, B.S., *Developmental patterns of renal functional maturation compared in the human neonate.* J Pediatr, 1978. **92**(5): p. 705-712.
24. Kearns, G.L., et al., *Developmental pharmacology—drug disposition, action, and therapy in infants and children.* New England Journal of Medicine, 2003. **349**(12): p. 1157-1167.
25. McNamara, P.J. and J. Alcorn, *Protein binding predictions in infants.* AAPS PharmSci, 2002. **4**(1): p. E4.
26. Bonner, J.J., et al., *Does age affect gastric emptying time? A model-based meta-analysis of data from premature neonates through to adults.* Biopharmaceutics & drug disposition, 2015. **36**(4): p. 245-257.
27. Maharaj, A.R. and A.N. Edginton, *Examining Small Intestinal Transit Time as a Function of Age-Is There Evidence to Support Age-Dependent Differences Among Children?* Drug Metabolism and Disposition, 2016: p. dmd. 115.068700.
28. Maharaj, A.R., A.N. Edginton, and N. Fotaki, *Assessment of age-related changes in pediatric gastrointestinal solubility.* Pharmaceutical research, 2016. **33**(1): p. 52-71.

29. Hines, R.N., *Ontogeny of human hepatic cytochromes P450.* J Biochem Mol Toxicol, 2007. **21**(4): p. 169-75.
30. Ratanasavanh, D., et al., *Intralobular distribution and quantitation of cytochrome P-450 enzymes in human liver as a function of age.* Hepatology, 1991. **13**(6): p. 1142-1151.
31. Edginton, A.N. and G. Joshi, *Have physiologically-based pharmacokinetic models delivered?* Expert opinion on drug metabolism & toxicology, 2011. **7**(8): p. 929-934.
32. Manolis, E. and G. Pons, *Proposals for model-based paediatric medicinal development within the current European Union regulatory framework.* British journal of clinical pharmacology, 2009. **68**(4): p. 493-501.
33. Cole, S., et al., *European regulatory perspective on pediatric physiologically based pharmacokinetic models.* International journal of Pharmacokinetics, 2017. **2**(2): p. 113-124.
34. Shebley, M., et al., *Physiologically Based Pharmacokinetic Model Qualification and Reporting Procedures for Regulatory Submissions: A Consortium Perspective.* Clin Pharmacol Ther, 2018. **104**(1): p. 88-110.
35. Yoshida, K., N. Budha, and J.Y. Jin, *Impact of physiologically based pharmacokinetic models on regulatory reviews and product labels: Frequent utilization in the field of oncology.* Clin Pharmacol Ther, 2017. **101**(5): p. 597-602.
36. Wagner, C., et al., *Application of physiologically based pharmacokinetic (PBPK) modeling to support dose selection: report of an FDA public workshop on PBPK.* CPT: pharmacometrics & systems pharmacology, 2015. **4**(4): p. 226-230.
37. Krauss, M., et al., *Using Bayesian-PBPK Modeling for Assessment of Inter-Individual Variability and Subgroup Stratification.* Journal of Pharmacokinetics and Pharmacodynamics, 2013. **40**: p. S33-S34.
38. Bernillon, P. and F.Y. Bois, *Statistical issues in toxicokinetic modeling: a bayesian perspective.* Environ Health Perspect, 2000. **108 Suppl 5**: p. 883-93.
39. Bois, F.Y., M. Jamei, and H.J. Clewell, *PBPK modelling of inter-individual variability in the pharmacokinetics of environmental chemicals.* Toxicology, 2010. **278**(3): p. 256-67.
40. Gilks, W.R., S. Richardson, and D. Spiegelhalter, *Markov chain Monte Carlo in practice*. 1995: CRC press.
41. Leong, R., et al., *Regulatory experience with physiologically based pharmacokinetic modeling for pediatric drug trials.* Clinical Pharmacology & Therapeutics, 2012. **91**(5): p. 926-931.
42. Holford, N., Y.A. Heo, and B. Anderson, *A pharmacokinetic standard for babies and adults.* J Pharm Sci, 2013. **102**(9): p. 2941-52.
43. Björkman, S., *Prediction of cytochrome P450-mediated hepatic drug clearance in neonates, infants and children.* Clinical pharmacokinetics, 2006. **45**(1): p. 1-11.
44. Edginton, A.N., et al., *A mechanistic approach for the scaling of clearance in children.* Clin Pharmacokinet, 2006a. **45**(7): p. 683-704.

45. Edginton, A.N., W. Schmitt, and S. Willmann, *Development and evaluation of a generic physiologically based pharmacokinetic model for children.* Clinical pharmacokinetics, 2006. **45**(10): p. 1013-1034.
46. Maharaj, A.R., J.S. Barrett, and A.N. Edginton, *A workflow example of PBPK modeling to support pediatric research and development: case study with lorazepam.* AAPS J, 2013. **15**(2): p. 455-64.
47. Maharaj, A.R. and A.N. Edginton, *Physiologically Based Pharmacokinetic Modeling and Simulation in Pediatric Drug Development.* CPT Pharmacometrics Syst Pharmacol, 2014. **3**(11): p. 1-13.
48. Agency, E.M., *Guideline on the qualification and reporting of physiologically based pharmacokinetic (PBPK) modelling and simulation.* 2016.
49. Yellepeddi, V., et al., *State-of-the-Art Review on Physiologically Based Pharmacokinetic Modeling in Pediatric Drug Development.* Clinical pharmacokinetics, 2018: p. 1-13.
50. Barrett, J.S., et al., *Physiologically based pharmacokinetic (PBPK) modeling in children.* Clin Pharmacol Ther, 2012. **92**(1): p. 40-9.
51. Edginton, A.N. and L. Ritter, *Predicting plasma concentrations of bisphenol A in children younger than 2 years of age after typical feeding schedules, using a physiologically based toxicokinetic model.* Environmental health perspectives, 2009. **117**(4): p. 645.
52. Willmann, S., et al., *PK-Sim (R): a physiologically based pharmacokinetic'whole-body'model.* Biosilico, 2003. **4**(1): p. 121-124.
53. Eissing, T., et al., *A computational systems biology software platform for multiscale modeling and simulation: integrating whole-body physiology, disease biology, and molecular reaction networks.* Frontiers in Physiology, 2011. **2**.
54. Peters, S.A., *Physiologically-based pharmacokinetic (PBPK) modeling and simulations: principles, methods, and applications in the pharmaceutical industry*. 2012: John Wiley & Sons.
55. McNally, K., R. Cotton, and G.D. Loizou, *A workflow for global sensitivity analysis of PBPK models.* Frontiers in pharmacology, 2011. **2**: p. 31.
56. Malik, P.R., et al., *Population PBPK modelling of trastuzumab: a framework for quantifying and predicting inter-individual variability.* Journal of pharmacokinetics and pharmacodynamics, 2017. **44**(3): p. 277-290.
57. McLanahan, E.D., et al., *The Use of PBPK Models to Inform Human Health Risk Assessment: Case Study on Perchlorate and Radioiodide Human Lifestage Models.* Risk Analysis, 2014. **34**(2): p. 356-366.
58. Ginsberg, G., et al., *Physiologically based pharmacokinetic (PBPK) modeling of caffeine and theophylline in neonates and adults: implications for assessing children's risks from environmental agents.* J Toxicol Environ Health A, 2004. **67**(4): p. 297-329.
59. Daston, G., et al., *A framework for assessing risks to children from exposure to environmental agents.* Environ Health Perspect, 2004. **112**(2): p. 238-56.

60. Mork, A.K., F. Jonsson, and G. Johanson, *Adjustment factors for toluene, styrene and methyl chloride by population modeling of toxicokinetic variability.* Regul Toxicol Pharmacol, 2014. **69**(1): p. 78-90.
61. Valcke, M. and K. Krishnan, *Evaluation of the impact of the exposure route on the human kinetic adjustment factor.* Regul Toxicol Pharmacol, 2011. **59**(2): p. 258-69.
62. Nong, A., et al., *Modeling interchild differences in pharmacokinetics on the basis of subject-specific data on physiology and hepatic CYP2E1 levels: A case study with toluene.* Toxicology and Applied Pharmacology, 2006. **214**(1): p. 78-87.
63. Gerlowski, L.E. and R.K. Jain, *Physiologically Based Pharmacokinetic Modeling - Principles and Applications.* Journal of Pharmaceutical Sciences, 1983. **72**(10): p. 1103-1127.
64. World Health Organization, *Chemical-specific adjustment factors for interspecies differences and human variability: guidance document for use of data in dose/concentration-response assessment*. Vol. 2. 2005: World Health Organization.
65. Ginsberg, G., et al., *A framework and case studies for evaluation of enzyme ontogeny in children's health risk evaluation.* J Toxicol Environ Health A, 2017. **80**(10-12): p. 569-593.
66. Khadra, I., et al., *Statistical investigation of simulated intestinal fluid composition on the equilibrium solubility of biopharmaceutics classification system class II drugs.* Eur J Pharm Sci, 2015. **67**: p. 65-75.
67. European Medicines Agency, *Guideline on the qualification and reporting of physiologically based pharmacokinetic (PBPK) modelling and simulation.* 2016.
68. Zhao, P., *Report from the EMA workshop on qualification and reporting of physiologically based pharmacokinetic (PBPK) modeling and simulation.* CPT Pharmacometrics Syst Pharmacol, 2017. **6**(2): p. 71-72.
69. Zhou, W., et al., *Predictive Performance of Physiologically Based Pharmacokinetic and Population Pharmacokinetic Modeling of Renally Cleared Drugs in Children.* CPT Pharmacometrics Syst Pharmacol, 2016. **5**(9): p. 475-83.
70. Zhou, W.D., et al., *Predictive Performance of Physiologically Based Pharmacokinetic (PBPK) Modeling of Drugs Extensively Metabolized by Major Cytochrome P450s in Children.* Clinical Pharmacology & Therapeutics, 2018. **104**(1): p. 188-200.
71. Samant, T.S., V. Lukacova, and S. Schmidt, *Development and Qualification of Physiologically Based Pharmacokinetic Models for Drugs With Atypical Distribution Behavior: A Desipramine Case Study.* Cpt-Pharmacometrics & Systems Pharmacology, 2017. **6**(5): p. 315-321.
72. Burghaus, R., *PBPK for Paediatric Development: Qualification of the PBPK platform for the Intended Purpose. Presented at EMA workshop on qualification and reporting of PBPK modelling and simulation.* 2016.
73. Huwaldt, J.A. and S. Steinhorst, *Plot digitizer URL http://plotdigitizer.sourceforge.net*. 2013.

74. Hozo, S.P., B. Djulbegovic, and I. Hozo, *Estimating the mean and variance from the median, range, and the size of a sample.* BMC Med Res Methodol, 2005. **5**: p. 13.
75. Hynynen, M., et al., *Plasma concentration and protein binding of alfentanil during highdose infusion for cardiac surgery.* BJA: British Journal of Anaesthesia, 1994. **72**(5): p. 571-576.
76. Macfie, A.G., A.D. Magides, and C.S. Reilly, *Disposition of alfentanil in burns patients.* Br J Anaesth, 1992. **69**(5): p. 447-50.
77. Scheytt, T., et al., *1-Octanol/water partition coefficients of 5 pharmaceuticals from human medical care: carbamazepine, clofibric acid, diclofenac, ibuprofen, and propyphenazone.* Water, air, and soil pollution, 2005. **165**(1-4): p. 3-11.
78. Riess, W., et al., *Kinetik und biotransformation von diclofenac in tier und mensch.* Therapiewoche, 1976. **26**: p. 18-27.
79. Radermacher, J., et al., *Diclofenac concentrations in synovial fluid and plasma after cutaneous application in inflammatory and degenerative joint disease.* Br J Clin Pharmacol, 1991. **31**(5): p. 537-41.
80. Andersson, T., et al., *Pharmacokinetic studies with esomeprazole, the (S)-isomer of omeprazole.* Clin Pharmacokinet, 2001. **40**(6): p. 411-26.
81. O'Neil, M.J., *The Merck index: an encyclopedia of chemicals, drugs, and biologicals*. 2013: RSC Publishing.
82. Kristl, A., *Acido-basic properties of proton pump inhibitors in aqueous solutions.* Drug Dev Ind Pharm, 2009. **35**(1): p. 114-7.
83. Landes, B.D., J.P. Petite, and B. Flouvat, *Clinical pharmacokinetics of lansoprazole.* Clin Pharmacokinet, 1995. **28**(6): p. 458-70.
84. Moj, D., et al., *Clarithromycin, Midazolam, and Digoxin: Application of PBPK Modeling to Gain New Insights into Drug-Drug Interactions and Co-medication Regimens.* AAPS J, 2017. **19**(1): p. 298-312.
85. Bjorkman, S., et al., *Prediction of the disposition of midazolam in surgical patients by a physiologically based pharmacokinetic model.* J Pharm Sci, 2001. **90**(9): p. 1226-1241.
86. Elkomy, M.H., et al., *Ondansetron pharmacokinetics in pregnant women and neonates: towards a new treatment for neonatal abstinence syndrome.* Clin Pharmacol Ther, 2015. **97**(2): p. 167-76.
87. Saynor, D.A. and C.M. Dixon, *The Metabolism of Ondansetron.* European Journal of Cancer & Clinical Oncology, 1989. **25**: p. S75-S77.
88. Meuldermans, W.E., R.M. Hurkmans, and J.J. Heykants, *Plasma protein binding and distribution of fentanyl, sufentanil, alfentanil and lofentanil in blood.* Arch Int Pharmacodyn Ther, 1982. **257**(1): p. 4-19.
89. Roy, S.D. and G.L. Flynn, *Solubility and related physicochemical properties of narcotic analgesics.* Pharm Res, 1988. **5**(9): p. 580-6.

90. Saari, T.I., et al., *Influence of intensive care treatment on the protein binding of sufentanil and hydromorphone during pain therapy in postoperative cardiac surgery patients.* British Journal of Anaesthesia, 2014. **113**(4): p. 677-687.
91. Haley, T.J., *Metabolism and pharmacokinetics of theophylline in human neonates, children, and adults.* Drug Metab Rev, 1983. **14**(2): p. 295-335.
92. Simons, K.J., et al., *Theophylline protein binding in humans.* J Pharm Sci, 1979. **68**(2): p. 252-3.
93. Yalkowsky, S.H., Y. He, and P. Jain, *Handbook of Aqueous Solubility Data*. 2016: CRC press. pp. 394-395.
94. T'Jollyn, H., et al., *Physiology-based IVIVE predictions of tramadol from in vitro metabolism data.* Pharm Res, 2015a. **32**(1): p. 260-74.
95. T'jollyn, H., et al., *Physiologically Based Pharmacokinetic Predictions of Tramadol Exposure Throughout Pediatric Life: an Analysis of the Different Clearance Contributors with Emphasis on CYP2D6 Maturation.* AAPS J, 2015b. **17**(6): p. 1376-1387.
96. Law, V., et al., *DrugBank 4.0: shedding new light on drug metabolism.* Nucleic Acids Res, 2014. **42**(Database issue): p. D1091-7.
97. Egan, T.D., et al., *Remifentanil versus alfentanil: comparative pharmacokinetics and pharmacodynamics in healthy adult male volunteers.* Anesthesiology, 1996. **84**(4): p. 821-33.
98. Ferrier, C., et al., *Alfentanil pharmacokinetics in patients with cirrhosis.* Anesthesiology, 1985. **62**(4): p. 480-4.
99. Meistelman, C., et al., *A comparison of alfentanil pharmacokinetics in children and adults.* Anesthesiology, 1987. **66**(1): p. 13-6.
100. den Hollander, J.M., et al., *Alfentanil in infants and children with congenital heart defects.* J Cardiothorac Anesth, 1988. **2**(1): p. 12-7.
101. Goresky, G.V., et al., *The pharmacokinetics of alfentanil in children.* Anesthesiology, 1987. **67**(5): p. 654-9.
102. Willis, J.V., et al., *The pharmacokinetics of diclofenac sodium following intravenous and oral administration.* Eur J Clin Pharmacol, 1979. **16**(6): p. 405-10.
103. Mermelstein, F., et al., *Single-dose and multiple-dose pharmacokinetics and dose proportionality of intravenous and intramuscular HPbetaCD-diclofenac (Dyloject) compared with other diclofenac formulations.* Pharmacotherapy, 2013. **33**(10): p. 1012-21.
104. Korpela, R. and K.T. Olkkola, *Pharmacokinetics of intravenous diclofenac sodium in children.* Eur J Clin Pharmacol, 1990. **38**(3): p. 293-5.
105. Hassan-Alin, M., et al., *Pharmacokinetics of esomeprazole after oral and intravenous administration of single and repeated doses to healthy subjects.* Eur J Clin Pharmacol, 2000. **56**(9-10): p. 665-70.
106. Niazi, M., et al., *Pharmacokinetics of esomeprazole following varying intravenous administration rates.* Basic Clin Pharmacol Toxicol, 2005. **97**(6): p. 351-4.

107. Sandstrom, M., et al., *Phase I, multicenter, randomized, open-label study evaluating the pharmacokinetics and safety profile of repeated once-daily doses of intravenous esomeprazole in children 0 to 17 years of age.* Clin Ther, 2012. **34**(8): p. 1828-38.
108. Mouton, J.W., et al., *Pharmacokinetics of itraconazole and hydroxyitraconazole in healthy subjects after single and multiple doses of a novel formulation.* Antimicrob Agents Chemother, 2006. **50**(12): p. 4096-102.
109. Heykants, J., et al., *The clinical pharmacokinetics of itraconazole: an overview.* Mycoses, 1989. **32 Suppl 1**: p. 67-87.
110. Abdel-Rahman, S.M., et al., *Single-dose pharmacokinetics of intravenous itraconazole and hydroxypropyl-beta-cyclodextrin in infants, children, and adolescents.* Antimicrob Agents Chemother, 2007. **51**(8): p. 2668-73.
111. Gerloff, J., et al., *Pharmacokinetics and absolute bioavailability of lansoprazole.* Eur J Clin Pharmacol, 1996. **50**(4): p. 293-7.
112. Amer, F., et al., *Comparison of the pharmacokinetics of lansoprazole 15- and 30-mg sachets for suspension versus intact capsules.* Clin Ther, 2004. **26**(12): p. 2076-83.
113. Hussein, Z., et al., *Age-related differences in the pharmacokinetics and pharmacodynamics of lansoprazole.* Br J Clin Pharmacol, 1993. **36**(5): p. 391-8.
114. Zhang, W., et al., *Age-dependent pharmacokinetics of lansoprazole in neonates and infants.* Paediatr Drugs, 2008. **10**(4): p. 265-74.
115. Tran, A., et al., *Pharmacokinetic-pharmacodynamic study of oral lansoprazole in children.* Clinical Pharmacology & Therapeutics, 2002. **71**(5): p. 359-367.
116. Heizmann, P., M. Eckert, and W.H. Ziegler, *Pharmacokinetics and bioavailability of midazolam in man.* Br J Clin Pharmacol, 1983. **16 Suppl 1**: p. 43S-49S.
117. Smith, M.T., M.J. Eadie, and T.O. Brophy, *The pharmacokinetics of midazolam in man.* Eur J Clin Pharmacol, 1981. **19**(4): p. 271-8.
118. Rey, E., et al., *Pharmacokinetics of midazolam in children: comparative study of intranasal and intravenous administration.* Eur J Clin Pharmacol, 1991. **41**(4): p. 355-7.
119. Reed, M.D., et al., *The single-dose pharmacokinetics of midazolam and its primary metabolite in pediatric patients after oral and intravenous administration.* J Clin Pharmacol, 2001. **41**(12): p. 1359-69.
120. Payne, K., et al., *The pharmacokinetics of midazolam in paediatric patients.* Eur J Clin Pharmacol, 1989. **37**(3): p. 267-72.
121. Blake, J.C., et al., *The pharmacokinetics of intravenous ondansetron in patients with hepatic impairment.* Br J Clin Pharmacol, 1993. **35**(4): p. 441-3.
122. VanDenBerg, C.M., et al., *Pharmacokinetics of three formulations of ondansetron hydrochloride in healthy volunteers: 24-mg oral tablet, rectal suppository, and i.v. infusion.* Am J Health Syst Pharm, 2000. **57**(11): p. 1046-50.
123. Colthup, P.V., et al., *Determination of ondansetron in plasma and its pharmacokinetics in the young and elderly.* J Pharm Sci, 1991. **80**(9): p. 868-71.

124. Mondick, J.T., et al., *Population pharmacokinetics of intravenous ondansetron in oncology and surgical patients aged 1-48 months.* Eur J Clin Pharmacol, 2010. **66**(1): p. 77-86.
125. Spahr-Schopfer, I.A., et al., *Pharmacokinetics of intravenous ondansetron in healthy children undergoing ear, nose, and throat surgery.* Clin Pharmacol Ther, 1995. **58**(3): p. 316-21.
126. Bovill, J.G., et al., *The pharmacokinetics of sufentanil in surgical patients.* Anesthesiology, 1984. **61**(5): p. 502-6.
127. Taverne, R.H., T.I. Ionescu, and S.T. Nuyten, *Comparative absorption and distribution pharmacokinetics of intravenous and epidural sufentanil for major abdominal surgery.* Clin Pharmacokinet, 1992. **23**(3): p. 231-7.
128. Bartkowski, R.R., et al., *Sufentanil Disposition - Is It Affected by Erythromycin Administration.* Anesthesiology, 1993. **78**(2): p. 260-265.
129. Davis, P.J., et al., *Pharmacodynamics and pharmacokinetics of high-dose sufentanil in infants and children undergoing cardiac surgery.* Anesth Analg, 1987. **66**(3): p. 203-8.
130. Greeley, W.J., N.P. de Bruijn, and D.P. Davis, *Sufentanil pharmacokinetics in pediatric cardiovascular patients.* Anesth Analg, 1987. **66**(11): p. 1067-72.
131. Guay, J., et al., *Pharmacokinetics of sufentanil in normal children.* Can J Anaesth, 1992. **39**(1): p. 14-20.
132. Gisclon, L.G., et al., *Absence of a pharmacokinetic interaction between intravenous theophylline and orally administered levofloxacin.* The Journal of Clinical Pharmacology, 1997. **37**(8): p. 744-750.
133. Steinijans, V.W., et al., *Absolute bioavailability of theophylline from a sustained-release formulation using different intravenous reference infusions.* Eur J Clin Pharmacol, 1987. **33**(5): p. 523-6.
134. Simons, F.E. and K.J. Simons, *Pharmacokinetics of theophylline in infancy.* J Clin Pharmacol, 1978. **18**(10): p. 472-6.
135. Loughnan, P.M., et al., *Pharmacokinetic analysis of the disposition of intravenous theophylline in young children.* J Pediatr, 1976. **88**(5): p. 874-9.
136. Arnold, J.D., G.N. Hill, and L.N. Sansom, *A comparison of the pharmacokinetics of theophylline in asthmatic children in the acute episode and in remission.* Eur J Clin Pharmacol, 1981. **20**(6): p. 443-7.
137. Lintz, W., et al., *Pharmacokinetics of tramadol and bioavailability of enteral tramadol formulations. 4th communication: drops (without ethanol).* Arzneimittelforschung, 2000. **50**(2): p. 99-108.
138. Lintz, W., H. Beier, and J. Gerloff, *Bioavailability of tramadol after i.m. injection in comparison to i.v. infusion.* Int J Clin Pharmacol Ther, 1999. **37**(4): p. 175-83.
139. Murthy, B.V., et al., *Pharmacokinetics of tramadol in children after i.v. or caudal epidural administration.* Br J Anaesth, 2000. **84**(3): p. 346-9.

140. Rodgers, T. and M. Rowland, *Physiologically based pharmacokinetic modelling 2: Predicting the tissue distribution of acids, very weak bases, neutrals and zwitterions.* Journal of Pharmaceutical Sciences, 2006. **95**(6): p. 1238-1257.
141. Rodgers, T., D. Leahy, and M. Rowland, *Physiologically based pharmacokinetic modeling 1: predicting the tissue distribution of moderate-to-strong bases.* Journal of pharmaceutical sciences, 2005. **94**(6): p. 1259-1276.
142. Lin, L.I., *A concordance correlation coefficient to evaluate reproducibility.* Biometrics, 1989. **45**(1): p. 255-68.
143. International Commission on Radiological Protection (ICRP), *Basic anatomical and physiological data for use in radiological protection: reference values: ICRP Publication 89.* Ann ICRP, 2002. **32**(3-4): p. 1-277.
144. Willmann, S., et al., *Development of a physiology-based whole-body population model for assessing the influence of individual variability on the pharmacokinetics of drugs.* J Pharmacokinet Pharmacodyn, 2007. **34**(3): p. 401-31.
145. Benedetti, M.S. and K. Tipton, *Monoamine oxidases and related amine oxidases as phase I enzymes in the metabolism of xenobiotics*, in *MAO—The Mother of all Amine Oxidases*, M.B.H.Y. John P.M. Finberg, Peter Riederer, K.F. Tipton, Editor. 1998, Springer. p. pp. 149-171.
146. Fernandez, E., et al., *Factors and Mechanisms for Pharmacokinetic Differences between Pediatric Population and Adults.* Pharmaceutics, 2011. **3**(1): p. 53-72.
147. Morgan, E.T., *Impact of infectious and inflammatory disease on cytochrome P450-mediated drug metabolism and pharmacokinetics.* Clin Pharmacol Ther, 2009. **85**(4): p. 434-8.
148. Zanger, U.M. and M. Schwab, *Cytochrome P450 enzymes in drug metabolism: regulation of gene expression, enzyme activities, and impact of genetic variation.* Pharmacol Ther, 2013. **138**(1): p. 103-41.
149. van der Weide, J. and L.S. Steijns, *Cytochrome P450 enzyme system: genetic polymorphisms and impact on clinical pharmacology.* Ann Clin Biochem, 1999. **36 (Pt 6)**: p. 722-9.
150. Efron, B., *Bootstrap methods: another look at the jackknife*, in *Breakthroughs in statistics. Springer Series in Statistics (Perspectives in Statistics).* N.L.J. Kotz S., Editor. 1992, Springer, New York, NY. p. pp. 569-593.
151. R Core Team, *R: A language and environment for statistical computing R Foundation for Statistical Computing, Vienna, Austria, 2021.*
152. Marino, S., et al., *A methodology for performing global uncertainty and sensitivity analysis in systems biology.* J Theor Biol, 2008. **254**(1): p. 178-96.
153. Campbell, A., *Development of PBPK model of molinate and molinate sulfoxide in rats and humans.* Regul Toxicol Pharmacol, 2009. **53**(3): p. 195-204.
154. Johnson, T.N., et al., *Changes in liver volume from birth to adulthood: a meta-analysis.* Liver Transpl, 2005. **11**(12): p. 1481-93.

155. International Programme on Chemical Safety, *Chemical-Specific Adjustment Factors (CSAFs) for Interspecies Differences and Human Variability: Guidance Document for the Use of Data in Dose/Concentration-Response Assessment*. 2005, WHO/IPCS/01.4, 1–96 International Panel on Chemical Safety, World Health Organization.
156. Renwick, A.G., *Safety Factors and Establishment of Acceptable Daily Intakes.* Food Addit Contam, 1991. **8**(2): p. 135-150.
157. Renwick, A.G. and N.R. Lazarus, *Human variability and noncancer risk assessment - An analysis of the default uncertainty factor.* Regulatory Toxicology and Pharmacology, 1998. **27**(1): p. 3-20.
158. Valcke, M. and K. Krishnan, *Assessing the impact of the duration and intensity of inhalation exposure on the magnitude of the variability of internal dose metrics in children and adults.* Inhalation Toxicology, 2011. **23**(14): p. 863-877.
159. Hasegawa, R., et al., *Safety assessment of boron by application of new uncertainty factors and their subdivision.* Regulatory Toxicology and Pharmacology, 2013. **65**(1): p. 108-114.
160. Willmann, S., et al., *Whole-body physiologically based pharmacokinetic population modelling of oral drug administration: inter-individual variability of cimetidine absorption.* J Pharm Pharmacol, 2009. **61**(7): p. 891-9.
161. Sutphen, J.L. and V.L. Dillard, *Effects of maturation and gastric acidity on gastroesophageal reflux in infants.* Am J Dis Child, 1986. **140**(10): p. 1062-4.
162. Lacroix, D., et al., *Expression of CYP3A in the human liver--evidence that the shift between CYP3A7 and CYP3A4 occurs immediately after birth.* Eur J Biochem, 1997. **247**(2): p. 625-34.
163. Stevens, J.C., et al., *Developmental expression of the major human hepatic CYP3A enzymes.* J Pharmacol Exp Ther, 2003. **307**(2): p. 573-82.
164. Kim, H., et al., *Successful empirical antifungal therapy of intravenous itraconazole with pharmacokinetic evidence in pediatric cancer patients undergoing hematopoietic stem cell transplantation.* Clin Drug Investig, 2015. **35**(7): p. 437-46.
165. Isoherranen, N., et al., *Role of itraconazole metabolites in CYP3A4 inhibition.* Drug Metab Dispos, 2004. **32**(10): p. 1121-31.
166. Open Systems Pharmacology, *PK-Sim® Ontogeny Database Version 7.3.* 2018.
167. Pang, K.S. and M. Rowland, *Hepatic clearance of drugs. I. Theoretical considerations of a "well-stirred" model and a "parallel tube" model. Influence of hepatic blood flow, plasma and blood cell binding, and the hepatocellular enzymatic activity on hepatic drug clearance.* J Pharmacokinet Biopharm, 1977. **5**(6): p. 625-53.
168. Wilkinson, G.R. and D.G. Shand, *Commentary: a physiological approach to hepatic drug clearance.* Clin Pharmacol Ther, 1975. **18**(4): p. 377-90.
169. Delco, F., et al., *Dose adjustment in patients with liver disease.* Drug Saf, 2005. **28**(6): p. 529-45.
170. Scholz, J., M. Steinfath, and M. Schulz, *Clinical pharmacokinetics of alfentanil, fentanyl and sufentanil. An update.* Clin Pharmacokinet, 1996. **31**(4): p. 275-92.

171. Alcorn, J. and P.J. McNamara, *Ontogeny of hepatic and renal systemic clearance pathways in infants: part I.* Clin Pharmacokinet, 2002. **41**(12): p. 959-98.
172. Butler, M.A., et al., *Human Cytochrome P-450pa (P-450ia2), the Phenacetin O-Deethylase, Is Primarily Responsible for the Hepatic 3-Demethylation of Caffeine and N-Oxidation of Carcinogenic Arylamines - (Aromatic-Amines Heterocyclic Amines Carcinogen Metabolism).* Proceedings of the National Academy of Sciences of the United States of America, 1989. **86**(20): p. 7696-7700.
173. Sonnier, M. and T. Cresteil, *Delayed ontogenesis of CYP1A2 in the human liver.* Eur J Biochem, 1998. **251**(3): p. 893-8.
174. WHO Multicentre Growth Reference Study Group, *WHO Child Growth Standards based on length/height, weight and age.* Acta Paediatr Suppl, 2006. **450**: p. 76-85.
175. de Onis, M., et al., *Development of a WHO growth reference for school-aged children and adolescents.* Bull World Health Organ, 2007. **85**(9): p. 660-7.
176. European Food Safety Authority, *Opinion of the Scientific Panel on Food Additives, Flavourings, Processing Aids and Materials in Contact with Food on a request from the Commission related to 2,2-BIS(4-HYDROXYPHENYL)PROPANE (Bisphenol A) Question number EFSA-Q-2005-100.* EFSA J, 2006. **428**: p. 1-75.
177. T'Jollyn, H., A. Vermeulen, and J. Van Bocxlaer, *PBPK and its Virtual Populations: the Impact of Physiology on Pediatric Pharmacokinetic Predictions of Tramadol.* AAPS J, 2018. **21**(1): p. 8.
178. Pearce, R.E., et al., *Developmental Expression of CYP2B6: A Comprehensive Analysis of mRNA Expression, Protein Content and Bupropion Hydroxylase Activity and the Impact of Genetic Variation.* Drug Metab Dispos, 2016. **44**(7): p. 948-58.
179. Burton, M.E., et al., *Applied pharmacokinetics & pharmacodynamics: principles of therapeutic drug monitoring*. 4th ed. 2006: Lippincott Williams & Wilkins.
180. Yun, Y.E. and A.N. Edginton, *Model qualification of the PK-Sim® pediatric module for pediatric exposure assessment of CYP450 metabolized compounds.* Journal of Toxicology and Environmental Health, Part A, 2019: p. 1-26.
181. Pacifici, G.M. and A. Viani, *Methods of determining plasma and tissue binding of drugs. Pharmacokinetic consequences.* Clin Pharmacokinet, 1992. **23**(6): p. 449-68.
182. Bowers, W.F., S. Fulton, and J. Thompson, *Ultrafiltration vs equilibrium dialysis for determination of free fraction.* Clin Pharmacokinet, 1984. **9 Suppl 1**: p. 49-60.
183. Oravcova, J., B. Bohs, and W. Lindner, *Drug-protein binding sites. New trends in analytical and experimental methodology.* J Chromatogr B Biomed Appl, 1996. **677**(1): p. 1-28.
184. Bohnert, T. and L.S. Gan, *Plasma Protein Binding: From Discovery to Development.* Journal of Pharmaceutical Sciences, 2013. **102**(9): p. 2953-2994.
185. Lambrinidis, G., T. Vallianatou, and A. Tsantili-Kakoulidou, *In vitro, in silico and integrated strategies for the estimation of plasma protein binding. A review.* Adv Drug Deliv Rev, 2015. **86**: p. 27-45.

186. Ingle, B.L., et al., *Informing the Human Plasma Protein Binding of Environmental Chemicals by Machine Learning in the Pharmaceutical Space: Applicability Domain and Limits of Predictability.* Journal of Chemical Information and Modeling, 2016. **56**(11): p. 2243-2252.
187. Obach, R.S., F. Lombardo, and N.J. Waters, *Trend analysis of a database of intravenous pharmacokinetic parameters in humans for 670 drug compounds.* Drug Metab Dispos, 2008. **36**(7): p. 1385-405.
188. Zhu, X.W., et al., *The Use of Pseudo-Equilibrium Constant Affords Improved QSAR Models of Human Plasma Protein Binding.* Pharmaceutical Research, 2013. **30**(7): p. 1790-1798.
189. Votano, J.R., et al., *QSAR modeling of human serum protein binding with several modeling techniques utilizing structure-information representation.* Journal of Medicinal Chemistry, 2006. **49**(24): p. 7169-7181.
190. Moda, T.L., et al., *PK/DB: database for pharmacokinetic properties and predictive in silico ADME models.* Bioinformatics, 2008. **24**(19): p. 2270-1.
191. Wetmore, B.A., et al., *Incorporating High-Throughput Exposure Predictions With Dosimetry-Adjusted In Vitro Bioactivity to Inform Chemical Toxicity Testing.* Toxicol Sci, 2015. **148**(1): p. 121-36.
192. Wetmore, B.A., et al., *Integration of dosimetry, exposure, and high-throughput screening data in chemical toxicity assessment.* Toxicol Sci, 2012. **125**(1): p. 157-74.
193. US-EPA, *Toxicity Forecaster (ToxCast) Fact Sheet* *https://www.epa.gov/sites/production/files/2019-01/documents/toxcast_factsheet_dec2018.pdf*.
194. Watanabe, R., et al., *Predicting Fraction Unbound in Human Plasma from Chemical Structure: Improved Accuracy in the Low Value Ranges.* Mol Pharm, 2018. **15**(11): p. 5302-5311.
195. Moriwaki, H., et al., *Mordred: a molecular descriptor calculator.* Journal of Cheminformatics, 2018. **10**(1): p. 4.
196. Yap, C.W., *PaDEL-descriptor: an open source software to calculate molecular descriptors and fingerprints.* J Comput Chem, 2011. **32**(7): p. 1466-74.
197. Gaulton, A., et al., *The ChEMBL database in 2017.* Nucleic Acids Res, 2017. **45**(D1): p. D945-D954.
198. SA RELX Intellectual Properties, *PharmaPendium* *https://www.pharmapendium.com*. 2016, Elsevier.
199. Kanehisa, M., et al., *KEGG: new perspectives on genomes, pathways, diseases and drugs.* Nucleic Acids Res, 2017. **45**(D1): p. D353-D361.
200. Kanehisa, M. and S. Goto, *KEGG: kyoto encyclopedia of genes and genomes.* Nucleic Acids Res, 2000. **28**(1): p. 27-30.
201. Kanehisa, M., et al., *New approach for understanding genome variations in KEGG.* Nucleic Acids Res, 2019. **47**(D1): p. D590-D595.

202. Kalvass, J.C., T.S. Maurer, and G.M. Pollack, *Use of plasma and brain unbound fractions to assess the extent of brain distribution of 34 drugs: comparison of unbound concentration ratios to in vivo p-glycoprotein efflux ratios.* Drug Metabolism and Disposition, 2007. **35**(4): p. 660-666.
203. Li, G.F., et al., *Quantitative Estimation of Plasma Free Drug Fraction in Patients With Varying Degrees of Hepatic Impairment: A Methodological Evaluation.* J Pharm Sci, 2018. **107**(7): p. 1948-1956.
204. Patsalos, P.N., et al., *Serum protein binding of 25 antiepileptic drugs in a routine clinical setting: A comparison of free non-protein-bound concentrations.* Epilepsia, 2017. **58**(7): p. 1234-1243.
205. Sethi, P.K., et al., *Ontogeny of plasma proteins, albumin and binding of diazepam, cyclosporine, and deltamethrin.* Pediatr Res, 2016. **79**(3): p. 409-15.
206. Kim, S., et al., *PubChem 2019 update: improved access to chemical data.* Nucleic Acids Research, 2019. **47**(D1): p. D1102-D1109.
207. Food and Drug Administration, *In vitro metabolism-and transporter-mediated drug-drug interaction studies: Guidance for industry.* Center for Drug Evaluation and Research, US Food and Drug Administration, US Department of Health and Human Services, Rockville, MD, 2017.
208. Kuhn, M., *Building predictive models in R using the caret package.* J Stat Softw, 2008. **28**(5): p. 1-26.
209. Lipscomb, J.C., et al., *In vitro to in vivo extrapolation for trichloroethylene metabolism in humans.* Toxicol Appl Pharmacol, 1998. **152**(2): p. 376-87.
210. Heuberger, J., S. Schmidt, and H. Derendorf, *When is protein binding important?* Journal of pharmaceutical sciences, 2013. **102**(9): p. 3458-3467.
211. McNamara, P.J. and D. Meiman, *Predicting Drug Binding to Human Serum Albumin and Alpha One Acid Glycoprotein in Diseased and Age Patient Populations.* J Pharm Sci, 2019. **108**(8): p. 2737-2747.
212. Clewell, H.J., 3rd, *The application of physiologically based pharmacokinetic modeling in human health risk assessment of hazardous substances.* Toxicol Lett, 1995. **79**(1-3): p. 207-17.
213. Gleeson, M.P., *Plasma protein binding affinity and its relationship to molecular structure: an in-silico analysis.* J Med Chem, 2007. **50**(1): p. 101-12.
214. Sjoholm, I., et al., *The specificity of three binding sites as studied with albumin immobilized in microparticules.* Mol Pharmaco116, 1979.
215. Sudlow, G., D.J. Birkett, and D.N. Wade, *The characterization of two specific drug binding sites on human serum albumin.* Mol Pharmacol, 1975. **11**(6): p. 824-32.
216. Sjoholm, I., et al., *Binding of drugs to human serum albumin:XI. The specificity of three binding sites as studied with albumin immobilized in microparticles.* Mol Pharmacol, 1979. **16**(3): p. 767-77.
217. Tillement, J.P., et al., *Binding of digitoxin, digoxin and gitoxin to human serum albumin.* Eur J Drug Metab Pharmacokinet, 1980. **5**(3): p. 129-34.

218. Sengupta, A. and D.S. Hage, *Characterization of minor site probes for human serum albumin by high-performance affinity chromatography.* Anal Chem, 1999. **71**(17): p. 3821-7.
219. Wanwimolruk, S., D.J. Birkett, and P.M. Brooks, *Structural requirements for drug binding to site II on human serum albumin.* Mol Pharmacol, 1983. **24**(3): p. 458-63.
220. Xu, Z., et al., *Halogen bond: its role beyond drug-target binding affinity for drug discovery and development.* J Chem Inf Model, 2014. **54**(1): p. 69-78.
221. Tan, Y.-M., et al., *Reconstructing human exposures using biomarkers and other "clues".* J Toxicol Environ Health, 2012. **15**(1): p. 22-38.
222. Yin, Y., et al., *Essential set of molecular descriptors for ADME prediction in drug and environmental chemical space*. 2014, Research.
223. Thomas, R.S., et al., *Incorporating new technologies into toxicity testing and risk assessment: moving from 21st century vision to a data-driven framework.* Toxicol Sci, 2013. **136**(1): p. 4-18.
224. Tropsha, A., P. Gramatica, and V.K. Gombar, *The importance of being earnest: Validation is the absolute essential for successful application and interpretation of QSPR models.* Qsar & Combinatorial Science, 2003. **22**(1): p. 69-77.
225. Tropsha, A., *Application of predictive QSAR models to database mining.* Chemoinformatics in Drug Discovery, 2004. **23**: p. 437-455.
226. Kovatcheva, A., et al., *Combinatorial QSAR of ambergris fragrance compounds.* Journal of chemical information and computer sciences, 2004. **44**(2): p. 582-595.
227. Ekins, S., et al., *Towards a new age of virtual ADME/TOX and multidimensional drug discovery.* Mol Divers, 2002. **5**(4): p. 255-75.
228. Wang, H., et al., *Understanding and reducing the experimental variability of in vitro plasma protein binding measurements.* J Pharm Sci, 2014. **103**(10): p. 3302-9.
229. US-EPA, *Guidance for Applying Quantitative Data to Develop Data-Derived Extrapolation Factors for Interspecies and Intraspecies Extrapolation. EPA/100/R-14/002F. Washington, DC: US EPA.* 2014.
230. Notarianni, L.J., *Plasma protein binding of drugs in pregnancy and in neonates.* Clin Pharmacokinet, 1990. **18**(1): p. 20-36.
231. Lehman-McKeeman, L.D., *Chapter 5. Absorption, Distribution, and Excretion of Toxicants. Casarett & Doull's Essentials of Toxicology* 2ed. 2010: McGraw Hill Professional.
232. Putnam, F.W., *Alpha, beta, gamma, omega—the roster of the plasma proteins*, in *The plasma proteins*. 1975, Elsevier. p. 57-131.
233. Israili, Z.H. and P.G. Dayton, *Human alpha-1-glycoprotein and its interactions with drugs.* Drug Metab Rev, 2001. **33**(2): p. 161-235.
234. Barre, J., et al., *Decreased alpha 1-acid glycoprotein in liver cirrhosis: consequences for drug protein binding.* Br J Clin Pharmacol, 1984. **18**(4): p. 652-3.
235. Lemaire, M., et al., *Lipoprotein binding of drugs.* Drug–Protein Binding. Reidenberg MM, Erill S (Eds). Praeger Publishers, NY, USA, 1986: p. 93-108.

236. Ehrnebo, M., et al., *Age differences in drug binding by plasma proteins: studies on human foetuses, neonates and adults.* Eur J Clin Pharmacol, 1971. **3**(4): p. 189-93.
237. Cartlidge, P.H. and N. Rutter, *Serum albumin concentrations and oedema in the newborn.* Arch Dis Child, 1986. **61**(7): p. 657-60.
238. Pacifici, G.M., et al., *Effects of Development, Aging, and Renal and Hepatic Insufficiency as Well as Hemodialysis on the Plasma-Concentrations of Albumin and Alpha-1-Acid Glycoprotein - Implications for Binding of Drugs.* Therapeutic Drug Monitoring, 1986. **8**(3): p. 259-263.
239. Fujita, H., et al., *Low-density lipoprotein profile changes during the neonatal period.* J Perinatol, 2008. **28**(5): p. 335-40.
240. Yaster, M., *The dose response of fentanyl in neonatal anesthesia.* Anesthesiology, 1987. **66**(3): p. 433-5.
241. Koehntop, D.E., et al., *Pharmacokinetics of fentanyl in neonates.* Anesth Analg, 1986. **65**(3): p. 227-32.
242. Meistelman, C., et al., *Effects of age on plasma protein binding of sufentanil.* Anesthesiology, 1990. **72**(3): p. 470-3.
243. Johnson, T.N., A. Rostami-Hodjegan, and G.T. Tucker, *Prediction of the clearance of eleven drugs and associated variability in neonates, infants and children.* Clin Pharmacokinet, 2006. **45**(9): p. 931-56.
244. Maharaj, A.R., et al., *Improving Pediatric Protein Binding Estimates: An Evaluation of alpha1-Acid Glycoprotein Maturation in Healthy and Infected Subjects.* Clin Pharmacokinet, 2018. **57**(5): p. 577-589.
245. Kim, Y.S., et al., *Serum Albumin as a Biomarker of Poor Prognosis in the Pediatric Patients in Intensive Care Unit.* Acute and Critical Care, 2017. **32**(4): p. 347-355.
246. Mayer, H., et al., *A novel approach to estimate ontogenies for PBPK applications– From literature data to simulations.* 2018.
247. Weaving, G., G.F. Batstone, and R.G. Jones, *Age and sex variation in serum albumin concentration: an observational study.* Ann Clin Biochem, 2016. **53**(Pt 1): p. 106-11.
248. Holt, D.W., A.M. Hayler, and G.F. Healey, *Effect of age and plasma concentrations of albumin and alpha 1-acid glycoprotein on protein binding of disopyramide.* Br J Clin Pharmacol, 1983. **16**(3): p. 344-5.
249. Kanakoudi, F., et al., *Serum concentrations of 10 acute-phase proteins in healthy term and preterm infants from birth to age 6 months.* Clin Chem, 1995. **41**(4): p. 605-8.
250. Brodersen, R., et al., *The chemical nature of fetal albumin*, in *Neonatal Jaundice*. 1984, Springer. p. 51-54.
251. Wallace, S., *Altered plasma albumin in the newborn infant.* Br J Clin Pharmacol, 1977. **4**(1): p. 82-5.
252. Windorfer, A., W. Kuenzer, and R. Urbanek, *The influence of age on the activity of acetylsalicylic acid-esterase and protein-salicylate binding.* Eur J Clin Pharmacol, 1974. **7**(3): p. 227-31.

253. Besunder, J.B., M.D. Reed, and J.L. Blumer, *Principles of drug biodisposition in the neonate. A critical evaluation of the pharmacokinetic-pharmacodynamic interface (Part I).* Clin Pharmacokinet, 1988. **14**(4): p. 189-216.
254. Fredholm, B.B., A. Rane, and B. Persson, *Diphenylhydantoin Binding to Proteins in Plasma and Its Dependence on Free Fatty-Acid and Bilirubin Concentration in Dogs and Newborn-Infants.* Pediatric Research, 1975. **9**(1): p. 26-30.
255. Urien, S., et al., *In vitro studies on the distribution of probucol among human plasma lipoproteins.* Molecular pharmacology, 1984. **26**(2): p. 322-327.
256. Maliwal, B.P. and F.E. Guthrie, *Chemical Modifications of the Insecticide Binding-Sites on Human-Serum Albumin - Role of Indole, Bilirubin, and Fatty-Acid Binding-Sites.* Pesticide Biochemistry and Physiology, 1983. **19**(1): p. 104-113.
257. Mohammed, A., et al., *Distribution of Toxaphene, Ddt, and Pcb among Lipoprotein Fractions in Rat and Human Plasma.* Archives of Toxicology, 1990. **64**(7): p. 567-571.
258. Sethi, P.K., et al., *Measurement of plasma protein and lipoprotein binding of pyrethroids.* J Pharmacol Toxicol Methods, 2014. **70**(1): p. 106-11.
259. Wasan, K.M. and S.M. Cassidy, *Role of plasma lipoproteins in modifying the biological activity of hydrophobic drugs.* J Pharm Sci, 1998. **87**(4): p. 411-24.
260. Peters Jr, T., *All about albumin: biochemistry, genetics, and medical applications*. 1995: Academic press.
261. Ferguson, A., R. Penney, and H. Solo-Gabriele, *A review of the field on children's exposure to environmental contaminants: A risk assessment approach.* International journal of environmental research and public health, 2017. **14**(3): p. 265.
262. Thomas, R.S., et al., *The Next Generation Blueprint of Computational Toxicology at the US Environmental Protection Agency.* Toxicological Sciences, 2019. **169**(2): p. 317-332.
263. Wambaugh, J.F., et al., *High throughput heuristics for prioritizing human exposure to environmental chemicals.* Environ Sci Technol, 2014. **48**(21): p. 12760-7.
264. McLanahan, E.D., et al., *Physiologically Based Pharmacokinetic Model Use in Risk Assessment-Why Being Published Is Not Enough.* Toxicological Sciences, 2012. **126**(1): p. 5-15.
265. Mostrag-Szlichtyng, A., J.M.Z. Comenges, and A.P. Worth, *Computational toxicology at the European Commission's Joint Research Centre.* Expert Opinion on Drug Metabolism & Toxicology, 2010. **6**(7): p. 785-792.
266. Krewski, D., et al., *Toxicity testing in the 21st century: progress in the past decade and future perspectives.* Arch Toxicol, 2020. **94**(1): p. 1-58.
267. Alcorn, J. and P.J. McNamara, *Pharmacokinetics in the newborn.* Adv Drug Deliv Rev, 2003. **55**(5): p. 667-86.
268. Yun, Y.E., et al., *Evaluation of quantitative structure property relationship algorithms for predicting plasma protein binding in humans.* Computational Toxicology. **17**: p. 100142.

269. Bteich, M., *An overview of albumin and alpha-1-acid glycoprotein main characteristics: highlighting the roles of amino acids in binding kinetics and molecular interactions.* Heliyon, 2019. **5**(11): p. e02879.
270. Yun, Y.E. and A.N. Edginton, *Evaluation of models for predicting pediatric fraction unbound in plasma for human health risk assessment.* Journal of Toxicology and Environmental Health-Part a-Current Issues, 2020.
271. Asali, L.A. and K.F. Brown, *Naloxone protein binding in adult and foetal plasma.* Eur J Clin Pharmacol, 1984. **27**(4): p. 459-63.
272. Pacifici, G.M., G. Taddeucci-Brunelli, and A. Rane, *Clonazepam serum protein binding during development.* Clin Pharmacol Ther, 1984. **35**(3): p. 354-9.
273. Pacifici, G.M., A. Viani, and G. Taddeucci-Brunelli, *Serum protein binding of furosemide in newborn infants and children.* Dev Pharmacol Ther, 1987. **10**(6): p. 413-21.
274. Pacifici, G.M., et al., *Plasma-Protein Binding of Dicloxacillin - Effects of Age and Diseases.* International Journal of Clinical Pharmacology and Therapeutics, 1987. **25**(11): p. 622-626.
275. Schaad, U.B., W.L. Hayton, and K. Stoeckel, *Single-dose ceftriaxone kinetics in the newborn.* Clin Pharmacol Ther, 1985. **37**(5): p. 522-8.
276. Schaad, U.B. and K. Stoeckel, *Single-dose pharmacokinetics of ceftriaxone in infants and young children.* Antimicrob Agents Chemother, 1982. **21**(2): p. 248-53.
277. Nau, H., et al., *Serum protein binding of diazepam, desmethyldiazepam, furosemide, indomethacin, warfarin, and phenobarbital in human fetus, mother, and newborn infant.* Pediatr Pharmacol (New York), 1983. **3**(3-4): p. 219-27.
278. Smits, A., et al., *Cefazolin plasma protein binding and its covariates in neonates.* Eur J Clin Microbiol Infect Dis, 2012. **31**(12): p. 3359-65.
279. Rane, A., et al., *Plasma Protein Binding of Diphenylhydantoin in Normal and Hyperbilirubinemic Infants.* Journal of Pediatrics, 1971. **78**(5): p. 877-+.
280. Kurz, H., A. Mauser-Ganshorn, and H.H. Stickel, *Differences in the binding of drugs to plasma proteins from newborn and adult man. I.* Eur J Clin Pharmacol, 1977. **11**(6): p. 463-7.
281. Kurz, H., H. Michels, and H.H. Stickel, *Differences in the binding of drugs to plasma proteins from newborn and adult man. II.* Eur J Clin Pharmacol, 1977. **11**(6): p. 469-72.
282. Wood, M. and A.J. Wood, *Changes in plasma drug binding and alpha 1-acid glycoprotein in mother and newborn infant.* Clin Pharmacol Ther, 1981. **29**(4): p. 522-6.
283. Sudhakaran, S., et al., *Differential protein binding of indinavir and saquinavir in matched maternal and umbilical cord plasma.* Br J Clin Pharmacol, 2007. **63**(3): p. 315-21.
284. Belpaire, F.M., et al., *Protein binding of propranolol and verapamil enantiomers in maternal and foetal serum.* Br J Clin Pharmacol, 1995. **39**(2): p. 190-3.

285. Loughnan, P.M., et al., *Pharmacokinetic observations of phenytoin disposition in the newborn and young infant.* Arch Dis Child, 1977. **52**(4): p. 302-9.
286. Zsila, F., et al., *Determination of Human Serum alpha(1)-Acid Glycoprotein and Albumin Binding of Various Marketed and Preclinical Kinase Inhibitors.* Current Medicinal Chemistry, 2009. **16**(16): p. 1964-1977.
287. Yang, F., Y. Zhang, and H. Liang, *Interactive association of drugs binding to human serum albumin.* Int J Mol Sci, 2014. **15**(3): p. 3580-95.
288. Nishi, K., et al., *Involvement of disulfide bonds and histidine 172 in a unique beta-sheet to alpha-helix transition of alpha(1)-acid glycoprotein at the biomembrane interface.* Proteins-Structure Function and Bioinformatics, 2006. **63**(3): p. 611-620.
289. Kremer, J.M., J. Wilting, and L.H. Janssen, *Drug binding to human alpha-1-acid glycoprotein in health and disease.* Pharmacol Rev, 1988. **40**(1): p. 1-47.
290. Valko, K., et al., *Fast gradient HPLC method to determine compounds binding to human serum albumin. Relationships with octanol/water and immobilized artificial membrane lipophilicity.* Journal of pharmaceutical sciences, 2003. **92**(11): p. 2236-2248.
291. European Medicines Agency, *Guideline on the investigation of medicinal products in the term and preterm neonate* 2009.
292. Pellegatti, M., et al., *Plasma protein binding and blood-free concentrations: which studies are needed to develop a drug?* Expert Opinion on Drug Metabolism & Toxicology, 2011. **7**(8): p. 1009-1020.
293. Food and Drug Administration, *General Clinical Pharmacology Considerations for Neonatal Studies for Drugs and Biological Products Guidance for Industry.* . 2019.
294. BOXENBAUM, H. and R.W. D'SOUZA, *Interspecies pharmacokinetic scaling, biological design and neoteny*, in *Advances in drug research*. 1990, Elsevier. p. 139-196.
295. Wajima, T., et al., *Prediction of human clearance from animal data and molecular structural parameters using multivariate regression analysis.* Journal of Pharmaceutical Sciences, 2002. **91**(12): p. 2489-2499.
296. Mahmood, I. and J.D. Balian, *Interspecies scaling: predicting pharmacokinetic parameters of antiepileptic drugs in humans from animals with special emphasis on clearance.* J Pharm Sci, 1996. **85**(4): p. 411-4.
297. Mahmood, I. and J.D. Balian, *Interspecies scaling: A comparative study for the prediction of clearance and volume using two or more than two species.* Life Sciences, 1996. **59**(7): p. 579-585.
298. Sharma, V. and J.H. McNeill, *To scale or not to scale: the principles of dose extrapolation.* British journal of pharmacology, 2009. **157**(6): p. 907-921.
299. Wetmore, B.A., et al., *Incorporating population variability and susceptible subpopulations into dosimetry for high-throughput toxicity testing.* Toxicological Sciences, 2014. **142**(1): p. 210-224.

300. Alcorn, J. and P.J. McNamara, *Ontogeny of hepatic and renal systemic clearance pathways in infants: part II.* Clin Pharmacokinet, 2002. **41**(13): p. 1077-94.
301. Barter, Z.E., et al., *Scaling factors for the extrapolation of in vivo metabolic drug clearance from in vitro data: reaching a consensus on values of human microsomal protein and hepatocellularity per gram of liver.* Curr Drug Metab, 2007. **8**(1): p. 33-45.
302. Rhodin, M.M., et al., *Human renal function maturation: a quantitative description using weight and postmenstrual age.* Pediatric nephrology, 2009. **24**(1): p. 67.
303. Tod, M., V. Jullien, and G. Pons, *Facilitation of drug evaluation in children by population methods and modelling.* Clin Pharmacokinet, 2008. **47**(4): p. 231-43.
304. Upreti, V.V. and J.L. Wahlstrom, *Meta-Analysis of Hepatic Cytochrome P450 Ontogeny to Underwrite the Prediction of Pediatric Pharmacokinetics Using Physiologically Based Pharmacokinetic Modeling.* Journal of Clinical Pharmacology, 2016. **56**(3): p. 266-283.
305. Edginton, A.N., et al., *The integration of allometry and virtual populations to predict clearance and clearance variability in pediatric populations over the age of 6 years.* Clin Pharmacokinet, 2013. **52**(8): p. 693-703.
306. Savage, V.M., et al., *The predominance of quarter-power scaling in biology.* Functional Ecology, 2004. **18**(2): p. 257-282.
307. Germovsek, E., et al., *Scaling clearance in paediatric pharmacokinetics: all models are wrong, which are useful?* British journal of clinical pharmacology, 2017. **83**(4): p. 777-790.
308. Mahmood, I., *Dosing in children: a critical review of the pharmacokinetic allometric scaling and modelling approaches in paediatric drug development and clinical settings.* Clin Pharmacokinet, 2014. **53**(4): p. 327-46.
309. Holford, N.H. and B.J. Anderson, *Why standards are useful for predicting doses.* Br J Clin Pharmacol, 2017. **83**(4): p. 685-687.
310. Varma, M.V., et al., *Predicting Clearance Mechanism in Drug Discovery: Extended Clearance Classification System (ECCS).* Pharm Res, 2015. **32**(12): p. 3785-802.
311. Hunt, P.A., M.D. Segall, and J.D. Tyzack, *WhichP450: a multi-class categorical model to predict the major metabolising CYP450 isoform for a compound.* J Comput Aided Mol Des, 2018. **32**(4): p. 537-546.
312. Olsen, L., et al., *SMARTCyp 3.0: enhanced cytochrome P450 site-of-metabolism prediction server.* Bioinformatics, 2019. **35**(17): p. 3174-3175.
313. Shin, Y.G., et al., *Comparison of Metabolic Soft Spot Predictions of CYP3A4, CYP2C9 and CYP2D6 Substrates Using MetaSite and StarDrop.* Combinatorial Chemistry & High Throughput Screening, 2011. **14**(9): p. 811-823.
314. Aliagas, I., et al., *A probabilistic method to report predictions from a human liver microsomes stability QSAR model: a practical tool for drug discovery.* J Comput Aided Mol Des, 2015. **29**(4): p. 327-38.

315. Ekins, S. and R.S. Obach, *Three-dimensional quantitative structure activity relationship computational approaches for prediction of human in vitro intrinsic clearance.* J Pharmacol Exp Ther, 2000. **295**(2): p. 463-73.
316. Pirovano, A., et al., *QSARs for estimating intrinsic hepatic clearance of organic chemicals in humans.* Environ Toxicol Pharmacol, 2016. **42**: p. 190-7.
317. Paixao, P., L.F. Gouveia, and J.A.G. Morais, *Prediction of the in vitro intrinsic clearance determined in suspensions of human hepatocytes by using artificial neural networks.* European Journal of Pharmaceutical Sciences, 2010. **39**(5): p. 310-321.
318. Watanabe, R., et al., *Development of an in silico prediction system of human renal excretion and clearance from chemical structure information incorporating fraction unbound in plasma as a descriptor.* Sci Rep, 2019. **9**(1): p. 18782.
319. Kim, S., et al., *PubChem in 2021: new data content and improved web interfaces.* Nucleic acids research, 2021. **49**(D1): p. D1388-D1395.
320. Iwatsubo, T., et al., *Prediction of in vivo drug metabolism in the human liver from in vitro metabolism data.* Pharmacol Ther, 1997. **73**(2): p. 147-71.
321. Davies, B. and T. Morris, *Physiological parameters in laboratory animals and humans.* Pharm Res, 1993. **10**(7): p. 1093-5.
322. Yun, Y.E. and A.N. Edginton, *Prediction of fraction unbound in plasma in children in data-limited scenarios for human health risk assessment.* Computational Toxicology, 2021. **18**: p. 100168.
323. Yun, Y.E., C.A. Cotton, and A.N. Edginton, *Development of a decision tree to classify the most accurate tissue-specific tissue to plasma partition coefficient algorithm for a given compound.* Journal of pharmacokinetics and pharmacodynamics, 2014. **41**(1): p. 1-14.
324. Pritchard, J.F., *Ondansetron metabolism and pharmacokinetics.* Semin Oncol, 1992. **19**(4 Suppl 10): p. 9-15.
325. Ito, S., et al., *Intravenous and oral propafenone for treatment of tachycardia in infants and children: pharmacokinetics and clinical response.* J Clin Pharmacol, 1998. **38**(6): p. 496-501.
326. Delgado Iribarnegaray, M.F., et al., *Carbamazepine population pharmacokinetics in children: mixed-effect models.* Ther Drug Monit, 1997. **19**(2): p. 132-9.
327. Hill, K.D., et al., *Pharmacokinetics of intravenous sildenafil in children with palliated single ventricle heart defects: effect of elevated hepatic pressures.* Cardiol Young, 2016. **26**(2): p. 354-62.
328. Mukherjee, A., et al., *Population pharmacokinetics of sildenafil in term neonates: evidence of rapid maturation of metabolic clearance in the early postnatal period.* Clin Pharmacol Ther, 2009. **85**(1): p. 56-63.
329. Kunze, C., et al., *Pharmacokinetics and safety of macrocyclic gadobutrol in children aged younger than 2 years including term newborns in comparison to older populations.* Investigative radiology, 2016. **51**(1): p. 50-57.

330. An, S.H., J.Y. Kim, and H.S. Gwak, *Outcomes of a new dosage regimen of amikacin based on pharmacokinetic parameters of Korean neonates.* Am J Health Syst Pharm, 2014. **71**(2): p. 122-7.
331. Treluyer, J.M., et al., *Nonparametric population pharmacokinetic analysis of amikacin in neonates, infants, and children.* Antimicrob Agents Chemother, 2002. **46**(5): p. 1381-7.
332. Chien, S., et al., *Levofloxacin pharmacokinetics in children.* J Clin Pharmacol, 2005. **45**(2): p. 153-60.
333. James, L.P., et al., *Pharmacokinetics and pharmacodynamics of famotidine in infants.* J Clin Pharmacol, 1998. **38**(12): p. 1089-95.
334. Nahata, M.C., et al., *Tobramycin kinetics in newborn infants.* The Journal of Pediatrics, 1983. **103**(1): p. 136-138.
335. Blumer, J.L., et al., *Sequential, single-dose pharmacokinetic evaluation of meropenem in hospitalized infants and children.* Antimicrob Agents Chemother, 1995. **39**(8): p. 1721-5.
336. Kuti, J.L., et al., *Pharmacokinetic properties and stability of continuous-infusion meropenem in adults with cystic fibrosis.* Clin Ther, 2004. **26**(4): p. 493-501.
337. Pettit, R.S., et al., *Population pharmacokinetics of meropenem administered as a prolonged infusion in children with cystic fibrosis.* Journal of Antimicrobial Chemotherapy, 2016. **71**(1): p. 189-195.
338. Sipes, N.S., et al., *An Intuitive Approach for Predicting Potential Human Health Risk with the Tox21 10k Library.* Environ Sci Technol, 2017. **51**(18): p. 10786-10796.
339. Wambaugh, J.F., et al., *Evaluating In Vitro-In Vivo Extrapolation of Toxicokinetics.* Toxicol Sci, 2018. **163**(1): p. 152-169.
340. Villeneuve, D.L., et al., *High-throughput screening and environmental risk assessment: State of the science and emerging applications.* Environ Toxicol Chem, 2019. **38**(1): p. 12-26.
341. Pearce, R.G., et al., *httk: R Package for High-Throughput Toxicokinetics.* J Stat Softw, 2017. **79**(4): p. 1-26.
342. Anissimov, Y.G., *Mathematical models for skin toxicology.* Expert Opin Drug Metab Toxicol, 2014. **10**(4): p. 551-60.
343. Dancik, Y., et al., *Design and performance of a spreadsheet-based model for estimating bioavailability of chemicals from dermal exposure.* Adv Drug Deliv Rev, 2013. **65**(2): p. 221-36.
344. Dancik, Y., P.L. Bigliardi, and M. Bigliardi-Qi, *What happens in the skin? Integrating skin permeation kinetics into studies of developmental and reproductive toxicity following topical exposure.* Reproductive Toxicology, 2015. **58**: p. 252-281.
345. HWA, C., E.A. BAUER, and D.E. COHEN, *Skin biology.* Dermatologic Therapy, 2011. **24**(5): p. 464-470.
346. Anissimov, Y.G., et al., *Mathematical and pharmacokinetic modelling of epidermal and dermal transport processes.* Adv Drug Deliv Rev, 2013. **65**(2): p. 169-90.

347. Gorzelanny, C., et al., *Skin Barriers in Dermal Drug Delivery: Which Barriers Have to Be Overcome and How Can We Measure Them?* Pharmaceutics, 2020. **12**(7).
348. Jepps, O.G., et al., *Modeling the human skin barrier--towards a better understanding of dermal absorption.* Adv Drug Deliv Rev, 2013. **65**(2): p. 152-68.
349. Law, R.M., M.A. Ngo, and H.I. Maibach, *Twenty Clinically Pertinent Factors/Observations for Percutaneous Absorption in Humans.* Am J Clin Dermatol, 2020. **21**(1): p. 85-95.
350. Roberts, M.S., *Targeted drug delivery to the skin and deeper tissues: role of physiology, solute structure and disease.* Clin Exp Pharmacol Physiol, 1997. **24**(11): p. 874-9.
351. Debeer, S., et al., *Comparative histology and immunohistochemistry of porcine versus human skin.* Eur J Dermatol, 2013. **23**(4): p. 456-66.
352. Kanitakis, J., *Anatomy, histology and immunohistochemistry of normal human skin.* Eur J Dermatol, 2002. **12**(4): p. 390-9; quiz 400-1.
353. McLafferty, E., C. Hendry, and F. Alistair, *The integumentary system: anatomy, physiology and function of skin.* Nurs Stand, 2012. **27**(3): p. 35-42.
354. Menon, G.K., *New insights into skin structure: scratching the surface.* Advanced Drug Delivery Reviews, 2002. **54**: p. S3-S17.
355. Wong, R., et al., *The dynamic anatomy and patterning of skin.* Experimental Dermatology, 2016. **25**(2): p. 92-98.
356. Wysocki, A.B., *Skin anatomy, physiology, and pathophysiology.* Nurs Clin North Am, 1999. **34**(4): p. 777-97, v.
357. Cices, A., et al., *Poisoning Through Pediatric Skin: Cases from the Literature.* Am J Clin Dermatol, 2017. **18**(3): p. 391-403.
358. Sanchez-Prado, L., et al., *Content of suspected allergens and preservatives in marketed baby and child care products.* Analytical Methods, 2013. **5**(2): p. 416-427.
359. French Agency for Food Environmental and Occupational Health & Safety (ANSES), *Sécurité des couches pour bébé.*
360. Lansdown, A.B., *Epidermal differentiation in normal and growth-retarded infants: studies in two animal models and in human babies.* Br J Dermatol, 1978. **99**(2): p. 139-46.
361. Evans, N.J. and N. Rutter, *Development of the epidermis in the newborn.* Biol Neonate, 1986. **49**(2): p. 74-80.
362. Stamatas, G.N., et al., *Infant skin physiology and development during the first years of life: A review of recent findings based on in vivo studies.* International Journal of Cosmetic Science, 2011. **33**(1): p. 17-24.
363. Hamadeh, A., J. Troutman, and A.N. Edginton, *Assessment of Vehicle Volatility and Deposition Layer Thickness in Skin Penetration Models.* Pharmaceutics, 2021. **13**(6): p. 807.

364. Hewitt, N.J., et al., *Measurement of the penetration of 56 cosmetic relevant chemicals into and through human skin using a standardized protocol.* Journal of Applied Toxicology, 2020. **40**(3): p. 403-415.
365. Kasting, G.B. and M.A. Miller, *Kinetics of finite dose absorption through skin 2: Volatile compounds.* Journal of Pharmaceutical Sciences, 2006. **95**(2): p. 268-280.
366. Baty, F., et al., *A toolbox for nonlinear regression in R: the package nlstools.* Journal of Statistical Software, 2015. **66**(5): p. 1-21.
367. James, G., et al., *An introduction to statistical learning*. Vol. 112. 2013: Springer.
368. Barrett, D., et al., *Buprenorphine permeation through premature neonatal skin.* PHARMACEUTICAL SCIENCE COMMUNICATIONS, 1994. **4**: p. 125-125.
369. Barrett, D.A., N. Rutter, and S.S. Davis, *An in vitro study of diamorphine permeation through premature human neonatal skin.* Pharmaceutical research, 1993. **10**(4): p. 583-587.
370. Bonina, F., et al., *In vitro percutaneous absorption evaluation of phenobarbital through hairless mouse, adult and premature human skin.* International journal of pharmaceutics, 1993. **98**(1-3): p. 93-99.
371. World Health Organization, *Born too soon: the global action report on preterm birth.* 2012.
372. Kushner IV, J., et al., *First-principles, structure-based transdermal transport model to evaluate lipid partition and diffusion coefficients of hydrophobic permeants solely from stratum corneum permeation experiments.* Journal of Pharmaceutical Sciences, 2007. **96**(12): p. 3236-3251.
373. Abd, E., et al., *Skin models for the testing of transdermal drugs.* Clinical pharmacology : advances and applications, 2016. **8**: p. 163-176.
374. Stamatas, G.N., et al., *Infant Skin Microstructure Assessed In Vivo Differs from Adult Skin in Organization and at the Cellular Level.* Pediatric Dermatology, 2010. **27**(2): p. 125-131.
375. Liu, Q., et al., *Infant Skin Barrier, Structure, and Enzymatic Activity Differ from Those of Adult in an East Asian Cohort.* Biomed Res Int, 2018. **2018**: p. 1302465.
376. Miyauchi, Y., et al., *Developmental Changes in Neonatal and Infant Skin Structures During the First 6 Months: In Vivo Observation.* Pediatr Dermatol, 2016. **33**(3): p. 289-95.
377. Fairley, J.A. and J.E. Rasmussen, *Comparison of stratum corneum thickness in children and adults.* J Am Acad Dermatol, 1983. **8**(5): p. 652-4.
378. Tsugita, T., et al., *Positional differences and aging changes in Japanese woman epidermal thickness and corneous thickness determined by OCT (optical coherence tomography).* Skin Res Technol, 2013. **19**(3): p. 242-50.
379. Anderson, R.L. and J.M. Cassidy, *Variation in physical dimensions and chemical composition of human stratum corneum.* J Invest Dermatol, 1973. **61**(1): p. 30-2.
380. HI, M. and B. EK, *Neonatal Skin-Structure and Function*. 1982: New York, NY, Marcel Dekker.

381. Walters, R.M., et al., *Developmental Changes in Skin Barrier and Structure during the First 5 Years of Life.* Skin Pharmacology and Physiology, 2016. **29**(3): p. 111-118.
382. de Viragh, P.A. and M. Meuli, *Human scalp hair follicle development from birth to adulthood: Statistical study with special regard to putative stem cells in the bulge and proliferating cells in the matrix.* Archives of Dermatological Research, 1995. **287**(3): p. 279-284.
383. Mogensen, M., et al., *Morphology and epidermal thickness of normal skin imaged by optical coherence tomography.* Dermatology, 2008. **217**(1): p. 14-20.
384. Cross, S.E. and M.S. Roberts, *Use of In Vitro Human Skin Membranes to Model and Predict the Effect of Changing Blood Flow on the Flux and Retention of Topically Applied Solutes.* Journal of Pharmaceutical Sciences, 2008. **97**(8): p. 3442-3450.
385. Alkilani, A.Z., M.T.C. McCrudden, and R.F. Donnelly, *Transdermal Drug Delivery: Innovative Pharmaceutical Developments Based on Disruption of the Barrier Properties of the stratum corneum.* Pharmaceutics, 2015. **7**(4): p. 438-470.
386. Kakasheva-Mazhenkovska, L., et al., *Variations of the histomorphological characteristics of human skin of different body regions in subjects of different age.* Prilozi, 2011. **32**(2): p. 119-28.
387. Hughes-Formella, B., et al., *Comparison of Skin Structural and Functional Parameters in Well-Nourished and Moderately Undernourished Infants.* Skin Pharmacology and Physiology, 2019. **32**(4): p. 212-223.
388. Marcos-Garcés, V., et al., *Age-related dermal collagen changes during development, maturation and ageing - a morphometric and comparative study.* J Anat, 2014. **225**(1): p. 98-108.
389. Ryatt, K.S., et al., *Methodology to measure the transient effect of occlusion on skin penetration and stratum corneum hydration in vivo.* Br J Dermatol, 1988. **119**(3): p. 307-12.
390. Berardesca, E., C. European Group for Efficacy Measurements on, and P. Other Topical, *EEMCO guidance for the assessment of stratum corneum hydration: electrical methods.* Skin Research and Technology, 1997. **3**(2): p. 126-132.
391. Chittock, J., et al., *Development of stratum corneum chymotrypsin-like protease activity and natural moisturizing factors from birth to 4 weeks of age compared with adults.* Br J Dermatol, 2016. **175**(4): p. 713-20.
392. Fluhr, J.W., et al., *Infant epidermal skin physiology: adaptation after birth.* Br J Dermatol, 2012. **166**(3): p. 483-90.
393. Garcia Bartels, N., et al., *Influence of bathing or washing on skin barrier function in newborns during the first four weeks of life.* Skin Pharmacol Physiol, 2009. **22**(5): p. 248-57.
394. Garcia Bartels, N., et al., *Effect of Standardized Skin Care Regimens on Neonatal Skin Barrier Function in Different Body Areas.* Pediatric Dermatology, 2010. **27**(1): p. 1-8.

395. Hoeger, P.H. and C.C. Enzmann, *Skin Physiology of the Neonate and Young Infant: A Prospective Study of Functional Skin Parameters During Early Infancy.* Pediatric Dermatology, 2002. **19**(3): p. 256-262.
396. Minami-Hori, M., et al., *Developmental alterations of physical properties and components of neonatal-infantile stratum corneum of upper thighs and diaper-covered buttocks during the 1st year of life.* Journal of Dermatological Science, 2014. **73**(1): p. 67-73.
397. Saijo, S. and H. Tagami, *Dry skin of newborn infants: functional analysis of the stratum corneum.* Pediatr Dermatol, 1991. **8**(2): p. 155-9.
398. Visscher, M.O., et al., *Changes in diapered and nondiapered infant skin over the first month of life.* Pediatr Dermatol, 2000. **17**(1): p. 45-51.
399. Yosipovitch, G., et al., *Skin barrier properties in different body areas in neonates.* Pediatrics, 2000. **106**(1 Pt 1): p. 105-8.
400. Fluhr, J.W., S. Pfisterer, and M. Gloor, *Direct comparison of skin physiology in children and adults with bioengineering methods.* Pediatr Dermatol, 2000. **17**(6): p. 436-9.
401. Fujimura, T., et al., *Ethnic differences in stratum corneum functions between Chinese and Thai infants residing in Bangkok, Thailand.* Pediatric dermatology, 2018. **35**(1): p. 87-91.
402. Stamatas, *Assessment of infant stratum corneum composition and thickness with Raman spectroscopy.* Journal of the American Academy of Dermatology, 2012. **66**(4, Supplement 1): p. AB35.
403. Stamatas, G.N., E. Boireau, and J. Nikolovski, *Compositional differences between infant and adult stratum corneum determined by in vivo Raman confocal microspectroscopy.* Journal of Investigative Dermatology, 2010. **130**(SUPPL. 1): p. S69.
404. Narendran, V., et al., *Biomarkers of Epidermal Innate Immunity in Premature and Full-Term Infants.* Pediatric Research, 2010. **67**(4): p. 382-386.
405. Kretsos, K. and G.B. Kasting, *Dermal capillary clearance: physiology and modeling.* Skin Pharmacol Physiol, 2005. **18**(2): p. 55-74.
406. Kretsos, K. and G.B. Kasting, *A geometrical model of dermal capillary clearance.* Mathematical Biosciences, 2007. **208**(2): p. 430-453.
407. Holbrook, K., *A histological comparison of infant and adult skin.* Neonatal Skin: Structure and Function, 1982: p. 3-31.
408. Pöschl, J., et al., *Periodic variations in skin perfusion in full-term and preterm neonates using laser Doppler technique.* Acta Pædiatrica, 1991. **80**(11): p. 999-1007.
409. Fluhr, J.W. and R. Darlenski, *Skin Surface pH in Newborns: Origin and Consequences.* Curr Probl Dermatol, 2018. **54**: p. 26-32.
410. Fluhr, J.W. and P.M. Elias, *Stratum corneum pH: Formation and Function of the 'Acid Mantle'.* Exogenous Dermatology, 2002. **1**(4): p. 163-175.
411. Lynde, C., et al., *Skin Surface pH.* J Drugs Dermatol, 2019. **18**(12): p. 214.

412. Giusti, F., et al., *Skin barrier, hydration, and pH of the skin of infants under 2 years of age.* Pediatr Dermatol, 2001. **18**(2): p. 93-6.
413. Marchini, G., et al., *Erythema Toxicum Neonatorum Is an Innate Immune Response to Commensal Microbes Penetrated into the Skin of the Newborn Infant.* Pediatric Research, 2005. **58**(3): p. 613-616.
414. Kakasheva-Mazhenkovska, L., et al., *Histomorphometrical characteristics of human skin from capillitium in subjects of different age.* Prilozi, 2011. **32**(2): p. 105-18.
415. Wang, T.F., G.B. Kasting, and J.M. Nitsche, *A multiphase microscopic diffusion model for stratum corneum permeability. I. Formulation, solution, and illustrative results for representative compounds.* J Pharm Sci, 2006. **95**(3): p. 620-48.
416. Anderson, B.D. and P.V. Raykar, *Solute structure-permeability relationships in human stratum corneum.* J Invest Dermatol, 1989. **93**(2): p. 280-6.
417. Nitsche, J.M., T.F. Wang, and G.B. Kasting, *A two-phase analysis of solute partitioning into the stratum corneum.* J Pharm Sci, 2006. **95**(3): p. 649-66.
418. Khiao In, M., et al., *Histological and functional comparisons of four anatomical regions of porcine skin with human abdominal skin.* Anat Histol Embryol, 2019. **48**(3): p. 207-217.
419. Choe, C., et al., *Human skin in vivo has a higher skin barrier function than porcine skin ex vivo-comprehensive Raman microscopic study of the stratum corneum.* J Biophotonics, 2018. **11**(6): p. e201700355.
420. Sauermann, K., et al., *Age related changes of human skin investigated with histometric measurements by confocal laser scanning microscopy in vivo.* Skin Res Technol, 2002. **8**(1): p. 52-6.
421. Therkildsen, P., et al., *Epidermal thickness measured by light microscopy: a methodological study.* Skin Res Technol, 1998. **4**(4): p. 174-9.
422. Sandby-Moller, J., T. Poulsen, and H.C. Wulf, *Epidermal thickness at different body sites: relationship to age, gender, pigmentation, blood content, skin type and smoking habits.* Acta Derm Venereol, 2003. **83**(6): p. 410-3.
423. Robertson, K. and J.L. Rees, *Variation in epidermal morphology in human skin at different body sites as measured by reflectance confocal microscopy.* Acta Derm Venereol, 2010. **90**(4): p. 368-73.
424. Barrett, D.A. and N. Rutter, *Percutaneous lignocaine absorption in newborn infants.* Arch Dis Child Fetal Neonatal Ed, 1994. **71**(2): p. F122-4.
425. Delgado-Charro, M.B. and R.H. Guy, *Effective use of transdermal drug delivery in children.* Advanced Drug Delivery Reviews, 2014. **73**: p. 63-82.
426. Evans, N., et al., *Transdermal Drug Delivery to Neonates.* International Journal of Pharmaceutics, 1985. **24**(2-3): p. 259-265.
427. West, D.P., S. Worobec, and L.M. Solomon, *Pharmacology and toxicology of infant skin.* J Invest Dermatol, 1981. **76**(3): p. 147-50.
428. Telofski, L.S., et al., *The infant skin barrier: can we preserve, protect, and enhance the barrier?* Dermatology research and practice, 2012. **2012**.

429. Potts, R.O. and R.H. Guy, *Predicting skin permeability.* Pharmaceutical research, 1992. **9**(5): p. 663-669.
430. Food and Drug Administration, *Code of Federal Regulations Title 21 PART 320 Sec. 320.23 Basis for measuring in vivo bioavailability or demonstrating bioequivalence. https://www.accessdata.fda.gov/scripts/cdrh/cfdocs/cfcfr/CFRSearch.cfm?fr=320.23.*
431. Salamanca, C.H., et al., *Franz Diffusion Cell Approach for Pre-Formulation Characterisation of Ketoprofen Semi-Solid Dosage Forms.* Pharmaceutics, 2018. **10**(3).
432. Food and Drug Administration, *Transdermal and Topical Delivery Systems - Product Development and Quality Considerations Draft Guidance https://www.fda.gov/media/132674/download.* 2019.
433. Ginsberg, G., et al., *Pediatric pharmacokinetic data: implications for environmental risk assessment for children.* Pediatrics, 2004. **113**(4 Suppl): p. 973-83.
434. Ginsberg, G., et al., *Incorporating children's toxicokinetics into a risk framework.* Environmental health perspectives, 2004. **112**(2): p. 272-283.
435. Matta, M.K., et al., *Effect of Sunscreen Application Under Maximal Use Conditions on Plasma Concentration of Sunscreen Active Ingredients A Randomized Clinical Trial.* Jama-Journal of the American Medical Association, 2019. **321**(21): p. 2082-2091.
436. Orakzai SA, S.K., Ayub M, Saeed AK, *Serum proteins in infants.* J Pak Med Assoc., 1987. **37**(10): p. 251-255.
437. Zemlickis, D., et al., *Cisplatin protein binding in pregnancy and the neonatal period.* Med Pediatr Oncol, 1994. **23**(6): p. 476-9.
438. Herngren, L., M. Ehrnebo, and L.O. Boreus, *Drug binding to plasma proteins during human pregnancy and in the perinatal period. Studies on cloxacillin and alprenolol.* Dev Pharmacol Ther, 1983. **6**(2): p. 110-24.
439. Miller, P.F., et al., *Pharmacokinetics of prednisolone in children with nephrosis.* Arch Dis Child, 1990. **65**(2): p. 196-200.
440. Ritter, D.A. and J.D. Kenny, *Bilirubin binding in premature infants from birth to 3 months.* Arch Dis Child, 1986. **61**(4): p. 352-6.
441. Echizen, H., et al., *Plasma-Protein Binding of Disopyramide in Pregnant and Postpartum Women, and in Neonates and Their Mothers.* British Journal of Clinical Pharmacology, 1990. **29**(4): p. 423-430.
442. Anell-Olofsson, M., et al., *Plasma concentrations of alpha-1-acid glycoprotein in preterm and term newborns: influence of mode of delivery and implications for plasma protein binding of local anaesthetics.* Br J Anaesth, 2018. **121**(2): p. 427-431.
443. Lerman, J., et al., *Effects of age on the serum concentration of α1-acid glycoprotein and the binding of lidocaine in pediatric patients.* Clinical Pharmacology & Therapeutics, 1989. **46**(2): p. 219-225.
444. Mazoit, J.X., D.D. Denson, and K. Samii, *Pharmacokinetics of bupivacaine following caudal anesthesia in infants.* Anesthesiology, 1988. **68**(3): p. 387-91.

445. Rapp, H.J., et al., *Ropivacaine in neonates and infants: a population pharmacokinetic evaluation following single caudal block.* Pediatric Anesthesia, 2004. **14**(9): p. 724-732.
446. Fairley, J.A. and J.E. Rasmussen, *Comparison of stratum corneum thickness in children and adults.* Journal of the American Academy of Dermatology, 1983. **8**(5): p. 652-654.
447. Leveque, J.L., et al., *In vivo studies of the evolution of physical properties of the human skin with age.* Int J Dermatol, 1984. **23**(5): p. 322-9.
448. sMichel, M., et al., *From newborn to adult: phenotypic and functional properties of skin equivalent and human skin as a function of donor age.* J Cell Physiol, 1997. **171**(2): p. 179-89.
449. Akutsu, N., et al., *Functional characteristics of the skin surface of children approaching puberty: age and seasonal influences.* Acta Derm Venereol, 2009. **89**(1): p. 21-7.
450. Eberlein-König, B., et al., *Skin surface pH, stratum corneum hydration, trans-epidermal water loss and skin roughness related to atopic eczema and skin dryness in a population of primary school children.* Acta Derm Venereol, 2000. **80**(3): p. 188-91.
451. Fluhr, J.W., S. Pfisterer, and M. Gloor, *Direct Comparison of Skin Physiology in Children and Adults with Bioengineering Methods.* Pediatric Dermatology, 2000. **17**(6): p. 436-439.
452. Fujimura, T., et al., *Ethnic differences in stratum corneum functions between Chinese and Thai infants residing in Bangkok, Thailand.* Pediatric Dermatology, 2018. **35**(1): p. 87-91.
453. Man, M.Q., et al., *Variation of skin surface pH, sebum content and stratum corneum hydration with age and gender in a large Chinese population.* Skin Pharmacol Physiol, 2009. **22**(4): p. 190-9.
454. Yuan, C., et al., *Properties of Skin in Chinese Infants: Developmental Changes in Ceramides and in Protein Secondary Structure of the Stratum Corneum.* Biomed Res Int, 2017. **2017**: p. 3594629.
455. Zhu, Y.H., et al., *Characterization of skin friction coefficient, and relationship to stratum corneum hydration in a normal Chinese population.* Skin Pharmacol Physiol, 2011. **24**(2): p. 81-6.
456. Fluhr, J.W., et al., *Development and organization of human stratum corneum after birth: electron microscopy isotropy score and immunocytochemical corneocyte labelling as epidermal maturation's markers in infancy.* Br J Dermatol, 2014. **171**(5): p. 978-86.
457. Kashibuchi, N., et al., *Three-dimensional analyses of individual corneocytes with atomic force microscope: morphological changes related to age, location and to the pathologic skin conditions.* Skin Res Technol, 2002. **8**(4): p. 203-11.
458. Paus, R. and G. Cotsarelis, *The biology of hair follicles.* N Engl J Med, 1999. **341**(7): p. 491-7.

Appendices

Appendix for Chapter 2

Appendix 1. Sensitivity analysis results presenting input parameters that exhibited high (absolute SC ≥ 40%) or age-dependent (Δ(SCadult - SCchild) ≥ 30%)) sensitivity for the prediction of AUCinf in a newborn, an infant and an adult.

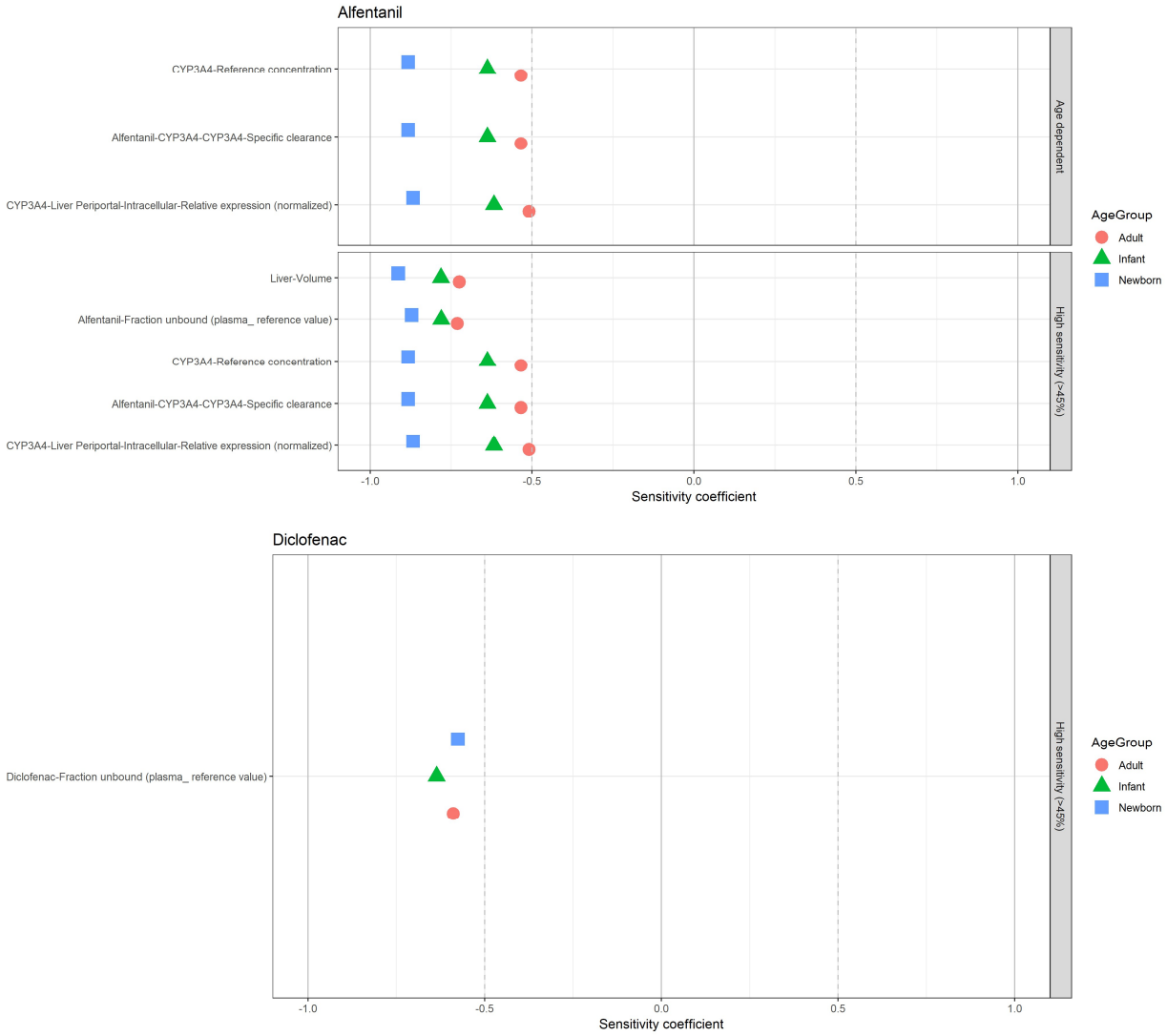
Alfentanil
CYP3A4-Reference concentration
Alfentanil-CYP3A4-CYP3A4-Specific clearance
CYP3A4-Liver Periportal-Intracellular-Relative expression (normalized)
Liver-Volume
Alfentanil-Fraction unbound (plasma_ reference value)
CYP3A4-Reference concentration
Alfentanil-CYP3A4-CYP3A4-Specific clearance
CYP3A4-Liver Periportal-Intracellular-Relative expression (normalized)
Age dependent
High sensitivity (>45%)
-1.0
-0.5
0.0
0.5
1.0
Sensitivity coefficient
AgeGroup
Adult
Infant
Newborn
Diclofenac
Diclofenac-Fraction unbound (plasma_ reference value)
High sensitivity (>45%)
-1.0
-0.5
0.0
0.5
1.0
Sensitivity coefficient
AgeGroup
Adult
Infant
Newborn

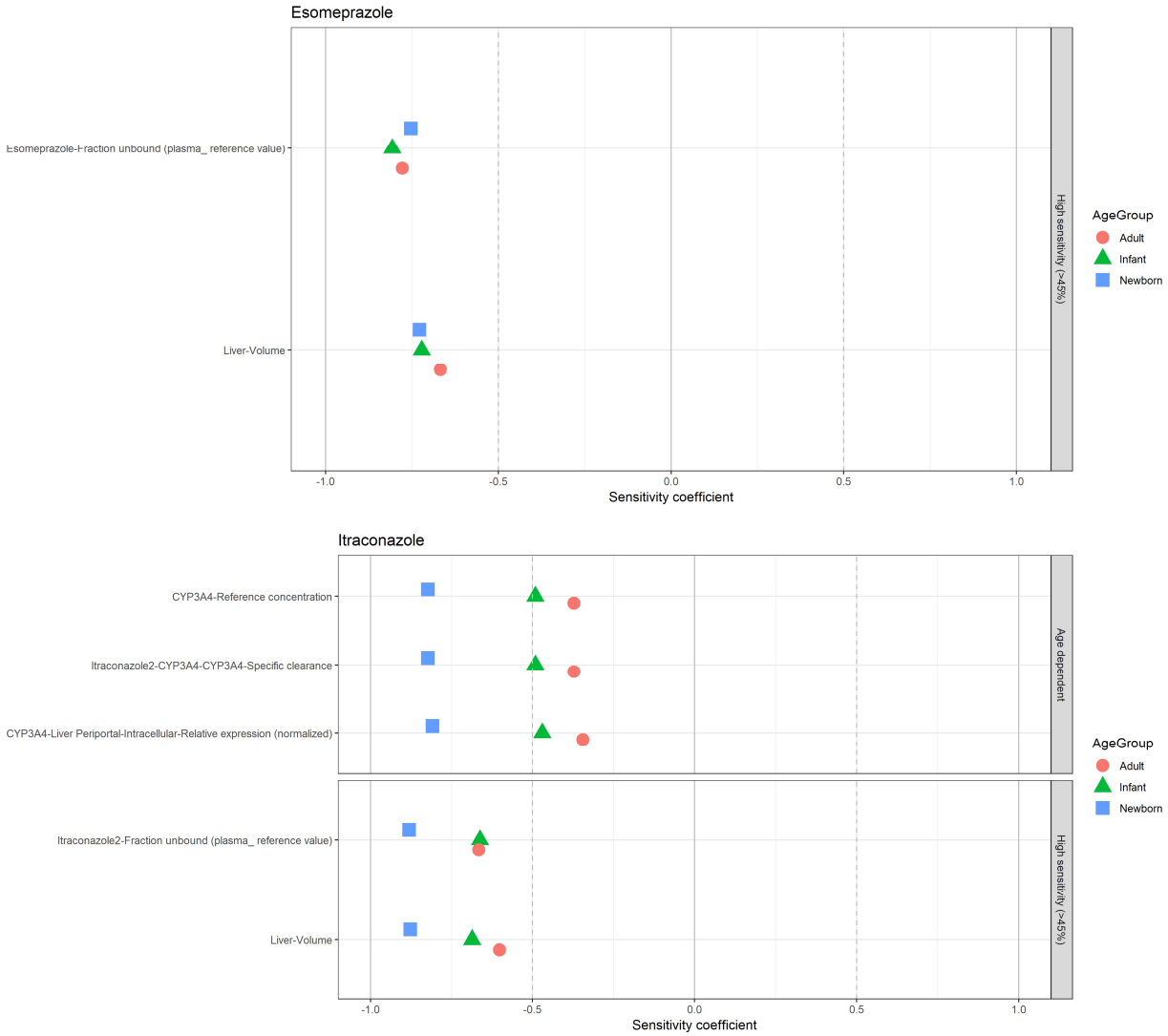
Esomeprazole
Esomeprazole-Fraction unbound (plasma_ reference value)
Liver-Volume
High sensitivity (>45%)
-1.0
-0.5
0.0
0.5
1.0
Sensitivity coefficient
AgeGroup
Adult
Infant
Newborn
Itraconazole
CYP3A4-Reference concentration
Itraconazole2-CYP3A4-CYP3A4-Specific clearance
CYP3A4-Liver Periportal-Intracellular-Relative expression (normalized)
Age dependent
Itraconazole2-Fraction unbound (plasma_ reference value)
Liver-Volume
High sensitivity (>45%)
-1.0
-0.5
0.0
0.5
1.0
Sensitivity coefficient
AgeGroup
Adult
Infant
Newborn

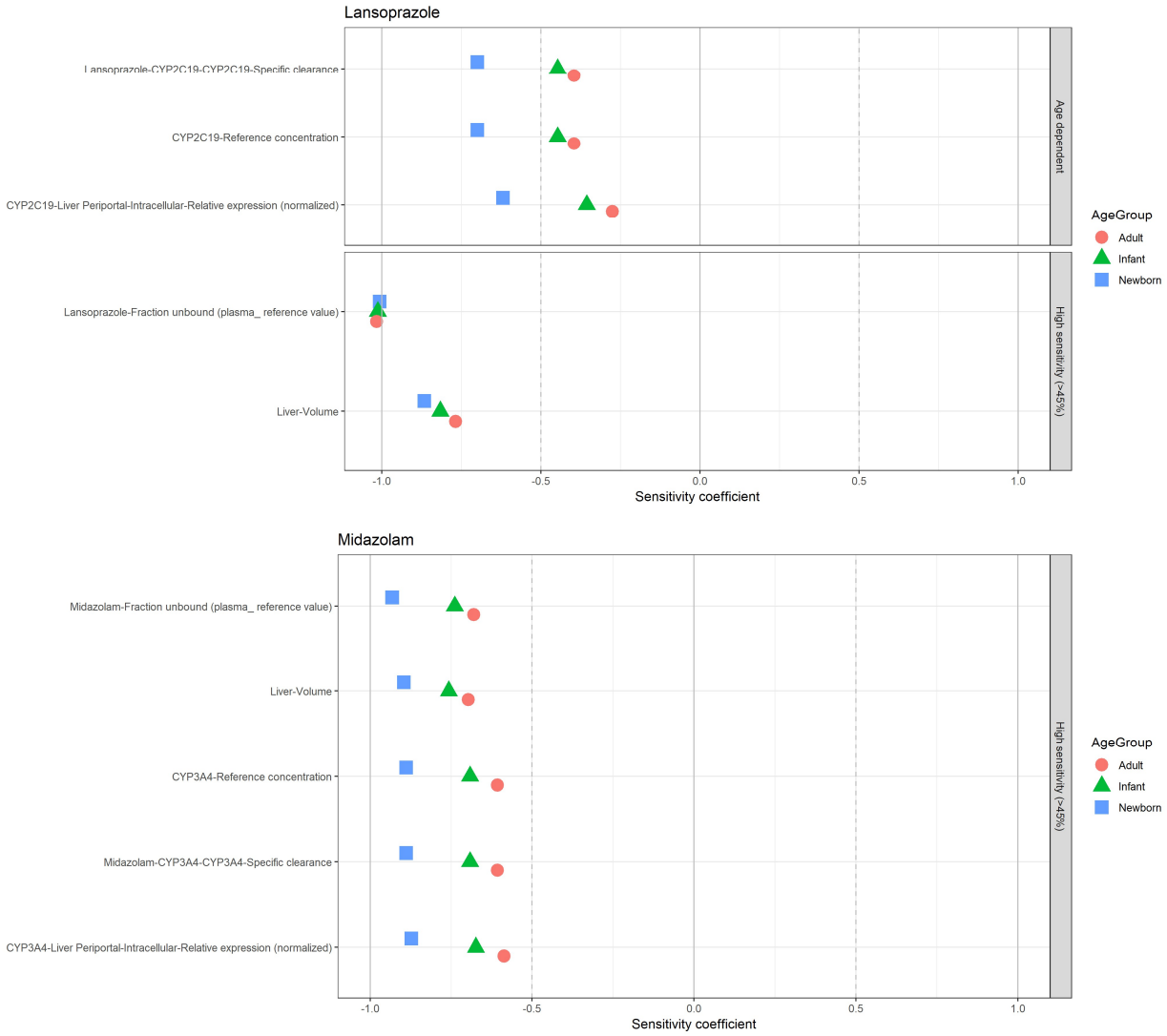
Lansoprazole
Lansoprazole-CYP2C19-CYP2C19-Specific clearance
CYP2C19-Reference concentration
CYP2C19-Liver Periportal-Intracellular-Relative expression (normalized)
Lansoprazole-Fraction unbound (plasma_ reference value)
Liver-Volume
Age dependent
High sensitivity (>45%)
-1.0
-0.5
0.0
0.5
1.0
Sensitivity coefficient
AgeGroup
Adult
Infant
Newborn
Midazolam
Midazolam-Fraction unbound (plasma_ reference value)
Liver-Volume
CYP3A4-Reference concentration
Midazolam-CYP3A4-CYP3A4-Specific clearance
CYP3A4-Liver Periportal-Intracellular-Relative expression (normalized)
High sensitivity (>45%)
-1.0
-0.5
0.0
0.5
1.0
Sensitivity coefficient
AgeGroup
Adult
Infant
Newborn

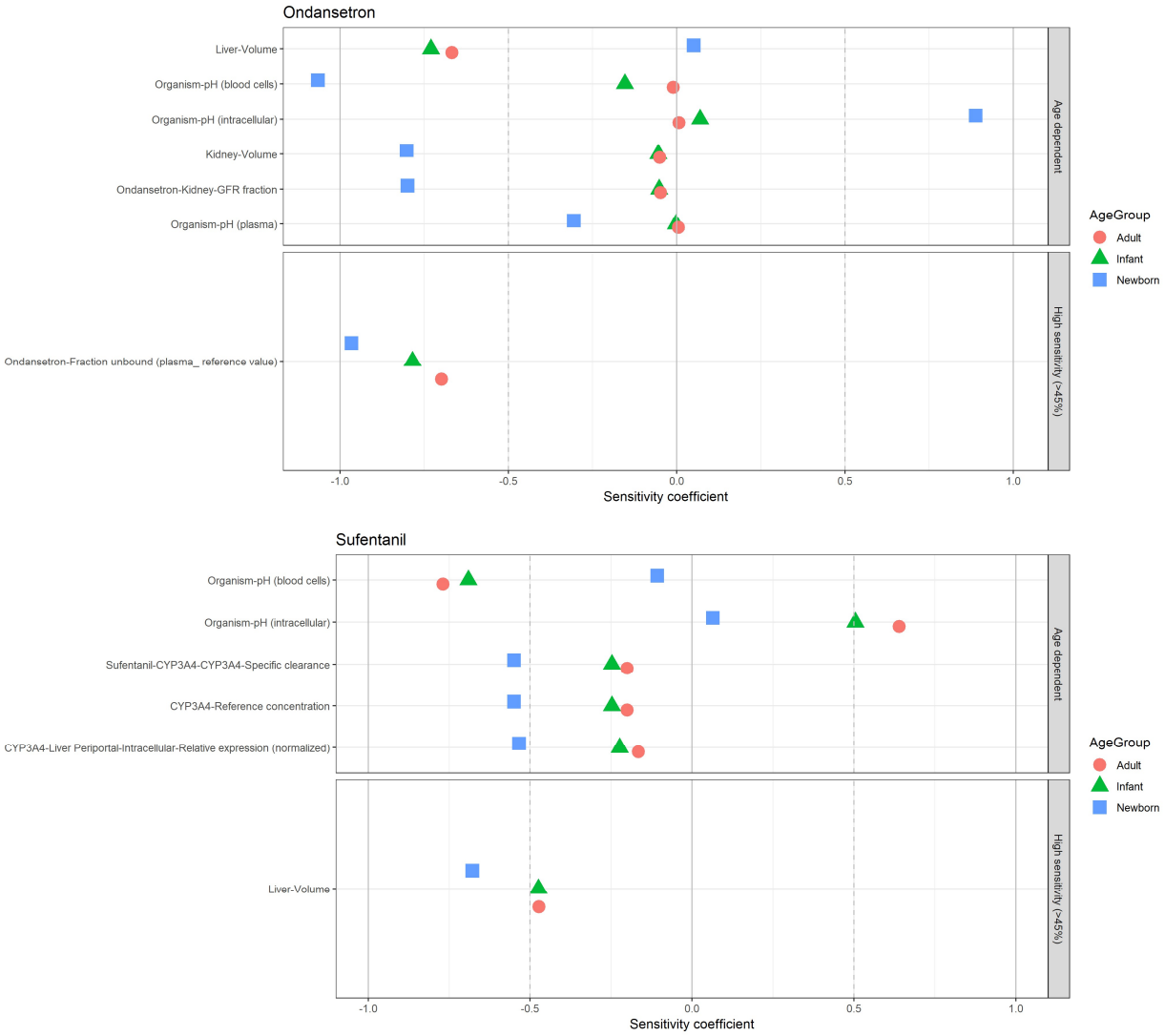
Ondansetron
Liver-Volume
Organism-pH (blood cells)
Organism-pH (intracellular)
Kidney-Volume
Ondansetron-Kidney-GFR fraction
Organism-pH (plasma)
Ondansetron-Fraction unbound (plasma_ reference value)
Age dependent
High sensitivity (>45%)
-1.0
-0.5
0.0
0.5
1.0
Sensitivity coefficient
AgeGroup
Adult
Infant
Newborn
Sufentanil
Organism-pH (blood cells)
Organism-pH (intracellular)
Sufentanil-CYP3A4-CYP3A4-Specific clearance
CYP3A4-Reference concentration
CYP3A4-Liver Periportal-Intracellular-Relative expression (normalized)
Liver-Volume
Age dependent
High sensitivity (>45%)
-1.0
-0.5
0.0
0.5
1.0
Sensitivity coefficient
AgeGroup
Adult
Infant
Newborn

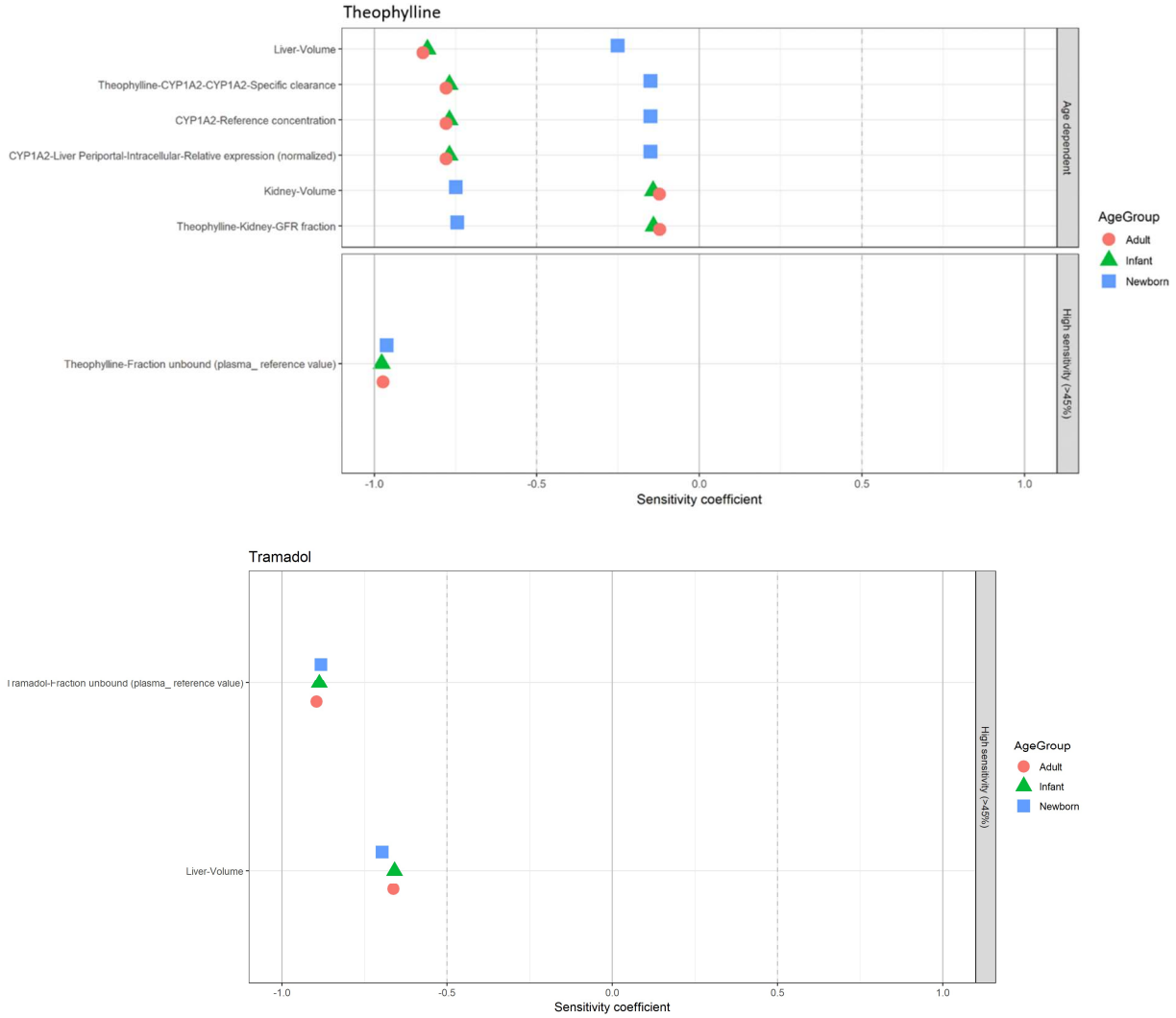

Supplementary Materials for Chapter 2

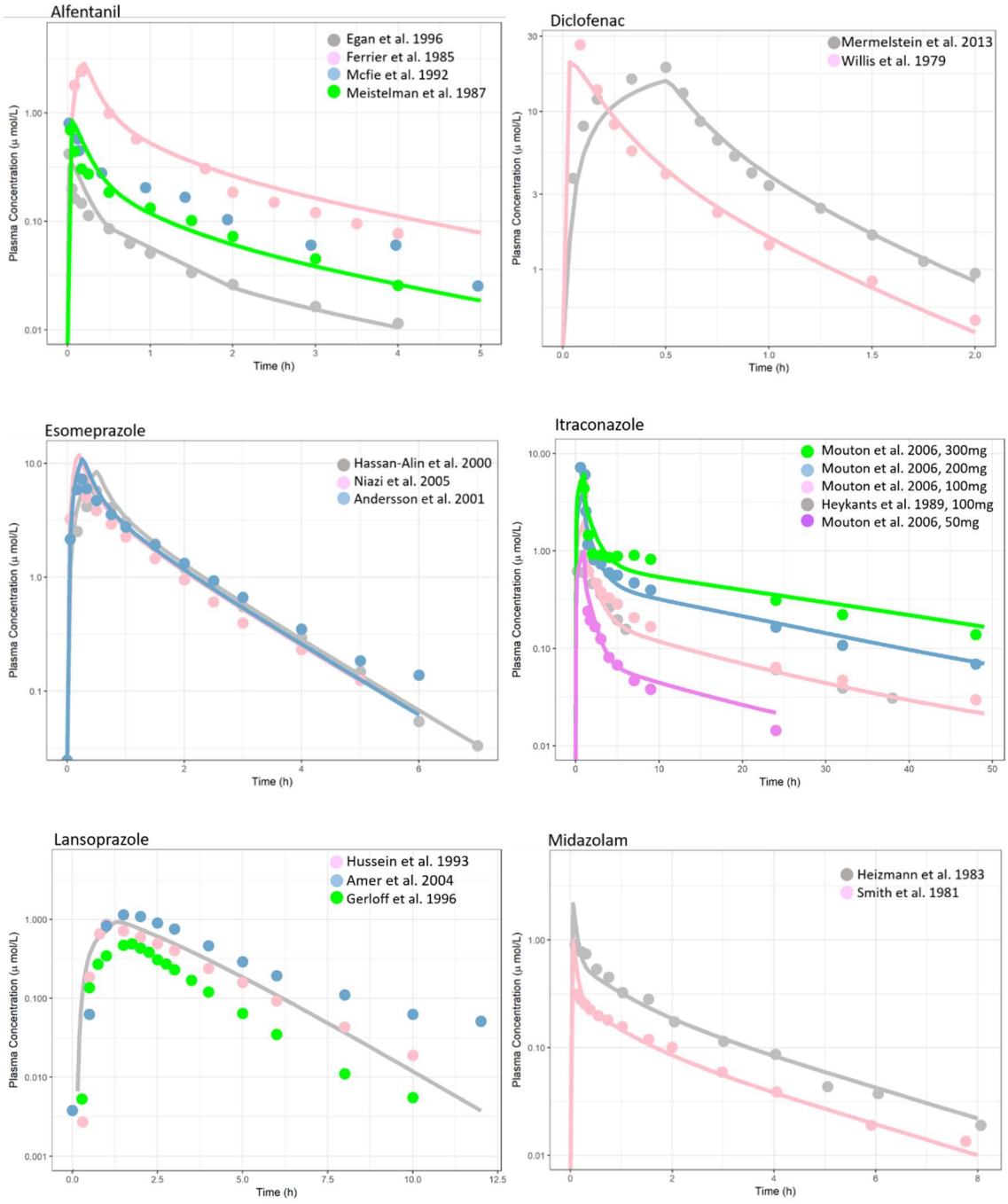
Alfentanil
Egan et al. 1996
Ferrier et al. 1985
Mcfie et al. 1992
Meistelman et al. 1987
Plasma Concentration (µ mol/L)
Time (h)
Diclofenac
Mermelstein et al. 2013
Willis et al. 1979
Plasma Concentration (µ mol/L)
Time (h)
Esomeprazole
Hassan-Alin et al. 2000
Niazi et al. 2005
Andersson et al. 2001
Plasma Concentration (µ mol/L)
Time (h)
Itraconazole
Mouton et al. 2006, 300mg
Mouton et al. 2006, 200mg
Mouton et al. 2006, 100mg
Heykants et al. 1989, 100mg
Mouton et al. 2006, 50mg
Plasma Concentration (µ mol/L)
Time (h)
Lansoprazole
Hussein et al. 1993
Amer et al. 2004
Gerloff et al. 1996
Plasma Concentration (µ mol/L)
Time (h)
Midazolam
Heizmann et al. 1983
Smith et al. 1981
Plasma Concentration (µ mol/L)
Time (h)

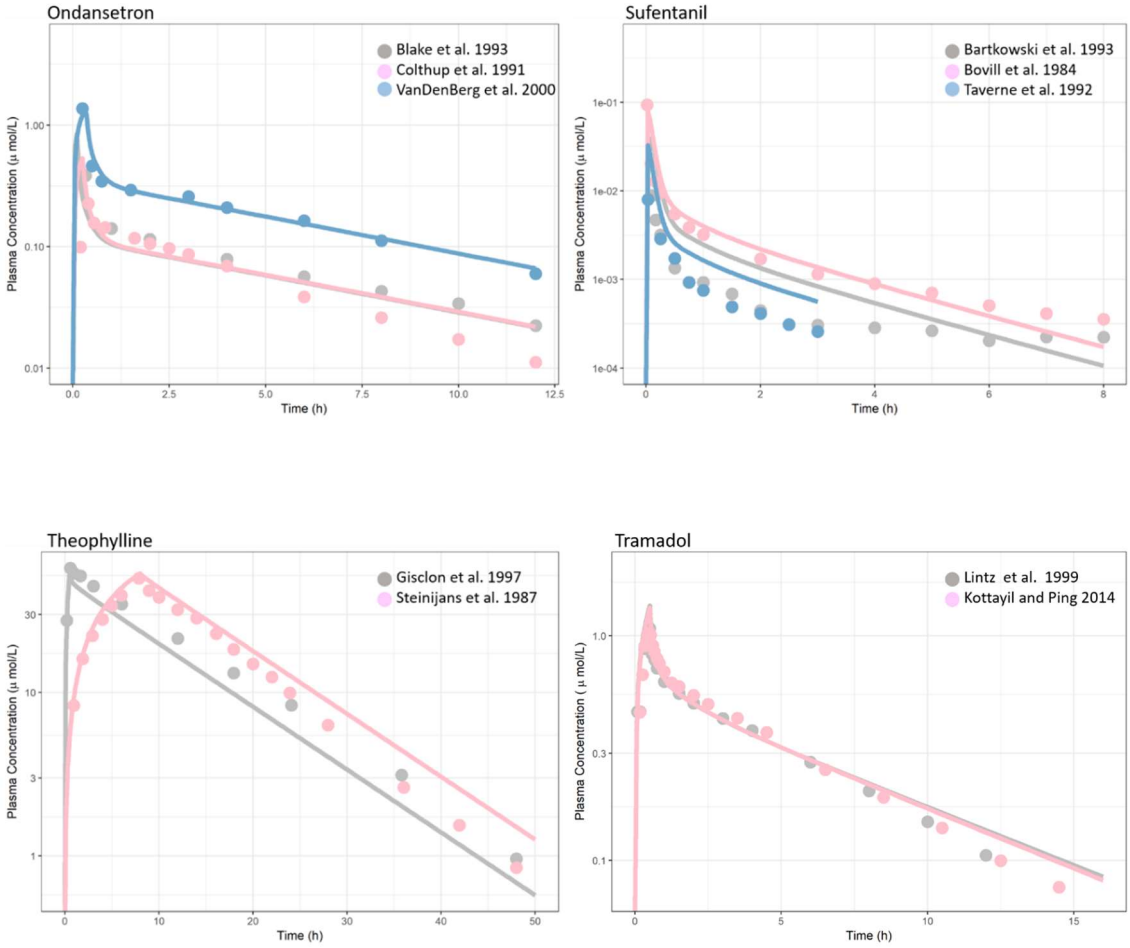

Figure S1. Predicted and observed plasma concentrations vs. time profiles of 10 compounds in adults. Solid lines represent the predicted plasma concentrations by PBPK modeling. Dots represent observed data from clinical studies. Administration protocols were listed in Table 2.2.

Table S1. Estimation equations for a standard deviation.

Standard deviation for the case where median and range were available.	Eqn (8) $S \approx \sqrt{\frac{1}{12}\left[\frac{(min-2*median+max)^2}{4} + (max-min)^2\right]}$ Where S is a standard deviation, min is minimum, max is maximum. This equation was taken from Hozo et al. This equation was used when observed SDs were not available in the data source. Of note, this equation was used for estimating SD from the reported CL range for esomeprazole data taken from Sandstrom et al. 2012. In the calculation, the reported geometric mean was assumed to be equivalent to median.
Standard deviation of each bootstrap replicate	Eqn (9) $s_i = \sqrt{\frac{\sum_{j=1}^{n}(x_j-\bar{x}_i)^2}{n-1}}$ Where si is a standard deviation of ith bootstrap replicates. Xj is a CL value (jth) of a virtual individual and $\bar{x}_i$ is an arithmetic mean in an ith bootstrap replicate. n is the sample size of an ith bootstrap replicate. The SD values calculated by this equation were used in Figure 1 and in the calculation of t-test and CVpred,i.
Standard deviation of means of bootstrap replicates	Eqn (10) $s = \sqrt{\frac{\sum_{k=1}^{100}(m_k-\bar{m})^2}{100-1}}$

	Where s is a standard deviation of means of bootstrap replicates. mk is an arithmetic mean of kth bootstrap replicate and $\overline{m}$ is an arithmetic mean of 100 bootstrap replicates' means. This SD was used in Figure 2.

Table S2. Concordance correlation coefficients (ρ_c) for plasma concentration vs. time profiles in adults.

compound	ρ_c
Alfentanil	0.98
Diclofenac	0.91
Esomeprazole	0.87
Itraconazole	0.75
Lansoprazole	0.78
Midazolam	0.91
Ondansetron	0.94
Sufentanil	0.84
Theophylline	0.97
Tramadol	0.95

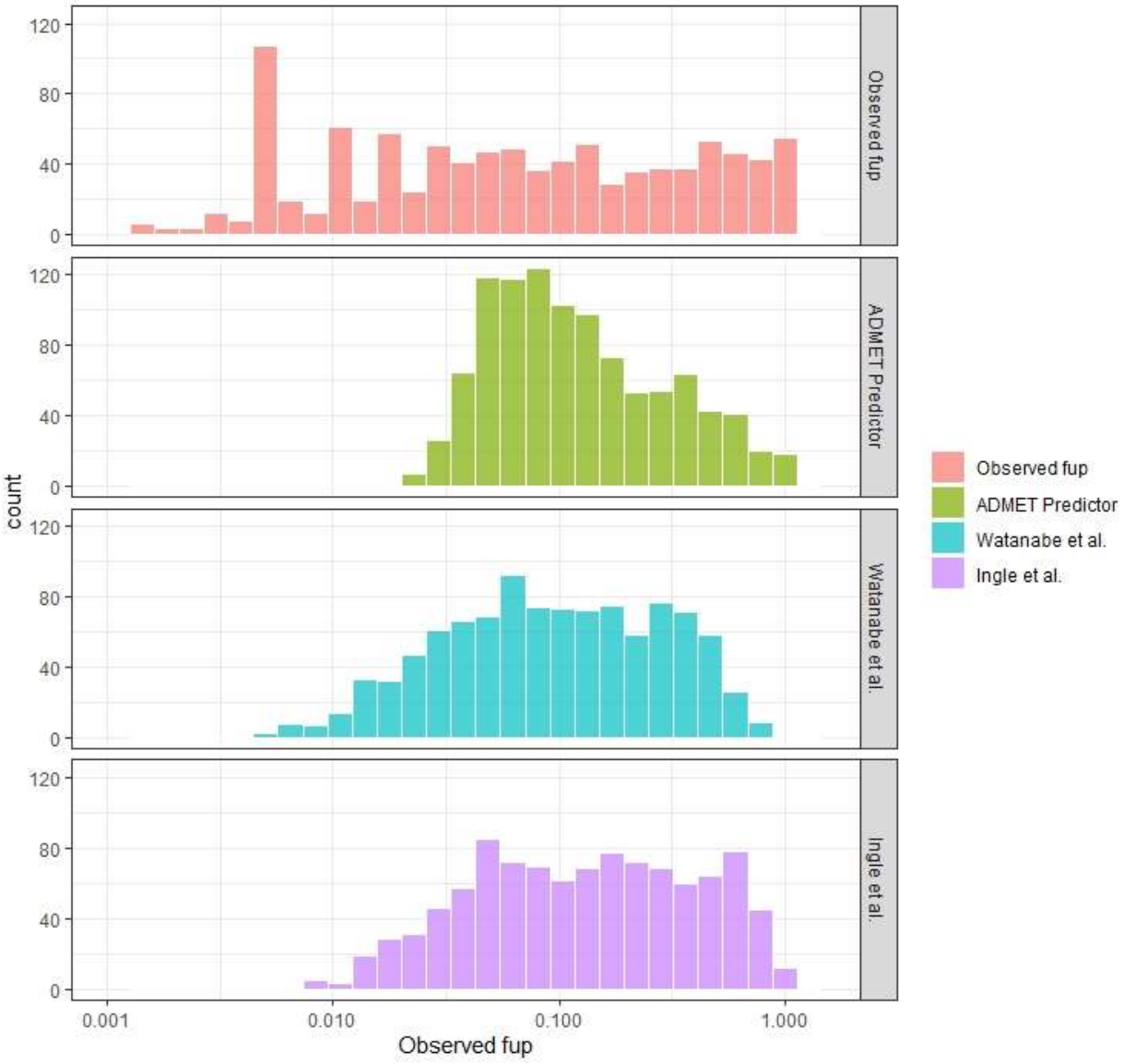

Figure S1. The distributions of the observed fup values and the predicted values according to each QSPR model.

Supplementary Materials for Chapter 4

Table S1. Observed albumin concentrations obtained from literature

PNA (days)	PNA SD	Albumin conc. (g/dL)	Albumin conc. SD	Reference
1	-	2.9	0.4	[277]
2	-	3	0.5	[277]
4	-	3.4	0.4	[277]
6	-	3.4	0.4	[277]
1	-	3.5	0.4	[249]
30	-	3.6	0.3	[249]
90	-	4	0.3	[249]
180	-	4	0.2	[249]
1	-	3.9	0.1	[436]
90	-	4.3	0.1	[436]
180	-	4.3	0.1	[436]
270	-	4.4	0.1	[436]
360	-	4.5	0.1	[436]
450	-	4.5	0.1	[436]
540	-	4.5	0.1	[436]
1	-	3.7	0.2	[236]
1	-	3.7	0.2	[236]

1	-	3.7	0.2	[236]
1	-	3.7	0.2	[236]
1	-	3.7	0.2	[236]
1	-	3.8	0.3	[437]
1	-	3.9	0.3	[438]
1	-	4.2	0.1	[273]
5110	-	4.6	0.3	[439]
365	-	4.3	-	[247]
730	-	4.3	-	[247]
1095	-	4.3	-	[247]
1460	-	4.3	-	[247]
1825	-	4.3	-	[247]
2190	-	4.4	-	[247]
2555	-	4.4	-	[247]
2920	-	4.4	-	[247]
3285	-	4.5	-	[247]
3650	-	4.5	-	[247]
4015	-	4.4	-	[247]
4380	-	4.2	-	[247]
4745	-	4.4	-	[247]
5110	-	4.5	-	[247]

5475	-	4.4	-	[247]
5840	-	4.4	-	[247]
6205	-	4.4	-	[247]
6570	-	4.4	-	[247]
6935	-	4.4	-	[247]
7300	-	4.3	-	[247]
365	-	4.2	-	[247]
730	-	4.2	-	[247]
1095	-	4.3	-	[247]
1460	-	4.3	-	[247]
1825	-	4.3	-	[247]
2190	-	4.3	-	[247]
2555	-	4.3	-	[247]
2920	-	4.3	-	[247]
3285	-	4.4	-	[247]
3650	-	4.4	-	[247]
4015	-	4.4	-	[247]
4380	-	4.3	-	[247]
4745	-	4.4	-	[247]
5110	-	4.4	-	[247]
5475	-	4.5	-	[247]

5840	-	4.5	-	[247]
6205	-	4.6	-	[247]
6570	-	4.6	-	[247]
6935	-	4.5	-	[247]
7300	-	4.6	-	[247]
1	-	3	0.2	[440]
3	1	3.2	0.3	[440]
7	-	3.4	0.2	[440]
14	-	3.4	0.3	[440]
28	-	3.6	0.3	[440]
56	-	3.2	0.2	[440]
80.5	14.8	3.6	0.2	[440]
1	-	3.5	-	[260]
109.5	-	3.8	-	[260]
365	-	4.2	-	[260]
1825	-	4.6	-	[260]
3650	-	4.5	-	[260]
4745	-	4.3	-	[260]
PNA: post natal age, SD: standard deviation, conc.: concentration, - : not available				

Table S2. Observed AAG concentrations data in children

PNA (days)	PNA SD	AAG conc. g/L	AAG conc. SD	Reference
1	-	0.1	0.2	[441]
1	-	0.3	0.1	[242]
180	120	0.6	0.1	[242]
2482	1095	0.7	0.2	[242]
1	-	0.2	-	[442]
1	-	0.2	0.1	[271]
1	-	0.1	0.1	[284]
1	-	0.2	0.1	[438]
15.5	7.3	0.6	0.3	[248]
380.5	174.8	0.8	0.5	[248]
3285.5	1277.3	0.9	0.6	[248]
1	-	0.3	0.1	[249]
30	-	0.5	0.2	[249]
90	-	0.7	0.1	[249]
180	-	0.7	0.3	[249]
1	-	0.2	0.05	[443]
168	83.8	0.5	0.1	[443]
103.1	51.7	0.3	0.1	[444]
66	-	0.4	2.7	[445]

1	-	0.2	0.05	[282]
SD: standard deviation, - : not available				

Table S3. Summary of chemical properties of the data set

Data type	N
Total data set	61
Albumin binding compounds	41
AAG binding compounds	20
Acids	24
Bases	24
Neutrals	13

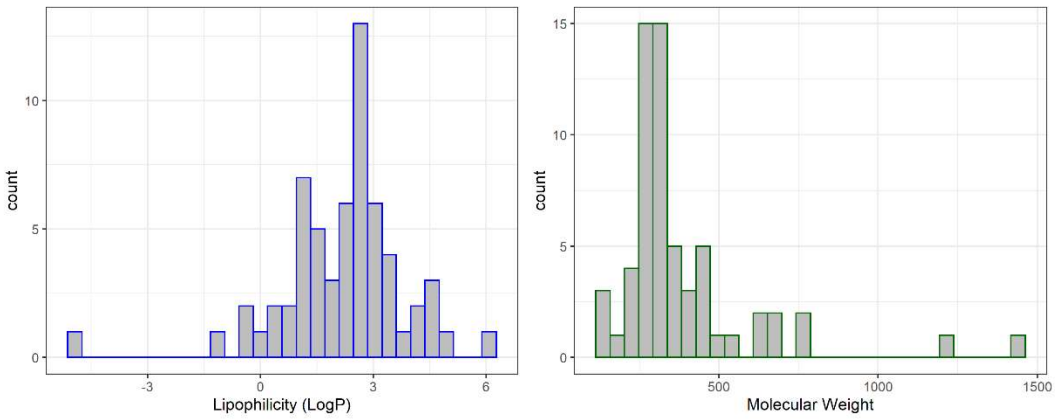

Figure S1. Histograms of key chemical properties of the dataset

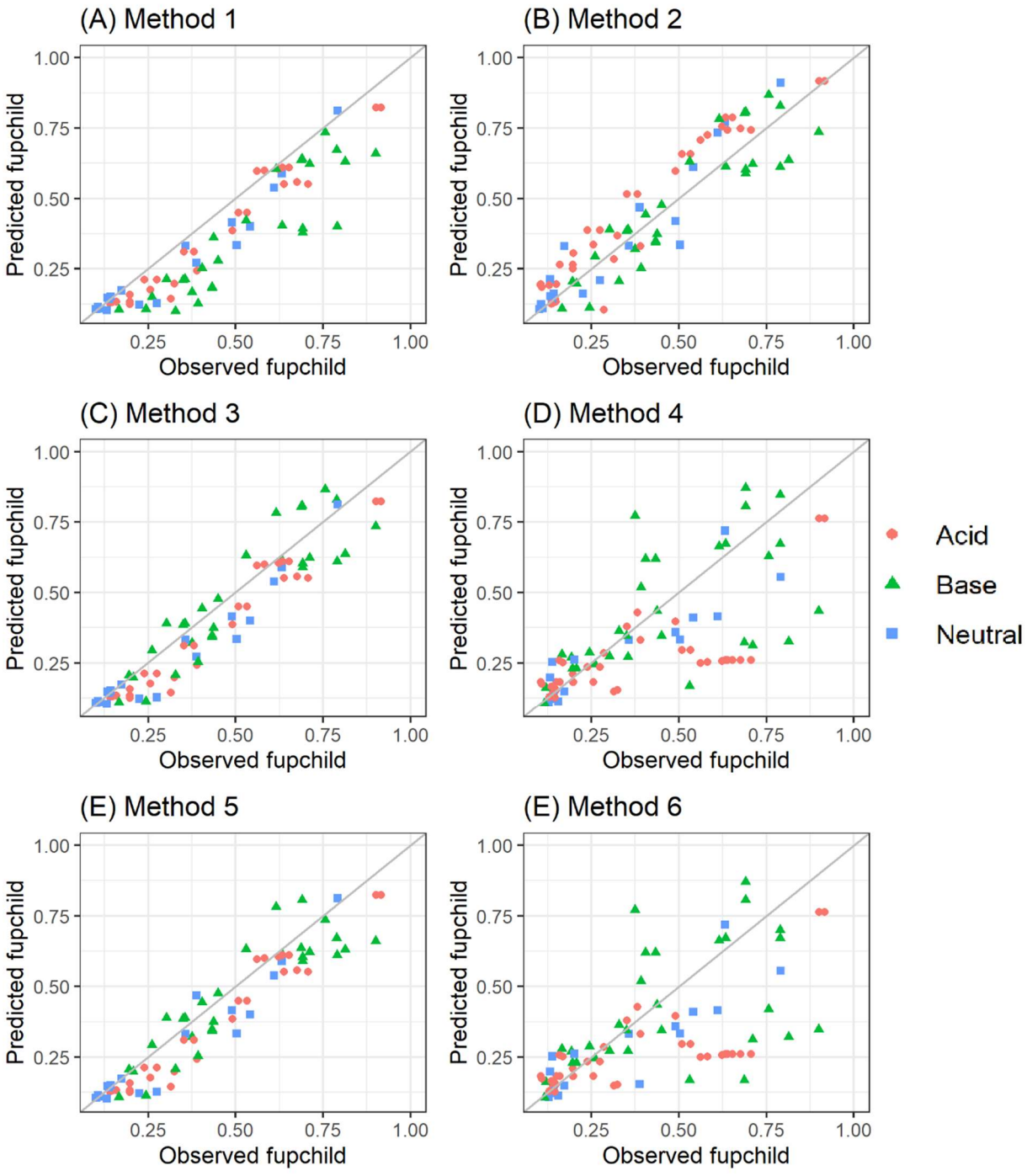
(A) Method 1
(B) Method 2
(C) Method 3
(D) Method 4
(E) Method 5
(E) Method 6
Predicted fupchild
Observed fupchild
1.00
0.75
0.50
0.25
Acid
Base
Neutral

Figure S1. Comparison between observed fup_{child} values and QSPR-based fup_{child} calculated using Johnson et al. according to different data-availability scenarios.

Supplementary Materials for Chapter 6

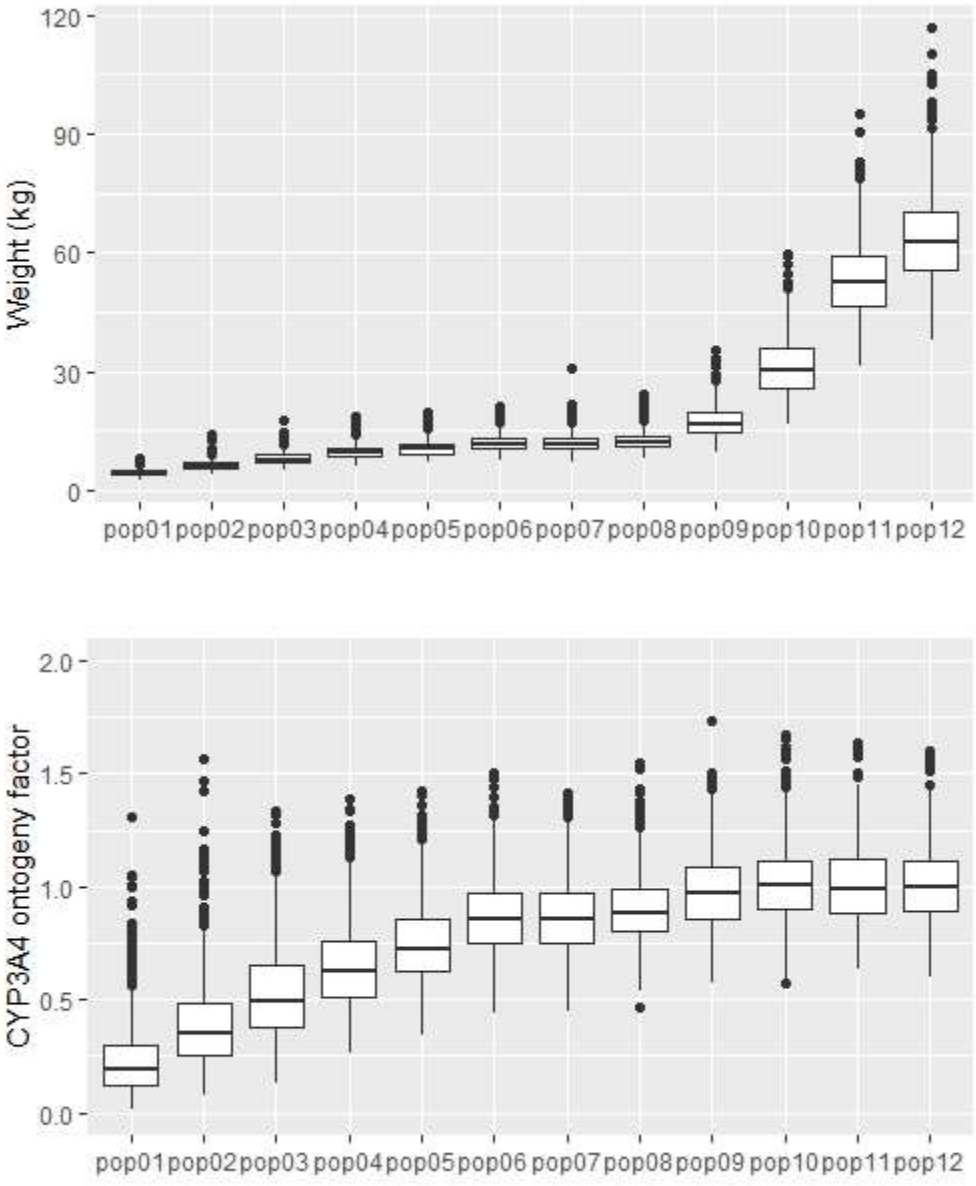

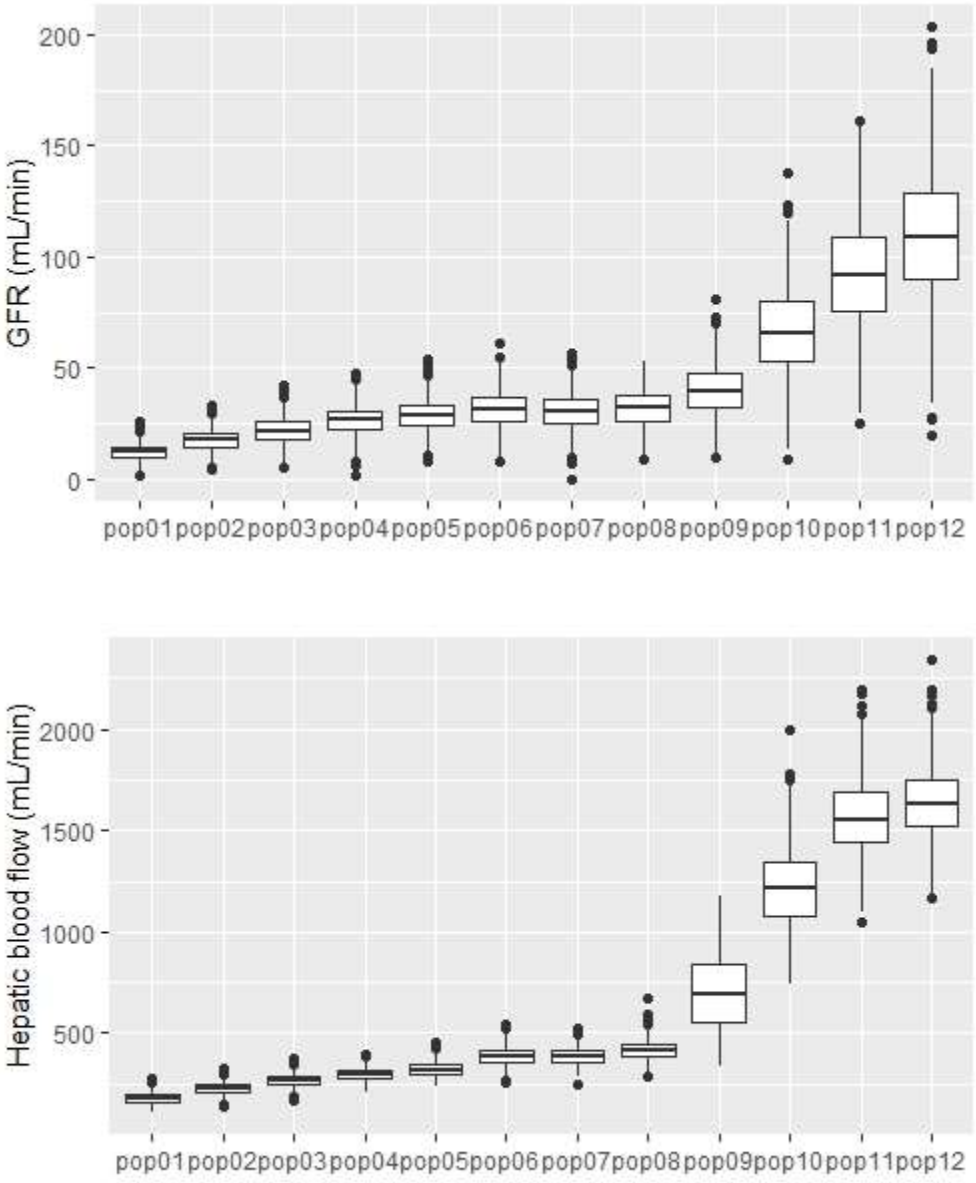

Figure S1. System-specific parameters that contribute to the inter-individual variability of CLchild.

Table S1. Stratum corneum (SC) thickness in infants and children.

Measurement Type	In vivo/ in vitro/ ex vivo & Room conditions	Body Area	Age	Notes	Trend	Reference
Hematoxylin and Eosin (H&E)	*Ex vivo*	Abdomen	Child (n=30): average=28 months/3.9 years (3 months – 11 years) Infant <3 months (n=10): average = 17.1 days Adult (n=10): average=26 years (17-46 years)	Values don't represent an absolute value for SC thickness, values are just used for relative comparison	No significant differences in SC thickness between any of the groups Adult SC = 35.4 μm, SD = 6.4 Child 3mo – 11 years. = 28.8 μm, SD = 10.6 Infant SC= 35.4 μm, SD=11.3	[446]
Confocal laser scanning microscopy	*In vivo* 22-28°C, 63-85% relative humidity	Buttock Upper thigh Ventral forearm	Full-term neonates (n=15) Measurements (4 times per site) at 4-7 days, 1,3,6 months after birth Mothers of infants n=15 (only measured ventral forearm)		Significant decrease in forearm skin observed from 4-7 days(~22μm) to 3 months of age (~10 μm). Similar changes in buttock and thigh skin but degree of decrease was relatively lower. SC thickness was almost the same as adults from 1 month of age in forearm skin. After 4-7 days SC thickness from all sites ranged from ~10-15 μm.	[376]
Modified starrett gauge, dry thickness of stratum corneum	*Ex vivo*	Hip	8 years – 65 years, n=10 donors total (3 females, 7 males) one section from each donor	Focus was to obtain reproducible results from single donor not the accuracy of measurement. Cell layers were counted on at least 6 locations and averaged	SC thickness for the only 8 years old: 8.1 μm 30-45 years old SC thickness ranged from: 6.2 – 19.1 μm Sc thickness positively correlated with dry mass (r=0.93).	[379]

				to determine purity of stratum corneum isolation.	Can't correlate thickness with age given only one donor <30 years and one > 45 years	
Reflectance Confocal Microscopy	*In vivo* No topical products and cosmetics for at least 24 h prior to study	44 adults (25-40 years): Caucasian Fitzpatrick skin type I–III (n = 25) and African American (n = 19) Infants (3-49 months old)	Upper inner arm (n=142) Dorsal forearm (n=151)	Children were grouped into 7 age bins (average n=11 per age bin): All 44 adults (average age 32 years) were placed into one age bin	SC thickness increases until 4 years of age from ~8 to 14μm, where it becomes similar to adult SC thickness (~13-14 μm) SC thickness of dorsal forearm and inner arms are similar in thickness	[381]
Reflectance Confocal Microscopy	*In vivo*	Infants: 6-24 months Mothers: 25-46 years old N=20 per group	Lower thigh	SC thickness was calculated from top of corneocyte layer to where granular cells can be detected	Infant SC thickness was on average 30% lower than that of adult: Infant: 7.3 ± 1.1 μm Adult: 10.5 ± 2.1 μm	[374]
Reflectance Confocal Microscopy	*In vivo* Avoid skin care products for 24 hours 20–25°C 40-60% humidity	Infants: 3-24 months (n=52) Adult mothers: 20-40 years (n=27) Asian Descent	Upper inner arm Lower thigh	SC thickness is measured from top of corneocyte layer to granular cells	On average SC thickness was lower than adults. Upper inner arm: infant SC was ~ 18% thinner than adults (5.3±1.4μm vs 7.9±1.8μm) Thigh: 34% thinner SC in infants These thickness values are thinner than Caucasian counterparts found in [374] No significant differences between male and female infants	[375]
Optical Coherence Tomography	*In vivo*	Healthy female Japanese volunteers (n= 116)	Forehead Cheek	Note: Quantitative values were thinner than reported in conventional textbooks	Thickest SC: back of hand Thinnest SC: shin	[378]

		Age: teens (14-17 years old) to sixties	Inner side of upper arm Inner side of forearm Outer side of forearm Back of hand Abdomen Back Inner side of femur Inner side of leg Shin		SC thickness showed no correlation to aging (unlike epidermal thickness). No trend was observed in SC thickness as aging occurs. Only cheek SC thickness became significantly less in the forties but in the sixties it returned to almost the same level as that in the twenties. Back of hand also seems to increase with age, but not stat significant.	
Histological sections, light microscopy	*Ex vivo* Post-mortem skin samples	Infants (n=169) Gestation: 24-40 weeks 3 groups: 36-40 weeks (n=88) 31-35 (n=22) <31 (n=59)	Upper abdominal margin of the midline	SC thickness was measured based on a scoring system: Barely visible (0) Thin layer (1) Medium layer (2) Thick layer (3)	SC thickness increases with gestational age, SC is very thin or barely there until 34 weeks gestational age. After 34 weeks gestation, SC forms and most have medium to thick SC layer. SC thickness in term babies doesn't increase over 16 weeks. More infants have SC in the thick or medium layer category after 6 weeks of age, but many also have the same scoring from 0-4 weeks of age. Very few full term babies have thin SC. Histologically, the SC thickness also showed similar structure and thickness in term baby at 1 day old and 4 months (16 weeks) old	[361]

Table S2. Thickness of viable epidermis in infants and children.

Measurement Type	In vivo/ in vitro/ ex vivo & room conditions	Body Area	Age	Notes	Trend	Reference

Holtain Skin Caliper	*In vivo*	Dorsal forearm	Age: 8-89 years old (n=145) No skin disorders		Measured whole skin thickness. Thickness: bell curve distribution with peak at 25 years old for women and 45 years old for men. Women's skin was always thinner than men skin after the peak of thickness for women at 25 years old.	[447]
Reflectance Confocal microscopy	*In vivo*	Lower thigh	Infants 6-24 months old (n=20) Infant Mothers: 25-46 years old (n=20)	Epidermal thickness calculated from the top corneocyte layer (thickness includes Stratum Corneum) to the top of the dermal papilla	Infant supra-papillary epidermis was on average 20% thinner than that of adults (29.7±3.4 μm versus 36.2±5.2 μm) Differences between child and adult were statistically significant	[374]
Histology, paraffin, hematoxylin and eosin	Skin biopsies *ex vivo*	Capillitium Forehead Cheeks Anterior neck Thorax Axilla Abdomen Back Gluteus Anterior arm Anterior forearm Palm Anterior leg, Anterior lower leg Sole	Divided into age groups: full term to 1 years 1-12 years 13-22 years 23-55 years 56-73 years 10 donors per age group, N=750 skin biopsies	Open-source journal	No stat analysis shown. Appears total skin thickness increases with age. Epidermis thickens from 0-1 years old to adulthood (23-53 years old) in forehead, palm, and sole. For covered skin areas the epidermis thickness stays relatively constant from 0-1 years old. Epidermis thickness decreases from 1 to 12 years and reaches similar thickness to adults	[386]

Histology, paraffin, hematoxylin and eosin	Skin biopsies of healthy human skin at autopsy, *ex vivo*	Capitillium (epidermis and corium aka dermis)	Neonate: full term to 1 years Childhood: 1-12 years Puberty/adolescence: 13-22 years Adult: 23-55 years Elderly: 56-73 years N=60 biopsy specimens, 12 samples per age groups	Open-source journal	Epidermal thickness was higher in infants less than 1years old (160.8 μm) then decreased in children aged 1-12 years old (98.3 μm). From then epidermal thickness increased into adulthood (158.7-174.6 μm), then decreased after 56 years old (112 μm). Percentage of each epidermal layer in whole epidermis also changes with age.	[414]
Reflectance confocal laser scanning microscopy	*In vivo* 20–25°C 40-60% humidity	Upper inner arm Lower thigh	Infants: 3-24 months (n=52) Infant mothers: 20-40 years (n=27)	Thickness of the suprapapillary epidermis (SPE) was measured from the top corneocyte layer to the top of the dermal papilla (epidermal thickness includes Stratum corneum thickness)	On average infant SPE thickness was lower than adults. Upper inner arm: infant SPE ~ 22% thinner Thigh: Infant SPE 8% thinner These thickness values are thinner than Caucasian counterparts found in [374].	[375]
Histology, light microscopy	*In vitro*	Human foreskin	Newborn: 2-5 days old Child: 3-11 years Old Adult: 17-58 years old	Two different donors for each age category: Newborn- 2 and 3 day old Child- 4 and 10 years old Adult- 15 and 26 years. old	After 1 week of submerged culture, epidermal thickness decreased with age. Adult keratinocytes formed 1-2 cell layer thick epidermis. Newborn epidermis was 6-8 cell layers thick Child epidermis was 4-5 cell layers thick. The same was seen when cultured at air-liquid interface.	[448]
Confocal laser scanning microscopy	*In vivo* 22-28°C	Full-term neonates (n=15)	Buttock Upper thigh	Epidermal thickness determined in two ways:	Dermal papilla not observed up to 4-7 days post birth but gradually observed up to 3 months of age.	[376]

	63-85% humidity	Measurements at 4-7 days, 1,3,6 months after birth Infant Mothers: n=15 (only ventral forearm measured)	Ventral forearm	1. Skin surface to top of dermal area (dermal papillae) 2. Skin surface to the bottom of epidermal layer (rete ridges) Epidermis thickness includes SC thickness	Dermal papilla increases in size and number up to 6 months of age, but the most drastic changes occur in the first 3 months. **Skin surface to top of dermal area:** Increase in epidermal thickness at each site from 4-7 days old to 1 month old. After 1 month, thickness was mostly the same as in adults (21 μm ±3): Ventral forearm: ~20 μm to 25 μm Buttock: ~21 μm to 26 μm Thigh: similar thickness from 4-7days to 1 month **Epidermal thickness from skin surface to bottom of the epidermal layer, i**ncreased significantly between 4 to 7 days and 1 month of age in all areas. This change with growth after birth almost stopped before 1 month of age, and from 1 month of age, epidermal thickness from the skin surface to the bottom of the epidermal layer was mostly the same as in adults (ventral forearm only: ~60μm). Ventral forearm: ~25μm at 4-7 days to 55μm at 1 month old	
Histological sections, light microscopy	*Ex vivo*	Upper abdominal margin of the midline	Gestation at birth ranged from 24-40 weeks 3 groups: 36-40 weeks (n=88) 31-35 (n=22) <31 (n=59)		Epidermal thickness increases with increasing gestational age Epidermis increases with increasing postnatal age. The increase in epidermal thickness stops after 16 wks. of age	[361]

					The undulation of the epidermis also increases with increased age post birth. Premature babies develop epidermis in 2 weeks of life with increase thickness and cell layers. However, the undulation of the epidermis does not develop during this time.	
Histology sections	Biopsy specimens	Parietal scalp	Age: 2 weeks – 21 years (n=100) 62 males, 38 females	Minimum and maximum epidermis thickness was measured	Minimum epidermis thickness did not appear to vary with age (25μm). But maximal epidermal thickness increased slightly with age (80 μm at birth to 160 μm at 21 years old): Linear regression: 80.5 + 3.0y R=0.5, p<0.0001 Units in μm	[382]

Table S3. Thickness of Dermis in infants and children.

Method of measurement	In vivo/ in vitro/ ex vivo & room conditions	Body Area	Age	Notes	Trend	Reference
Histology sections	Biopsy specimens	Parietal scalp	Post-natal Age: 2 weeks – 21 years (n=100) 62 males, 38 females	Dermis measured from dermal papilla to least and most prominent projection of collagen fibres. Adventitial dermis not considered	Both the minimum and maximum dermis thickness values increased with age (y=years) in parallel (units = μm) Minimum Dermis: <1-year-old: 850 μm 21 years old: 1500 μm Maximum Dermis: <1-year-old: 1125 μm 21 years old: 2200 μm **Regression Lines:** Min dermis: 777.5 + 32.9y (r=0.64, p<0.0001) Max dermis: 1143.1 + 34.2y (r=0.53, p<0.0001)	[382]
Histology, paraffin, hematoxylin and eosin	Skin biopsies	Capillitium Forehead Cheeks Anterior neck Thorax Axilla Abdomen Back	Divided into age groups: full term to 1 year 1-12 years 13-22 years 23-55 years 56-73 years	Open-source journal No in-text references	No stat analysis shown. Appears total skin thickness increases with age. Dermis thickness is higher in the 1-12 age group compared to the 0-1 year old age group at all regions measured except capillitium (scalp). Dermis also is higher in the 13-22 age groups compared to the 1-12 age group After this age, unsure whether it stays the same given no statistical analysis.	[386]

		Gluteus Anterior arm Anterior forearm Palm Anterior leg Anterior lower leg Sole	N=10 per age group			
20 MHz sonography (allows depiction of the dermis, but not separate resolution of the epidermis)	*In vivo*	Cheek Volar forearm Thigh Calf	N=310 7 age groups (n=21-24 per group): 1wk ±5 days old 4weeks± 7 days old 6 months ± 20 days old 9months ± 20 days old 12 months ± 20 days old 24 months ± 84 days old 36months ± 84 days old	Did not mention the bounds of the dermis that were measured to get thickness values.	Measured **total skin thickness.** Dermal thickness at cheek appears highest at 1 week of age (1200μm) then slightly decreases at 4 weeks of age (1100μm), where it is similar from 6- 36 months of age (1000μm). Dermal thickness at forearm appears highest at 1 week of age (1200μm) then slightly decreases at 4 weeks of age (1100μm), where it is similar from 6- 36 months of age (1050μm)	[387]
Histology and microscopy	*Ex vivo*	Abdominal skin: periumbilical region adjacent to the midline.	N=45 Age 5 months old to 95 years Old		**Thickness of papillary dermis increases with age.** It followed a linear regression model in a statistically significant way ($P < 0.0001$, $R^2 = 0.26$):	[388]

	Area assumed to be protected from sun exposure	Average age: 57.02 ± 27.68 years	from 63.24-μm-thick in the moment of birth until 100 μm at 100 years old (predicted). Reticular dermis thickness followed a quadratic function: $P = 0.011$, $R^2 = 0.193$ The thickness was minimum in the first and last stages of life, with values of 1603.88 μm at the moment of birth and 1303.48 μm predicted for 100-year-olds, and maximum values in adult skin, reaching a thickness of 3236.18 μm at 50 years of age.	

Table S4. Stratum corneum (SC) hydration in infants and children.

Method of measurement	In vivo/ in vitro/ ex vivo & room conditions	Body Area	Age	Trend	Reference
Corneometer	24°C 50% humidity *In vivo*	Cheek Forearm	10-14 years old (N=32) Mothers: 40±4 years old	Skin hydration is lower in children compared to adults. Cheek Summer (AU): Children: 45.7±8.4 Adult: 56.3±8.8 P<0.0001 Cheek Winter (AU): Children: 31.8±11.2 Adult: 49.2±9.9 P<0.0001 Forearm Summer Children: 30.7±3.3 Adult: 37.2±5.0 P<0.0001 Forearm Winter Children: 27.7±3.2	[449]

				Adult: 31.2±5.0 P=0.0026	
Capacitance	20.6±0.62°C35.71±6.51 % humidity *In vivo*	Forearm Thigh	Birth (<72h old)- 4 weeks old (N=39) Compared to unrelated adults (N=20)	Skin hydration increases significantly from birth Birth: 17·66 ± 4·55 relative capacitance units (RCU) Early infancy (4 weeks): 41·79 ± 9·65 RCU Newborn infant skin was dryer than adults 17.66 RCU (infants) vs 31.47± 6.9 RCU (adults)	[391]
Capacitance	*In vivo*	Forearm	6.4 ± 0.31 years old Eczema versus no eczema	Skin hydration measured as 62.29 ± 6.34 AU	[450]
Corneometer	20 ± 2 °C 50 ± 10% humidity *In vivo*	Forearm	Age groups (n=18 per group): 1-15 days old 5-6 weeks old 6± 1 months Old 1-2 years old 4-5 years old Adult: 20-35 years	Mean skin hydration value for newborns 1-15 days old (17.4AU) was significantly lower compared with older age groups. The 5-6 week old (41.2AU) and the 6 month old age group (41.5AU) had higher skin hydration compared to the other age groups.	[392]
Corneometer	21-25°C Mean Humidity=43.6% Range humidity=33-55% humidity *In vivo*	Forearm	1-6 years old (n=44) Compared to adult parent 21-44 years old (n=44)	Skin hydration not significantly different between children and adults. Child: 75.4 ± 11.4 AU Adult: 76.1 ± 8.4 AU	[451]
Corneometer	22-26°C 40-60% humidity *In vivo*	Upper arm Thigh Buttock	6-24 months of age (n=60)	No significant differences in skin hydration at any site from 6 months to 24 months of age.	[452]

Corneometer	*In vivo*	Forehead Abdomen Upper leg Buttock	Newborns ≤48h old followed to 8 weeks of age (n=64)	Hydration increased with age at all four sites. Hydration in 2-day old neonate was ~25 AU and increased to ~55AU at 8 weeks of age.	[394]
Corneometer	21.6 ±1 .5°C 46.4 ± 7.45% humidity *In vivo*	Forehead Cheek Forearm Gluteal surface	3 days old newborns (n=202) Followed up at 4 and 12 weeks Mothers: 18-40 years old	Hydration increased significantly at all tested sites during the neonatal period then remained stable after 30 days post birth.	[395]
Corneometer	*In vivo*	Forehead Abdomen Upper leg Buttock	Neonates ≤48h old followed until 4 weeks old. Product applied after 7 days	Hydration significantly increased from day 2 -7 post birth. The highest increase in hydration was in the abdomen, which increased by 7 AU. An overall increase in hydration is also seen from age 2 days to 28 days old in the control group bathed with water and the group bathed with a washcloth and water.	[393]
Corneometer	22–24°C 45–55% Humidity *In vivo*	Forehead Forearm	0.5 - 94 years of age N=713	Skin hydration increases to age 40-50 years then decreases	[453]
Corneometer	25°C 40% Humidity *In vivo*	Upper thigh Diaper covered buttock	Neonates 3 days old followed up to 1 year old (n=19) Mothers (n=5)	Skin hydration is lower than adults in the thigh and buttock, then increases rapidly until 1 month of age and remains higher than adult hydration throughout the first year of life.	[396]
High frequency conductance	22-26°C 40-53% Humidity *In vivo*	Forearm	Newborn infants 0-5 days old (n=46) Children 1-5 years old (n=16) Adults 22-47 years old (n=10)	Newborns had lower conductance than adults. Conductance was higher in 1 month and 2-month-old infants compared to newborns.	[397]

Dermal Phase Meter	*In vivo*	Non-diapered skin above waistband Forearm (mother)	Newborn infants (n=31) Followed from one day old to 28 days of age Mothers	Skin surface hydration of non-diapered region increases in the first 2 postnatal weeks then plateaus. Adult value (4.76 Log capacitive reactance) was higher than value in the first week of life but lower than value at one month of age.	[398]
Corneometer	22°C to 24°C 50% humidity *In vivo*	Forehead Upper black Forearm Palm Abdomen Inguinal region Soles	Newborns (n=44) 5-10 hours post-partum and followed until 24 hours post-partum Adults: mean age of 24 (n=20)	Hydration was significantly lower in neonates compared with adults in forehead, back, abdomen. Hydration was significantly higher in neonates than adults in forearm and palms.	[399]
Corneometer	24–26°C 40–60% humidity *In vivo*	Inner upper arm Buttock Cheek	Infants 2-24 months old (n=63) Mothers (n=60)	Water content decreased in an age-dependent manner: Infants 2-12 months old had highest capacitance 13–24-month-old group: **Buttock:** higher water content than mothers **Upper arms and cheeks:** significantly lower water content than mothers	[454]
Corneometer	16–20°C 44–47% humidity *In vivo*	Dorsal Hand Forehead Canthus	0.15 -79-year-old volunteers (n=633) 125 volunteers aged 0-10 years old	Increased hydration from the first decade of life to ~40 years, then decreases.	[455]

AU: arbitrary units; RCU: relative capacitance units.

Table S5. Corneocyte Volume Fraction.

Method of measurement	In vivo/ in vitro/ ex vivo & room conditions	Body Area	Age	Notes	Trend	Reference

				Not a direct measure of corneocyte volume fraction of SC.		
Scanning Electron Microscopy	Adhesive disc to isolate and analyze surface of Stratum Corneum 20 ± 2 °C 50 ± 10% relative humidity	Volar forearm	1 day old to 5 years old Adult patients were parents of children whenever possible. 6 age groups created (n=6 or 5 per group): (i) full term newborns (1–15 days; mean 0·3 months), (ii) young babies (5–6 weeks old; mean 1·5 months), (iii) older babies (6 ± 1 months old; mean 6·2 months), (iv) young children (2 years old; mean 22·7 months), (v) older children (4–5 years old; mean 50·4 months), (vi) adults (20–35 years old; mean 336·0 months)	1-2 year old age group was analysed separately given larger age gap in enrolled individuals Developed isotropy score based on SEM images. Score parameters: (i) cell density (× 30 magnification); (ii) cluster formation (× 30 magnification); (iii) cell shape and adhesion (× 500 magnification); and (iv) resolution (× 500 magnification) Score from 0-3 points per parameter (12 max per sample), total score divided into 3 categories: anisotropy(immature), intermediate isotropy, good isotropy (mature)	Correlation: Younger age group had lower score. Child 6 months to 4-5 years had lower scores than adults too. Under age 2, change in score was very fast, then the rate increased at a slower rate to adult hood. Irregular corneocyte distribution was observed under age 1, and the projected area showed a progressive age dependent increase. Overall: Skin matured quickly until age 2 years old, then slows until adulthood in the morphology of the corneocytes.	[456]
Atomic Force Microscopy	*In vitro* Tape striped corneocyte from surface of skin Indoor ordinary environment	Cheek Flexor surface of upper arm	N=12 females Age: 1 -82 years old 7 participants were < 20 years old: 1 years old: n=1	2D and 3D parameters of corneocytes were measured: Average thickness Projected cell surface area (as it increases, cell turnover decreases)	Average corneocyte thickness was greater in the upper arm than the cheek regardless of age. Corneocyte thickness decreased with age for the upper arm but not for the cheek due to too much individual variation.	[457]

			2 years old: n=2 4 years old: n=1 9 years old: n=2 16 years old: n=1	Real surface area Volume Flatness Index (projected area/average thickness X 10^{-3})	Projected surface area of corneocytes in the flexor upper arm increased with age (relationship was not as prominent in the cheek). Corneocytes from forearm were larger than the cheek. Flatness index of forearm corneocytes also increased with age (as age increases, corneocytes become bigger and flatter). This was not observed for cheek corneocytes.	
Reflectance Confocal Microscopy	*In vivo* One tape strip of surface corneocytes	Infants 6-24 months Mothers 25-46 years old N=20 per group	Upper inner arm Dorsal forearm Lower thigh area		Size of infant corneocytes was smaller than adult corneocytes at all sites. The size of corneocytes between the different sites were not significantly different in adults or children. Corneocyte size (μm^2): Upper inner arm: Infant: 949.9 ± 19.1 Adult: 1077.6 ± 26.9 Dorsal forearm: Infant: 907.3 ± 23.4 Adult: 1071.0 ± 25.7 Thigh: Infant: 953.0 ± 23.8 Adult: 1154.4 ± 33.7 Smaller size of corneocytes was attributed to higher cell proliferation rate.	[374]

					Volume of corneocytes from the upper arm were higher than the cheek corneocytes. No clear correlation between the volume of corneocytes and the age of the participants in cheek or upper arm samples due to large individual variations at both sites.	
Several	*In vivo*	8 years old – 89 years old	Ventral side of arm	The main focus is older age. Measured number of corneocytes and surface area	Corneocyte count increases linearly with age. Number of corneocytes increase very sharply after 60 years of age. Projected surface area of corneocytes increases with age.	[447]

Table S6. Follicle Size and Volume.

Method	**In vivo/ in vitro/ ex vivo & room conditions**	**Body Area**	**Age**	**Notes**	**Trend**	**Ref.**
Transmission Electron Microscopy Scanning Electron Microscopy	3mm Punch biopsies for only 6 infants without Erythema toxicum	Lower leg	Infants: 1 day old (≥24h <48h) (n=69) Adults: n=4	None of the babies were bathed before sample collection	The number of visible hair structures/mm^2 was 3.5 ± 0.08 in infants (n =2) and 0.3 ± 0.15 (mean ± SD) in adults (n =4) Newborn infants have ~10 times more hair follicles than adults (comes from a textbook stating that newborns have approximately 5 million hair follicles on their body but no reference to this number [458])	[413]
Histology, hematoxylin and eosin	*Ex vivo*		Neonatal full-term infants to elderly up to 73 years old	Unpublished data	Length and width of hair follicles changes with age Follicle diameter increases from 0.13mm to 0.558 in elderly. In newborns the length of longitudinal follicle is 1.113 and increases up to 4.5mm in adolescence	[414]

Table S7. Stratum Corneum Thickness Literature Review and Search Strategy.

The following search strategy was inputted into PubMed to identify publications that contained quantitative stratum corneum thickness measurements in infants and children.

Input	Results
"stratum corneum" AND (thick* OR thickness OR depth OR deep OR width OR thin*) AND (development OR develop* OR time OR life OR growth OR progress OR change OR age OR maturation)	1191
English language and full text filters	1039
Exclude review articles	980
Human only filter	609
Relevant articles	43
Final Selected	17

Table S8. Epidermis Thickness Literature Review and Search Strategy.

The following search strategy was inputted into PubMed to identify publications that contained quantitative epidermis thickness measurements in infants and children.

Input	Filters	Results
(Epidermis [mesh] OR "Epidermal cells" OR epidermal) AND (Thick* OR thickness OR depth OR deep OR width OR thin*) AND (Development [tiab] OR develop*[tiab] OR time OR life OR growth OR progress OR change [tiab] OR maturation [tiab] OR matur*) NOT "stem cell" NOT "growth factor" NOT burn NOT graft NOT Langerhans NOT review [pt] NOT treatment [tiab]	English Human Full-Text	1262
Relevant articles		27
Final Selected		9

Table S9. Dermis Thickness Literature Review and Search Strategy.

The following search strategy was inputted into PubMed to identify publications that contained quantitative dermis thickness measurements in infants and children.

Input	Filters	Results
(Dermis [mesh] OR papillary dermis) AND (Thick* OR thickness OR width OR depth[tiab] OR thin*) AND (Development [tiab] OR develop*[tiab] OR time [tiab] OR "early life" OR growth [tiab] OR progress* OR change [tiab] OR age OR maturation [tiab])	English Human Full-Text	509
Relevant articles		7
Final Selected		4

Table S10. Stratum Corneum Hydration Literature Review and Search Strategy.

The following search strategy was used to search MEDLINE and EMBASE using OVID to identify publications that quantitatively measured the water content or fraction in the stratum corneum of infants or children.

Number	Searches	EMBASE Results	MEDLINE Results
1	horny layer.mp. [mp=title, abstract, heading word, drug trade name, original title, device manufacturer, drug	838	697

	manufacturer, device trade name, keyword, floating subheading word, candidate term word]		
2	cornified cell envelope.mp. [mp=title, abstract, heading word, drug trade name, original title, device manufacturer, drug manufacturer, device trade name, keyword, floating subheading word, candidate term word]	267	219
3	exp stratum corneum/	11603	0
4	stratum corneum.mp. [mp=title, abstract, heading word, drug trade name, original title, device manufacturer, drug manufacturer, device trade name, keyword, floating subheading word, candidate term word]	15894	9335
5	hydration.mp. or exp hydration/ or exp skin hydration meter/	54620	36122
6	chemical composition/ or exp lipid composition/ or exp tissue water/ or exp water content/	123638	0
7	(water adj4 (content or fraction or percent*)).mp. [mp=title, abstract, heading word, drug trade name, original title, device manufacturer, drug manufacturer, device trade name, keyword, floating subheading word, candidate term word]	46162	33771
8	exp infant/	985694	1139847
9	(infant* or newborn* or full term or neonat* or child or children).mp. [mp=title, abstract, heading word, drug trade name, original title, device manufacturer, drug manufacturer, device trade name, keyword, floating subheading word, candidate term word]	3279134	3096201
10	1 or 2 or 3 or 4	16569	10068
11	5 or 6 or 7	203833	68485
12	8 or 9	3283560	3096201
13	10 and 11 and 12	219	134

14	limit 13 to (human and english language)	171	101
	Duplicates	82	
	Final Selection	15	

Table S11. Corneocyte Volume Fraction Literature Review and Search Strategy.

The following search strategy was used to search MEDLINE and EMBASE using OVID to identify publications that quantitatively measured size, volume, or surface area of corneocytes in the stratum corneum of infants or children.

Number	Searches	EMBASE Results	MEDLINE Results
1	horny layer.mp. [mp=title, abstract, heading word, drug trade name, original title, device manufacturer, drug manufacturer, device trade name, keyword, floating subheading word, candidate term word]	838	697
2	cornified cell envelope.mp. [mp=title, abstract, heading word, drug trade name, original title, device manufacturer, drug manufacturer, device trade name, keyword, floating subheading word, candidate term word]	267	219
3	exp stratum corneum/	11603	0
4	stratum corneum.mp. [mp=title, abstract, heading word, drug trade name, original title, device manufacturer, drug manufacturer, device trade name, keyword, floating subheading word, candidate term word]	15892	9334
5	corneocyte.mp. [mp=title, abstract, heading word, drug trade name, original title, device manufacturer, drug manufacturer, device trade name, keyword, floating subheading word, candidate term word]	639	416
6	(corneocyte adj3 size).mp. [mp=title, abstract, heading word, drug trade name, original title, device manufacturer, drug manufacturer, device trade name, keyword, floating subheading word, candidate term word]	36	25
7	(corneocyte adj6 volume).mp. [mp=title, abstract, heading word, drug trade name, original title, device manufacturer, drug manufacturer, device trade name, keyword, floating subheading word, candidate term word]	4	1

8	(corneocyte adj6 phase).mp. [mp=title, abstract, heading word, drug trade name, original title, device manufacturer, drug manufacturer, device trade name, keyword, floating subheading word, candidate term word]	11	9
9	(corneocyte adj6 fraction).mp. [mp=title, abstract, heading word, drug trade name, original title, device manufacturer, drug manufacturer, device trade name, keyword, floating subheading word, candidate term word]	1	1
10	*infant/ or *Infant, Newborn/	43411	18885
11	(full term or neonat* or child).mp. [mp=title, abstract, heading word, drug trade name, original title, device manufacturer, drug manufacturer, device trade name, keyword, floating subheading word, candidate term word]	2580392	2371036
12	1 or 2 or 3 or 4	16567	10067
13	5 or 6 or 7 or 8 or 9	639	416
14	10 or 11	2599884	2379691
15	12 and 13 and 14	21	20
	Duplicates		14
	Total Selected		26
	Final Selection		4

Table S12. Lipid and Protein Ratio Literature Review and Search Strategy.

The following search strategy was used to search EMBASE and MEDLINE using OVID to identify publications that quantitatively measured the lipid and protein quantities in the stratum corneum of infants or children.

Number	Search	Results
1	exp lipid/ or exp lipid bilayer/ or exp skin lipid/	1548059
2	(content* or fraction or amount).mp. [mp=title, abstract, heading word, drug trade name, original title, device manufacturer, drug manufacturer, device trade name, keyword, floating subheading word, candidate term word]	1980619
3	*stratum corneum/	2843
4	(horny layer or cornified envelope).mp. [mp=title, abstract, heading word, drug trade name, original title, device manufacturer, drug manufacturer, device trade name, keyword, floating subheading word, candidate term word]	1661
5	(infant* or neonat* or child*).mp. [mp=title, abstract, heading word, drug trade name, original title, device manufacturer, drug manufacturer, device trade name, keyword, floating subheading word, candidate term word]	3213267
6	exp pediatrics/	106644
7	3 or 4	4338
8	5 or 6	3237629
9	exp phospholipid/	191370
10	free fatty acid.mp. or fatty acid/	113305
11	lipid matrix.mp. [mp=title, abstract, heading word, drug trade name, original title, device manufacturer, drug manufacturer, device trade name, keyword, floating subheading word, candidate term word]	1305
12	1 or 9 or 10 or 11	1550458
13	2 and 7 and 8 and 12	22
Final Selection	2	

*Medline: no results for final search.

Table S13. Follicle Size, Density, Volume Literature Review and Search Strategy.

The following search strategy was used to search MEDLINE and EMBASE using OVID to identify publications that quantitatively measured follicle physical properties in the skin of infants or children.

Number	Searches	EMBASE Results	MEDLINE Results
1	exp Infant/	985694	1138991
2	(neonat* or newborn* or child or children or infant* or preschool age or school age).mp.	3274956	3089674
3	exp Hair Follicle/	14897	6400
4	(hair? adj3 (follicle? or appendage? or structure?)).mp.	20705	14465
5	(count or counted or number or microscopy).mp.	3880791	2945093
6	exp Microscopy/	824006	549293
7	1 or 2	3279469	3089674
8	3 or 4	20705	18177
9	5 or 6	3893008	2955727
10	7 and 8 and 9	496	327
11	limit 10 to (english language and humans)	313	190
	Duplicates	117	
	Final selection	2	

Table S14. Albumin Concentration Literature Review and Search Strategy.

The following search strategy was used to search MEDLINE and EMBASE using OVID to identify publications that quantitatively measured albumin content or fraction in the epidermis of infants or children.

Number	Searches	EMBASE Results	MEDLINE Results
1	exp albumin/ or exp albumin level/	131881	0
2	exp epidermis/	159372	27270
3	exp infant/	946163	1151595
4	newborn*.mp. [mp=title, abstract, heading word, drug trade name, original title, device manufacturer, drug manufacturer, device trade name, keyword, floating subheading word, candidate term word]	614911	768034
5	(full term or neonat* or child or children).mp. [mp=title, abstract, heading word, drug trade name, original title, device manufacturer, drug manufacturer, device trade name, keyword, floating subheading word, candidate term word]	2728408	2613394
6	3 or 4 or 5	3089382	3050030
7	1 and 2 and 6	39	0
Final Selection	1		